# Total Radical Production and Degradation Products from Alkene Ozonolysis

by

Mohammed Salim Alam

A thesis submitted to the
University of Birmingham
for the degree of
DOCTOR OF PHILOSOPHY

School of Geography, Earth and Environmental Sciences
University of Birmingham
May 2011

# Abstract

The gas-phase reactions of ozone with alkenes can be significant sources of free radicals (OH, $HO_2$ and $RO_2$) in the Earth's atmosphere. Radical formation *via* ozonolysis is of interest as it may substantially influence the radical budget in urban and rural environments. While there are a number of quantitative indirect OH and $HO_2$ yield measurements from ozonolysis in the literature, obtained, for example, through the use of radical tracer / scavenger species, few direct observations have been reported. This thesis presents the first direct measurements of OH and $HO_2$ by Laser Induced Fluorescence (LIF) for a homologous series of alkenes.

The total radical production and degradation products from ethene, propene, 1-butene, 2-methylpropene, *cis*-2-butene, *trans*-2-butene and 2,3-dimethyl-2-butene ozonolysis have been observed, under conditions relevant to the troposphere. The experiments were carried out in the EUropean PHOtoREactor (EUPHORE) atmospheric simulation chamber (Valencia, Spain), utilising various instrumentation including Fourier Transform Infrared Spectroscopy (FTIR) measuring volatile organic compounds / oxygenated volatile organic compounds (VOCs / OVOCs), a Laser Induced Fluorescence (LIF) system for measuring OH and $HO_2$ radical products and a PEroxy Radical Chemical Amplification (PERCA) instrument measuring $HO_2 + \Sigma RO_2$. The alkene-ozone reaction systems were investigated with and without an OH radical scavenger, in order to suppress side reactions. Radical concentrations were measured under dry and humid conditions and interpreted through detailed chemical chamber box modelling, incorporating the Master Chemical Mechanism (MCMv3.1) degradation scheme for each specific alkene, which was updated to include a more explicit representation of the alkene-ozone reaction mechanism. The observed yields are interpreted in terms of branching ratios for each channel within the postulated alkene ozonolysis mechanism, and their implications for atmospheric radical production were considered under representative scenarios.

786/92/110

To Mum and Dad,

With love

# Acknowledgements

First and Foremost, I would like to thank my supervisor Dr Bill Bloss for giving me the opportunity to join such a stimulating research group. I thank him not only for putting up with me over the last few years but for his expert guidance, support and endless encouragement.

I would like to show my gratitude to NERC for a studentship that allowed me to take part in the TRAPOZ project, alongside a great team; whom it has been a privilege to meet and work beside. I would like to thank Dr Andrew Rickard for his expert guidance and making it an enjoyable experience in Port Saplaya – those locks on those doors were hard to open! I am also grateful for the assistance of Dr Marie Camredon, where I will always remember the car that she (impossibly) got stuck on top of a rock. Not to mention the legend Dr Kev Wyche – those open top bus tours and valor ice-creams were sublime.

To those others who have helped, discussed and made it an enjoyable experience, I owe many thanks; in particularly Jess and Kate and our magnificent periodic table. I would like to wish Paula all the best in catching her ghost and apologise for not being able to help, "I had a valid excuse!" Special thanks, love and respect also goes to Vivien, Shana, Juan and Adam.

Finally, I'd like to thank my *amazing* family, Shakil, Farhana, Aniqa, Moonisah, Ridwan and Tasnim, but *most importantly* Mum and Dad. Without *all* you guys, I would not have been able to get through life, let alone this PhD. I will be thankful and indebted to your endless love, support, prayers and encouragement forever! Thank you for your absolute patience and loyal support in all that I have done and will do. I would also like to thank my spiritual father Syed Mohamed Hashmi and family for their endless guidance and prayers.

# Table of Contents

# List of Figures

## *Chapter 1*



## *Chapter 2*

## *Chapter 3*

## *Chapter 4*

## *Chapter 5*

## *Chapter 6*

# List of Tables

## *Chapter 1*



## *Chapter 2*



## *Chapter 3*

## *Chapter 4*

## *Chapter 5*



## *Chapter 6*

# List of Abbreviations

| | |
|---|---|
| BVOC | Biogenic Volatile Organic Compound |
| CI | Criegee Intermediate |
| CIR-TOF-MS | Chemical Ionisation Reaction Time Of Flight Mass Spectrometry |
| CLD | Chemiluminescene Detector |
| EUPHORE | EUropean PHOtoREactor Facility |
| FTIR | Fourier Transform Infra Red spectroscopy |
| HPLC | High Performance Liquid Chromatography |
| IR | Infrared |
| LIF | Laser Induced Fluorescence |
| MCM | Master Chemical Mechanism |
| NMHC | Non Methane Hydrocarbon |
| PERCA | PEroxy Radical Chemical Amplifier |
| POZ | Primary Ozonide |
| ppmV | parts per trillion ($10^6$), by volume |
| ppbV | parts per trillion ($10^9$), by volume |
| pptV | parts per trillion ($10^{12}$), by volume |
| SCI | Stabilised Criegee Intermediate |
| SOA | Secondary Organic Aerosol |
| SVOC | Semi-Volatile Organic Compound |
| $Y_{HO_2}$ | Yield of $HO_2$ |
| $Y_{OH}$ | Yield of OH |
| $Y_{SCI}$ | Yield of Stabilised Criegee Intermediate |

# Chapter 1. Introduction

It is fundamental to study detailed chemistry of the atmosphere, in order to gain a fuller understanding of current global problems that exist and are continuing to form. Issues such as biomass burning, fossil fuel consumption and increasing transport emissions have led to a rapid rise in the concentration of atmospheric greenhouse gases and particulate matter over the last few decades. These emissions not only lead to the degradation of air quality, acidic precipitation and stratospheric ozone destruction, but can also have detrimental effects on human health and vegetation. A comprehensive understanding of atmospheric chemistry is therefore imperative for elucidation of local, regional and global scale alterations in the atmosphere.

This introductory chapter provides a basis for the primary focus of this thesis; the investigation of gas-phase alkene-ozone reactions and their importance in the troposphere.

## 1.1 Composition of the Atmosphere

The atmosphere is a thin layer of gas that surrounds the Earth, consisting of a mixture of different species. The bulk composition of dry atmospheric air principally consists of $N_2$ (78 %), $O_2$ (21 %), Ar (0.9 %) and $CO_2$ (0.04 %) with trace amounts of many other species. One of the most important trace atmospheric gases is water vapour, the composition of which is highly variable throughout the atmosphere, but generally

constitutes approximately 1 – 1.5 % in surface air over Europe (Ehhalt, 1999). Other trace constituents include $O_3$, NO, $NO_2$, OH and $HO_2$, all of which are present in low concentrations, and will be explored in subsequent sections of this chapter. The average abundances of selected atmospheric constituents are listed in Table 1.1.

**Table 1.1.** Mixing ratios of selected trace constituents. Adapted from Jacob (2000)

| **Atmospheric species** | **Mixing ratio (mol/mol)*** |
|---|---|
| Nitrogen ($N_2$) | 0.78 |
| Oxygen ($O_2$) | 0.21 |
| Argon (Ar) | $0.90 \times 10^{-2}$ |
| Carbon dioxide ($CO_2$) | $3.70 \times 10^{-4}$ |
| Methane ($CH_4$) | $0.17 \times 10^{-5}$ |
| Hydrogen ($H_2$) | $0.05 \times 10^{-5}$ |
| Nitrous oxide ($N_2O$) | $0.32 \times 10^{-5}$ |
| Ozone ($O_3$) [a] | $0.01 – 10 \times 10^{-8}$ |
| Carbon monoxide (CO) [b] | $0.04 – 0.20 \times 10^{-6}$ |

* mixing ratios of trace gases are commonly given in parts per million (or billion) volume.
1 ppmV = $1 \times 10^{-6}$ mol/mol; 1 ppbV = $1 \times 10^{-9}$ mol/mol
[a] Atmospheric levels of ozone differ with altitude (see Section 1.2)
[b] Data from Wayne (2000)

## 1.2 Structure of the Atmosphere

### 1.2.1 Pressure

The mixing ratios listed in Table 1.1 predominantly correspond to averages for the lower atmosphere, as approximately 99 % of the mass of the atmosphere lies below 30 km (Wayne, 2000). This is due to the exponential decrease in pressure, *P*, with increasing altitude, *z*, which is given by the hydrostatic equation (EQ1.1)

$$P = P_0 \exp\left( - z \Big/ \frac{RT}{Mg} \right) \qquad \text{(EQ1.1)}$$

where $P_0$ is the pressure at zero altitude, $M$ is the relative molar mass of air (28.8 g $mol^{-1}$), $g$ is the acceleration due to gravity (9.8 m $s^{-2}$), $R$ is the universal gas constant (8.314 J $K^{-1}$ $mol^{-1}$) and $T$ is the temperature (K). The quantity ($RT/Mg$) represents the distance over which the pressure drops by a factor of $1/e$ and is often referred to as the scale height ($H$), which is approximately 7 km. The decrease in pressure with increasing altitude is illustrated in Figure 1.1.

### 1.2.2 Temperature

The atmosphere can be divided into various regions on the basis of the vertical temperature profile, each with different physical and chemical characteristics, as illustrated in Figure 1.1. The lowest altitude region, the troposphere, contains the majority of the total atmospheric mass, and has a depth of between 10 and 17 km (Wayne, 2000), depending upon season and latitude. The troposphere is thickest in the tropics during the summer, owing to high temperatures causing rapid vertical expansion. For example, incoming solar radiation and infrared emission from the Earth's surface heats the air above it, causing it to rise. The rising air will then expand, as it does work against the surrounding atmosphere, and cool. This decrease in temperature with increasing altitude is known as the dry adiabatic lapse rate, which is approximately -9.8 K $km^{-1}$. However, the actual temperature gradient observed at the Earth's surface is -6.5 K $km^{-1}$, which is due to the condensation of water vapour,

releasing latent heat. This negative temperature gradient leads to strong vertical mixing, allowing fast transport of chemicals within the troposphere. The lowest region of the troposphere, the boundary layer, is where the greatest mixing takes place due to mechanical turbulence. It is the boundary layer where many of the chemical transformations that occur in the troposphere take place or are initiated.

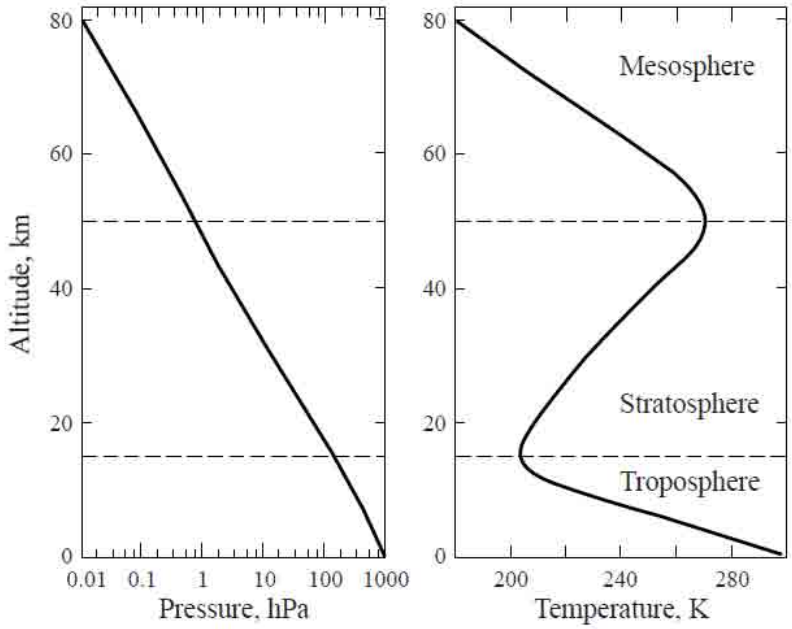


**Figure 1.1.** Pressure (left) and Temperature (right) profiles of the atmosphere. Data from Jacob (1999)

The tropopause is the boundary at which a temperature inversion prevents rapid mixing between the troposphere and the region above, the stratosphere (Figure 1.1). In order to explain this temperature inversion, the vertical distribution of ozone within the stratosphere must be considered; first explained by the chemical scheme suggested by Chapman in the 1930s (R1.1 – R1.4).

$$O_2 + h\nu\ (\lambda<242\ nm) \rightarrow 2O \quad \text{(R1.1)}$$

$$O + O_2 + M \rightarrow O_3 + M \quad \text{(R1.2)}$$

$$O_3 + h\nu\ (\lambda < 1180\ nm) \rightarrow O + O_2 \quad \text{(R1.3)}$$

$$O + O_3 \rightarrow 2O_2 \quad \text{(R1.4)}$$

Where, M is the reaction third body. A maximum mixing ratio of ozone exists in the altitude region of 20 – 40 km. This is because the optimum altitude for the production of ozone is determined by: (*i*) the concentration of $O_2$ available to undergo photodissociation; this increases with decreasing altitude; and (*ii*) the intensity of solar radiation at $\lambda < 242$ nm, which decreases with decreasing altitude. The Chapman cycle (R1.1 – R1.4) in isolation cannot, however, account for the observed mixing ratios of ozone in the stratosphere, as additional loss processes are required. The general catalytic cycle (R1.5 – R1.6) provides this additional ozone loss through the action of other trace constituent reactions in the stratosphere.

$$X + O_3 \rightarrow XO + O_2 \quad \text{(R1.5)}$$

$$XO + O \rightarrow X + O_2 \quad \text{(R1.6)}$$

net: $O + O_3 \rightarrow 2O_2$

Where, X can be H, OH, NO, Cl, Br, *etc*. The temperature inversion in the stratosphere arises due to the absorption of shortwave UV radiation by ozone. The O atom also reacts exothermically with $O_2$ to reform $O_3$ (R1.2), thus giving rise to the warm stratosphere. The positive temperature gradient of the stratosphere results in very little vertical mixing.

The stratosphere extends from the tropopause to an altitude of approximately 50 km, where the mesosphere begins. The mesosphere is characterised by a negative temperature gradient (Figure 1.1), as the concentration of ozone is too low to affect this region. The next region of the atmosphere, the thermosphere, begins at approximately 90 km, where a further temperature inversion is observed, owing to the absorption of highly energetic solar radiation, photodissociation and photoionisation processes.

The primary focus of this thesis will be on the chemical reactions that occur within the lowest layer of the atmosphere; the troposphere.

## 1.3 Tropospheric Chemistry

As described in Section 1.1, the bulk composition of the atmosphere principally consists of $N_2$, $O_2$, Ar and $H_2O$ (Table 1.1). However, although they are present in limited abundance, it is the trace constituents that dominate the chemistry of the troposphere.

A large number of species are emitted to the troposphere from both anthropogenic and natural sources, including $NO_x$ ($NO + NO_2$), $O_3$, CO, $SO_2$ and particulate matter (PM); all of which have human health and environmental impacts. Approximately 10 % of atmospheric $O_3$ exists in the troposphere, which is of fundamental importance for a number of reasons, other than being an atmospheric oxidant. For example, global levels of $O_3$ are of particular concern, owing to its impact on human health,

phytotoxic (*i.e.* detrimental to plant cells, inhibiting photosynthesis) behaviour and its ability to act as a greenhouse gas.

The atmospheric oxidation processes that occur within the troposphere do so by the action of sunlight, by reactions with free radicals (OH and $NO_3$) and by reaction with $O_3$. In this section, each initialisation process (*i.e.* atmospheric oxidation by OH, $NO_3$ and $O_3$) will be considered in turn.

### 1.3.1 OH Chemistry

The hydroxyl radical (OH) initiates the degradation of most hydrocarbon based species emitted into the troposphere. It is therefore imperative to understand the sources and concentration of OH in the atmosphere, as its high reactivity means that it determines the fate of many trace constituents. OH radicals are formed primarily from the photolysis of ozone to produce excited $O(^1D)$ atoms (R1.7), which can then go on to react with water vapour and form OH (R1.9). The wavelength threshold for significant formation of excited $O(^1D)$ is approximately 310 nm, however, production (albeit small) has also been reported through spin-forbidden processes and up to at least 330 nm (Ravishankara et al., 1998).

$$O_3 + h\nu\ (\lambda \leq 310\ nm) \rightarrow O(^1D) + O_2 \quad (R1.7)$$

$$O_3 + h\nu\ (\lambda < 1180\ nm) \rightarrow O(^3P) + O_2 \quad (R1.8)$$

$$O(^1D) + H_2O \rightarrow 2OH \quad (R1.9)$$

$O(^1D)$ can also be collisionally quenched, by collision with molecular oxygen or nitrogen (R1.10), to form ground state $O(^3P)$ which will proceed to regenerate $O_3$ (R1.2).

$$O(^1D) + M \rightarrow O(^3P) + M \quad \text{(R1.10)}$$

$$O(^3P) + O_2 + M \rightarrow O_3 + M \quad \text{(R1.2)}$$

Under typical European conditions, an estimated 10 % of excited $O(^1D)$ formed from R1.7, will generate OH radicals *via* R1.9 (Ehhalt, 1999). Other primary sources of OH radicals include the photolysis of nitrous acid (HONO, (R1.11)) and the reactions of ozone with alkenes; which is discussed in greater detail in subsequent sections.

$$HONO + h\nu\ (\lambda < 400\ nm) \rightarrow OH + NO \quad \text{(R1.11)}$$

In an unpolluted environment (low $NO_x$ levels), OH reacts primarily with CO (and $CH_4$) leading to the cycle described by reaction R1.12 – R1.14. Radical terminating steps involve the formation of soluble species (*e.g.* $H_2O_2$) which are removed from the troposphere by washout or surface deposition.

$$OH + CO \rightarrow H + CO_2 \quad \text{(R1.12)}$$

$$H + O_2 + M \rightarrow HO_2 + M \quad \text{(R1.13)}$$

$$HO_2 + O_3 \rightarrow OH + 2O_2 \quad \text{(R1.14)}$$

The oxidation of CO shown above leads to a net loss of $O_3$: $CO + O_3 \rightarrow CO_2 + O_2$. However, in an environment where anthropogenic emissions of $NO_x$ are high NO can

compete with $O_3$ for reaction with $HO_2$. OH termination under high $NO_x$ conditions can involve the formation of nitric acid ($HNO_3$).

$$HO_2 + NO \rightarrow OH + NO_2 \quad \text{(R1.15)}$$

$$NO_2 + h\nu\ (\lambda < 400\ \text{nm}) \rightarrow NO + O(^3P) \quad \text{(R1.16)}$$

$$O + O_2 + M \rightarrow O_3 + M \quad \text{(R1.2)}$$

The oxidation of CO in the presence of $NO_x$ therefore leads to the net production of $O_3$: $CO + 2O_2 \rightarrow CO_2 + O_3$. The balance between ozone production and destruction therefore, depends on the relative rates of reactions R1.14 and R1.15; where net ozone production exceeds destruction at NO levels of approximately 14 – 55 pptV (Carpenter et al., 1997, Salisbury et al., 2002).

A similar effect with more complex reaction cycles is observed when considering the OH initiated oxidation of other volatile organic compounds (VOCs). Figure 1.2 illustrates the importance of $NO_x$ in the OH initiated oxidation of $CH_4$ (the simplest hydrocarbon). In the presence of $NO_x$, the net reaction is that one molecule of $CH_4$ gives rise to two conversions of NO to $NO_2$ through the reactions of the peroxy radicals: $CH_3O_2$ and $HO_2$, which in turn leads to the production of $O_3$ *via* R1.16 and R1.2. Further $O_3$ production will also result from the subsequent oxidation of HCHO. The oxidation of VOCs in the presence of high $NO_x$ generating $O_3$ may lead to the formation of photochemical smog in urban environments.

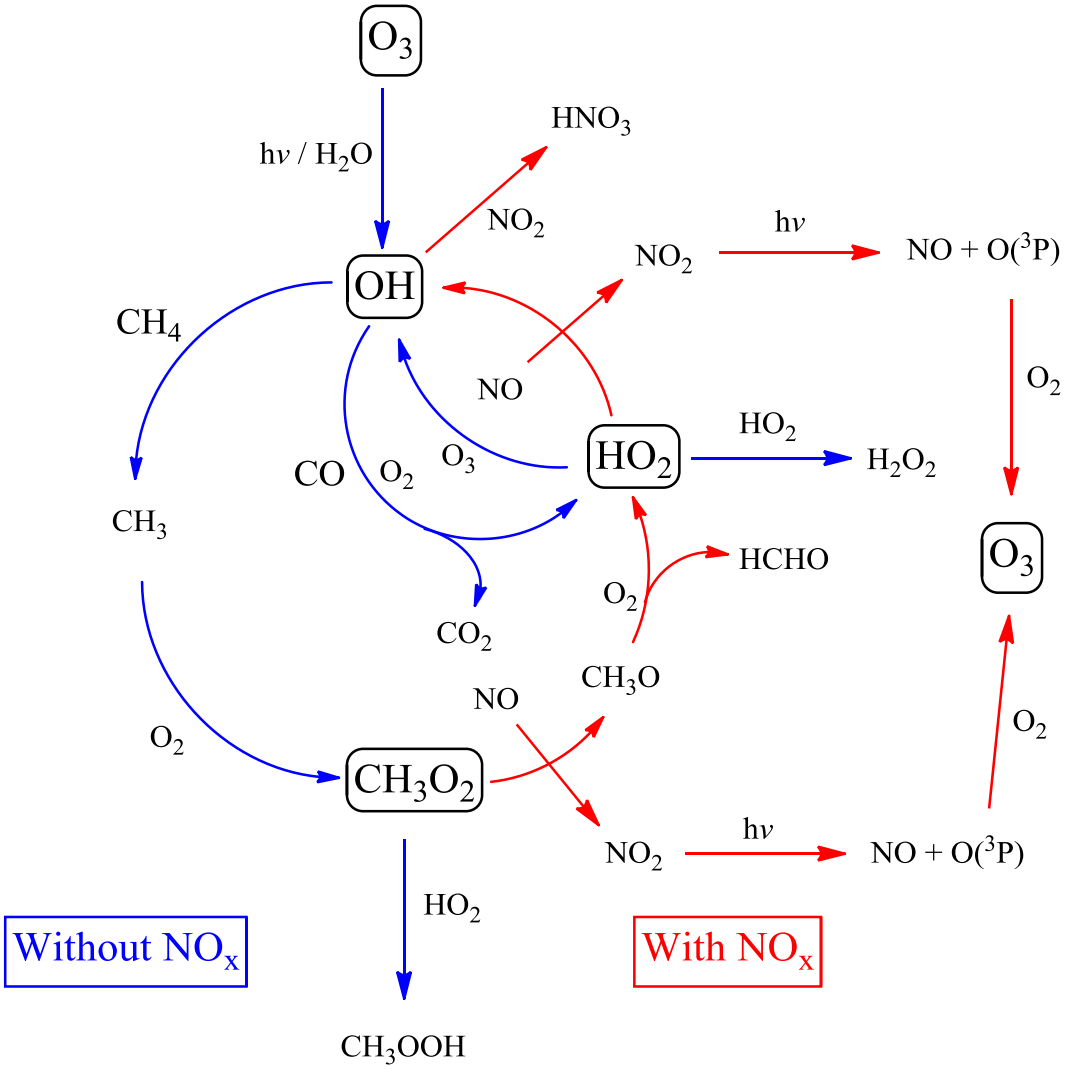


**Figure 1.2.** Tropospheric OH-initiated oxidation of methane and CO. Adapted from Wayne (2000).

The OH radical in the $HO_x$ cycle described above can oxidise CO, $CH_4$ and other VOCs. The OH initiated oxidation of VOCs involves a series of reaction pathways that can eventually lead to the formation of $CO_2$ and $H_2O$. A generic reaction scheme for the degradation of a VOC is given in Figure 1.3, and the detailed OH-initiated oxidation of cyclohexane is discussed in Chapter 3. In the case of saturated hydrocarbons, the oxidation mechanism involves an initial hydrogen atom abstraction by OH to form an alkyl radical (R•). For unsaturated VOCs, the preferred route is the

addition of OH to the C=C double bond. The unstable alkyl radical formed from the initial oxidation step reacts near-instantaneously with $O_2$ to form a peroxy radical, $RO_2$, (Atkinson and Arey, 2003). These peroxy radicals are then converted to alkoxy radicals (RO), *via* reaction with NO or self and cross reactions. In the atmosphere $RO_2$ + $RO_2$ interactions generally involve reaction with $CH_3O_2$, as the methylperoxy radical is the most abundant $RO_2$ species in the atmosphere (Orlando et al., 2003). Alkoxy radicals (RO) can potentially follow a number of competing reaction pathways, including isomerisation, decomposition or reaction with $O_2$ (Atkinson, 1997a, Orlando et al., 2003) to form oxygenated VOCs (OVOCs) such as aldehydes and ketones. However, the rate constants and the competition between reaction pathways determining the fate of many alkoxy radicals are not well understood. Figure 1.4 illustrates the potential reaction pathways available for a typical alkoxy radical; chemistry of the 2-pentoxy radical, formed from the OH-initiated oxidation of pentane.

It is the competition between the potential RO reaction pathways that determines a hydrocarbon's impact on the atmosphere. For example, the RO decomposition channel leads to the formation of more reactive short chain carbonyl species, which ultimately results in a larger potential for photochemical ozone production (*i.e.* alkyl fragment + $O_2 \rightarrow RO_2$, followed by $RO_2 + NO \rightarrow RO + NO_2$, where the $NO_2$ can form $O_3$ *via* R1.14 and R1.2). In contrast reaction with $O_2$ or the isomerisation channel produce less reactive and more highly substituted oxygenated species, ultimately reducing the potential for photochemical ozone production.

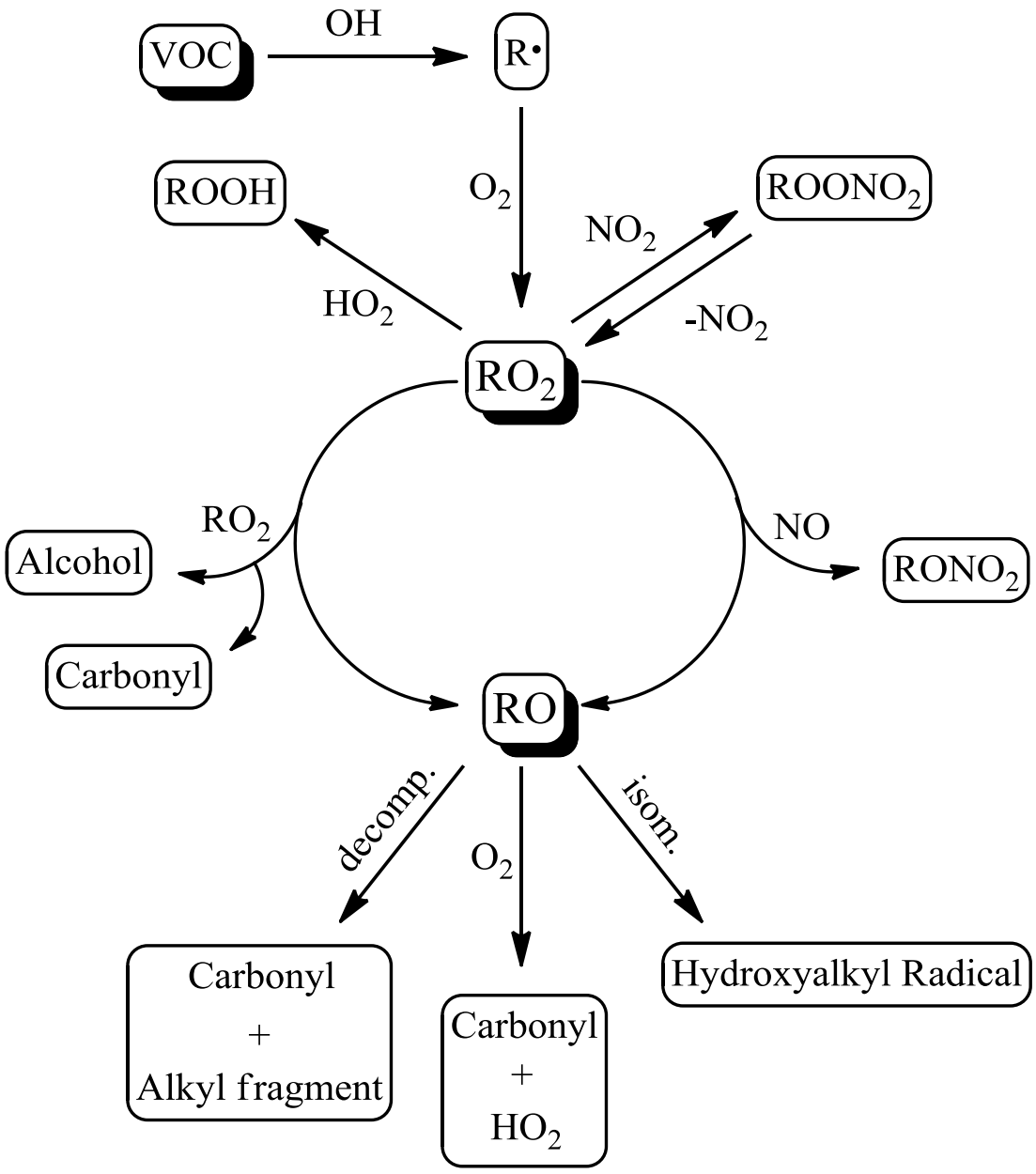


**Figure 1.3.** General chemical scheme for the oxidation of VOCs, producing alkyl or substituted alkyl radical products. Adapted from Atkinson and Arey (2003) and Orlando et al. (2003)

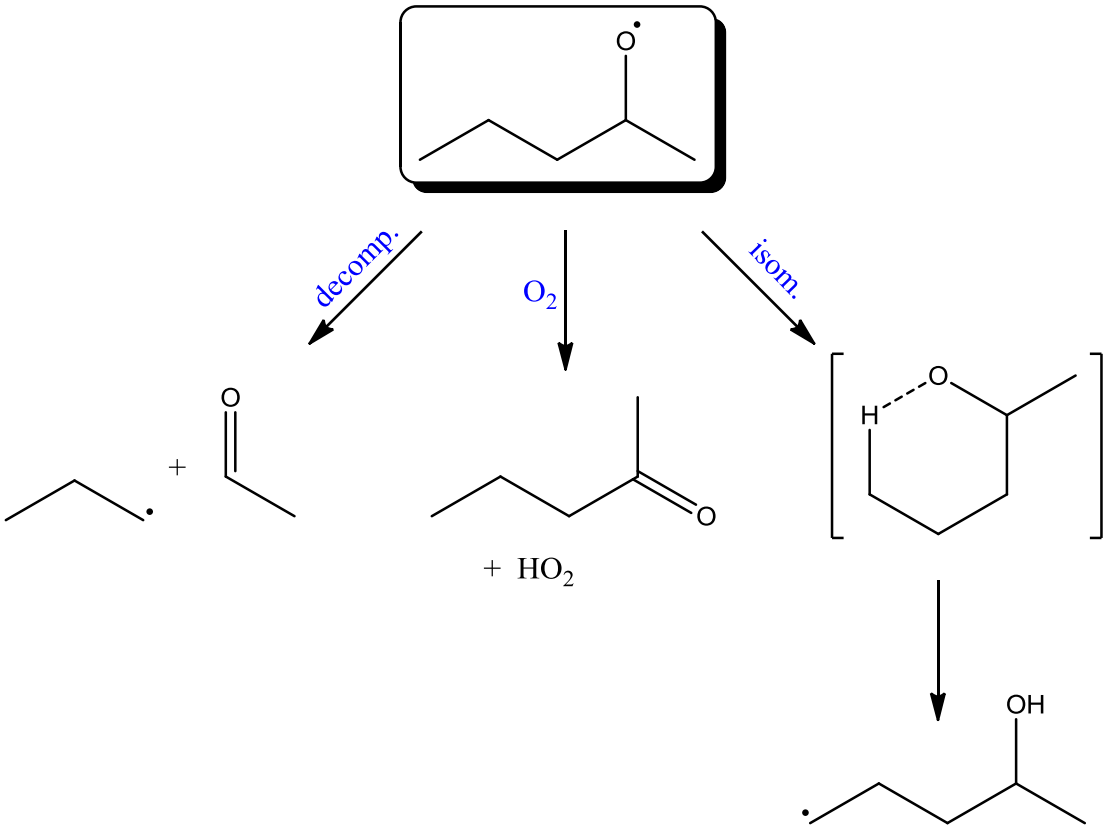


**Figure 1.4.** Competing reaction pathways of the 2-pentoxy radical formed from the OH-initiated oxidation of pentane.

The measure of an emitted species' reactivity towards OH provides useful information in regards to its impact upon the atmosphere. However, it does not take into account reactivity with other oxidants (*e.g.* $O_3$, $NO_3$) or the reactivity of subsequent degradation products. The differences in structure and reactivity towards OH for VOCs emitted to the troposphere, results in each VOC having a different ability to produce $O_3$, as described above. Derwent at al. (1996) developed a method for measuring a VOCs potential to form photochemical ozone. This measure, known as the Photochemical Ozone Creation Potential (POCP) was calculated for each VOC by using model simulations to incrementally increase the concentrations of each VOC independently, followed by an assessment of the change in $O_3$ concentration relative

to the change produced by ethene; the reference VOC (Derwent et al., 1996, Derwent et al., 1998). POCPs therefore, provide useful information for a particular VOCs potential to form $O_3$, which can be used to design control strategies of VOCs in the environment.

### 1.3.2 $NO_3$ Chemistry

In the absence of sunlight, it is the nitrate radical ($NO_3$) that is the dominant oxidising agent of the troposphere, initiating the degradation of many emitted VOCs. The role of $NO_3$ during the night is therefore similar to that of OH during the day. $NO_3$ is formed by the oxidation of $NO_2$ by $O_3$ (R1.17), and is rapidly photolysed during the day (R1.18, R1.19).

$$NO_2 + O_3 \rightarrow NO_3 + O_2 \quad \text{(R1.17)}$$

$$NO_3 + h\nu\ (585 < \lambda < 640\ \text{nm}) \rightarrow NO + O_2 \quad \text{(R1.18)}$$

$$NO_3 + h\nu\ (\lambda < 640\ \text{nm}) \rightarrow NO_2 + O \quad \text{(R1.19)}$$

Although $NO_3$ is generally not as reactive as OH, its reaction with unsaturated hydrocarbons can be comparable to that of the analogous reactions with OH, in terms of VOC removal. This is because of the higher night-time [$NO_3$] of approximately $10^9$ molecule $cm^{-3}$ in comparison to the lower daytime [OH] of approximately $10^6$ molecule $cm^{-3}$. The reaction of the nitrate radical with unsaturated hydrocarbons are thought to proceed *via* the addition of $NO_3$ to the C=C bond (R1.20), followed by addition of $O_2$ to form a peroxy radical (R1.21). The peroxy

nitrate radical can then participate in $NO_x$ cycling analogous to non-nitrogen containing $RO_2$ species (as discussed in Section 1.3.1, see Figure 1.3), forming OVOCs and $HO_2$.

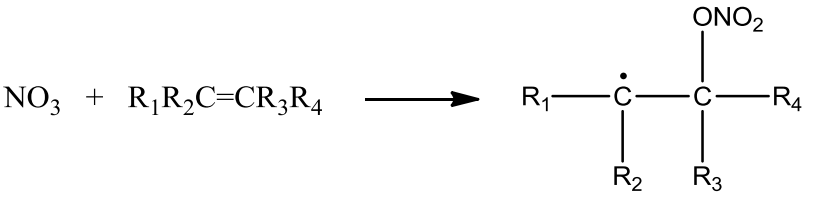


(R1.20)

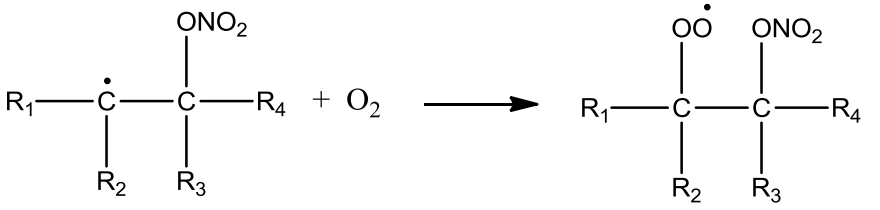


(R1.21)

The reactions of $NO_3$ with alkanes (R1.22) and aldehydes (R1.23) proceed *via* hydrogen abstraction, the latter being faster.

$$NO_3 + RH \rightarrow HNO_3 + R\bullet \quad \text{(R1.22)}$$

$$NO_3 + RCHO \rightarrow RCO + HNO_3 \quad \text{(R1.23)}$$

The alkyl and acyl radicals formed in R1.22 and R1.23 respectively, will react near-instantaneously with $O_2$ to form $RO_2$ and $RC(O)O_2$ which can go on to react with $NO_2$ to form peroxy nitrates, see Figure 1.3.

### 1.3.3 Ozone Chemistry

The main impact of $O_3$ upon the oxidative capacity of the atmosphere is its ability to create OH radicals (*via* R1.7 – R1.9) during the day and $NO_3$ radicals (*via* R1.15) during the night, that initiate primary chain oxidation reactions, as discussed previously.

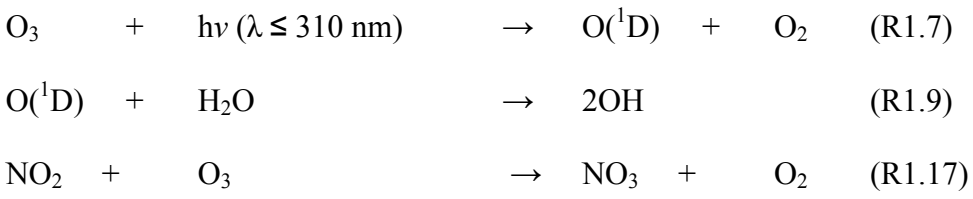

$$O_3 + h\nu\ (\lambda \leq 310\ nm) \rightarrow O(^1D) + O_2 \quad (R1.7)$$



$$O(^1D) + H_2O \rightarrow 2OH \quad (R1.9)$$



$$NO_2 + O_3 \rightarrow NO_3 + O_2 \quad (R1.17)$$

Ozone itself, can also act as an atmospheric oxidant *via* reaction with unsaturated hydrocarbons (alkenes). Table 1.2 gives the respective lifetimes of selected alkenes with respect to their oxidising species. The shorter lifetime of many alkenes with respect to $O_3$ means that the dominant loss pathway of alkenes can be *via* reaction with $O_3$. Alkene ozonolysis reactions can therefore act as a sink for ozone, particularly in areas where biogenic VOC (BVOC) emissions are high (Goldstein et al., 2004). Furthermore, alkene-ozone reactions are widely recognised as a non-photolytic source of OH, $HO_2$ and $RO_2$ radical products (Calvert et al., 2000, Johnson and Marston, 2008, Paulson et al., 1999a, Paulson and Orlando, 1996), which will be discussed in detail in the next section.

**Table 1.2.** Atmospheric lifetimes of selected alkene species with respect to OH, $NO_3$ and $O_3$ attack.

| | OH | | $NO_3$ | | $O_3$ | |
|---|---|---|---|---|---|---|
| Alkene | $10^{-12} \times k_{OH}$ (298 K) ($cm^3$ $molecule^{-1}$ $s^{-1}$) | Lifetime (hours) | $10^{-16} \times k_{NO_3}$ (298 K) ($cm^3$ $molecule^{-1}$ $s^{-1}$) | Lifetime (hours) | $10^{-18} \times k_{O_3}$ (298 K) ($cm^3$ $molecule^{-1}$ $s^{-1}$) | Lifetime (hours) |
| Ethene | 8.5 | 20.4 | 2.1 | 3780 | 1.6 | 231.5 |
| Propene | 26 | 6.7 | 95 | 83.5 | 10 | 37.0 |
| 1-Butene | 31 | 5.6 | 135 | 58.8 | 9.6 | 38.6 |
| 2-Methylpropene | 51 | 3.4 | 3400 | 2.3 | 11 | 33.7 |
| *cis*-2-Butene | 56 | 3.1 | 3500 | 2.3 | 125 | 3.0 |
| *trans*-2-Butene | 64 | 2.7 | 3900 | 2.0 | 190 | 2.0 |
| 2,3-Dimethyl-2-butene | 110 | 1.6 | 570,000 | 0.01 | 1100 | 0.3 |
| Isoprene | 101 | 1.7 | 6800 | 1.2 | 13 | 28.5 |

Rate constant data are from Calvert et al. (2000). Assumed [OH], [$NO_3$] and [$O_3$] are $1.6 \times 10^6$, $3.5 \times 10^8$, $7.5 \times 10^{11}$ molecule $cm^{-3}$, respectively.

## 1.4 Alkene Ozonolysis

Unsaturated hydrocarbons, alkenes, are emitted to the troposphere from a wide range of sources, which include combustion processes, vehicle and biogenic emissions. They are significant primary pollutants in the boundary layer, accounting for up to 30 % of the total OH sink (Calvert et al., 2000) and can contribute appreciably to ozone formation in urban environments in the presence of $NO_x$ (Ryerson et al., 2003). Although alkenes can react with OH and $NO_3$, their reaction with ozone may form the dominant loss pathway, depending on local conditions and the time of day (see Table 1.2) (Paulson and Orlando, 1996).

The gas phase reaction of alkenes with ozone has been subject to considerable interest since the reaction mechanism was first proposed by Criegee in the late 1940s. In recent years, however, research in this area has gained major importance owing to the reactions key role in the Earth's tropospheric chemistry (Johnson and Marston, 2008). The gas phase ozonolysis of alkenes is an important sink for both alkenes and ozone, and leads to the formation of a wide range of functionalised oxygenated products, including carbonyls (Tuazon et al., 1997), organic acids (Ma and Marston, 2009) and hydroperoxides (Hasson et al., 2001a, Hasson et al., 2001b). Larger biogenic alkenes, notably terpenes ($C_{10}$) and sesquiterpenes ($C_{15}$), are known to lead to the production of semi-volatile oxygenated compounds (SVOCs) that have been detected in secondary organic aerosol (SOA) (Camredon et al., 2010, Kroll and Seinfeld, 2008).
Alkene-ozone reactions are widely recognised as a non-photolytic source of OH, $HO_2$ and $RO_2$ radical products (Calvert et al., 2000, Johnson and Marston, 2008, Paulson et

al., 1999a, Paulson and Orlando, 1996), where their contribution to the overall $HO_x$ budget has been recognised in a number of studies. For example, Paulson and Orlando (1996) outlined that alkene ozonolysis can be the dominant $HO_x$ source during both urban and rural case studies in Los Angeles and in a forested site in Alabama, respectively. Heard et al. (2004) reported that under polluted urban conditions, at a site in Birmingham, UK, alkene ozonolysis accounted for 46 % of the daytime radical production in the summer and 62 % during winter. More recently, it was reported that the reaction of alkenes with ozone was responsible for 33 % of the peak radical production observed during the day in Mexico City (Volkamer et al., 2010). In summertime conditions in Santiago de Chile, alkene ozonolysis comprised ~ 24 % of the total daytime primary OH radical source (Elshorbany et al., 2009). The radical formation potential from the ozonolysis of unsaturated hydrocarbons is therefore of significant interest, as it has a substantial influence on the $HO_x$ budget in both urban and rural environments. The impacts of alkene-ozone reactions on $HO_x$ production in the light of experiments reported here will be discussed in detail in Chapter 5.

The reaction mechanism for alkene ozonolysis is discussed in detail in Chapters 3 and 4, and thus will only be introduced briefly in this section. Gas-phase alkene ozonolysis is believed to proceed *via* the Criegee mechanism (Criegee, 1975), illustrated in Figure 1.5. Ozonolysis is initiated by the electrophilic cycloaddition of ozone across the C=C double bond to form an unstable 1,2,3-trioxolane, also called a primary ozonide (POZ) (R1.24). This intermediate is high in energy and rapidly decomposes at the central C-C bond and one of the O-O bonds. Given that the O-O bond can break at two different sites, a pair of carbonyl oxides (hereafter referred to

as Criegee Intermediate) and stable carbonyl molecules can be formed (R1.25a and R1.25b). The fate of the vibrationally excited Criegee intermediate (CI) is somewhat complex, as different CIs (formed from different alkenes) behave as different chemical entities (see Chapter 4, Section 4.3).

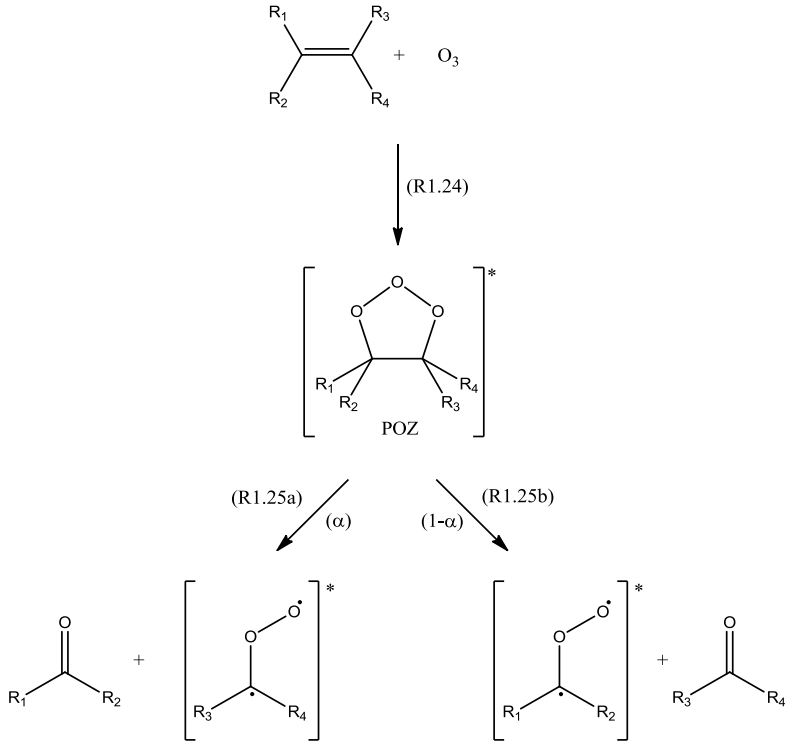


**Figure 1.5.** Cycloaddition of ozone across the alkene double bond and subsequent decomposition of the POZ.

In general, at low pressures, energy rich CIs can undergo prompt decomposition to yield OH and a vinoxy radical (See Figure 1.6, R1.26a) (the vinoxy radical subsequently reacts near-instantaneously with $O_2$ to form a peroxy radical, which then reacts according to the mechanism illustrated in Figure 1.3) (Donahue et al., 2011). At higher pressures (*e.g.* 760 Torr) the CI is collisionally stabilised (R1.27) and can thermally decompose to generate OH and a vinoxy radical (R1.26b) or undergo

rearrangement through a dioxirane structure. The dioxirane structure can decompose to various products including $HO_2$ (R1.28), *via* a 'hot' acid intermediate.

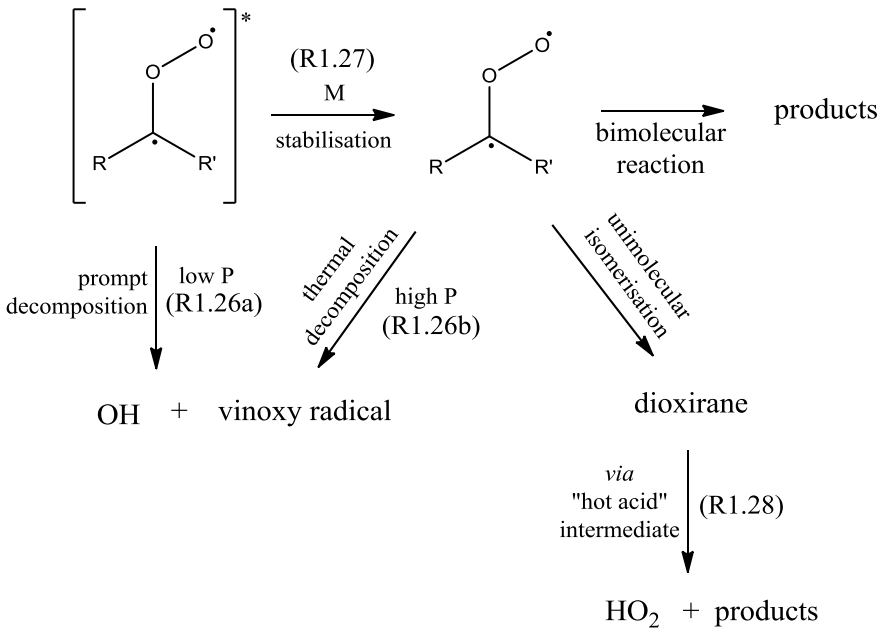


**Figure 1.6.** Fate of the Criegee intermediate

The stabilised Criegee intermediate (SCI) formed in R1.27 can undergo bimolecular reactions with a number of atmospheric abundant species, including $H_2O$, CO and $SO_2$. The reaction with $H_2O$ can produce organic acids, carbonyls and hydroperoxides including the phytotoxic hydroxymethyl hydroperoxide ($HOCH_2OOH$, HMHP) *via* R1.29.

$$CH_2OO + H_2O \rightarrow HOCH_2OOH \qquad \text{(R1.29)}$$

For small chain alkenes, α-hydroxy-hydroperoxides, such as $HOCH_2OOH$ formed from R1.29, are expected to decompose by loss of $H_2O_2$ (Hasson et al., 2001b).

α-Hydroxy-hydroperoxides from the SCI + $H_2O$ reaction from the ozonolysis of terpenes, however, have been identified in the aerosol phase (Kroll and Seinfeld, 2008).

The SCI reaction with $SO_2$ can produce $SO_3$ (R1.30) which in turn can react heterogeneously with $H_2O$ to form $H_2SO_4$ (R1.31) contributing to acid deposition in the troposphere.

$$R_1R_2COO + SO_2 \rightarrow R_1R_2CO + SO_3 \quad \text{(R1.30)}$$

$$SO_3 + H_2O \rightarrow H_2SO_4 \quad \text{(R1.31)}$$

As mentioned previously, alkene ozonolysis is widely recognised as a non-photolytic source of OH (R1.27), $HO_2$ (R1.28) and $RO_2$ (Calvert et al., 2000, Johnson and Marston, 2008, Paulson et al., 1999a). This is of major importance in the troposphere, as the ozonolysis of alkenes may contribute to the $HO_x$ (OH + $HO_2$) source during both day and night. For a complete understanding of alkene-ozone chemistry in the troposphere, it is essential to understand the mechanism of formation of these products. Despite advances made in recent years, however, a complete understanding of the gas-phase reactions of alkene with ozone remains elusive. In this study, a detailed investigation has been performed to aid to the evaluation of alkene ozonolysis mechanisms for a range of small chain alkenes ($C_2$ – $C_6$).

## 1.5 Models of Atmospheric Chemistry

The interpretation of atmospheric processes can be assessed by comparing calculations from numerical simulations with observations of the atmosphere. In general, such numerical models may consist of two components, dynamical and chemical, operating over a range of temporal and spatial conditions. The transport of a chemical species is incorporated in the dynamical component, whereas the chemical component concerns the rate of change of concentration of a species.

Zero-dimensional box models enable the evaluation of detailed chemical reactions performed in laboratories. These models simulate very few physical processes and primarily consist of the chemical component, where the production and loss rates for atmospheric constituents are calculated iteratively from specified initial concentrations at each time step. The chemical mechanism within these numerical models is an integral part of how the chemistry is simulated, as the mechanism predicts the evolution of an emitted species into its oxidation products. In this thesis, zero-dimensional box modelling has been utilised to improve the representation of chemical mechanisms of alkene ozonolysis reactions.

## 1.6 The Master Chemical Mechanism

The Master Chemical Mechanism (MCM) is a near explicit chemical mechanism, describing the detailed gas-phase chemical processes involved in the atmospheric degradation of important primary emitted VOCs (Jenkin et al., 1997). The current

version, MCMv3.1, contains approximately 13,500 elementary reactions and 5,900 primary, secondary and radical species to describe the degradation of 135 VOCs (Bloss et al., 2005, Jenkin et al., 1997, Saunders et al., 1997). The selected VOCs in the MCM are major emitted anthropogenic species listed in the National Atmospheric Emissions Inventory (NAEI), UK; and cover approximately 90 % of the total mass of identified emitted VOCs in the boundary layer (Derwent et al., 2007).

The protocol on which the MCM is based is divided into several parts, including initiation reactions, reactions with radical intermediates, and degradation of first and subsequent generation products. Initiation reactions of a given VOC can occur through reaction with OH, $NO_3$ and $O_3$ or by photolysis, generating RO / $RO_2$ radicals or Criegee intermediates. These generated products can undergo further reactions forming of a wide range of functionalised oxygenated products, including alcohols, carboxylic acids, hydroperoxides, nitrates *etc.* This process is continued until each degradation pathway is broken down to CO, $CO_2$ or an organic product (or radical), for which the subsequent chemistry is represented elsewhere in the mechanism.

The MCM utilises published laboratory, atmospheric simulation chamber and theoretical data to describe the kinetics and mechanisms of reactions of VOCs and their degradation products. For unstudied reactions where kinetic and mechanistic data are not available, the MCM utilises the results of studied reactions of a smaller subset or similar chemical species, by analogy and with the use of structure activity relationships (SARs). The difficulty in including *explicit* mechanisms for each VOC is that the numerical model would run at a tremendous cost. Thus, important simplifications have been made to the MCM to limit its size, for example: (*i*) low probability pathways resulting from oxidation of VOCs have been neglected (*ii*)

degradation chemistry of minor reaction products have been simplified and (*iii*) parameterisation of the reactions of peroxy radicals ($RO_2$) with each other.

In this study, the results of alkene-ozone atmospheric simulation chamber experiments have been interpreted through chemical box modelling, drawing upon the MCMv3.1 (see Chapter 2). The alkene photo-oxidation mechanisms were updated to include a more explicit representation of the ozonolysis reaction mechanisms (see Chapter 4, Section 4.3).

## 1.7 Thesis Motivation

As mentioned previously, a complete understanding of the gas phase reactions of alkenes with ozone remains elusive and therefore the aims of this study are:

- Determination of the radical yields (OH and $HO_2$) from the ozonolysis of a range of alkenes of biogenic and anthropogenic origin.

- Measurement and identification of the gas-phase degradation products from the ozonolysis of a range of alkenes.

- Improvement of the representation of radical production from alkene ozonolysis and degradation pathways for volatile organic compounds in a detailed atmospheric model (the Master Chemical Mechanism, MCMv3.1)

These objectives have been achieved through a series of experiments using the EUropean PHOtoREactor (EUPHORE) atmospheric simulation chamber, in Valencia, Spain. A combination of OH, $HO_2$ (and $RO_2$) instrumentation was used to perform

comprehensive measurements of radical production from the studied alkene-ozone reactions. Degradation products were constrained using a suite of instrumentation described in Chapter 2.

During the course of alkene-ozone experiments performed at EUPHORE, an increase in the apparent NO signal was observed (by chemiluminescence $NO_x$ analyser) on addition of alkene to the chamber. Reasons for this potential interference are also investigated.

## 1.8 Thesis Overview

This thesis is subdivided into 6 subsequent chapters:

Chapter 2 describes the EUPHORE facility and instrumentation utilised to study the alkene-ozone reactions. This is followed by a description of the experimental approach and a detailed description of the zero-dimensional box modelling approach employed to optimise reaction rate coefficients and product yields.

In Chapter 3, the importance of understanding the fate and kinetics of the gas-phase ozonolysis reaction of the simplest unsaturated hydrocarbon, ethene, is outlined. The decomposition of the ethene Criegee intermediate is evaluated, focusing on OH and $HO_2$ radical yields. The results underpin interpretation of experimental measurements of radical production from the ozonolysis of larger alkenes. This chapter has been published following peer review (Alam et al. 2011).

Chapter 4 includes a detailed description of the gas-phase ozonolysis mechanism, focusing on the decomposition of each Criegee intermediate studied. Optimised reaction rate coefficients and derived stable and radical product yields are presented. The results are compared with literature and discussed in terms of branching ratios for various channels within their corresponding postulated reaction mechanisms.

The radical formation potential from the ozonolysis of various alkenes and their influence on the $HO_x$ budget of an urban environment is discussed in Chapter 5. This includes the use of the derived product and radical (OH and $HO_2$) yields determined in Chapters 3 and 4, in a zero-dimensional photochemical box model to evaluate the contribution of alkene-ozone reactions to the primary initiation to OH and $HO_2$.

Chapter 6 discusses the importance of accurately measuring ambient concentrations of the oxides of nitrogen ($NO_x$), with particular emphasis on the use of chemiluminescence in NO / $NO_2$ detection monitors. Potential interferences of a range of alkenes studies in chemiluminescence $NO_x$ monitors are described.

Finally, Chapter 7 summarises the findings of this study, with a discussion of possible future work that could be carried out.

# Chapter 2. Experimental & Methodology

This chapter describes the experimental facility in which the alkene-ozone experiments were conducted, together with a description of the range of instrumentation used. This is followed by comprehensive details of the experimental and modelling approach utilised to determine the radical and stable products from alkene ozonolysis. The chapter is subdivided into the following two sections: Section (*A*) - describes the EUropean PHOtoREactor (EUPHORE) facility and instrumentation utilised for observations of stable and radical products from gas-phase alkene ozonolysis reactions. Section (*B*) - describes the approach used for the alkene-ozone chamber experiments and the detailed modelling performed to interpret the observations of radical and carbonyl products.

## *Section A*

## 2.1 European Photoreactor (EUPHORE) Facility

The alkene ozonolysis experiments were carried out in the EUropean PHOtoREactor Facility (EUPHORE) in Valencia, Spain, over two 4 week campaigns. EUPHORE is a large scale atmospheric simulation chamber (see Figure 2.1), used for studying the mechanisms of atmospheric processes. More in depth details of the chamber and its instrumentation are given elsewhere (Becker, 1996, Becker, 1999). Briefly, it consists of two identical 197 $m^3$ simulation chambers, formed from fluorine-ethene-propene (FEP) Teflon foil (127 μm thickness), fitted with housings that can exclude ambient

light. This foil has a transmission of > 80 % for sunlight in the near UV / visible range between 280 and 640 nm; the range at which most tropospheric photo-oxidation reaction processes take place (see Chapter 1). The chamber is operated with an excess pressure of 0.75 – 1.5 Torr to keep the foil in shape. The heating of chamber air by solar radiation is compensated by a cooling system integrated into the chamber floor. The chamber is filled with scrubbed ambient air (NMHC < 0.2 ppbV, $CH_4$ = ambient *i.e.* 1800 ppbV, $NO_y$ < 1 ppbV, $H_2O$ ~ 75 ppm)[1] prior to experiments, and is fitted with large horizontal and vertical fans to ensure rapid mixing (*ca*. 2 - 3 min).

**Figure 2.1.** The EUropean PHOtoREactor (EUPHORE) atmospheric simulation chamber in Valencia, Spain

[1] NMHC – non-methane hydrocarbon. $NO_y$ – sum of $NO_x$ (NO + $NO_2$) and all oxidised nitrogen species that represent sources or sinks of $NO_x$ through processes that occur on relatively short timescales.

In this study a range of analytical instrumentation was used (Table 1), including a Laser Induced Fluorescence (LIF) system for the direct measurement of $HO_x$ (OH + $HO_2$) radicals (Bloss et al., 2004, Siese et al., 2001). In addition, the EUPHORE facility was supplemented with a PEroxy Radical Chemical Amplifier (PERCA) and a Chemical Ionisation Reaction Time-Of-Flight Mass-Spectrometer (CIR-TOF-MS) for the measurement of $HO_2$ + $\Sigma RO_2$ and volatile organic / oxygenated volatile organic compounds (VOCs / OVOCs), respectively (Green et al., 2006, Wyche et al., 2007).

**Table 2.1.** Instruments used during this work

| Instrumentation | Target Species |
|---|---|
| Laser Induced Fluorescence (LIF) | OH, $HO_2$ |
| Peroxy Radical Chemical Amplifier (PERCA) | ($HO_2$ + $\Sigma RO_2$) |
| Fourier Transform Infra Red Spectroscopy, Nicolet Magna 550 (FT-IR) | Alkene, $O_3$, VOCs, $SF_6$ |
| Chemical Ionisation Reaction Time-of-Flight Mass Spectrometer (CIR-TOF-MS) | VOCs / OVOCs |
| High Performance Liquid Chromatography UV/FLD (HPLC) | Hydroperoxides |
| Nitric Oxide(s) Analyser, CLD770 (chemiluminescence / photolytic $NO_2$) | NO, $NO_2$, $NO_x$ |
| Ozone Analyser ML9810 (UV absorption) | $O_3$ |
| CO Analyser TE48C | CO |
| Dew Point Hygrometer, Walz | $H_2O$ |

The analytical instrumentation was operated by staff from the EUPHORE facility, with the exception of the PERCA and CIR-TOF-MS measurements, which were carried out by researchers from the University of Leicester, and the laboratory NO interference experiments described in Chapter 6, which were performed in Birmingham. The data analysis described in this and following chapters is the focus of this thesis.

## 2.2 Instrumentation

### 2.2.1 Laser Induced Fluorescence (LIF)

$HO_x$ radicals formed from alkene ozonolysis were measured by Laser Induced Fluorescence (LIF), in particular the FAGE (fluorescence assay by gas expansion) technique (Hard et al., 1984, Heard and Pilling, 2003), illustrated in Figure 2.2.

OH radicals are detected by sampling a continuous jet of air by gas expansion through a 0.38 mm nozzle, into a low pressure fluorescence cell (1.3 Torr). An OH molecule in the sample analyte is promoted into an electronically excited state by laser excitation at $\lambda \sim 308$ nm, where the low pressure gas expansion serves to extend the lifetime of the OH fluorescence enabling detection of light ($\lambda \sim 308$ nm) by gated photon counting (Bloss et al., 2003, Commane et al., 2010, Smith et al., 2006). $HO_2$ is detected by chemical conversion to OH by reaction with added NO (R2.1), followed by detection of the generated OH using the FAGE technique (Fuchs et al., 2010, Heard and Pilling, 2003).

$$HO_2 + NO \rightarrow OH + NO_2 \qquad \text{(R2.1)}$$

Potential interferences in the $HO_2$ mode of detection of the LIF system are described in Chapter 5. The LIF system was calibrated before, during and after each measurement campaign using the $H_2O$ photolysis / ozone actinometry approach (Aschmutat et al., 1994); calibrations were consistent to within a few percent. The

estimated uncertainty in the LIF data from a single calibration is 27 % (combined systematic error and precision). The detection limits for OH and $HO_2$ are approximately $1 \times 10^6$ and $2 \times 10^6$ molecule $cm^{-3}$, respectively.

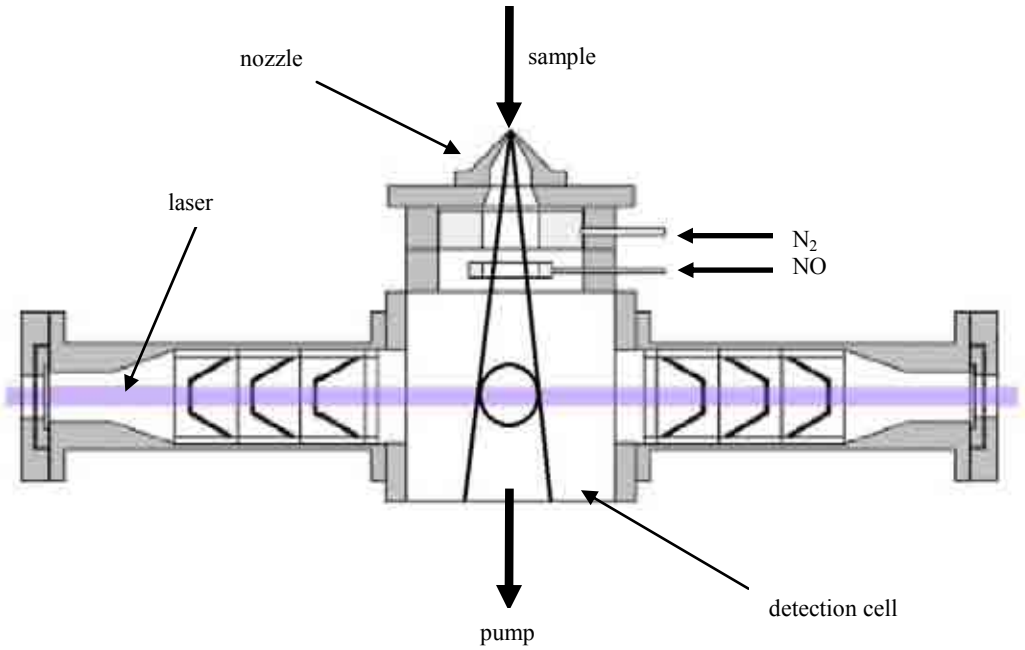


**Figure 2.2.** Diagrammatic representation of Laser Induced Fluorescence (LIF) setup. From Fuchs et al. (2011).

## 2.2.2 Peroxy Radical Chemical Amplifier (PERCA)

Total peroxy radicals ($HO_2$ + $\Sigma RO_2$) were measured by Peroxy Radical Chemical Amplification (PERCA), supplied by the University of Leicester, UK. The technique converts reactive radicals (OH, $HO_2$ + $RO_2$) into $NO_2$ and $CO_2$ (R2.1 – R2.4) (Cantrell et al., 1984). $RO_2$ radicals are converted into $HO_2$ *via* R2.2 – R2.3 and $HO_2$ is converted into OH *via* R2.1, by reaction with NO. The OH formed *via* R2.1 is

converted back to $HO_2$ by reaction with CO *via* R2.4 – R2.5. This results in the formation of multiple $NO_2$ molecules for each $HO_2$ and $RO_2$ radical, which are detected by luminol chemiluminescence.

$$RO_2 + NO \rightarrow RO + NO_2 \quad (R2.2)$$

$$RO + O_2 \rightarrow HO_2 + R'CHO \quad (R2.3)$$

$$HO_2 + NO \rightarrow OH + NO_2 \quad (R2.1)$$

$$OH + CO \rightarrow H + CO_2 \quad (R2.4)$$

$$H + O_2 + M \rightarrow HO_2 + M \quad (R2.5)$$

The number of inter-conversion $HO_2$/OH cycles that occur (*i.e.* the amplification cycle) before radical termination is the chain length (CL), where radical termination can occur *via* R2.6 – R2.8 or by loss on the inlet walls.

$$OH + NO + M \rightarrow HONO + M \quad (R2.6)$$

$$OH + NO_2 + M \rightarrow HNO_3 + M \quad (R2.7)$$

$$HO_2 + NO_2 + M \rightarrow HO_2NO_2 + M \quad (R2.8)$$

The $NO_2$ resulting from the reaction of peroxy radicals must be distinguished from other sources, as ozone can also produce $NO_2$ through the oxidation of NO (R2.9). This is achieved by running the PERCA in 'termination' mode, by injecting CO approximately 1 – 2 seconds downstream of the NO addition point, rather than alongside NO, allowing sufficient time for R2.6 to occur.

$$NO + O_3 \rightarrow NO_2 + O_2 \quad (R2.9)$$

The measurements in the inlet were modulated with a cycle of 2 minutes, so that the radical signal produced from amplification alternated with the signal produced from radical termination. The difference in the two signal modes (amplification and termination) comprised the $NO_2$ formed by $HO_2$ and $RO_2$ radicals only (*i.e.* $\Delta NO_2$ = amplification signal – termination signal), and the total peroxy radical concentration is given by (EQ 2.1).

$$([OH]+[HO_2]+[\Sigma RO_2]) = \frac{\Delta NO_2}{CL} \qquad \text{(EQ2.1)}$$

Since the [OH] is typically 2 orders of magnitude lower than the concentration of peroxy radicals, then $\Delta NO_2$ / CL (in EQ2.1) is equivalent to $HO_2$ + $\Sigma RO_2$. $NO_2$ is measured by detection of the blue chemiluminescence produced from its reaction with luminol. The PERCA was calibrated using methyl iodide ($CH_3I$) photolysis at 253.7 nm, followed by subsequent reaction with $O_2$ generating methylperoxy radicals ($CH_3O_2$), thus determining the chain length of the chemical amplification (Clemitshaw et al., 1997). An $NO_2$ permeation device was used to determine the sensitivity of the luminol chemiluminescence detector to the $NO_2$ product of the amplification (Fleming et al., 2006). The overall uncertainty of peroxy radical measurements is 38 % (2σ) from a combination of uncertainties associated with the radical calibration, $NO_2$ quantification and humidity correction, discussed in detail elsewhere (Brookes, 2009). The PERCA instrument was setup on a raised platform below the atmospheric simulation chamber, with the inlet placed perpendicularly into the chamber floor, sampling approximately 10 cm above the chamber floor.

### 2.2.3 Fourier Transform Infrared Spectroscopy (FTIR)

VOCs, OVOCs, $O_3$ and $SF_6$ were measured using Fourier Transform Infrared Spectroscopy (FTIR). FTIR is a technique where infrared (IR) radiation passes through a sample, which may absorb some of the radiation, producing a spectrum that represents the molecular absorption and transmission of that sample. A given sample analyte will have a specific IR fingerprint with absorption peaks that correspond to frequencies of vibrations between the bonds of the atoms making up the compound. This analytical method can therefore qualitatively and quantitatively identify different species from the IR absorption spectrum, exploiting the Beer Lambert law (EQ2.2)

$$I = I_o \exp(-\sigma c l) \qquad \text{(EQ2.2)}$$

where $I$ and $I_o$ are the emerging and incident intensities respectively, $\sigma$ is the absorption cross section, $c$ is the concentration and $l$ is the path length.

A principle component of the FTIR spectrometer is the interferometer illustrated in Figure 2.3.

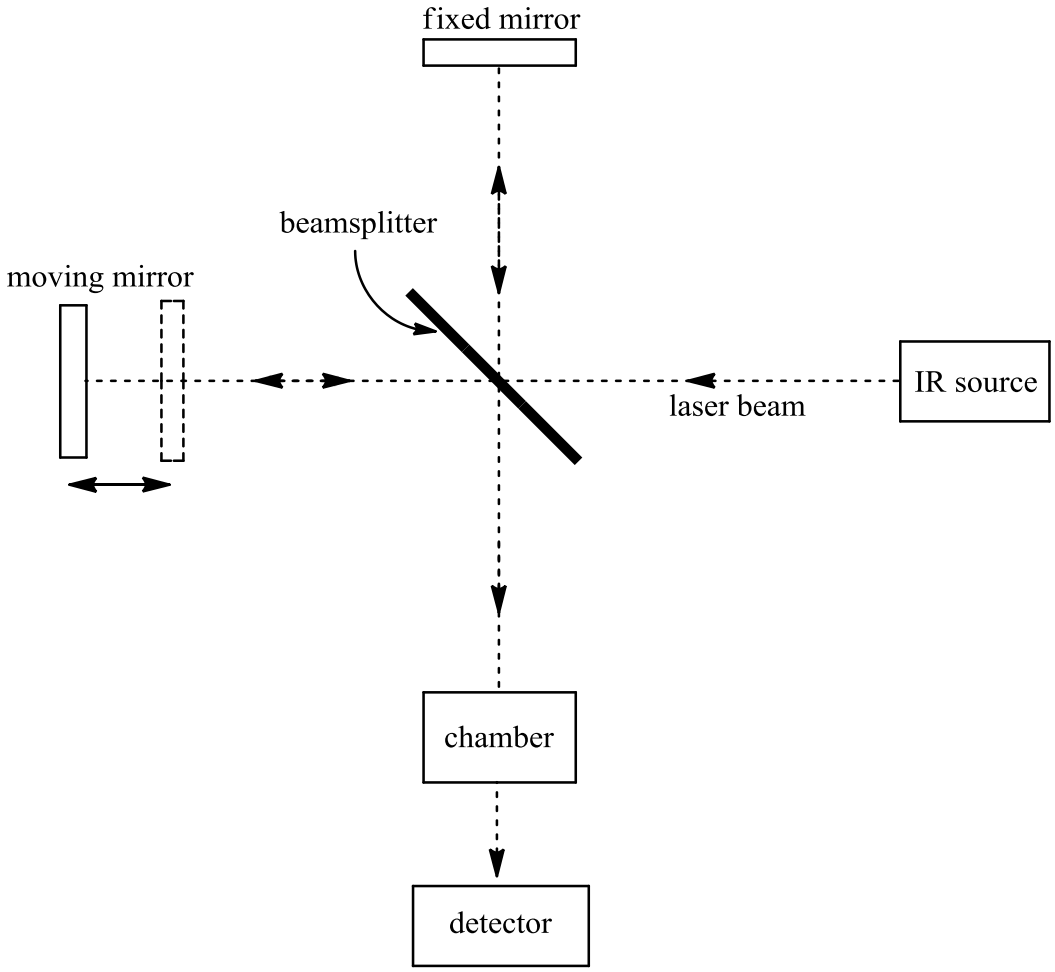


**Figure 2.3.** Diagrammatic representation of the interferometer component of the FTIR system.

An IR beam is guided, from the IR source, through the interferometer to an IR transparent beamsplitter. Approximately 50 % of the beam is reflected to a fixed mirror, which in turn reflects the light back to the beamsplitter, while the remaining 50 % of light passes through the beamsplitter to a continuously moving mirror, moving in the direction of the incoming beam, which also reflects the light back to the beamsplitter. At the beamsplitter the reflected light from the fixed and moving mirrors combine and is directed towards the EUPHORE chamber. Variable optical path lengths are achieved owing to the continuous moving mirror from the beam splitter resulting in different wavelengths of radiation entering the chamber. After the FTIR

beampath traverses the chamber an interferogram (a plot of light intensity *vs* optical path difference) is measured by the detector which through Fourier transform analysis produces an IR spectrum.

At EUPHORE the FTIR spectrometer is also used in combination with a long path (653.6 m) absorption system, with a spectral resolution of 0.5 $cm^{-1}$, a time resolution of 5 minutes and an infrared spectral range of 400 - 4000 $cm^{-1}$. This long optical path is needed in particularly for gas-phase measurements of chemical compounds in the low concentration range (Doussin et al., 1999, White, 1942). The long path system at EUPHORE is a White mirror arrangement consisting of three spherical, concave mirrors, erected inside the chamber at a height of 0.5 m above the chamber floor (Becker, 1996). VOCs and OVOCs were monitored by FTIR with the measurement accuracy limited by the uncertainty of the reference cross sections available and the fitting process involved. The estimated uncertainties and detection limits of a range of species measured during this study are as shown in Table 2.2.

**Table 2.2.** Species measured by FTIR and their associated uncertainties

| Species | Uncertainty / % | Detection limit / ppbV * |
|---|---|---|
| Ethene | 6.2 | 1.6 |
| Propene | 5.8 | 8.2 |
| 1-Butene | 30.0 | 3.0 |
| 2-Methylpropene | 8.0 | 1.0 |
| *trans*-2-Butene | 9.0 | 3.3 |
| *cis*-2-Butene | 6.8 | 7.2 |
| 2,3-Dimethyl-2-butene | 30.0 | 2.1 |
| Cyclohexane | 3.5 | 0.5 |
| Cyclohexanone | 30.0 | 6.0 |
| Cyclohexanol | 30.0 | 3.3 |
| Acetone | 14.0 | 2.0 |
| Formaldehyde | 3.3 | 3.0 |
| Glyoxal | 7.9 | 2.9 |
| Methyl-glyoxal | 15.0 | 3.0 |
| Propanal | 25.8 | 1.9 |
| Formic acid | 30.0 | 0.5 |
| Acetaldehyde | 13.0 | 2.9 |
| Ozone | 8.0 | 3.0 |

* detection limits are 3σ
Detection limits and uncertainties obtained from Instituto Universitario Centro de Estudios Ambientales del Mediterraneo, CEAM, group.

### 2.2.4 Chemical Ionisation Reaction Time-Of-Flight Mass Spectrometer (CIR-TOF-MS)

VOCs and OVOCs were also measured by Chemical Ionisation Reaction Time-Of-Flight Mass Spectrometry (CIR-TOF-MS). A diagrammatic representation of this technique is given in Figure 2.4.

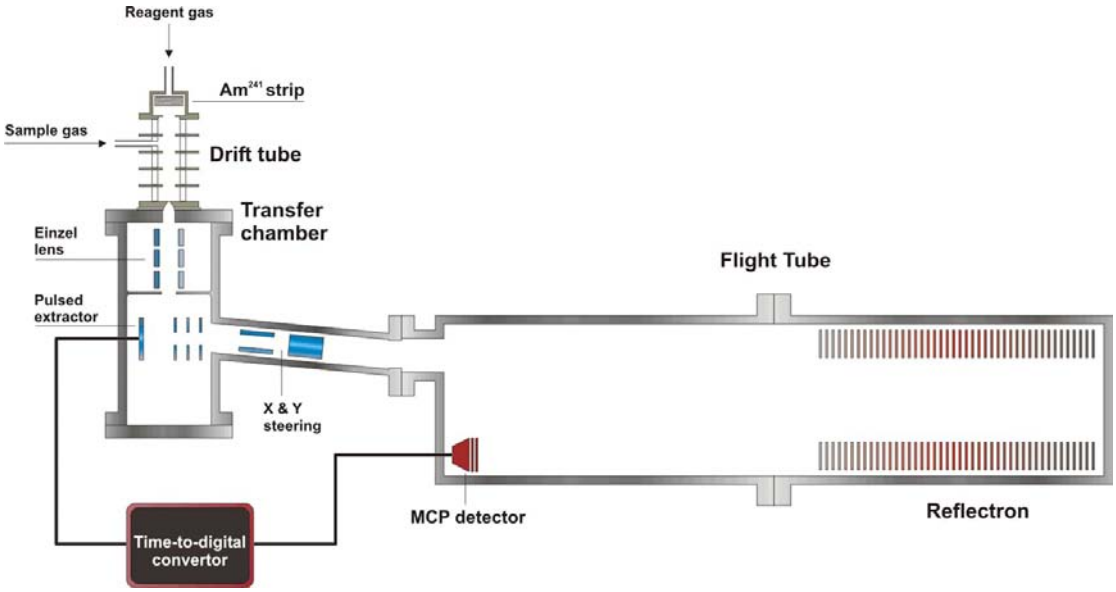


**Figure 2.4.** A diagrammatic representation of the CIR-TOF-MS instrument Taken from Wyche et al. (2007)

The CIR-TOF-MS technique employs a radioactive ion source ($^{241}$Am) and a reaction drift tube coupled to a reflection time-of-flight mass spectrometer (Blake et al., 2004). The radioactive $^{241}$Am α-particle source is used to chemically ionize $H_2O$ vapour to produce hydronium ($H_3O^+$) as a primary chemical ionisation reagent, this is then employed to facilitate the ionisation of an analyte target, R, by means of an ion-molecule reaction inside the reaction drift cell. Water vapour was delivered to the

ion source by bubbling $N_2$ carrier gas through a glass vessel containing high purity deionised water (Wyche et al., 2007). The resulting hydronium ions are then drawn into the drift tube by a voltage gradient, where a proton transfer reaction occurs with the continuously injected sample analyte; pumped from a single point from the centre of the EUPHORE chamber (R2.10).

$$H_3O^+ + R \rightarrow RH^+ + H_2O \qquad \text{(R2.10)}$$

The combined reagent and sample gas moves through the drift tube and into the transfer chamber, equipped with transfer optics. The ion transfer optics consists of a lens, which is used to focus the ions into a narrow beam that is then driven into the flight tube before entering a reflectron, equipped with a detector, which records an *m/z* spectrum.

The CIR-TOF-MS was calibrated after the chamber experiments using the following methods: (*i*) direct admission of a known gas standard (BOC Special Gases, UK) to the instrument inlet line, following dynamic dilution; (*ii*) sampling of "in-house" calibration material produced by the volumetric dilution and liquid injection of the calibrant (Sigma Aldrich, typical purity ≥ 99 %) into Tedlar sample bags and (*iii*) production of gas standards using certified permeation tubes (Eco-Scientific, UK), diluted, appropriately humidified and delivered to the CIR-TOF-MS sample inlet. Overall calculated uncertainties for formaldehyde, acetaldehyde, acetone and cyclohexanone for example, were between 27.6, 10.2, 12.8 and 20.2 %, respectively. These values comprise the combination of both instrument precision and calibration accuracy.

### 2.2.5 High Performance Liquid Chromatography (HPLC)

Organic hydroperoxides were determined by the high performance liquid chromatography (HPLC) – fluorescence method (Hellpointner and Gab, 1989). This technique employs an impinger to collect gaseous hydroperoxide in aqueous solution prior to analysis. Briefly, samples were taken by bubbling chamber air through dilute cold acidic solution (0 °C, $H_3PO_4$), as hydroxyalkyl hydroperoxides are stable under these conditions. The HPLC system was then used to separate the various hydroperoxides at ~ 0 °C. Immediately after separation, both the temperature and pH of the eluate ($H_3PO_4$) was increased to liberate $H_2O_2$ from the hydroxyalkyl hydroperoxides and *p*-hydrophenyl acetic acid and horseradish peroxidase were added. $H_2O_2$ and alkyl hydroperoxides, in the presence of peroxidase, oxidise *p*-hydrophenyl acetic acid to a biphenyl derivative, which after excitation at 285 nm shows a strong fluorescence at 410 nm (Becker, 1996). Sampling times ranged from 5 - 30 min, depending on environmental factors. Carbonyl compounds were determined by derivatisation with DNPH (2,4-dintrophenylhydrazine) and subsequent HPLC-UV detection of the corresponding hydrazones. The estimated uncertainty for observations made by HPLC was 30 %.

### 2.2.6 Nitric Oxide(s) ($NO_x$) Analyser

The alkene ozonolysis experiments were performed in zero $NO_x$ conditions, and thus the use of the nitric oxide(s) analyser was not crucial to the results of this study, other than to monitor the chamber and to ensure zero $NO_x$ conditions. The $NO_x$ analyser is

described in detail in Chapter 6. Briefly, the $NO_x$ analyser exploits the chemiluminescence reaction of NO + $O_3$ (Clough and Thrush, 1967, Clyne et al., 1964). The mechanism involves the formation of an electronically excited $NO_2$ molecule (R2.11) which can either undergo chemiluminescence (R2.13) or quenching (R2.14). Chemiluminescence is seen in the range $600 < \lambda < 3000$ nm, where only a small fraction of emission occurs below 800 nm and emission peaks at 1200 nm.

$$NO + O_3 \rightarrow NO_2^* + O_2 \qquad (R2.11)$$

$$NO + O_3 \rightarrow NO_2 + O_2 \qquad (R2.12)$$

$$NO_2^* \rightarrow NO_2 + h\nu \qquad (R2.13)$$

$$NO_2^* + M \rightarrow NO_2 + M \qquad (R2.14)$$

The chemiluminescence emission is measured with a temperature controlled red sensitive photomultiplier tube (PMT). Measurements of $NO_2$ are achieved by reduction to NO using a photolytic convertor. $NO_2$ is converted into NO *via* R2.15 and detected as previously described for NO, through the chemiluminescence reaction, thus giving a NO + $NO_2$ combined signal.

$$NO_2 + h\nu \rightarrow NO + O(^3P) \qquad (R2.15)$$

The $NO_2$ concentration is derived by the difference between the NO and the $NO_x$ signals. The instrument is connected by a short Teflon tube to the reaction chamber, thus minimizing wall effects during the sampling. The detection limits for NO and $NO_2$ are 5 pptV and 7 pptV respectively. Potential interferences for this technique are described in detail in Chapter 6.

### 2.2.7 Ozone Analyser

The measurement of ozone was performed using both FTIR and an $O_3$ analyser. The analyser utilises the absorption of UV light by $O_3$ at 254 nm. Few molecules found at significant concentrations in the troposphere are known to absorb at this wavelength, thus allowing detection with selectivity. Briefly, a mercury lamp (with light intensity $\lambda = 254$ nm) and photodiodes are located on opposite sides of two absorption cells. Sample analyte is drawn into the instrument, where a pair of valves alternately send $O_3$ scrubbed / unscrubbed analyte through the two cells. The light intensity that passes through $O_3$ scrubbed analyte ($I_o$) and unscrubbed analyte ($I$) is then measured and the $O_3$ concentration is calculated, according to the Beer Lambert law (EQ2.3, rearranged from EQ2.2):

$$[O_3] = \frac{1}{\sigma l} \ln\left(\frac{I}{I_0}\right) \qquad \text{(EQ2.3)}$$

where $l$ is the path length of the absorption cell and σ is the absorption cross section for $O_3$ at 254 nm ($1.15 \times 10^{-17}$ $cm^2$ $molecule^{-1}$) (NASA-JPL, 2006). The detection limit of this technique is approximately 1 ppbV. Interferences have been reported for this technique under humid conditions, owing to condensation on absorption cell surfaces, and for sampling in the presence of aromatic VOCs (Meyer et al., 1991, Kleindienst et al., 1993). The instrument is connected to the chamber by a short Teflon tube.

### 2.2.8 Carbon Monoxide Analyser

CO was measured using a Gas Filter Correlation (GFC) carbon monoxide analyser. This analyser operates on the principle that CO undergoes IR absorption at a wavelength of 4.6 μm. Briefly, the sample is drawn into the instrument from the chamber and into an absorption cell. An infrared source emits radiation that passes through a filter, screening out most wavelengths and subsequently allowing radiation that CO absorbs into the sample cell. The instrument contains a chopper wheel that rotates, containing pure $N_2$ and CO gases, in separate compartments. As it rotates, the CO gas filter absorbs all the IR radiation, effectively scrubbing any radiation that can be attenuated by CO in the sample cell. The $N_2$ compartment is IR transparent, allowing IR radiation to be absorbed by any CO present in the sample cell. The two measurements of IR intensity are then detected, and [CO] is calculated using the Beer Lambert law, rearranging EQ 2.2. The CO mixing ratio in the (scrubbed) chamber is approximately 150 ppbV.

### 2.2.9 Duplication of Species Measurements

Measurements of some species were made by two or more types of instrumentation. For example, $O_3$ was measured by both FTIR and UV-absorption spectroscopy, where both methods were in very good agreement (within 1 %). Similarly, HCHO was monitored by FTIR, CIR-TOF-MS and a formaldehyde monitor (IR absorption). The data from all techniques were in good agreement, confirming that the reactants are well mixed in the simulation chamber (on the timescale of the alkene-ozone decay) –

the FTIR beampath traverses the chamber, while the monitor and CIR-TOF-MS sampled from two different single points.

## *Section B*

The next section describes the alkene-ozone experiments conducted in the atmospheric simulation chamber. Details of the modelling performed to interpret the observations from the experiments conducted are also described and methodologies for determination of radical and carbonyl yields are outlined.

## 2.3 Experimental Approach

The ozonolysis experiments were performed with the chamber housing closed to exclude photochemical effects ($j(NO_2) < 2\times10^{-6}$ $s^{-1}$), at near atmospheric pressure and ambient temperature, as described in Section 2.1. All experiments were conducted under $NO_x$-free conditions ([NO] and [$NO_2$] below the monitor detection limit of 5 and 7 pptV, respectively). In the absence of $NO_x$ and sunlight, chamber wall radical production has been shown to be negligible (Zador et al., 2006). For "dry" experiments, the relative humidity was low (< 1.0 %, in simulation chamber terms: dew point *ca*. -45 ° C / 75 ppmV $H_2O$). The experimental procedure, starting with a clean flushed chamber, was to add $SF_6$ (as a dilution tracer), followed by ozone (50 – 500 ppbV) and in certain cases an OH scavenger (CO or cyclohexane, in concentrations such that ≥ 95 % of any OH produced was scavenged) was introduced prior to ozone injection. To initiate the reaction, a known aliquot of alkene (20 - 500

ppbV) was injected into the chamber and the evolution of reactants and products was then monitored (Table 2.1) over timescales of 1 - 3 hours. The experimental procedure for "wet" experiments, where the relative humidity was ~ 30 %, involved the addition of $O_3$ (and scavenger species) prior to the addition of water to the chamber, as increased humidity (> 40 %) inside the chamber may affect FTIR measurements, owing to condensation on optical surfaces. The chamber mixing time was of the order of 2 - 3 minutes.

Four types of ozonolysis experiments were carried out:

(*a*). ***Simple, alkene / $O_3$***: designed to produce OH, $HO_2$ and $RO_2$ radicals (R2.16). OH was removed initially by reaction with the parent alkene (R2.17), whereas $HO_2$ and $RO_2$ were removed by cross- and self-reaction. OH yields were readily obtainable from the OH steady state concentration, measured by LIF, using the reaction rate coefficients for alkene + ozone (R2.16), alkene + OH (R2.17), $HO_2 + O_3$ (R2.18) and $OH + O_3$ (R2.19), by EQ 2.4, where $\alpha$ is the OH yield.

$$\text{Alkene} + O_3 \rightarrow \text{OH} + HO_2 + RO_2 + \text{products} \quad \text{(R2.16)}$$

$$\text{Alkene} + \text{OH} \rightarrow \text{products} \quad \text{(R2.17)}$$

$$HO_2 + O_3 \rightarrow \text{OH} + 2O_2 \quad \text{(R2.18)}$$

$$\text{OH} + O_3 \rightarrow HO_2 + O_2 \quad \text{(R2.19)}$$

$$[\text{OH}]_{SS} = \frac{\alpha\, k_{\text{Alk}+O_3}[\text{Alk}][O_3] + k_{HO_2+O_3}[HO_2][O_3]}{\left(k_{\text{Alk}+\text{OH}}[\text{Alk}] + k_{\text{OH}+O_3}[O_3]\right)} \quad \text{(EQ 2.4)}$$

However, some degradation products (measured by FTIR and CIR-TOF-MS) formed from both alkene + ozone and alkene + OH reactions can also react with OH, leading to a change in the steady state approximation, as shown in (EQ 2.5), where reaction with observed products can be accounted for by $k_{prod}$. The steady state approximation expression (EQ2.5) was solved using zero dimensional box modelling, described in Section 2.4.

$$[OH]_{SS} = \frac{\alpha\ k_{VOC+O_3}[VOC][O_3] + k_{HO_2+O_3}[HO_2][O_3]}{\left(k_{VOC+OH}[VOC] + k_{OH+O_3}[O_3] + k_{Prod}[Prod]\right)} \qquad \text{(EQ 2.5)}$$

(*b*). ***Excess CO, alkene / $O_3$ / CO***: designed to convert OH to $HO_2$ by reaction with excess CO (Gutbrod et al., 1997b). This allowed the total (sum of) OH and $HO_2$ production to be monitored via measurement of $HO_2$, and simplified the interpretation of $RO_2$ data, as > 95 % of OH produced from alkene ozonolysis was scavenged by CO, suppressing side reactions. $HO_2$ removal was therefore dominated by self-reaction. Additionally, the stabilised Criegee intermediates (SCIs) were also effectively scavenged by CO to form an aldehyde (dependent upon the structure of the Criegee intermediate) and $CO_2$ (Brauers et al., 2007). This experiment type, with negligible OH-initiated oxidation, provides the clearest data for the identification of the alkene ozonolysis products.

(*c*). ***Excess cyclohexane, $C_2H_4$ / $O_3$ / c-$C_6H_{12}$***: designed to obtain an indirect OH yield by monitoring products formed from the OH + cyclohexane reaction (Atkinson et al., 1992). The excess cyclohexane experiments were designed to scavenge > 95 % of OH produced from ozonolysis. This experiment type was exploited to derive OH yields

for ethene (and *trans*-2-butene for comparison with that derived *via* EQ 2.1) as the steady state [OH] from ethene ozonolysis is below the detection limit of the LIF system (approximately $5 \times 10^5$ molecule $cm^{-3}$). This experiment type, with negligible OH-initiated oxidation of alkene, like experiment type (*b*), provides data for the identification of the alkene ozonolysis products. Details of the OH-initiated cyclohexane oxidation reaction are discussed in detail in Section 2.4.

(*d*). ***Increased humidity***: experiments (*a*) and (*b*) were performed with graduated addition of water to the chamber, to monitor the humidity dependence of the OH and $HO_2$ radical yields and the effect of the reaction of $H_2O$ + SCI.

Owing to limited chamber time, the numbers of experimental runs were limited. However, some experimental runs were repeated to assess the repeatability of the results obtained for this thesis (see Tables A1 – A7 in the Appendices), including as a function of humidity, and were found to be consistent, as shown in chapters 3 and 4.

## 2.4 Box Modelling & Mechanism Optimisation

$HO_x$ radicals are highly reactive in the alkene-ozone experimental system; therefore the results were interpreted through detailed chemical box modelling, thus accounting for secondary processes. The photochemical degradation schemes were extracted from the Master Chemical Mechanism (MCMv3.1) for each specific alkene (Bloss et al., 2005, Jenkin et al., 1997, Saunders et al., 1997). The MCMv3.1 is a near explicit

chemical mechanism, describing the detailed gas-phase chemical processes involved in the atmospheric degradation of important primary emitted VOCs (see Chapter 1). The complete gas-phase photo-oxidation mechanism for each alkene studied (ethene, propene, 1-butene, 2-methylpropene, *cis*- / *trans*-2-butene and 2,3-dimethyl-2-butene) was extracted (including a suitable set of inorganic reactions) directly from the MCM website (http://mcm.leeds.ac.uk/MCM) and incorporated into a chamber specific box model. The alkene photo-oxidation mechanisms were updated to include a more explicit representation of the ozonolysis reaction mechanisms (see Chapter 4, Section 4.3) and chamber processes (dilution) (Bloss et al., 2005). Within the model, the rapid reaction steps occurring after formation of the primary ozonide were assumed to proceed near-instantaneously on the 1 - 2 hour timescale of the experiments; *i.e.* the POZ and CIs were assumed to decompose effectively instantaneously to form radical products (yields optimised as described below) and stable species, or stabilised to form the SCI. The rate constants for the bimolecular reactions of the SCI were extracted directly from the MCM. For type (*c*) experiments the cyclohexane photo-oxidation mechanism, extracted from MCMv3.1, was also updated and extended as outlined below.

All chamber box model simulations were integrated using FACSIMILE (Curtis and Sweetenham, 1987). FACSIMILE software is used to solve differential equations numerically, by replacing derivations by differences over a finite time step. The software exploits the predictor-corrector technique, in which the values of a solution vector at the end of a time step is first predicted and then corrected to satisfy the differential equation by the Newton iteration method. The data fitting wizard within FACSIMILE is used to optimise unknown parameters such as rate constants and

product yields (see optimisation section below). The model completes this by tuning designated parameters to give the best fit to the supplied observations (*i.e.* concentration time profiles), by minimising the sum of the squares of the residuals between the measured and simulated data. The FACSIMILE output files contain the optimised and observed data with data fitting statistics and quantified parameters. A detailed description of data fitting process using FACSIMILE is given elsewhere (Curtis and Sweetenham, 1987).

The initial conditions used for the initialisation of the corresponding box models for each of the alkene-ozone experiments are shown in Tables A1 – A7 in the Appendices of this thesis. As the fundamental reactions occurring are understood, the model is applicable to all types of conditions (*e.g.* varying concentrations of parent alkene and ozone). For some experiments the use of the high initial concentrations of alkene and ozone does not reflect realistic tropospheric conditions owing to the constraints of experimental limitations (*i.e.* detection limitations of instrumentation). Temperature, relative humidity and dilution rates were averaged over the duration of each experiment, as the variation in these parameters was minimal, see Figure 2.5. The simulations were initialised at the time point at which the maximum alkene mixing ratio was observed.

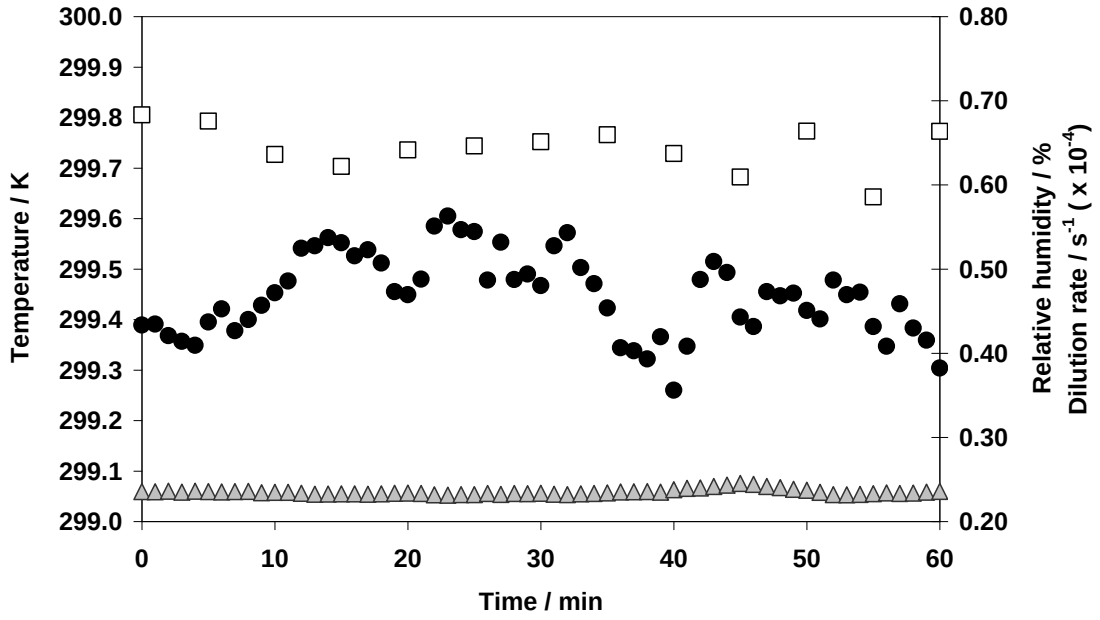


**Figure 2.5.** Variation of certain experimental parameters over the duration of a typical ozonolysis experiment. Temperature (black circles), relative humidity (grey triangles) and dilution rate (open squares, calculated from the FTIR $SF_6$ temporal profile).

To determine the overall yields of specific products from the overall fast ozonolysis reaction (*i.e.* CI formation and decomposition chemistry), four analytical steps were performed: (1) Reaction rate coefficient optimisation, (2) decomposition of POZ / SCI branching ratio calculation, (3) OH yield optimisation and (4) $HO_2$ yield optimisation. Flow charts summarising these analytical steps are given in Chapters 3 and 4.

1. ***Reaction rate coefficient ($k_{O_3+alkene}$) optimisation***

The recommended rate coefficients for the alkene + ozone ($k_{O_3+alkene}$) reactions have estimated uncertainties of the order 25 – 35 % (Calvert et al., 2000, http://www.iupac-kinetic.ch.cam.ac.uk/, 2007). Thus, the model representation of the alkene decay

could be improved by optimising $k_{O_3+alkene}$, to simulate (and reproduce) the observed alkene and ozone time profiles. This was achieved by using the FTIR observations of alkene and ozone and by minimising the sum of squares of residuals between the measured and modelled results within FACSIMILE. However, only OH scavenger experiments type (*b*) and (*c*) were exploited here as the OH + alkene reaction would be suppressed. Under these conditions, the loss of alkene can be assumed to be due to dilution (calculated from $SF_6$ decay) and reaction with ozone only, allowing the determination of the reaction rate coefficient between the alkene and ozone.

*For propene, 1-butene and 2-methylpropene only*

2. ***Decomposition of primary ozonide, POZ***

The POZ formed from the electrophilic addition of $O_3$ across the C=C double bond for these alkenes undergoes fragmentation, forming two pairs of CIs and 'primary' carbonyl compounds (see Chapter 4, Section 4.3). Recent literature suggests, however, that there is an unequal split between the formation of the two pairs of species (http://www.iupac-kinetic.ch.cam.ac.uk/, 2007). This branching ratio split was optimised by using the FTIR observations for the primary carbonyls and by minimising the sum of squares of residuals between the measured and modelled results within FACSIMILE.

*For ethene only*

2. ***SCI branching ratio calculation***

In type (b) experiments (excess CO), the production of HCHO arises from the decomposition of the POZ and the SCI + CO reaction, while the loss of HCHO is due to dilution only. It can be assumed from the postulated mechanism of ethene

ozonolysis (see Chapter 3, Figure 3.1) and previous studies (Grosjean et al., 1996, Grosjean and Grosjean, 1996b) that the primary formaldehyde yield (formed directly from the decomposition of the POZ) is unity; correspondingly measured yields above 1 are believed to result from the formation of HCHO *via* the reaction of the SCI + CO. Hence, assuming that the reaction with CO competes effectively with all other possible bimolecular fates of the SCI under the experimental conditions, an SCI yield can be determined. The HCHO yield was obtained from the regression of HCHO production *vs*. ethene consumption, following correction for dilution. The procedure for the dilution corrected derivation of stable carbonyl yields is discussed in Section 2.6.

*For ethene only (and trans-2-butene)*

3. ***OH yield optimisation (cyclohexane)***

OH yields from ethene ozonolysis were determined indirectly by exploiting type (*c*) experiments (excess cyclohexane), as the steady state [OH] generated in the "simple" type (*a*) system was below the detection limit of the LIF. The cyclohexane experiments were designed to scavenge ≥ 95 % of any OH produced from ethene ozonolysis, generating products illustrated in Figure 2.6 (Atkinson et al., 1992, Malkin et al., 2010) The cyclohexanone / cyclohexanol products formed from OH reacting with cyclohexane include both OH formed directly from the ozonolysis reaction, and that produced indirectly *via* $HO_2 + O_3$. The fate of the cyclohexyl peroxy radical (*c*-$C_6H_{11}O_2$) as well as the ratio of cyclohexanone / cyclohexyl-hydroperoxide formed is dependent upon the concentrations of $HO_2$ and $RO_2$, and identity of the $RO_2$, present in the system, as these compete for reaction with *c*-$C_6H_{11}O_2$ (see Figure 2.6). Hence, cyclohexanone "yields" from OH +

cyclohexane are not necessarily expected to be consistent between chemical systems, or indeed within the same chemical system at different (peroxy radical) concentration levels, with the key being the relative rates of the cyclohexyl peroxy + $RO_2$ and + $HO_2$ reactions (Alam et al., 2011). The OH yield was obtained by minimising the sum of the squares of residuals between the simulations and observations for cyclohexanone (as measured by CIR-TOF-MS), cyclohexyl-hydroperoxide (HPLC) and steady state $HO_2$ (LIF), whilst optimising the ratio $k_{2.21}/k_{2.22}$ (where $k_{2.21} = k_{2.21a} + k_{2.21b} + k_{2.21c}$, see Figure 2.6) and OH yield and constraining $C_2H_4$ and $O_3$ to their observed levels.

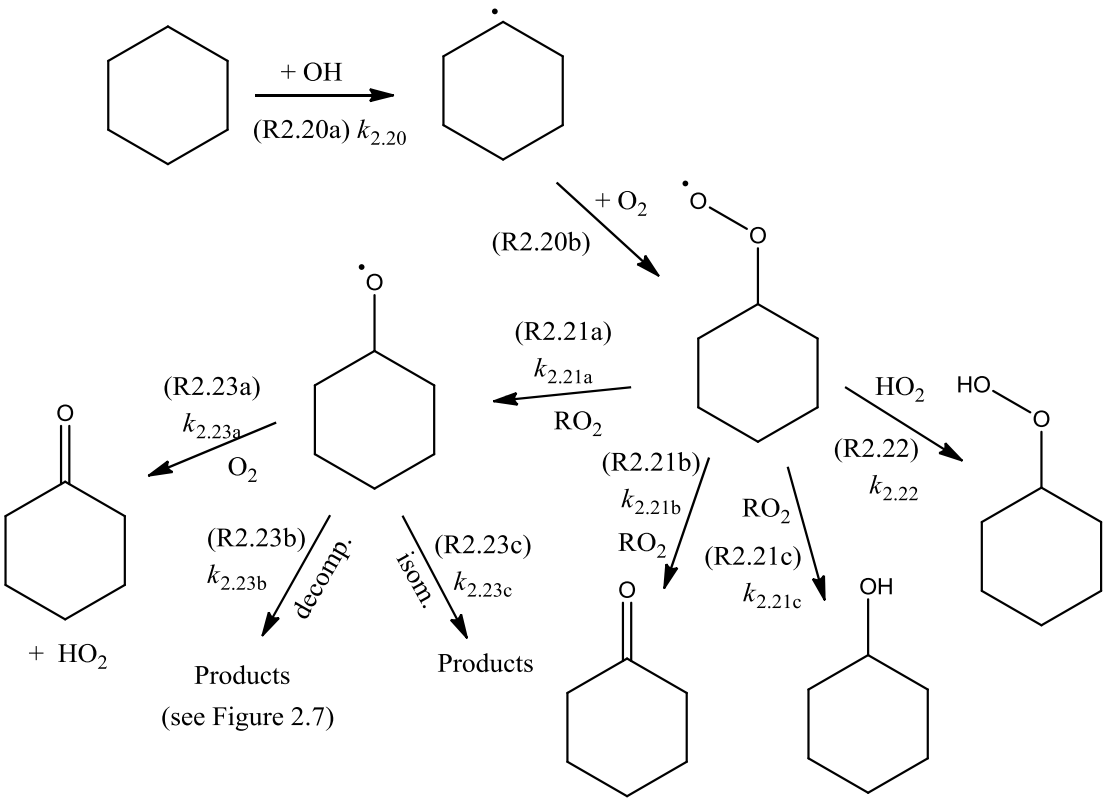


**Figure 2.6.** Cyclohexane-OH oxidation scheme (adapted from MCMv3.1; Atkinson et al. (2007) and Orlando et al. (2000).

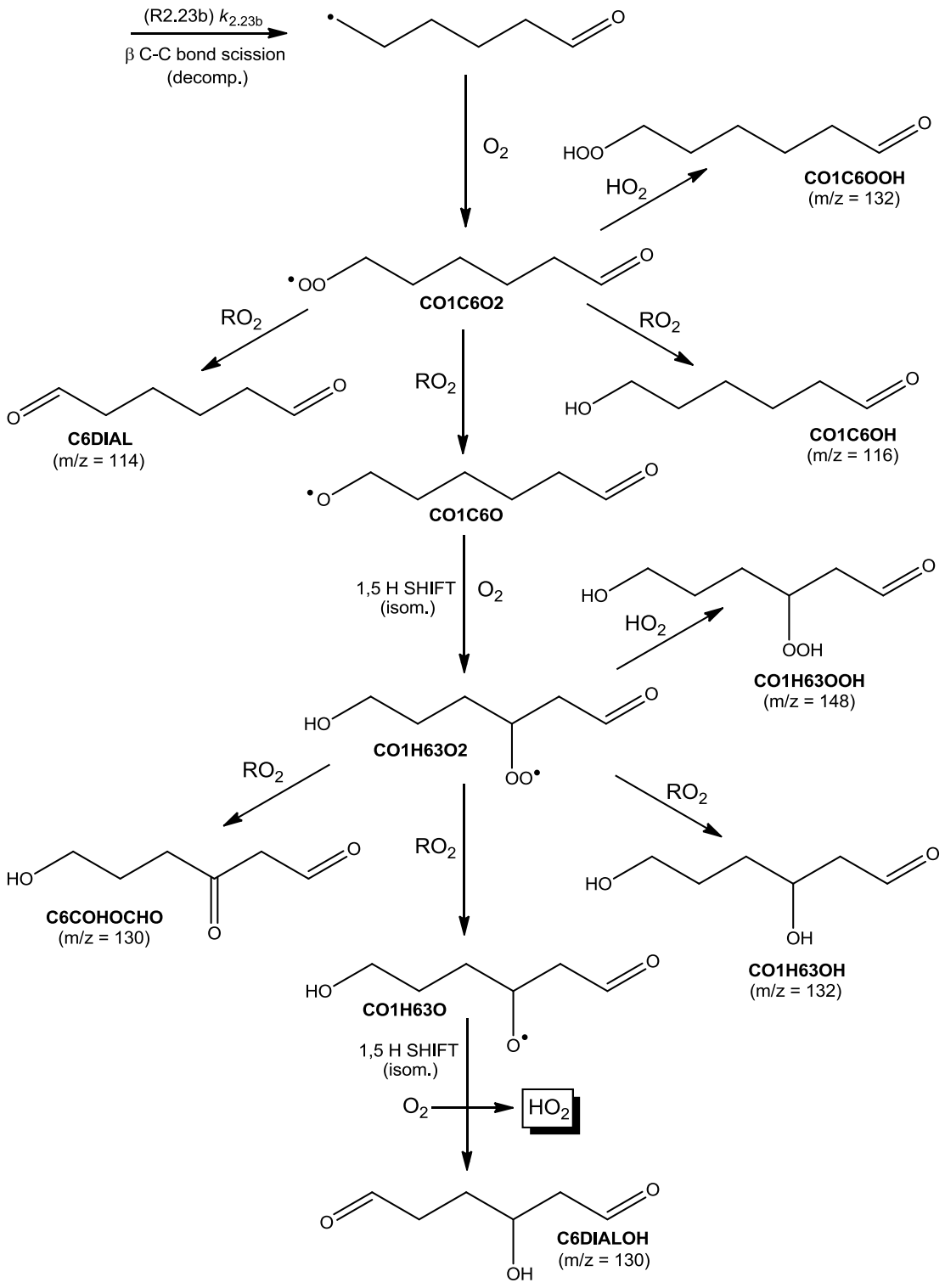


**Figure 2.7.** Schematic representation of the major decomposition (ring-opening) pathways of the cyclohexoxy radical chemistry under zero $NO_x$ conditions (subsequent reactions from pathway R2.23b in Figure 2.6). Adapted from MCMv3.1; Atkinson et al. (2007) and Orlando et al. (2000)

The MCMv3.1 cyclohexane mechanism was updated to include a more explicit representation of the OH-initiated oxidation. The inclusion of the ring opening chemistry, accounting for the decomposition / isomerisation reactions of the cyclohexoxy radical, is shown in Figures 2.6 and 2.7. The atmospheric chemistry of the cyclohexoxy radical involves competition between reaction with $O_2$ (R2.23a, Figure 2.6) and unimolecular decomposition *via* ring-opening (R2.23b). The unimolecular isomerisation of the cyclohexoxy radical (R2.23c) is found to be negligible owing to ring strain (Atkinson, 1997a, Orlando et al., 2000). The reaction rate coefficients of $2.5 \times 10^{-14} \exp^{(-300/T)}$ (Atkinson, 2007) and $3.8 \times 10^{-13} \exp^{(-6026/T)}$ $cm^3$ $molecule^{-1}$ $s^{-1}$ (Welz et al., 2008), were used for the cyclohexoxy radical + $O_2$ reaction (R2.23a) and the unimolecular decomposition of the cyclohexoxy radical (R2.23b), respectively. This corresponds to a yield of 0.43 for cyclohexanone from reaction R2.23a under atmospheric conditions, which is found to be in reasonable agreement with Orlando *et al*. (2000) (0.36 ± 0.06), and in very good agreement with Atkinson *et al.* (1992) (0.42 ± 0.05), and with the average yield of 0.41 ± 0.08 derived from various literature studies (Welz et al., 2008), (Orlando et al., 2003), (Platz et al., 1999), (Rowley et al., 1991), (Zhang et al., 2004), calculated using the recommended rate coefficient for secondary peroxy radical reactions with $O_2$ (Atkinson, 2007) in all cases, as above.

3. ***OH yield optimisation (LIF)***

Steady state [OH] was available for all alkenes except ethene, as the steady state [OH] from ethene ozonolysis is below the detection limit of the LIF system (*ca.* $5 \times 10^5$ molecule $cm^{-3}$). OH yields were determined by using the FTIR measurements for a given alkene and ozone and LIF observations for OH and minimising the sum of

squares of residuals between the simulated and observed concentrations. The branching ratio of the isomerisation / decomposition of the *syn*-CI was optimised in order to obtain an OH yield, while taking into account any secondary OH formed from R2.24, R2.25 and R2.26 in the model. The derived OH yield from the ozonolysis of ethene (see Chapter 3) was applied to $[CH_2OO]^*$ formed in the ozonolysis of propene, 1-butene and 2-methylpropene, while optimising the branching ratio of the co-produced CI that is assumed to form OH *via* the hydroperoxide mechanism.

$$HO_2 + O_3 \rightarrow 2O_2 + OH \quad \text{(R2.24)}$$

$$CH_3C(O)CH_2O_2 + HO_2 \rightarrow OH + CH_3C(O)CH_2O + O_2 \quad \text{(R2.25)}$$

$$CH_3C(O)O_2 + HO_2 \rightarrow OH + CH_3C(O)O + O_2 \quad \text{(R2.26)}$$

4. ***$HO_2$ optimisation (LIF)***

In general, the $HO_2$ yield was determined using FTIR measurements for a given alkene and ozone and LIF observations for $HO_2$ and minimising the sum of the squares of residuals between the simulated and observed $HO_2$ concentrations.

For ethene, the formation of OH is likely to be accompanied by a formyl radical (HCO) (as illustrated in Chapter 3, Figure 3.1, R3.2 and R3.3a), which under the experimental conditions employed would react rapidly with $O_2$ to form $HO_2$ + CO. Thus, the sum of channels R3.2 and R3.3a equates to the overall $Y_{OH}$ as well as a fraction of the $HO_2$ yield. As the overall $Y_{OH}$ is calculated during stage 3 (for ethene), channels R3.2 and R3.3a can be combined and quantified within the model. Using the postulated mechanism (see Chapter 3, Figure 3.1), the remaining channel producing

$HO_2$ in the ethene-ozone system to be quantified is R3.3b, where 2 H atoms react near-instantaneously with molecular oxygen to form 2 molecules of $HO_2$. Channel R3.3b was optimised within the model to improve the $HO_2$ model fit with the LIF observations and the sum of the combined branching ratios (R3.2 + R3.3a) (determined in stage 3 – OH yield optimisation) and 3b, determine the overall yield of $HO_2$. The $HO_2$ yield from ethene ozonolysis was determined prior to optimising the yields of $HO_2$ for all other alkenes studied and was attributed to $[CH_2OO]^*$ formed in terminal alkenes, propene, 1-butene and 2-methylpropene.

For propene ozonolysis, $HO_2$ formation is likely to result from the decomposition of both $[CH_2OO]^*$ and $[CH_3CHOO]^*$ (see Chapter 4, Figure 4.4). As a fraction of the $HO_2$ yield comes from the decomposition of $[CH_2OO]^*$, the remaining channel producing $HO_2$ in the propene-ozone system, using the postulated mechanism, to be quantified is R4.3c (decomposition of "hot" acid intermediate). The sum of the $HO_2$ formation from channels R4.3c and $[CH_2OO]^*$ is equal to the overall $HO_2$ yield from propene ozonolysis. Any secondary $HO_2$ formation is accounted for within the model. Similarly, for 1-butene $HO_2$ formation (other than formation *via* $[CH_2OO]^*$) is attributed to one channel from the decomposition of the "hot" acid intermediate. This fraction of $HO_2$ yield is optimised and added to the fraction of $HO_2$ determined from $[CH_2OO]^*$ to give an overall $HO_2$ yield for 1-butene ozonolysis. For *cis*-2-butene and *trans*-2-butene, $HO_2$ formation is likely to result from the decomposition of the "hot" acid (see Chapter 4, Figure 4.5, R4.3c), which was optimized to give an overall yield of $HO_2$ for the respective 2-butenes.

For 2-methylpropene, the postulated mechanism (see Chapter 4, Figure 4.6) indicates that $HO_2$ formation is restricted to $[CH_2OO]^*$. Thus, the $HO_2$ yield for 2-methylpropene was optimised in the same way as in the ethene-ozone system, described above. According to the postulated mechanism for 2,3-dimethyl-2-butene, there is no direct $HO_2$ formation channel (see Chapter 4, Figure 4.7). Little $HO_2$ formation is therefore expected from 2,3-dimethyl-2-butene which may be attributed to secondary sources. However, in the 2,3-dimethyl-2-butene-ozone system the observed $[HO_2]$ by LIF is larger than secondary sources would suggest, which may indicate a $HO_2$ formation channel. The yield of $HO_2$ for this system was therefore calculated by introducing (and optimising) an independent channel forming $HO_2$ from the decomposition of $[(CH_3)_2COO]^*$. The formation of $HO_2$ from the 2,3-dimethyl-2-butene-ozone system is discussed in detail in Chapters 4 and 5.

## 2.5 Dilution Correction of Carbonyl Yields

The formation of a product from the oxidation of a precursor is often expressed as a yield (*i.e.* the quantity of product formed as per amount of precursor oxidised). For the example of HCHO formation from ethene ozonolysis, HCHO overall yield, α, can be expressed as:

$$C_2H_4 + O_3 \xrightarrow{k} \alpha\,\mathrm{HCHO} + \mathrm{products} \qquad \text{(R2.27)}$$

where $k$ is the rate constant for ethene + ozone. The HCHO yield can be calculated as:

$$\alpha = \text{yield} = -\frac{\Delta[\text{HCHO}]}{\Delta[\text{C}_2\text{H}_4]} \qquad \text{(EQ2.6)}$$

where $\Delta[C_2H_4]$ is the $[C_2H_4]$ loss and $\Delta$[HCHO] is the amount of HCHO produced from (R2.23). The yield is generally obtained from the slope of the straight regression line of the graph $\Delta$HCHO *vs.* $\Delta C_2H_4$.

However, the yield of products formed from alkene ozonolysis studied in EUPHORE could not be directly calculated from alkene and stable product measurement, for two reasons:

(i) Product concentrations had chemical sinks (with OH) and other sources (coming from the precursor or secondary species oxidation by OH) if no OH scavenger was used in the experiment.

(ii) Chamber dilution significantly affected stable species' time profiles. The dilution loss of each stable species can be represented by a first order loss process. During each experiment, dilution is well constrained by the measured first order decay of $SF_6$ (as monitored by the FTIR). The dilution rate in the EUPHORE chamber is approximately $1 \times 10^{-5}$ $s^{-1}$. Figure 2.8 illustrates this problem in determining the HCHO yield directly from EQ2.6, where a curved plot is observed.

These sources and sinks need to be taken into account when calculating the yields of stable products and in most cases this was performed using the model, which

explicitly included these processes, minimising the sum of squares of residuals between the simulated and observed concentrations (FACSIMILE).

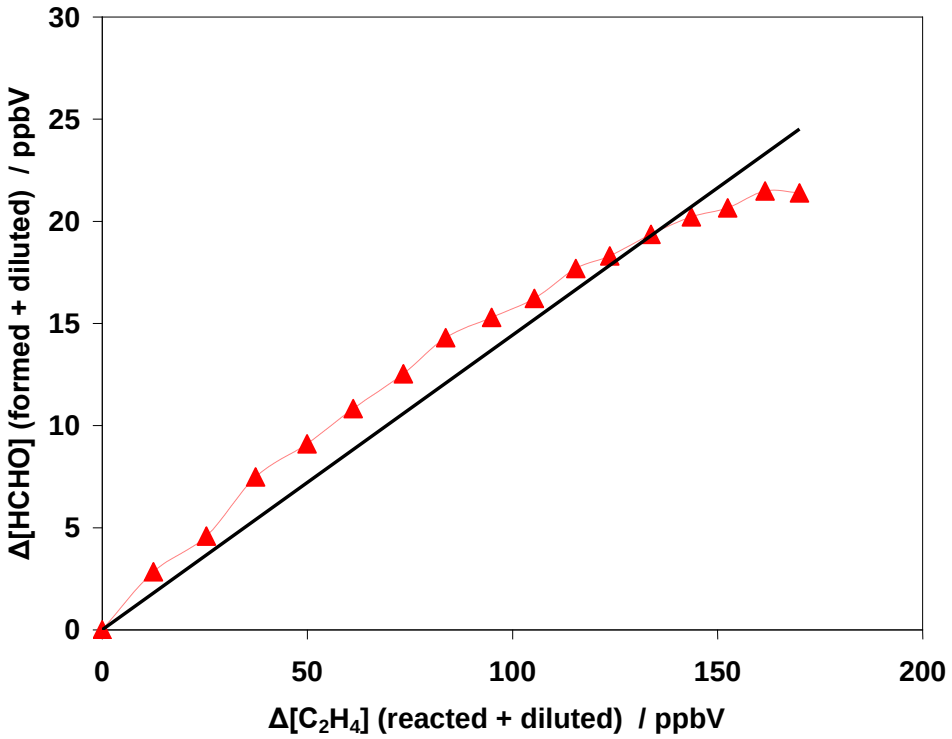


**Figure 2.8.** Typical observed regression line of HCHO formation as a function of ethene reacted, in the EUPHORE chamber. The slope of the graph generally determines the yield of HCHO, which in this case is not accurate due to the curvature of the plot – owing to ~ 60 % loss of ethene *via* dilution.

However, the stable product yields can also be calculated manually from the OH scavenger experiments, as under these conditions, alkene sinks are limited to reactions with ozone and dilution; and HCHO is formed by direct decomposition of the primary ozonide (and reaction of stabilised Criegee intermediate + CO, if from excess CO experiments):

$$\frac{d[C_2H_4]}{dt} = -k[C_2H_4][O_3] - k_{dil}[C_2H_4] \qquad \text{(EQ2.7)}$$

where $k_{dil}$ is the dilution rate constant. HCHO is formed from the $C_2H_4 + O_3$ reaction and is lost *via* dilution:

$$\frac{d[HCHO]}{dt} = +\alpha \quad k[C_2H_4][O_3] - k_{dil}[HCHO] \qquad \text{(EQ2.8)}$$

The variation of $C_2H_4$ and HCHO can be calculated considering a short time step, $\Delta t$:

$$\Delta[C_2H_4] = (-k[C_2H_4][O_3] - k_{dil}[C_2H_4])\Delta t \qquad \text{(EQ2.9)}$$

$$\Delta[HCHO] = (+\alpha k[HCHO][O_3] - k_{dil}[HCHO])\Delta t \qquad \text{(EQ2.10)}$$

Thus, the chemical loss of $C_2H_4$ ($\Delta[C_2H_4]_{chem}$) can be evaluated at any point in time by correcting the observed $C_2H_4$ loss for the dilution loss:

$$\Delta[C_2H_4]_{chem} = \Delta[C_2H_4] + k_{dil}[C_2H_4]\Delta t \qquad \text{(EQ2.11)}$$

$$\Delta[HCHO]_{chem} = \Delta[HCHO] + k_{dil}[HCHO]\Delta t \qquad \text{(EQ2.12)}$$

If the data are considered at a suitably small time-step (*e.g.* $\Delta t$ = 5 min, similar to that of the FTIR average sampling time), then the yield can be calculated from the measurements (between t and $\Delta t$) by EQ2.13, as there is little variation in $k_{dil}[C_2H_4]$ over $\Delta t$:

$$\alpha = \text{yield} = -\frac{\Delta[HCHO]_{chem}}{\Delta[C_2H_4]_{chem}} = \frac{[HCHO]_{t+\Delta t} - [HCHO]_t + k_{dil}([HCHO]_{t+\Delta t} + [HCHO]_t)/2 \quad \Delta t}{-([C_2H_4]_{t+\Delta t} - [C_2H_4]_t + k_{dil}([C_2H_4]_{t+\Delta t} + [C_2H_4]_t)/2 \quad \Delta t)}$$

(EQ2.13)

However, plotting the graph $\Delta[HCHO]_{chem}$ *vs*. $\Delta[C_2H_4]_{chem}$ does not allow us to access the HCHO yield, as the magnitudes of $\Delta[HCHO]_{chem}$ and $\Delta[C_2H_4]_{chem}$ during each FTIR 5 minute time step ($\Delta t$) is small in comparison to the error (precision) in the measurements, as illustrated in Figure 2.9.

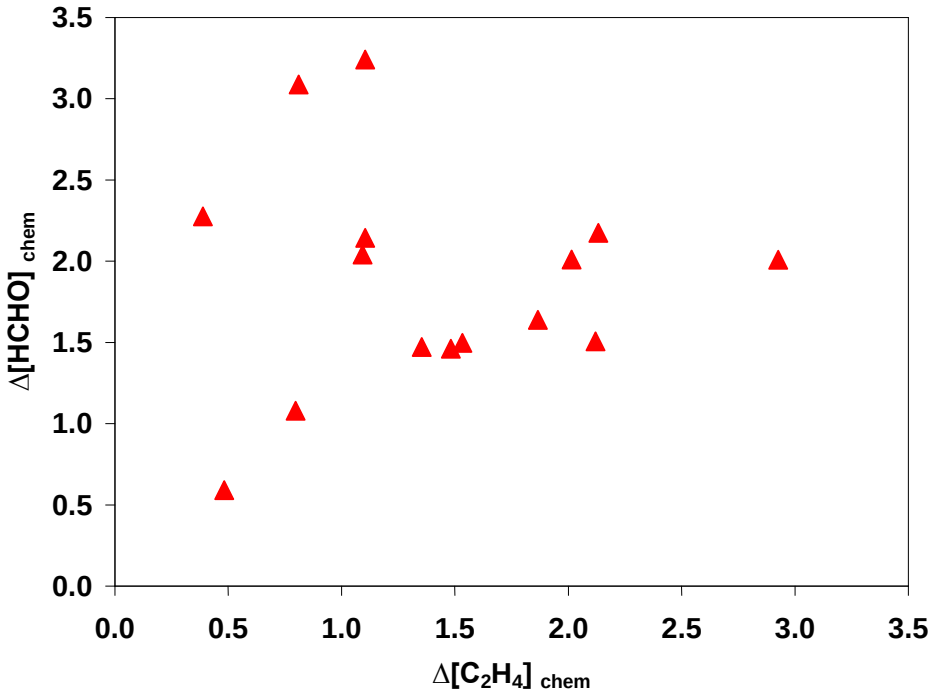


**Figure 2.9.** Dilution corrected correlation of $\Delta[HCHO]_{chem}$ and $\Delta[C_2H_4]_{chem}$ for each 5 minute time step ($\Delta t$)

The error in the measurements arises from the sum of the systematic and random errors. In order to decrease the random error and the scatter illustrated in Figure 2.9, the 'cumulative' HCHO production (and alkene loss) was used to calculate, from the slope of the graph, the overall yield ($\alpha$) of HCHO formed from $C_2H_4 + O_3$ (see Figure 2.10). However, while the random error of the measurements is decreased when using

the cumulative HCHO production yield, the systematic error is increased (due to the summation).

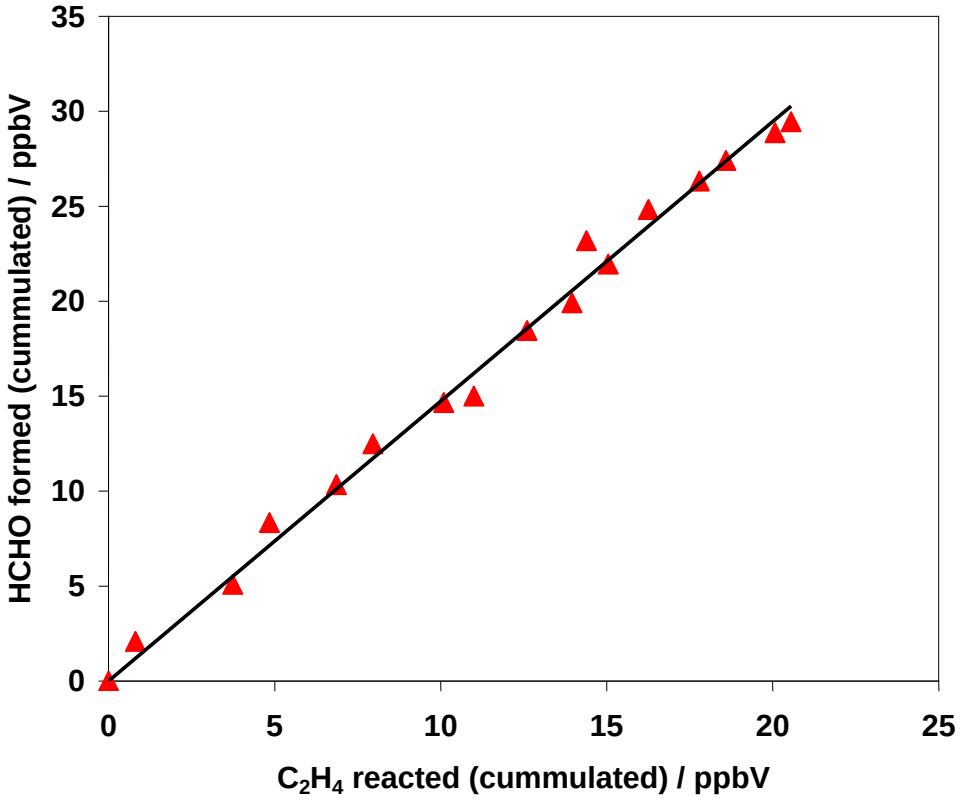


**Figure 2.10.** Formaldehyde production as a function of ethene reacted for an excess CO experiment. Data derived have been corrected for dilution as described in Section 2.6. The slope of the graph determines the yield of HCHO with respect to ethene reacted ($\alpha = 1.47$).

This method was utilised for the determination of all stable product yields from the ozonolysis of all alkenes studied and compared to those yields determined using the model; both of which were in excellent agreement. The following chapters (3 and 4), discuss the results obtained through application of the methodology described in this chapter.

# Chapter 3. Radical Production from Tropospheric Ethene Ozonolysis

In this chapter the results of a detailed study of ethene ozonolysis, performed under atmospherically relevant conditions, at the EUPHORE simulation chamber are presented. Experiments were performed with / without radical scavengers present, as discussed in Chapter 2. $HO_2$ and $HO_2 + \Sigma RO_2$ were observed using LIF and PERCA techniques, respectively; while stable species were measured by FTIR and CIR-TOF-MS. The observations were used to derive stable and radical product yields, using a detailed chemical mechanism based upon the MCM, to account for subsequent and secondary chemical reactions. The calculated yields for stable and radical products are then compared with recent literature and discussed in terms of branching ratios for various channels within the postulated reaction mechanisms.

## 3.1 Introduction

Ethene ($C_2H_4$), in terms of mass emission, is one of the most significant VOCs released into the environment; where its relatively high concentration enables detection at up to parts per billion (ppbV) levels in urban atmospheres (Altuzar et al., 2005, Ryerson et al., 2003). It has been estimated that exposure to 10 ppbV of ethene for one hour each week may lead to an increased lifetime risk of cancer amounting to approximately 70 cases per 100,000 people (Tornqvist, 1994). In terms of the

ozonolysis reaction mechanism, the simple structure of ethene ($H_2C=CH_2$) means that its reaction with ozone is unique, in that it cannot follow OH production *via* the hydroperoxide mechanism (Johnson and Marston, 2008, Calvert et al., 2000). The Criegee intermediate $[CH_2OO]^*$, formed from the ozonolysis of ethene is also a product formed from the ozonolysis of *all* terminal alkenes, including β–pinene, limonene, and the dominant non-methane hydrocarbon emitted into the atmosphere, isoprene. Thus it is essential to understand the fate and kinetics of the gas-phase reaction of ethene and ozone, as it is extremely difficult to interpret experimental measurements of ozonolysis of other terminal alkenes without first having a clear understanding of the reaction of simple chain alkenes.

## 3.2 Ethene Ozonolysis Mechanism

As mentioned in Chapter 1, the gas-phase ozonolysis of ethene is believed to proceed *via* the Criegee mechanism (Criegee, 1975) as illustrated in Figure 3.1. The reaction is initiated by the formation of a primary ozonide, POZ, (R3.1a), which rapidly decomposes, giving rise to a vibrationally excited Criegee intermediate and a stable (primary) formaldehyde molecule, R3.1b. The CI $[CH_2OO]^*$, has often been referred to as carbonyl oxide, dioxymethylene or peroxymethylene biradical, owing to its peculiar zwitterionic / biradical electronic structure. *Ab-initio* calculations have indicated that the ground state of the $[CH_2OO]^*$ CI is not the zwitterion or biradical, but may be regarded simply as a biradical, (Cremer et al., 1991, Gutbrod et al., 1997a, Olzmann et al., 1997) as illustrated in Figure 3.1. The significant amount of vibrational excitation retained within the carbonyl and CI co-products produced from

the exothermic decomposition of the POZ, R3.1b, enables further unimolecular reactions of the excited CI to occur, but the energy involved is not sufficient for the decomposition of the carbonyl compound to occur.

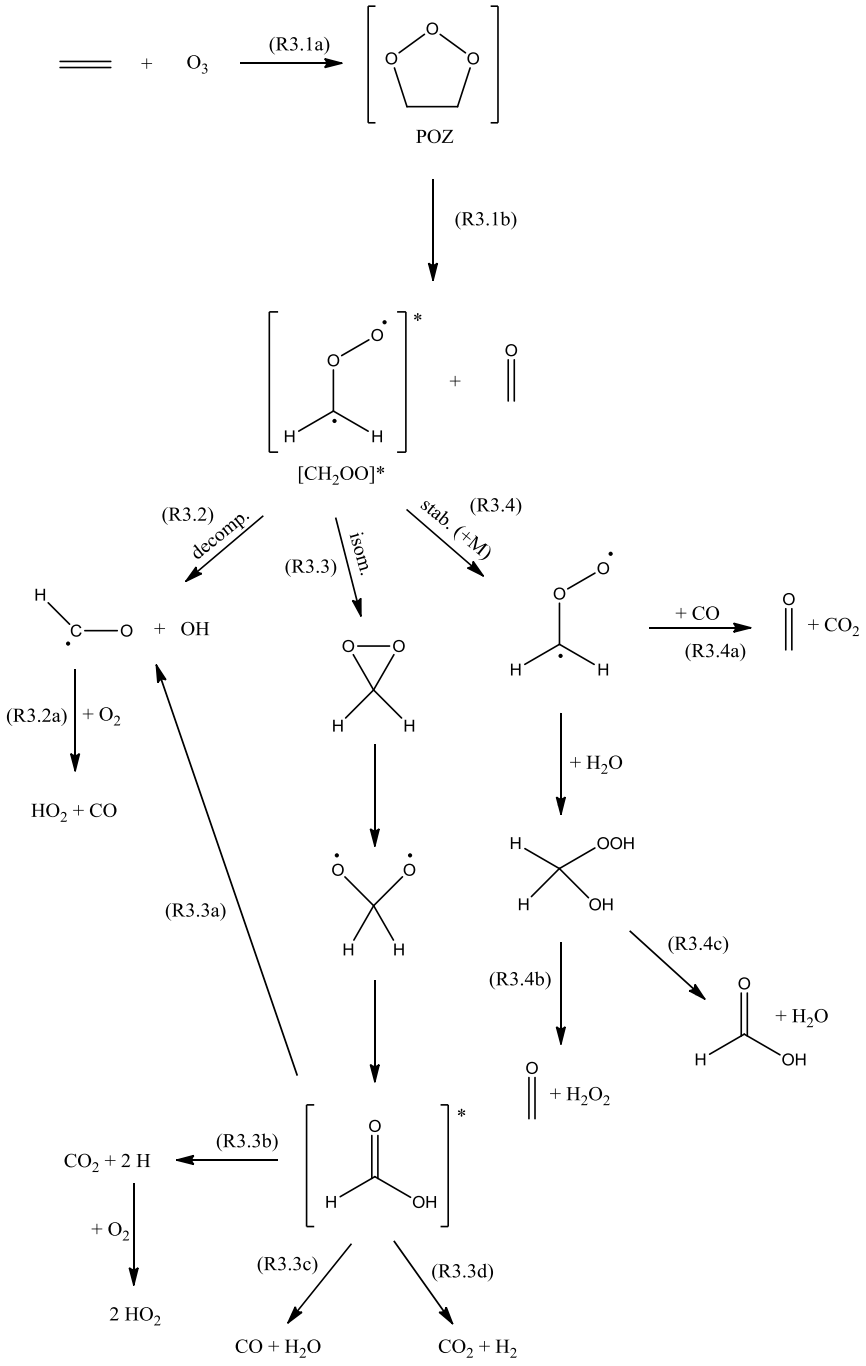


**Figure 3.1.** Schematic representation of the ethene ozonolysis reaction system. Adapted from Calvert et al. (2000); Johnson and Marston (2008) and Paulson et al. (1999).

Potential fates of the CI include:

(i) Direct rearrangement and decomposition via a four-membered transition state (R3.2).

(ii) Rearrangement through a dioxirane structure (R3.3) to a 'hot' acid intermediate, which can subsequently decompose to various products (R3.3a) – (R3.3d).

(iii) Stabilisation (R3.4) followed by bimolecular reactions R3.4a – R3.4c. The reaction mechanism shown in Figure 3.1, includes those possible fates of the stabilised Criegee intermediate (SCI), which could occur under the experimental conditions of this study. In the wider atmosphere, other reaction *e.g.* with $SO_2$ or $NO_2$ *etc.* may also occur, as discussed in Chapter 1.

*syn*-Mono and di-methyl substituted CIs are thought to predominantly decompose through isomerisation *via* a five-membered transition state to give an excited hydroperoxide species which subsequently decompose to give OH and a vinoxy radical; see Chapter 4 (Johnson and Marston, 2008). However, OH production is still observed in the ozonolysis of ethene, even in the absence of the so-called "hydroperoxide" mechanism, with the isomerisation / decomposition channels R3.2 and R3.3a postulated as the likely sources. There are a number of quantitative indirect OH yield measurements from the ozonolysis of ethene available in the literature, exploiting the use of radical tracer (Paulson et al., 1999b, Rickard et al., 1999) and scavenger (Chew and Atkinson, 1996, Gutbrod et al., 1997b) species. Direct observations at atmospheric pressure are scarce and challenging due to the reaction

rate coefficient for ethene + ozone ($1.59 \times 10^{-18}$ $cm^3$ $molecule^{-1}$ $s^{-1}$) being substantially slower than that for other alkenes (e.g. *ca*. 2 orders of magnitude slower than *cis*/*trans*-2-butene) (http://www.iupac-kinetic.ch.cam.ac.uk/, 2006) as well as the low OH yield, resulting in a low steady state [OH]. However, Donahue et al. (1998) and Kroll et al. (2001a) reported direct OH yield measurements at pressures between 10 – 60 Torr and at short timescales (*ca.* 10 ms). This was achieved as they found that the LIF sensitivity increased and OH-ethene rate constant decreased at low pressures, enabling the observation of steady state [OH]. The high barrier to reaction calculated for channel R3.2 (Gutbrod et al., 1996) together with pressure independent OH yields (Kroll et al., 2001a) leads to the suggestion that it is the fragmentation of the 'hot' acid (R3.3a) that is the dominant source of OH, rather than formation *via* the four-membered transition state (R3.2).

The recommended OH yield in the literature from ethene ozonolysis at atmospheric pressure is 0.16 (http://www.iupac-kinetic.ch.cam.ac.uk/, 2006). Measurements of $HO_2$ and/or potential $RO_2$ production, however, are much more limited and so the production of these contributors to $HO_x$ is uncertain. Ethene oxidation commonly occurs in moderate to high $NO_x$ environments (Ryerson et al., 2003) leading to rapid NO-mediated radical cycling, therefore $HO_2$ and/or potential $RO_2$ production can have a similar impact to direct OH production. Recently, $HO_2$ yields measured at atmospheric pressure from ethene ozonolysis reported by Qi et al. (2006) using PERCA of 0.38 ± 0.02 and Mihelcic et al. (1999) using matrix isolation with electron spin resonance (MIESR) of 0.39 ± 0.03, suggest that yields inferred from indirect studies may be underestimated by a factor of 3 (http://www.iupac-kinetic.ch.cam.ac.uk/, 2006). Wegener et al. (2007) indirectly inferred radical yields

for a range of alkenes, from long-duration (24 – 48 hr) experiments performed in the SAPHIR simulation chamber. The authors reported yields of 0.00 ± 0.05 for OH, and 0.50 ± 0.25 for $HO_2$, which were determined from $C_2H_4$ and $O_3$ temporal profiles, with indications that the radical yields may be dependent upon humidity.

A yield for H atoms of 0.076 ± 0.060 produced from ethene ozonolysis in the absence of $O_2$ (at 5 Torr), has also been reported by Kroll et al. (2001a), which may result from the decomposition of the formyl radical (HCO) formed *via* R3.2 and R3.3a and/or via the 'hot' acid R3.3b. Currently, atmospheric mechanisms, for example the Master Chemical Mechanism, employ radical yields which are largely inferred through the observation of associated stable products using assumed mechanisms (Saunders et al., 2003, Jenkin et al., 1997). The MCMv3.1 uses a value of 0.13 for both OH and $HO_2$ yields, similar to the earlier OH yield recommendation of 0.12 calculated using scavenger techniques (Atkinson, 1997b).

## 3.3 Experimental

The experimental approach, initial concentrations, box model and methodology is discussed in detail in Chapter 2. In this section, a brief methodology is presented in the form of the flow diagram below:

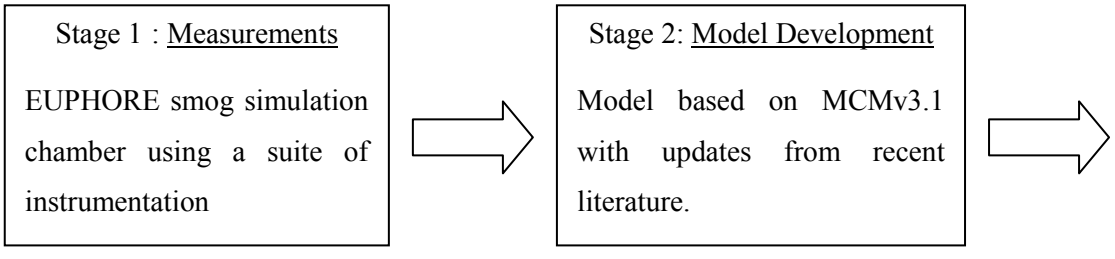

Stage 3: Rate Constant Optimisation

The ethene + ozone reaction rate coefficient was optimised using the FTIR observations for ethene and ozone.

Stage 4: Stabilised Criegee Intermediate Calculation

The stabilised Criegee intermediate yield was derived by calculating the overall HCHO yield from ethene ozonolysis in the presence of excess CO and subtracting 1. An appropriate branching ratio was then applied to the ozonolysis mechanism.

Stage 5: OH Optimisation

The yield of OH was optimised for ethene + ozone in the presence of cyclohexane. This was achieved by minimising the sum of the squares of residuals between the simulations and observations for cyclohexanone, cyclohexyl-hydroperoxide and $HO_2$, whilst optimising the ratio $k_{2.21}/k_{2.22}$ and OH yield and constraining $C_2H_4$ and $O_3$ to their observed levels. The derived branching ratio was then applied to the ozonolysis mechanism.

Stage 6: $HO_2$ Optimisation

The yield of $HO_2$ was optimised for all experiment types, by minimising the sum of squares of the residuals between the observations (LIF) and numerical simulations.

Stage 7: Branching Ratios

All experimental data were then used to derive branching ratios for various channels within the reaction mechanisms illustrated in Figure 3.1.

## 3.4 Results

### 3.4.1 Reaction Rate Coefficient, $k_{O_3+ethene}$

The ethene + ozone reaction rate coefficients, $k_{O_3+ethene}$, calculated from the scavenger experiments are shown in Table 3.1, where the indicated uncertainty is the combined precision (1σ) and systematic uncertainty of the instrumentation. The calculated $k_{O_3+ethene}$ of (1.45 ± 0.25) × $10^{-18}$ $cm^3$ $molecule^{-1}$ $s^{-1}$ at 298 K was subsequently used for all simulations performed. This value is in good agreement with previous studies (see Table 3.1) and is approximately 10 % lower than the IUPAC recommendation (http://www.iupac-kinetic.ch.cam.ac.uk/, 2006), which has an estimated uncertainty of ± 30 %. The rate constant for ethene ozonolysis is relatively slow in comparison to other small chain alkenes, such that the primary loss of ethene in the chamber is due to dilution (~ 60 %) rather than reaction with ozone.

### 3.4.2 Formaldehyde and Stabilised Criegee Intermediate Yields

The total HCHO yields (*i.e.* production *via* both pathways R3.1b and R3.4a) calculated from the excess CO experiments were 1.47 ± 0.11 and 1.61 ± 0.14, corresponding to a mean yield of 1.54 ± 0.12, where the indicated uncertainty is the combined precision (1σ) and systematic uncertainty of the instrumentation. The calculated branching ratio for the SCI ($Y_{SCI}$) is therefore 0.54. The HCHO yield was obtained from regression of the HCHO concentration as a function of the change in ethene concentration, after correction for dilution (as discussed in Chapter 2, see

Figure 2.10). The value is at the upper end of the previous reported literature range (Table 3.1). Figure 3.2 shows a comparison between the observed and modelled ethene, ozone and formaldehyde mixing ratios after optimisation of the ethene + ozone rate constant, and before / after optimisation of the SCI yield, for an excess CO experiment. Increasing the SCI yield from 0.37, as specified in MCMv3.1 to 0.54, calculated in this study, markedly improves the agreement between the HCHO observations and simulation.

**Table 3.1.** Comparison of reaction rate coefficient ($k_{O_3+ethene}$) and yield of stabilised Criegee intermediate $CH_2OO$ from this work and previous studies.

| **$10^{-18} \times k$ / $cm^3$ $molecule^{-1}$ $s^{-1}$ at 298 K** | **Yield of SCI ($Y_{SCI}$)** | **SCI Scavenger Type** | **Reference** |
|---|---|---|---|
| (1.33 ± 0.23) [a] | | | *This study* |
| (1.37 ± 0.24) [b] | | | *This study* |
| (1.55 ± 0.28) [c] | | | *This study* |
| (1.45 ± 0.25) | | | *This study (mean)* |
| (1.59 ± 0.30) | | | MCMv3.1 (IUPAC) |
| (1.45 ± 0.10) | | | Bahta et al. (1984) |
| (1.37 ± 0.08) | | | Treacy et al. (1992) |
| (1.59 ± 0.30) | | | Atkinson & Arey (2003) [e] |
| 1.44 [d] | | | Qi et al. (2006) |
| | 0.47 ± 0.11 | CO | *This study* |
| | 0.61 ± 0.14 | CO | *This study* |
| | 0.54 ± 0.12 | | *This study (mean)* |
| | 0.37 | | MCMv3.1 (IUPAC) |
| | 0.40 | | Atkinson & Lloyd (1984) |
| | 0.35 ± 0.05 | HCHO | Niki et al. (1981) |
| | 0.37 ± 0.02 | HCHO | Kan et al. (1981) |
| | 0.38 | HCHO | Su et al. (1980) |
| | 0.39 ± 0.11 | $H_2O$ and HCOOH | Hasson et al. (2001) |
| | 0.39 ± 0.05 | $SO_2$ | Hatakeyama et al. (1984) |
| | 0.47 ± 0.05 | Total yield of decomp., products | Horie & Moortgat (1991) |
| | 0.50 ± 0.04 | HCOOH | Neeb et al. (1996) |
| | 0.51 | Total yield of decomp., products | Neeb et al. (1998) |
| | 0.52 | $CF_3C(O)CF_3$ | Horie et al. 1999) |

[a] $k$ at 295.2 K [b] $k$ at 296.2 K [c] $k$ at 300.4 K [d] Error not specified. [e] Also recommendation of Calvert et al. (2000)

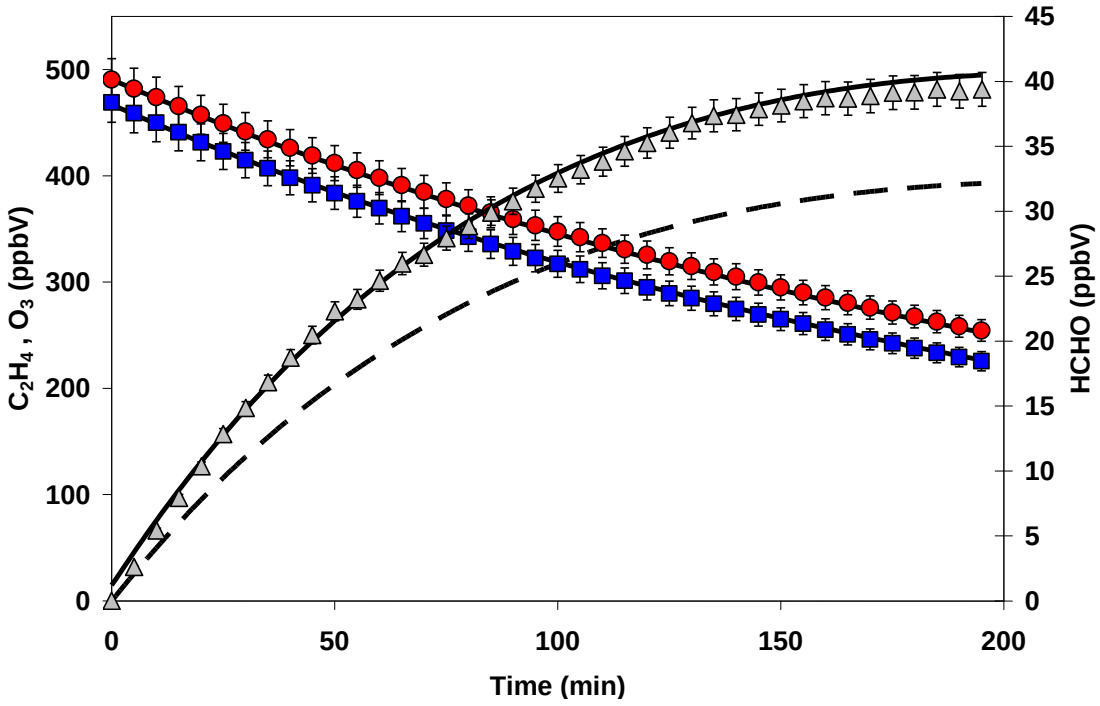


**Figure 3.2.** FT-IR Observed temporal profiles of $C_2H_4$ (red circles), $O_3$ (blue squares) and HCHO (grey triangles) plus model simulations (lines) for an excess CO experiment type (b). Model simulations for optimised $k_{O_3+ethene}$; with SCI branching ratio of 0.54 (solid line) and 0.37 (current IUPAC / MCMv3.1 recommended value) (dashed line).

### 3.4.3 OH Yield

The overall OH yield ($Y_{OH}$) for ethene ozonolysis in the presence of cyclohexane (OH scavenger experiment) was 0.17 ± 0.09 (shown in Table 3.2), which is thus attributed to the combined branching ratios R3.2 + R3.3a. The OH yield was determined by fitting the cyclohexanone, cyclohexyl-hydroperoxide and $HO_2$ observations (as described in Chapter 2, Section 2.5) and is shown in Figure 3.3. The importance of the knowledge of the detailed OH-initiated cyclohexane oxidation is demonstrated in Figure 3.3, where the current MCMv3.1 underestimates, the $HO_2$,

cyclohexyl-hydroperoxide and cyclohexanone yields. It was found that the best simultaneous fit to the OH-initiated cyclohexane oxidation products (*c*-$C_6H_{10}O$ and *c*-$C_6H_{11}OOH$), $HO_2$, ethene and ozone gave a $k_{2.21}/k_{2.22}$ (see Chapter 2, Figure 2.6) ratio of 0.44, which corresponds to the lower limit (*ca.* $5.0 \times 10^{-12}$ $cm^3$ $molecule^{-1}$ $s^{-1}$) of the previously determined literature values for $k_{2.22}$ of $1.70 \times 10^{-11}$ $cm^3$ $molecule^{-1}$ $s^{-1}$, (Boyd et al., 2003, Rowley et al., 1992) whilst using the MCMv3.1 $RO_2$ permutation rate coefficient (for > $C_3$ alkyl) of $2.5 \times 10^{-12}$ $cm^3$ $molecule^{-1}$ $s^{-1}$ for $k_{2.21a} + k_{2.21b} + k_{2.21c}$ overall (Jenkin et al., 1997). The branching ratios for reactions R2.21a, R2.21b and R2.21c used in the simulations were 0.6, 0.2 and 0.2 respectively, in good agreement with Rowley et al. (1991) who determined ratios of 0.58 and 0.42 for R2.21a and (R2.21b + R2.21c), respectively.

**Table 3.2.** Comparison of OH formation yields from this work and previous studies

| Yield of OH | Method | Reference |
|---|---|---|
| $0.17 \pm 0.09^*$ | *This Study* | *This study* |
| 0.16 | IUPAC | http://www.iupac-kinetic.ch.cam.ac.uk/ |
| 0.13 | MCMv3.1 | http://mcm.leeds.ac.uk/MCM |
| $0.18 \pm 0.06$ | Tracer | Paulson et al. (1999) |
| $0.14 \pm 0.07$ | Tracer | Rickard et al. (1999) |
| $0.20 \pm 0.02$ | MIESR | Mihelcic et al. (1999) |
| $0.12 \pm 0.06$ | Cyclohexane | Atkinson et al. (1992) |
| *ca*. 0.14 | Low pressure LIF | Kroll et al. (2001b) |
| $0.00 \pm 0.05$ | Stoichiometry | Wegener et al. (2007) |
| $\leq 0.05$ | Calculation | Gutbrod et al. (1996) |
| $0.08 \pm 0.01$ | CO | Gutbrod et al. (1997b) |
| $0.22 \pm 0.06$ | Tracer | Fenske et al. (2000) |

* The uncertainty in $Y_{OH}$ represents combined instrumental factors (51 %) and uncertainty associated with the branching ratio for decomposition of cyclohexoxy radical.

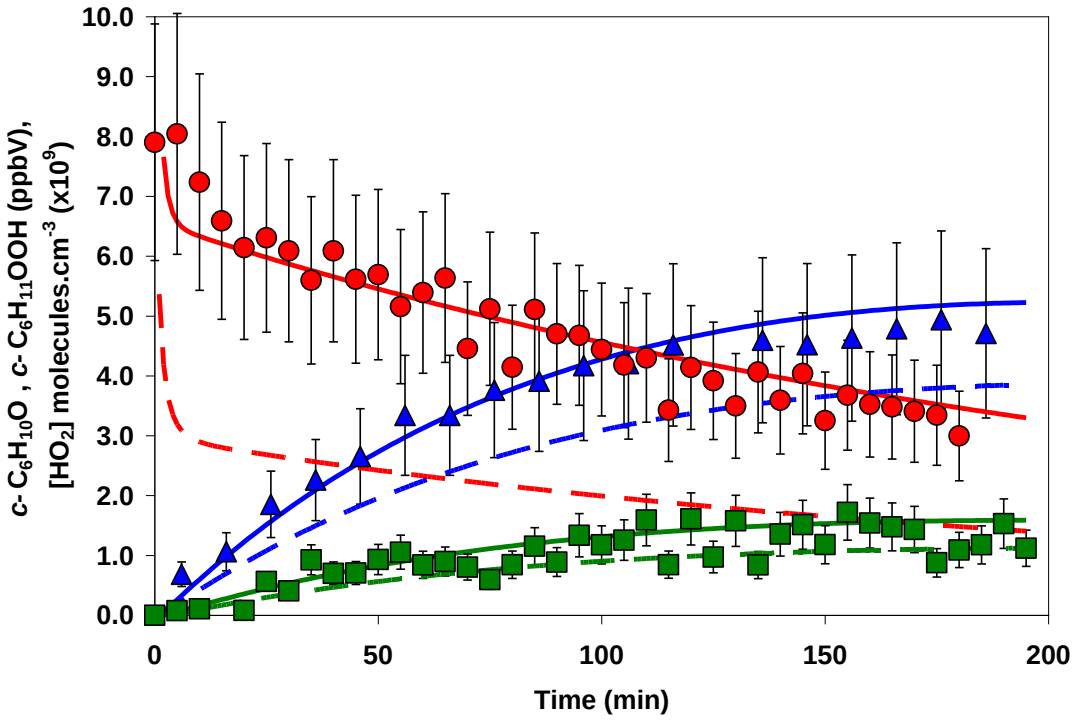


**Figure 3.3.** Observed temporal profiles of cyclohexanone (*c*-$C_6H_{10}O$ – green squares, from CIR-TOF-MS), cyclohexyl-hydroperoxide (*c*-$C_6H_{11}OOH$ – blue triangles, from HPLC) and steady state [$HO_2$] (red circles, from LIF) plus optimised (solid lines) and MCMv3.1 (dashed lines) model simulations for the excess cyclohexane scavenger experiment.

### 3.4.4 $HO_2$ Yield

The calculated yields of $HO_2$ ($Y_{HO_2}$) for the four types of experiments are shown in Table 3.3. For the simple ethene and ozone system (absence of scavenger) an $HO_2$ yield of 0.30 ± 0.08 was determined, where the indicated uncertainty arises from the uncertainty in the LIF system measurement. The value is derived from model simulations in which the ethene ozonolysis process (reactions R3.1 – R3.4 in Figure

3.1) is assumed to be effectively instantaneous on the timescale of the subsequent bimolecular chemistry ($HO_2$ + $HO_2$, $HO_2$ + $O_3$ *etc.*). The $Y_{HO_2}$ obtained is in reasonable agreement with the limited previous literature (Table 3.3).

**Table 3.3.** $HO_2$ yields derived *vs.* experimental conditions.

| Scavenger / Method | Yield of $HO_2$ | Reference |
|---|---|---|
| Simple $C_2H_4$ + $O_3$ | 0.30 ± 0.08 | *This study* |
| Excess CO (expt., 1) | 0.10 ± 0.03 | *This study* |
| Excess CO (expt., 2) | 0.10 ± 0.03 | *This study* |
| Excess cyclohexane | 0.24 ± 0.12 [a] | *This study* |
| Excess CO + $H_2O$ | 0.05 ± 0.01 | *This study* |
| Average [b] | 0.27 ± 0.07 | *This study* |
| MCMv3.1 | 0.13 | http://mcm.leeds.ac.uk/MCM |
| MI-ESR | 0.39 ± 0.03 | Mihelcic et al. (1999) |
| PERCA | 0.38 ± 0.02 | Qi et al. (2006) |
| Stoichiometry (Dry) | 0.50 ± 0.25 | Wegener et al. (2007) |
| Stoichiometry (Wet) | 0.40 ± 0.20 | Wegener et al. (2007) |

[a] The uncertainty in $Y_{HO_2}$ represents combined uncertainty from the instrumentation used (51 %) and uncertainty associated with the branching ratio for decomposition of cyclohexoxy radical.
[b] Average of simple + excess cyclohexane $HO_2$ yields.

A decrease in the observed $HO_2$ and $HO_2$ + $\Sigma RO_2$ measurements, performed by LIF and PERCA, respectively is seen when increasing the relative humidity from 0.2 to 29.0 %, as illustrated in Figure 3.4. The decrease seen in the observed $HO_2$ + $\Sigma RO_2$ measurements made by the PERCA instrument, however, is greater in comparison to the LIF measurements. $RO_2$ concentrations (which would presumably be $HOCH_2CH_2O_2$ and $CH_3O_2$ formed from OH + ethene and subsequent reactions) are expected to be minimal in this system, owing to the OH + ethene reaction being

suppressed by the excess CO in the system. Thus, the discrepancies between the two independent methods are likely owing to instrumental uncertainties or artefact(s). The LIF measurements are well simulated for the first ~ 95 minutes of the experiment, with an overall optimised yield of 0.10 for $HO_2$, but the model could not reproduce the observed decrease in $HO_2$ seen after increasing the humidity. The decrease in the simulated $HO_2$ observed when increasing the $H_2O$ concentration is solely due to the humidity dependence of the $HO_2$ self reaction, as there is no $H_2O$ dependence to the $HO_2$ yield from ethene ozonolysis in the basic mechanism within the model. The humidity dependence of the $HO_2 + HO_2$ reaction is well defined with an error of ~ 30 % (http://www.iupac-kinetic.ch.cam.ac.uk/, 2006); the reaction rate constant would have to be in error by a factor of 2 to account for the observations, suggesting that $Y_{HO_2}$ in the ozonolysis reaction decreases with increased humidity, under the conditions of these experiments (i.e. in the presence of excess CO).

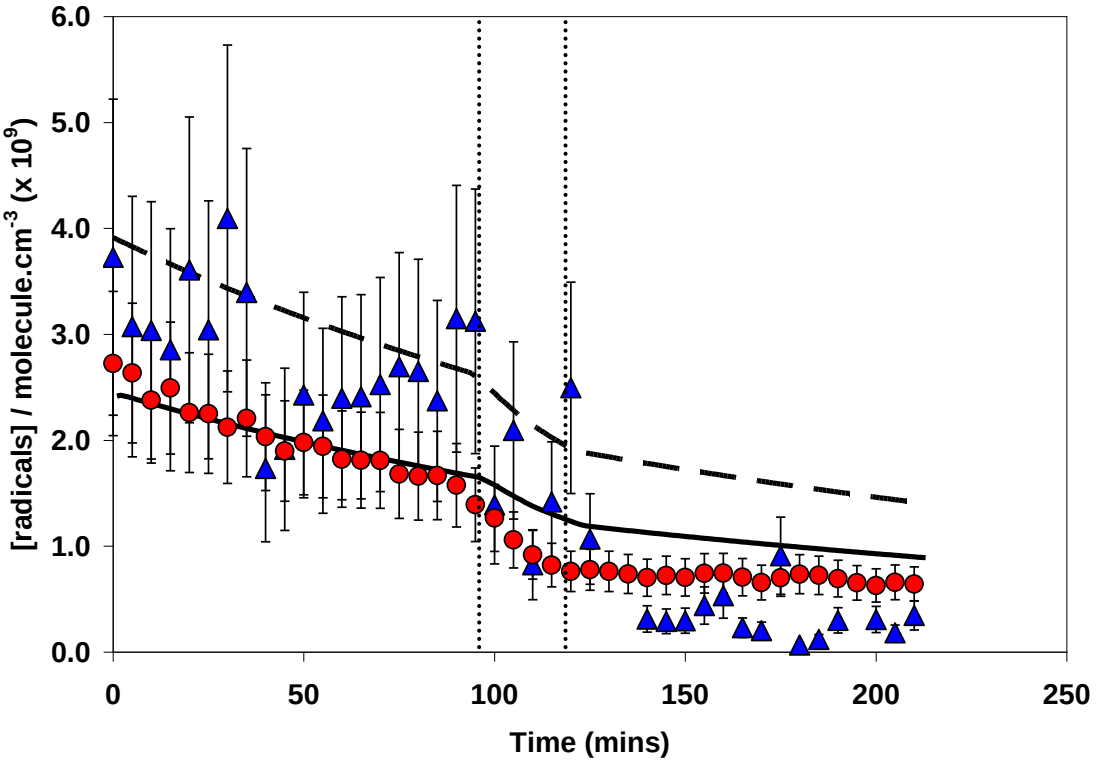


**Figure 3.4.** Temporal profile of $HO_2$ (LIF, grey circles) and $HO_2 + \Sigma RO_2$ (PERCA, black triangles) plus model simulations before (dashed line, base case MCMv3.1 chemistry) and after (solid line) optimising the $HO_2$ yield to the LIF data, for an excess CO scavenger experiment. $H_2O$ was added to increase the humidity from 0.2 % to 29 % RH over a 26 minute period from 97 min (dotted lines)**;** model includes impact of changed $HO_2$ upon secondary chemistry only (i.e. no change to $HO_2$ ozonolysis yield).

## 3.5 Discussion

### 3.5.1 Stabilised Criegee Intermediate Yield

The calculated SCI yield ($Y_{SCI}$) of 0.54 ± 0.12 is slightly larger than that found by the previous study of Hatakeyama et al. (1984) (0.39 ± 0.05), who measured the yield of sulphuric acid ($H_2SO_4$) formed from ethene ozonolysis in the presence of $SO_2$; where it was assumed that the SCI was scavenged by its reaction with $SO_2$, forming $SO_3$, which was further converted to $H_2SO_4$ aerosol (Hatakeyama et al., 1984). The similarity between both this study and that of Hatakeyama and co workers, is that the same reaction channel (R3.4) is exploited, but with the use of different scavengers. The yields determined by Su et al. (1980) and Niki et al. (1981) are also similarly lower than that obtained in this study, as shown in Table 3.1. These studies used long path FT-IR spectroscopy to measure the yield of hydroxy methyl formate (HMF, $HOCH_2OCHO$), a product from the reaction of $CH_2OO$ + HCHO. However, Neeb et al. (1995) later identified HMF as being hydroperoxy methyl formate (HPMF, $HOOCH_2OC(O)H$). The $Y_{SCI}$ value obtained here is, however, in good agreement with the studies of Neeb and co-workers who deduce the total yield of decomposition products from the excited CI (Neeb et al., 1998) and report a HPMF yield of 0.51 in the presence of excess HCOOH, exploiting the reaction SCI + HCOOH (Neeb et al., 1996). The $Y_{SCI}$ has also been found to be pressure dependent, where it is reported that a significant fraction (0.20 ± 0.03) of the initial $[CH_2OO]^*$ formed is thermally "cold" at low pressure (Hatakeyama et al., 1986) The authors determined this fraction by extrapolation of measurements over the range 13 mbar to 1.5 bar.

### 3.5.2 OH Yield Determination from Cyclohexane Scavenger Studies

The calculated $Y_{OH}$ of 0.17 ± 0.09 is in very good agreement with previous literature (Table 3.2). Paulson et al. (1999) and Rickard et al. (1999) employed OH radical tracer methods to obtain yields of 0.18 ± 0.06 and 0.14 ± 0.07 respectively, both of which are in good agreement with this study. Gutbrod *et al*. (1997b) used excess CO as an OH scavenger to deduce a $Y_{OH}$ of 0.08 ± 0.01 by detecting $CO_2$ as a product of the CO + OH reaction. The authors measure the increase in $CO_2$ upon addition of 30 Vol. % CO, on a background of a 26 % $CO_2$ yield without CO being added, which inherently leads to a less accurate determination of the OH yield from ethene ozonolysis (Gutbrod et al., 1997b). *Ab-initio* calculations made prior to their study, however, estimate a $Y_{OH}$ of ≤ 0.05 (Gutbrod et al., 1996). Atkinson and co workers reported an $Y_{OH}$ of 0.12 using cyclohexane as an OH scavenger, which is also found to be in reasonable agreement with the value determined in this study, but has a reported uncertainty of a factor of 1.5 (*i.e.* ± 0.06) owing to the unknown $HO_2$ concentration in the system, and therefore uncertain contribution of the $HO_2 + O_3$ reaction to the total OH (Atkinson et al., 1992). Previous studies exploiting excess cyclohexane as an OH scavenger have monitored the evolution of alkene ozonolysis relative to the production of cyclohexanone + cyclohexanol (or cyclohexanone itself) to determine an OH yield, providing that the yield of cyclohexanone (+ cyclohexanol) from the OH-initiated oxidation of cyclohexane was known. The yield of OH is then determined by using the following EQ3.1:

$$Y_{OH} = \frac{[\text{cyclohexanone}](+[\text{cyclohexanol}])/\Delta[\text{alkene}]}{[\text{cyclohexanone}](+[\text{cyclohexanol}])/\Delta[\text{cyclohexane}]} \qquad \text{(EQ3.1)}$$

Several studies have calculated the yield of cyclohexanone + cyclohexanol from the OH-initiated oxidation of cyclohexane, reporting a range of values between 0.50 – 0.88 (Atkinson and Aschmann, 1993, Atkinson et al., 1992, Rowley et al., 1991, Berndt et al., 2003) More recently, the $Y_{OH}$ has been determined by monitoring the evolution of the alkene relative to the production of cyclohexanone only (Malkin et al., 2010, Berndt et al., 2003, Winterhalter et al., 2009) where a range of yields of cyclohexanone from the OH-initiated oxidation of cyclohexane have also been reported: 0.26 – 0.53 (Atkinson et al., 1992, Berndt et al., 2003, Calvert et al., 2000, Malkin et al., 2010, Rowley et al., 1991). However, a study of the mechanism of the self reaction of $CH_3OCH_2O_2$, analogous to *c*-$C_6H_{11}O_2$, suggests that the yield of cyclohexanone from the OH-initiated oxidation of cyclohexane should always be close to 0.5 (Jenkin et al., 1993). The range in the reported yields is likely to arise from the varying flux through the $HO_2$ + *c*-$C_6H_{11}O_2$ reaction (see Figure 2.6, R2.22) between studies. The less than unity yield of cyclohexanone and cyclohexanol therefore arises owing to the yield of cyclohexyl-hydroperoxide being dependent on the $HO_2$ concentration, in competition with reactions R2.21a, R2.21b and R2.21c, as well as the decomposition / isomerisation reactions of the cyclohexoxy radical (reactions R2.23b and R2.23c in Figure 2.6). The yields of cyclohexanone and cyclohexanol observed will therefore depend upon the relative concentrations of $RO_2$ and $HO_2$ radicals (and $RO_2$ speciation) present, and will therefore be dependent on the specific reaction system, as well as the reagent concentrations used. Thus, this scavenger technique may result in a large variation in $Y_{OH}$ if applied to systems where the $HO_2$ and/or $RO_2$ present differ from those under which the cyclohexanone / cyclohexanol yields from cyclohexane were originally determined.

In addition, calculations show that owing to the slow ethene + $O_3$ rate coefficient and the low OH yield, approximately 40 % of the OH formed in the overall ethene + ozone system comes from R3.5, which should be taken into account when calculating $Y_{OH}$ using scavenger experiments, *via* EQ3.1:

$$HO_2 + O_3 \rightarrow OH + 2O_2 \qquad (R3.5)$$

Hence, if the $Y_{OH}$ were calculated using EQ3.1, while adopting an average cyclohexanone yield of 0.528 from recent cyclohexane + OH oxidation studies; (Berndt et al., 2003, Malkin et al., 2010) an overall OH yield of 0.09 ± 0.02 would be obtained, where ~ 40 % of this calculated OH yield would be due to the reaction of $HO_2 + O_3$, giving rise to an $Y_{OH}$ of 0.05 for the decomposition of $[CH_2OO]^*$. This value is a factor of 3 smaller than the value determined through the model optimisation approach, described in Chapter 2, Section 2.5. This highlights the importance of considering the detailed scavenger chemistry as well as the concentration of $HO_2$ under high $[O_3]$ / [ethene] conditions. Mihelcic et al. (1999) determined a $Y_{OH}$ of 0.20 ± 0.02, measuring $HOCH_2CH_2O_2$ using the MIESR technique, and attributed this to OH, as this peroxy radical is a direct product of the $C_2H_4$ + OH reaction. The larger $Y_{OH}$ can be explained if the additional secondary OH formation from $HO_2 + O_3$ is taken into account; which subsequently reacts with $C_2H_4$ forming additional $HOCH_2CH_2O_2$. Under the conditions of this study, if the secondary OH formation *via* R3.5 is combined with the 0.17 OH yield determined for the direct isomerisation / decomposition of $[CH_2OO]^*$, (calculated by OH yield optimisation simulations, in which the $HO_2 + O_3$ reaction is accounted for), an OH formation (primary and secondary) yield of 0.24 would be obtained.

The first direct evidence for OH formation in the ethene ozonolysis system was measured by LIF at a total pressure of 5 Torr, with a reported $Y_{OH}$ of 0.43 ± 0.20 (Donahue et al., 1998). Subsequent studies from the same laboratory suggested that there was no pressure dependence of the OH radical formation from ethene ozonolysis (Kroll et al., 2001b, Kroll et al., 2001c) and reported a refined $Y_{OH}$ of 0.14, corresponding to prompt OH production over short timescales (~ 30 ms) at pressures between 10 – 60 Torr (Kroll et al., 2001b). This finding suggests that OH is not formed by the direct dissociation of the excited CI $[CH_2OO]^*$, but rather *via* fragmentation of a 'hot' formic acid intermediate, as illustrated in Figure 3.1, reaction R3.3a. In contrast, however, the pressure dependence of OH yields was also investigated by Fenske et al. (2000) who reported an increase in the $Y_{OH}$ with decreasing pressure from 0.22 ± 0.06 at 760 Torr to 0.61 ± 0.18 at 20 Torr. The authors proposed an alternative biradical pathway at low pressures, but could not preclude that the 'hot' formic acid formed from the dioxirane could serve as a pressure dependent source of OH (Fenske et al., 2000b). The authors also outlined that the reduction in the $Y_{SCI}$ observed by Hatakeyama et al. (1986) at low pressures, may indicate that a larger proportion of the initially formed excited CI could undergo decomposition / isomerisation resulting in an increase in $Y_{OH}$ at lower pressures. Conversely, Kroll et al. (2001c) attributed this increase in OH production at low pressures to bimolecular reactions of reactive intermediates, which could be significant over longer timescales. To date, direct measurements of OH from ethene ozonolysis at atmospheric pressure have not been achieved. Thus, although there is strong evidence that the formation of OH comes from the fragmentation of 'hot' formic acid at low pressures (10 – 60 Torr) and short time scales (on the order of ms), the absence of direct measurements at atmospheric pressure for ethene ozonolysis,

both at short and long timescales, means that OH formation from the direct dissociation of the excited CI $[CH_2OO]^*$ cannot be precluded. As illustrated in Figure 3.1, the production of OH may result from both channels R3.2 and R3.3a. The data obtained in this study cannot distinguish between the two independent routes and so the channels R3.2 and R3.3a are summed to give an overall OH yield.

### 3.5.3 $HO_2$ Yield

The measured $HO_2$ yields ($Y_{HO_2}$) for the different types of experiments performed in this study are shown in Table 3.3, where the average derived $Y_{HO_2}$, together with recent literature, suggests that the yield of $HO_2$ currently used in the MCMv3.1 (0.13) is underestimated by a factor of 2. Recently, Wegener et al. (2007) exploited reaction R3.5 to evaluate $HO_2$ formation from assessing the additional ozone turnover (over and above that due to reaction with ethene) in excess CO experiments, deriving an $HO_2$ yield, $Y_{HO_2}$ of 0.50 ± 0.25. The secondary formation of OH *via* R3.5 disturbs the accurate determination of $Y_{OH}$, making it difficult to optimise reaction conditions to determine both $Y_{OH}$ and $Y_{HO_2}$ at the same time. Their reaction conditions were chosen such that OH would preferentially be produced by ozonolysis and consumed by reaction with ethene, while suppressing the turnover of R3.5. The contribution of ozone removal *via* reaction with $HO_2$, relative to the removal *via* reaction with ethene or dilution is therefore small, resulting in a large uncertainty in the derived $Y_{HO_2}$ of 0.50 ± 0.25, but is in agreement (within uncertainty) with this work. The PERCA $HO_2 + \Sigma RO_2$ data obtained here are consistent (within uncertainty) with the $HO_2$ observations for the ethene/ozone/CO system (Figure 3.4). The observations indicate

that organic peroxy radical levels in this system are small, which is in accord with the postulated mechanism shown in Figure 3.1. Additionally, the PERCA data, independently, display the same trend with the addition of water vapour as the LIF $HO_2$ observations, over and above that anticipated from the humidity dependence of the $HO_2$ self-reaction, as discussed in Section 3.3.4. The observed decrease in $Y_{HO_2}$ when increasing the relative humidity from 0.2 to 29.0 % is in qualitative agreement with Wegener et al. (2007) who report decreases, albeit with large uncertainty, in $Y_{HO_2}$ with enhanced humidity for ozonolysis of ethene (0.50 ± 0.25 to 0.40 ± 0.20), propene (1.50 ± 0.75 to 1.15 ± 0.60) and isobutene (2.00 ± 1.00 to 1.60 ± 0.08).

Mihelcic et al. (1999) measured $Y_{HO_2}$, using MIESR, in the presence and absence of excess CO as an OH scavenger. They found that the overall $Y_{HO_2}$ increased from 0.39 to 0.66 in the presence of excess CO, which they attributed to the total $HO_x$ radical yield (OH + $HO_2$) (Mihelcic et al., 1999). The observed increase in $Y_{HO_2}$ in the presence of CO is in contrast to this work, where a decrease in $Y_{HO_2}$ was observed (after accounting for additional $HO_2$ production via OH + CO). Mihelcic et al. (1999) however, used large initial concentrations of ethene (*ca*. 125 – 350 ppmV) so that the ozonolysis kinetics were kept pseudo-first-order with respect to $O_3$, and used a reaction rate coefficient, $k_{O_3+ethene}$, which is 40 % smaller than the currently accepted value for their calculations. The authors state that the use of the currently recommended value for $k_{O_3+ethene}$ in their calculations would result in the radical yields decreasing by ~ 40 %.

### 3.5.4 Possibilities for the reduced $Y_{HO2}$ in the presence of excess CO

There are three different product channels that form $HO_2$ from the ethene ozonolysis system:

i. Direct decomposition of the CI to form OH + HCO (HCO + $O_2$ → $HO_2$ + $CO_2$) (R3.2a, in Figure 3.1)
ii. The branching ratio product from the fragmentation of 'hot' formic acid forming OH + HCO (R3.3a) followed by HCO + $O_2$ → $HO_2$ + $CO_2$ (R3.2a, in Figure 3.1)
iii. Branching ratio R3.3b; $CO_2$ + 2H (H + $O_2$ + M → $HO_2$ + M).

The decrease in $Y_{HO_2}$ observed in this study in the presence of excess CO is not consistent with the mechanism presented in Figure 3.1, as one would expect the $Y_{HO_2}$ to remain the same while the observed [$HO_2$] would increase due to the formation of $HO_2$ *via* the reaction of OH + CO. In order to account for this behaviour, three potential explanations are considered:

#### 3.5.4.1 Bimolecular Reaction with the Partial SCI

Previous studies have shown that OH formation from alkene ozonolysis can result from both prompt formation from a vibrationally excited CI and formation from the decomposition of a "thermalised" CI, at longer timescales (Johnson and Marston, 2008, Kroll et al., 2001c). Thus, there may be a possibility for bimolecular reactions to occur with the thermalised CI, which would interrupt the decomposition process, particularly in the presence of excess CO, as illustrated in Figure 3.5. This theory,

however, has not been tested for the $CH_2OO$ CI and/or CO as the scavenger, but was partially tested by Johnson et al. (2001) for the ozonolysis of 2-methyl-2-butene in the presence of the Criegee scavengers $H_2O$, $SO_2$, butanone and acetic acid. The authors concluded that bimolecular reactions with the studied scavengers were too slow to inhibit OH formation (Johnson et al., 2001). In the ozonolysis of 2-methyl-2-butene, however, the likely fate for two of the CIs formed (*syn*-$[CH_3CHOO]^*$ and $[(CH_3)_2COO]^*$) are isomerisation / decomposition forming OH *via* the hydroperoxide mechanism which is reported in being 3 – 8 orders of magnitude faster than the thermalised CI reaction with water (Kuwata et al., 2010). Thus CI scavengers are more likely to interrupt the decomposition of thermalised *anti*-CIs (or $CH_2OO$) as the hydroperoxide mechanism is absent. The proposed bimolecular reaction of CO with the stabilised CI would, however, only account for approximately 60 % of the overall observed $HO_2$ reduction in the CO scavenger experiments, if it is assumed that as an upper limit 100 % of the OH formation from ethene ozonolysis at atmospheric pressure comes from the direct decomposition of $[CH_2OO]^*$ (as shown in Figure 3.5) and not from the 'hot' formic acid. Scavenging of the partially stabilised CI, by CO, would also contribute to the observed HCHO yield, as a product of the CO + SCI reaction, altering the overall SCI yield inferred in Section 3.3.2.

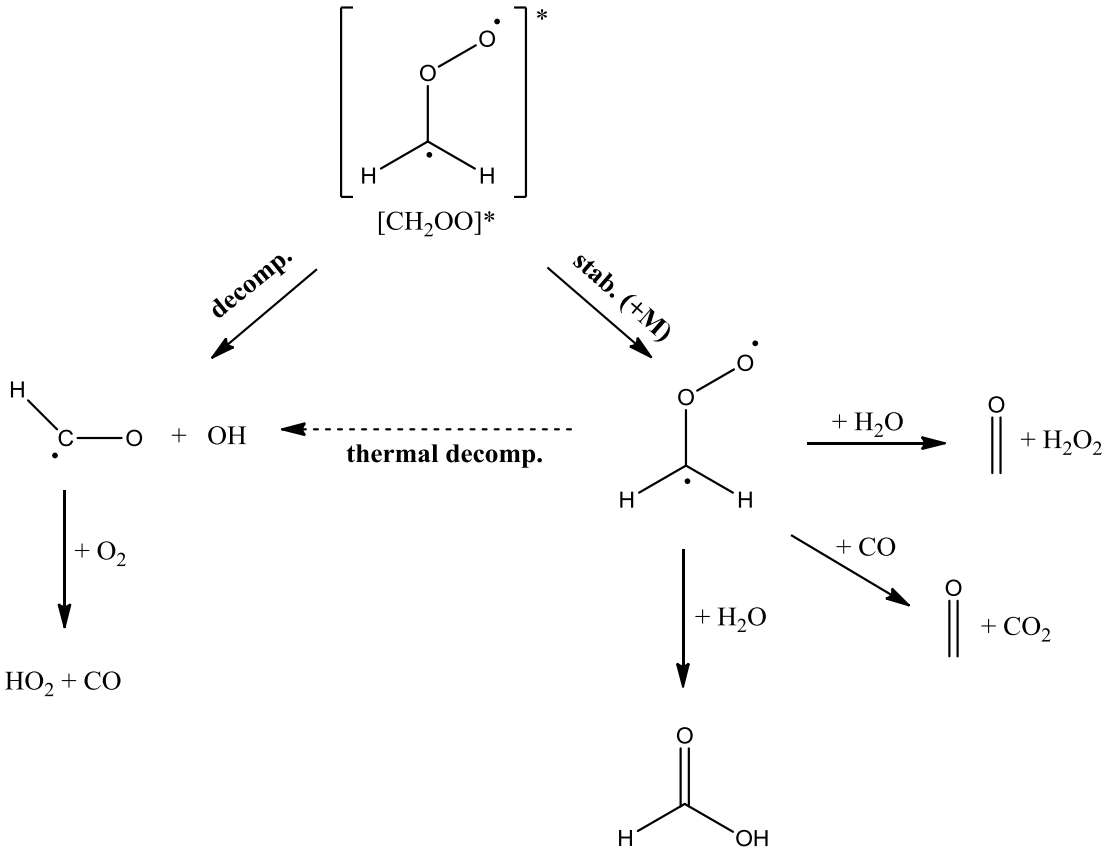


**Figure 3.5**. Possible routes to OH formation from the vibrationally excited CI. Adapted from Johnson and Marston (2008)

### 3.5.4.2 Formic Anhydride Formation from CO + dioxirane

The reaction of dioxirane with CO resulting in the formation of formic anhydride (FAN) (see Figure 3.6), is an additional possible explanation for the observed reduction in $Y_{HO_2}$ in the presence of excess CO (Kuhne et al., 1976, Hatakeyama and Akimoto, 1994) as this would interrupt the formation of $HO_2$ *via* channels R3.3a and R3.3b. Kuhne and co workers reported an increase in the yield of FAN in the presence of excess CO (Kuhne et al., 1976), while Su et al. (1980) reported a yield of

0.24 for FAN in the presence of excess CO, using FTIR. Kan et al. (1981) attributed the formation of FAN to the decomposition of hydroxyl methyl formate (HMF, $HOCH_2OCHO$), a product of the reaction of SCI + HCHO; however, more recently, the infrared spectrum attributed to HMF was reassigned to hydroperoxy methyl formate (HPMF, $HOOCH_2OCHO$) (Neeb et al., 1995), a product of the reaction of SCI + HCOOH, and a combined yield of 0.18 was assigned for both HPMF and FAN (Neeb et al., 1998). Wolff et al. (1997) not only confirmed the formation of HPMF from ethene ozonolysis in the presence of excess HCOOH using FTIR, but also observed HPMF in the absence of HCOOH using HPLC. All these studies, however, use relatively high levels of reactants, *i.e.* 2 – 10 ppmV of ethene and ozone, and either 5 – 50 ppmV of HCHO or 1 – 10 ppmV of HCOOH (larger concentrations, ≥ 100 ppmV, are used by Wolff et al. (1997)), in order to scavenge the SCI. Under the conditions of our experiments, the SCI would be expected to react with the excess CO present, rather than HCOOH and/or HCHO, and thus FAN would not be expected to arise from the decomposition of HPMF formed from the SCI + HCOOH reaction.

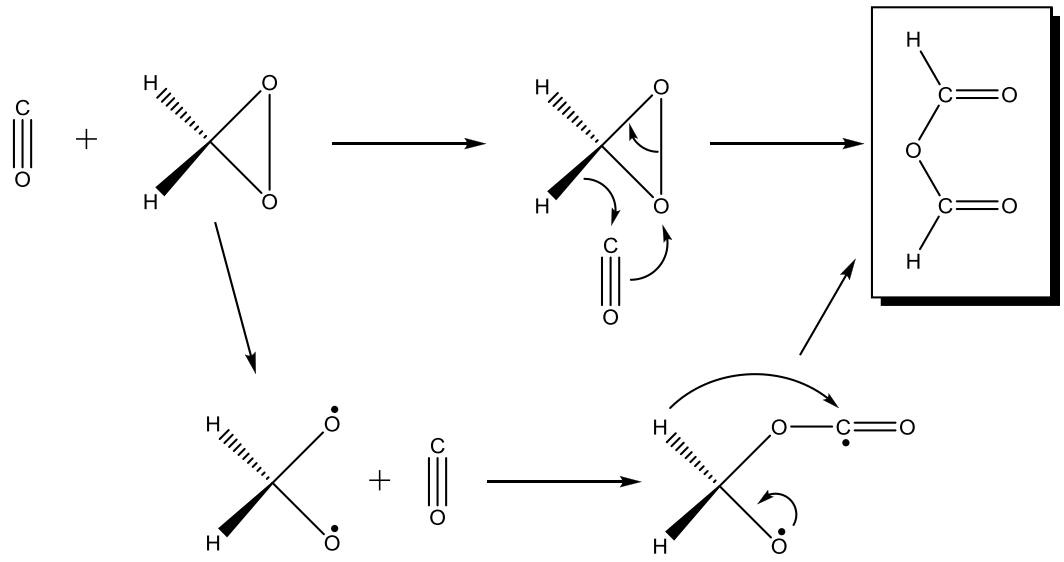

**Figure 3.6**. Proposed mechanism for the formation of formic anhydride (FAN). From Kuhne et al. (1976)

### 3.5.4.3 $HO_2$ Formation from SCI

The similar $HO_2$ yields obtained for the simple ethene-ozone experiment (0.30 ± 0.08) and in which excess cyclohexane was present (0.24 ± 0.12) may indicate that the presence of SCI scavengers could be responsible for the decrease in $Y_{HO_2}$. This could imply the occurrence of an independent $HO_2$ channel from the SCI, which may be inhibited in the presence of CO and/or $H_2O$. This radical pathway was proposed in a theoretical study investigating the unimolecular decomposition channels of hydroxymethyl hydroperoxide ($HOCH_2OOH$ or HMHP), the product of the $CH_2OO$ + $H_2O$ reaction (Crehuet et al., 2001). The authors reported that the water assisted decomposition of HMHP would yield further radical products (both OH and $HO_2$), which is in contrast to the results of this study.

## 3.6 Branching Ratios for the Decomposition of $[CH_2OO]^*$

The branching ratios for the postulated mechanism illustrated in Figure 3.1 were determined using the results reported in previous sections of this chapter. The calculated $Y_{SCI}$ (0.54, see Section 3.3.2) and $Y_{OH}$ (0.17, see Section 3.3.3), were attributed to channels R3.4 and the combined ratios (R3.2 + R3.3a), respectively. Using the average calculated $Y_{HO_2}$ (0.27 ± 0.07) from both for the simple (0.30 ± 0.08) and excess cyclohexane (0.24 ± 0.12) experiments, the product branching ratios R3.2, R3.3a and R3.3b can be assigned. The $Y_{OH}$ of 0.17 also corresponds to the total yield of HCO formed alongside OH; this HCO reacts near instantaneously with $O_2$

($5.1 \times 10^{-12}$ $cm^3$ $molecule^{-1}$ $s^{-1}$) (http://www.iupac-kinetic.ch.cam.ac.uk/, 2006) to form $HO_2$. The remaining branching ratio, R3.3b, is therefore 0.05, forming 2 molecules of $HO_2$. This also equates to a H atom yield of 0.10, which is in good agreement with the previously reported low pressure H atom yield of 0.076 ± 0.060 (Kroll et al., 2001a) suggesting that H atoms are formed *via* the hot acid channel, R3.3b, and not *via* HCO (R3.2a); in agreement with *ab-initio* calculations on the mechanism of HCO + $O_2$ (Martinez-Avila et al., 2003). Numerous studies have calculated the branching ratio for channel R3.3b, reporting a range of values between 0.06 – 0.10; (Calvert et al., 2000, Atkinson, 1997b, Atkinson and Lloyd, 1984, Herron and Huie, 1977, Horie and Moortgat, 1991, Thomas et al., 1993) all of which are in agreement, within uncertainty, with this study. With the quantification of the branching ratios determined during this study, the remaining branching ratios (R3.3c + R3.3d) are combined to 0.24. The branching ratios derived for reactions R3.1 – R3.4 are summarised in Table 3.4 and illustrated in Figure 3.7.

**Table 3.4.** Branching ratios derived for the $CH_2OO$* CI formed in the ozonolysis of ethene

| **Reaction Number (see Figure 3.7)** | **Reaction** | **Branching Ratio** |
|---|---|---|
| R3.2 + R3.3a | $CH_2OO^* \rightarrow OH + HCO$ | 0.17 |
| R3.3b | $CH_2OO^* \rightarrow CO_2 + 2\,H$ | 0.05 |
| R3.3c | $CH_2OO^* \rightarrow CO + H_2O$ | 0.24* |
| R3.3d | $CH_2OO^* \rightarrow CO_2 + H_2$ | |
| R3.4 | $CH_2OO^* \rightarrow CH_2OO$ | 0.54 |

* Combined branching ratio for reactions R3.3c and R3.3d

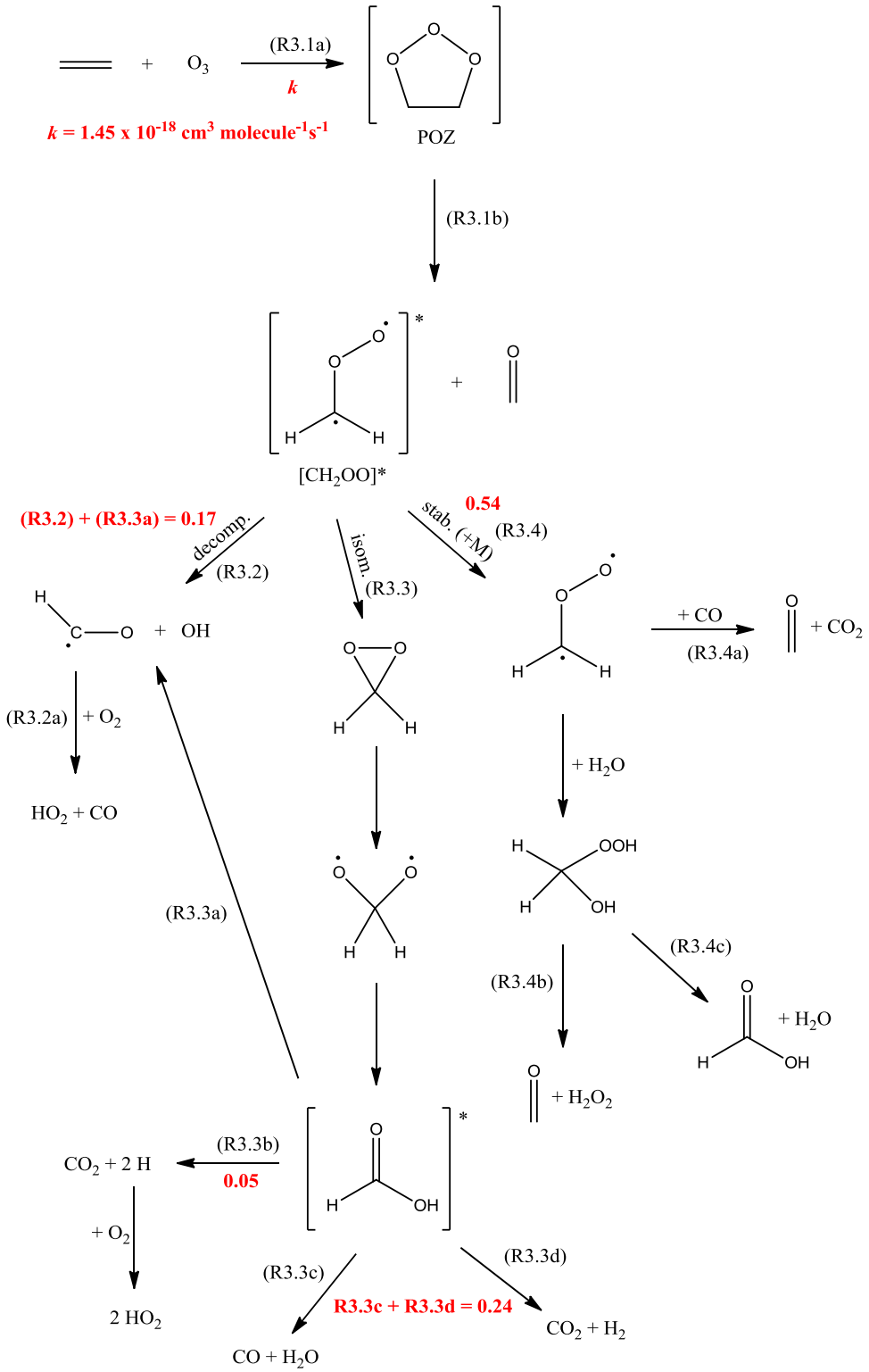


**Figure 3.7.** Schematic representation of the ethene ozonolysis reaction system with branching ratios. Adapted from Calvert et al. (2000); Johnson and Marston (2008) and Paulson et al. (1999).

# Chapter 4. Radical Yields from the Ozonolysis of Small Chain Alkenes ($C_2 – C_6$)

In this chapter a detailed study of small chain alkene (methyl (and alkyl) substituted ethenes, $C_2$ - $C_6$) ozonolysis, performed under tropospherically relevant conditions and as a function of humidity, in a large atmospheric simulation chamber, EUPHORE, is presented. OH and $HO_2$ radicals were observed using laser induced fluorescence (LIF), from experiments in the absence / presence of OH radical scavengers. These observations together with measurements from a suite of other instrumentation are used to derive yields for stable and radical products (from the fast ozonolysis process: CI formation and isomerisation / decomposition) using a detailed chemical mechanism based on the MCM to account for the subsequent and secondary chemical reactions. The calculated yields for stable and radical products are compared with recent literature and discussed in terms of branching ratios for various channels within the postulated reaction mechanisms.

## 4.1 Alkene Ozonolysis Mechanism

In general the gas-phase alkene ozonolysis reaction is believed to proceed via the Criegee mechanism (Criegee, 1975). Ozonolysis is initiated by a electrophilic cycloaddition of ozone across the double bond to form a primary ozonide (POZ). This intermediate is high in energy and rapidly decomposes at the central C-C bond and

one of the O-O bonds. Given that the O-O bond can break at two different sites, a pair of carbonyl oxides (hereafter referred to as Criegee Intermediates) and stable (primary) carbonyl molecules can be formed, as illustrated in Figure 4.1.

The Criegee Intermediate (CI) and carbonyl co-product produced from the exothermic decomposition of the POZ possess a significant amount of vibrational excitation. This energy enables further unimolecular reactions of the excited CI to occur but is not sufficient for the decomposition of the carbonyl molecule (Calvert et al., 2000). The distribution of decomposition products of the POZ is dependent upon the substitution of the alkene. For example, branched alkenes with an alkyl group attached to the C=C bond show a preference for forming a more highly substituted CI than the carbonyl co-product; whereas unbranched terminal alkenes (with the exception of 1-butene) (Grosjean and Grosjean, 1996a) show no preference for the less substituted aldehyde (*i.e.* HCHO) (Grosjean and Grosjean, 1996b, Paulson et al., 1999a, Tuazon et al., 1997).

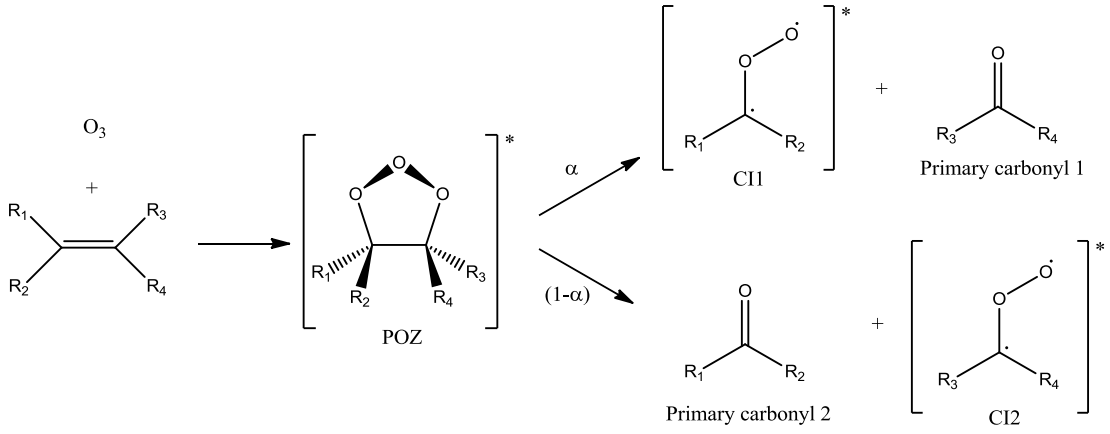


**Figure 4.1.** Cycloaddition of ozone across the alkene double bond and subsequent decomposition of the POZ. From Johnson and Marston (2008)

Different CIs behave as distinct and different chemical entities, which is demonstrated by the range of detected experimental products, depending on the extent of the substitution of the CI, and is discussed in detail in Section 4.3. Each CI can be formed in a *syn* (*i.e.* alkyl substituent is on the same side of the CI as the terminal O atom) or *anti* form, which determines their fates. Briefly, *syn*- and di-substituted CIs are thought to predominantly decompose through isomerisation via a five-membered transition state to give an excited hydroperoxide species which subsequently decomposes to give OH and a vinoxy radical (Calvert et al., 2000, Johnson and Marston, 2008) as illustrated in Figure 4.2. The proportion of the vibrationally excited CI that does not isomerise / decompose is suggested to be collisionally stabilised (Niki et al., 1987). Studies have shown that OH formation from vibrationally excited *syn* CI occurs on short timescales (*ca*. 10 ms) (Kroll et al., 2001c) and that the dominant route to OH production comes from the thermalised *syn* CI, *via* the hydroperoxide mechanism, as shown in Figure 4.2. It has been calculated that the 1,4-hydrogen shift forming OH proceeds approximately 3 – 8 orders of magnitude faster than collisional stabilisation followed by reaction with water, for the *syn* conformer (Kuwata et al., 2010).

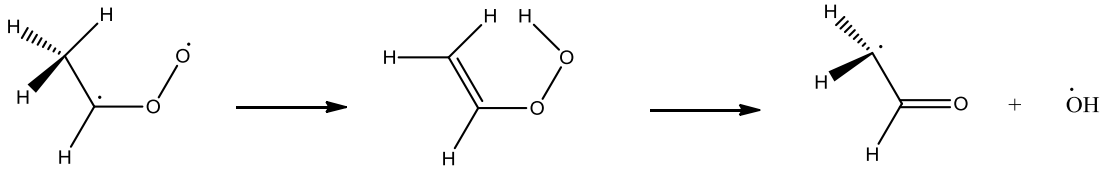


**Figure 4.2.** The "hydroperoxide" mechanism: 1,4-sigmatropic shift within the CI to form a vinyl hydroperoxide followed by bond fission to yield OH. Adapted from Niki et al. (1987)

The vinoxy radical formed alongside OH (see Figure 4.2) will react with oxygen in the atmosphere to form an excited β-oxo peroxy radical (Figure 4.3), which may be

stabilised (β pathway, Figure 4.3) or may undergo decomposition forming CO, a secondary stable carbonyl species and a further OH radical (1-β pathway, Figure 4.3) (Kuwata et al., 2005). However, this pathway to OH formation is only sufficient if an aldehydic hydrogen is present. The stabilised β-oxo peroxy may then react with other peroxy radicals, $HO_2$ or $RO_2$, to form stable species such as glyoxal, glycolaldehyde and secondary aldehydes, CO and $HO_2$ as shown in Figure 4.3.

The fate of the *anti*-CI and of the $CH_2OO$ CI formed from terminal alkenes is discussed in detail in Chapter 3. Briefly, the *anti*-CI (and $CH_2OO$) can undergo rearrangement through a dioxirane structure, which can decompose to various products including OH, $HO_2$, $CH_4$, CO, $CO_2$, $H_2O$ and methanol *via* a 'hot' acid/ester intermediate (Calvert et al., 2000, Nguyen et al., 2009a, Nguyen et al., 2009b). *syn* and *anti*-CIs can also undergo stabilisation followed by bimolecular reactions, but studies suggest that stabilisation is a minor process for di-substituted and *syn* mono-substituted CIs, as the lifetime with respect to the vinyl hydroperoxide mechanism is shorter than the time required for bimolecular processes to occur (Fenske et al., 2000a, Olzmann et al., 1997). Collisional stabilisation is therefore more likely to occur for the *anti*-CI enabling bimolecular reactions to proceed with many atmospherically relevant species such as $H_2O$, $NO_2$, $SO_2$ and CO (Calvert et al., 2000, Hatakeyama and Akimoto, 1994, Johnson et al., 2001). This is also shown by the computational studies performed by Kuwata et al. (2010), who predict that the *anti*-CI reacts ~ 40 000 times faster with water than does the *syn* CI.

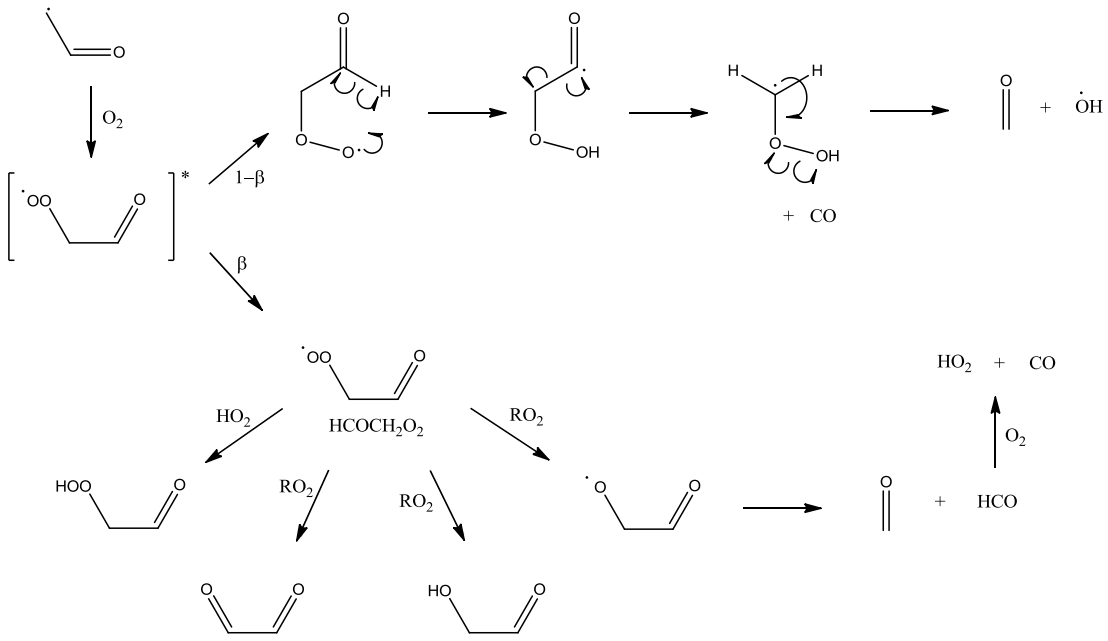


**Figure 4.3**. OH formation from excited β-oxo peroxy radical chemistry proposed by Kuwata et al. (2005), where calculations suggest that 1-β = 0.25, if an aldehydic hydrogen is available.

## 4.2 Decomposition Channels of Substituted Excited Criegee Intermediates

The alkenes discussed in this chapter are: propene, 1-butene, 2-methylpropene, *cis*-2-butene, *trans*-2-butene and 2,3-dimethyl-2-butene. The ozonolysis of each alkene studied gives rise to a range of products due to the differing nature of the Criegee intermediate (CI) formed from the initial POZ fragmentation (Rathman et al., 1999). As discussed in Section 4.2, the fate of the CI is dependent upon the degree of substitution of the alkene, as this determines whether the CI is mono or di-substituted or in a *syn* or *anti* configuration. The following section focuses on the products of the

decomposition channels of the CIs formed after the decomposition of each POZ in turn, followed by a brief overview of the $O_3$ initiated mechanisms of the alkenes studied.

### 4.2.1 Decomposition Channels of [$CH_3CHOO$]*

In this study the Criegee intermediate [$CH_3CHOO$]* is formed from the ozonolysis of propene, *cis*-2-butene and *trans*-2-butene, and can exist in an *anti*- or *syn*-configuration. In the case of propene (see Figure 4.4), the POZ decomposes nearly equally *via* two pathways: [$CH_3CHOO$]* + HCHO (R4.1a) and [$CH_2OO$]* + $CH_3CHO$ (R4.1b). This has been experimentally shown by Grosjean et al. (1996) and Tuazon et al.(1997) measuring an average yield of 0.48 ± 0.06 for $CH_3CHO$ in the presence of an OH scavenger. It is commonly assumed that 50 % of the [$CH_3CHOO$]* formed is in the *syn* configuration (Rickard et al., 1999) which predominantly undergoes decomposition to form OH radicals, *via* the vinyl hydroperoxide mechanism (R4.4). The *anti*-CI may undergo decomposition / isomerisation (R4.3) or be collisionally stabilised (R4.2). Stabilised CI (SCI) yields have been determined by Hatakeyama et al. (1984), Horie and Moortgat (1991), and Rickard et al. (1999). Hatakeyama et al. (1984) determined SCI yields of 0.25 ± 0.02 for propene (both $CH_2OO$ + $CH_3CHOO$) and 0.19 ± 0.03 for *trans*-2-butene, by measuring the yield of sulphuric acid ($H_2SO_4$) formed in the presence of $SO_2$. It was assumed that the SCI was scavenged by its reaction with $SO_2$, forming $SO_3$, and further converted to $H_2SO_4$ aerosol. Rickard et al. (1999) measured the increase in $CH_3CHO$ yield in the presence and absence of $SO_2$ (2000 ppmV), exploiting the reaction $SO_2 + CH_3CHOO \rightarrow SO_3 + CH_3CHO$, and reported SCI yields of 0.22 for

propene, 0.19 for *cis*-2-butene and 0.13 for *tran*-2-butene. The IUPAC recommendation for the SCI yield ($CH_3CHOO$) from $[CH_3CHOO]^*$ is 0.16. (http://www.iupac-kinetic.ch.cam.ac.uk/, 2007) The SCI may undergo bimolecular reaction with $H_2O$ in the troposphere to form hydroxy-alkyl-hydroperoxide (Neeb and Moortgat, 1999, Sauer et al., 1999) which may subsequently decompose to $CH_3C(O)OH + H_2O$ (R4.2c) or to $CH_3CHO + H_2O_2$ (R4.2b).

The IUPAC recommendation for the decomposition of $[CH_3CHOO]^*$ is shown below for propene (http://www.iupac-kinetic.ch.cam.ac.uk/, 2007)

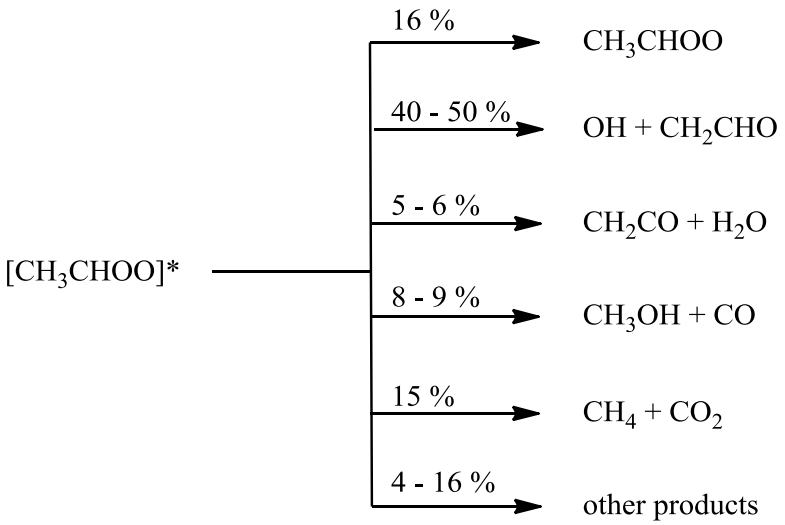


*cis*-2-Butene and *trans*-2-butene both form unity yields of $[CH_3CHOO]^*$ but the yields of their decomposition products may vary (see Figure 4.5). For example, the IUPAC recommendation for OH formation for *cis*-2-butene and *trans*-2-butene is 0.33 and 0.64, respectively (http://www.iupac-kinetic.ch.cam.ac.uk/, 2007). This may be due to the production of varying ratios of *syn* and *anti* CI configurations (Rathman et al., 1999). The chemical schemes used for the modelling purposes of this study are illustrated for propene in Figure 4.4 and *cis*- / *trans*-2-butene in Figure 4.5. The chemical mechanisms presented in Figures 4.4 and 4.5 show the fast ozonolysis

isomerisation / decomposition channels, as well as standard (slow) chemistry from the MCM *i.e.* peroxy radical and subsequent chemistry formed, *via* the hydroperoxide mechanism, to their reaction products (R4.5 – R4.8).

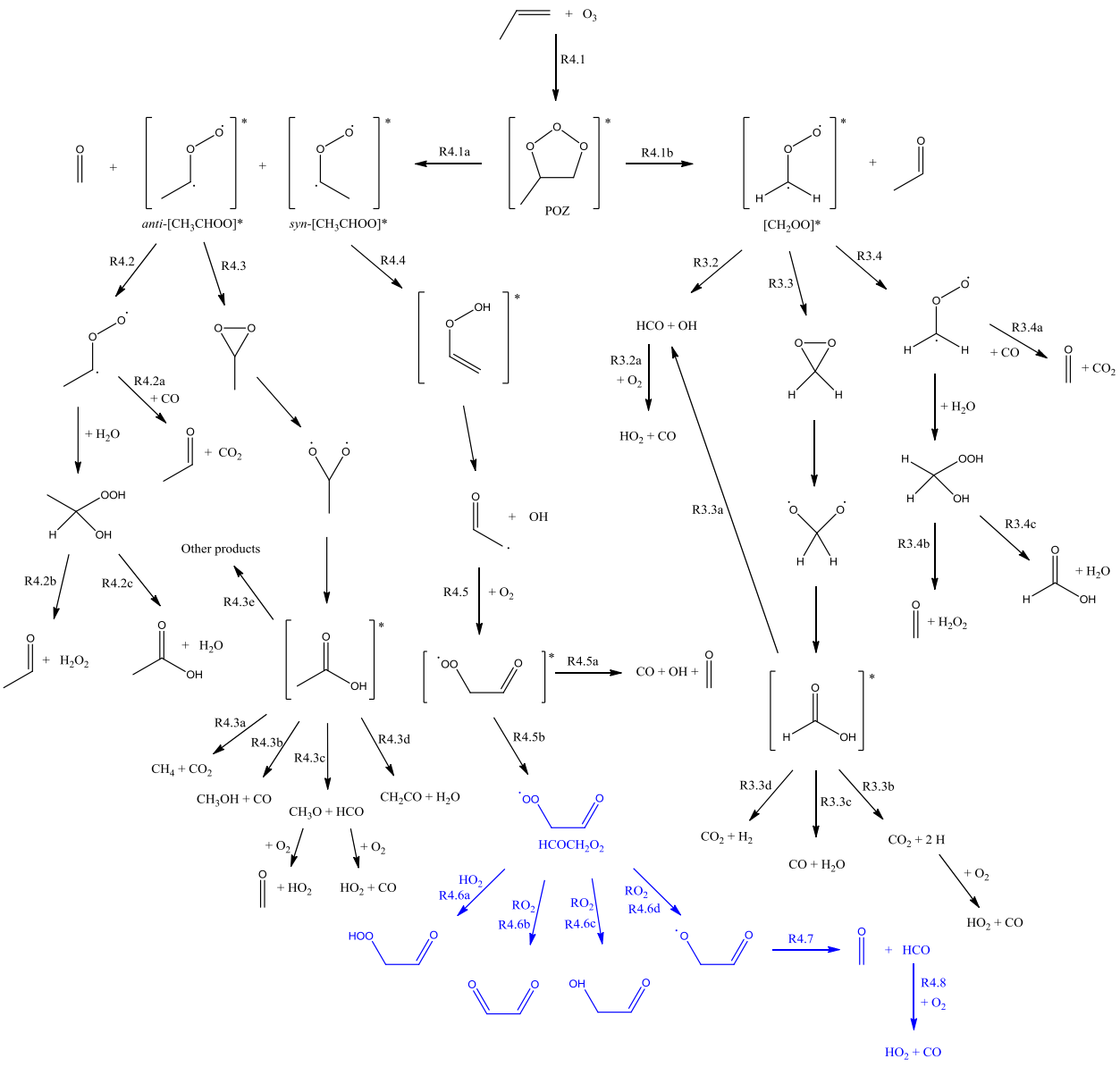


**Figure 4.4.** Schematic representation of the propene ozonolysis reaction system. Fast ozonolysis (black) – isomerisation / decomposition pathways adapted from IUPAC (2007), Johnson & Marston (2008) and Alam et al. (2011). Subsequent slow chemistry (blue) from standard MCM.

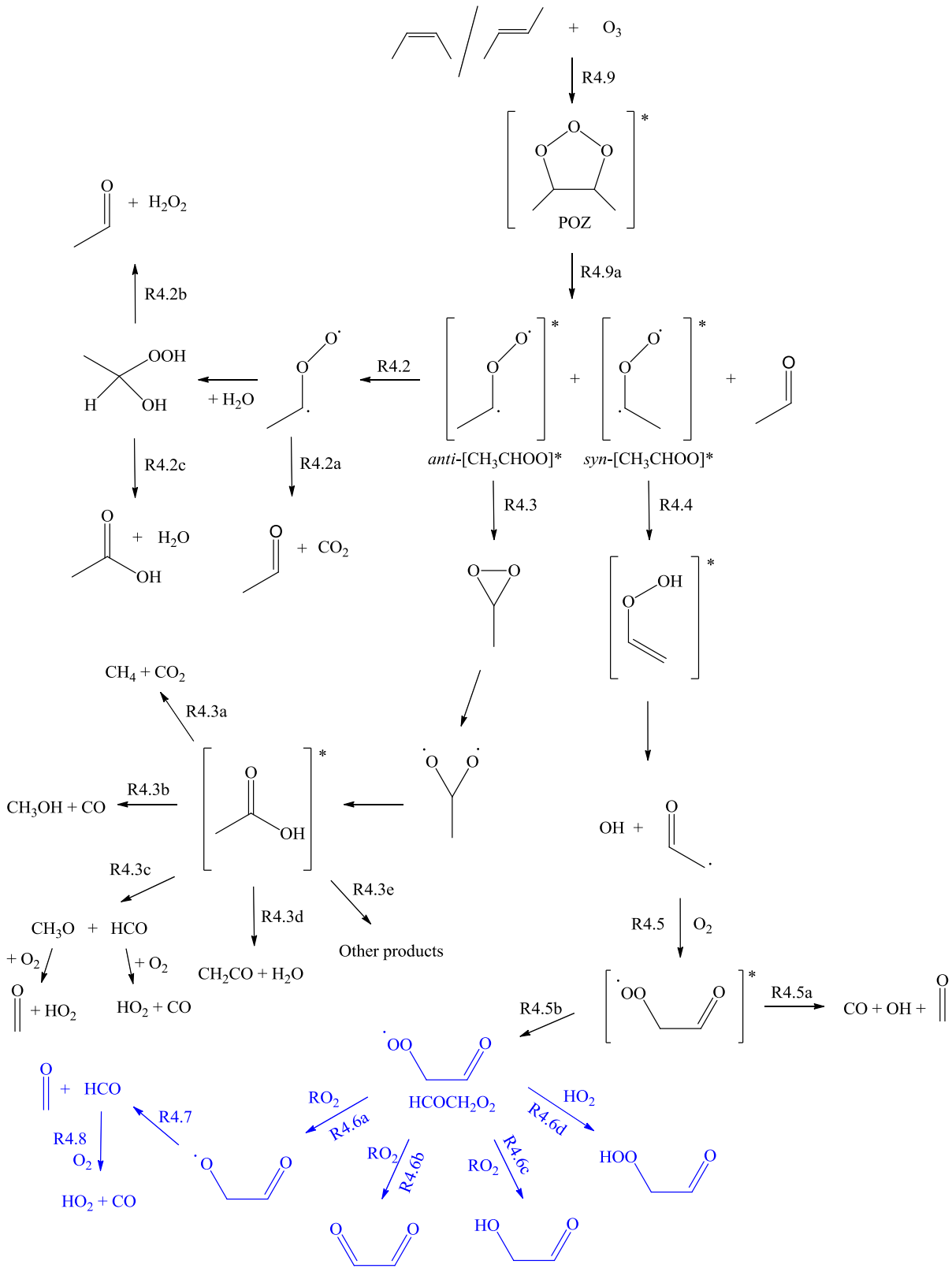


**Figure 4.5.** Schematic representation of the *cis*- and *trans*-2-butene ozonolysis reaction systems. Fast ozonolysis (black) – isomerisation / decomposition pathways adapted from IUPAC (2007), Johnson & Marston (2008) and Kuwata et al. (2005). Subsequent slow chemistry (blue) from standard MCM.

### 4.2.2 Decomposition Channels of $[(CH_3)_2COO]^*$

The Criegee intermediate $[(CH_3)_2COO]^*$ is formed from the fragmentation of the POZ formed from the ozonolysis of 2-methylpropene (Figure 4.6) and 2,3-dimethyl-2-butene (Figure 4.7). In the ozonolysis of 2-methylpropene, the POZ decomposes via two pathways: $[(CH_3)_2COO]^* + CH_3COCH_3$ (R4.10a) and $[CH_2OO]^* + HCHO$ (R4.10b). Acetone ($CH_3COCH_3$) yields of 0.340 ± 0.031 derived by Grosjean et al. (1996) and yields of 0.323 ± 0.030 and 0.294 ± 0.030 reported by Tuazon et al. (1997) were determined in the presence of OH scavenger which indicate (assuming the acetone yield is that for primary formation) branching ratios of ~ 0.32 and ~ 0.68 for (R4.10a) and (R4.10b), respectively. $[(CH_3)_2COO]^*$ can also be collisionally stabilised (R4.11) and may then undergo bimolecular reaction with $H_2O$ forming acetone and hydrogen peroxide ($H_2O_2$) (R4.11b). Hatakeyama *e*t al. (1984) derived an overall SCI yield of 0.174 ± 0.032 (both $CH_2OO + (CH_3)_2COO$) from the ozonolysis of 2-methylpropene. However, this yield may account for a significant amount of the stabilised $CH_2OO$ Criegee intermediate formed by the collisional stabilisation of $[CH_2OO]^*$. The current recommended yield of stabilised $CH_2OO$ CI is 0.37 (http://www.iupac-kinetic.ch.cam.ac.uk/, 2009) which is lower than the yield of 0.54 calculated in this study; see Chapter 3, Section 3.3.2.

The major fate of $[(CH_3)_2COO]^*$ is thought to be isomerisation / decomposition *via* the vinyl hydroperoxide mechanism to yield OH and a vinoxy radical (R4.12), which was first proposed by Niki et al. (1987). The authors studied the ozonolysis of 2,3-dimethyl-2-butene and suggested that ~ 30 % of the initially energy rich CIs were stabilised. However, experimental product studies suggest that stabilisation and/or

isomerisation (*i.e.* dimethyl-dioxirane formation) are minor fates of the $[(CH_3)_2COO]$*, which is evident in the absence of any decomposition products analogous to the "hot" acid isomerisation channel. OH yields of between 0.9 and 1.0 (for 2,3-dimethyl-2-butene), determined by various studies (http://www.iupac-kinetic.ch.cam.ac.uk/, 2009) also demonstrate that the major fate of $[(CH_3)_2COO]$* is isomerisation / decomposition *via* the vinyl hydroperoxide mechanism (see Figure 4.7, R4.12). Carbonyl product measurements from the ozonolysis of 2,3-dimethyl-2-butene in the presence of an OH scavenger have been made for acetone, HCHO, methylglyoxal and/or hydroxyacetone, $CH_3OH$ and $CO_2$ (Grosjean et al., 1996, Schafer et al., 1997, Tuazon et al., 1997). The chemical schemes used for the modelling purposes of this study for 2-methylpropene and 2,3-dimethyl-2-butene are shown in Figures 4.6 and 4.7, respectively. The chemical mechanisms presented in Figures 4.6 and 4.7 show the fast ozonolysis isomerisation / decomposition channels, as well as standard (slow) chemistry from the MCM *i.e.* peroxy radical and subsequent chemistry formed, *via* the hydroperoxide mechanism, to their reaction products (R4.13 – R4.17).

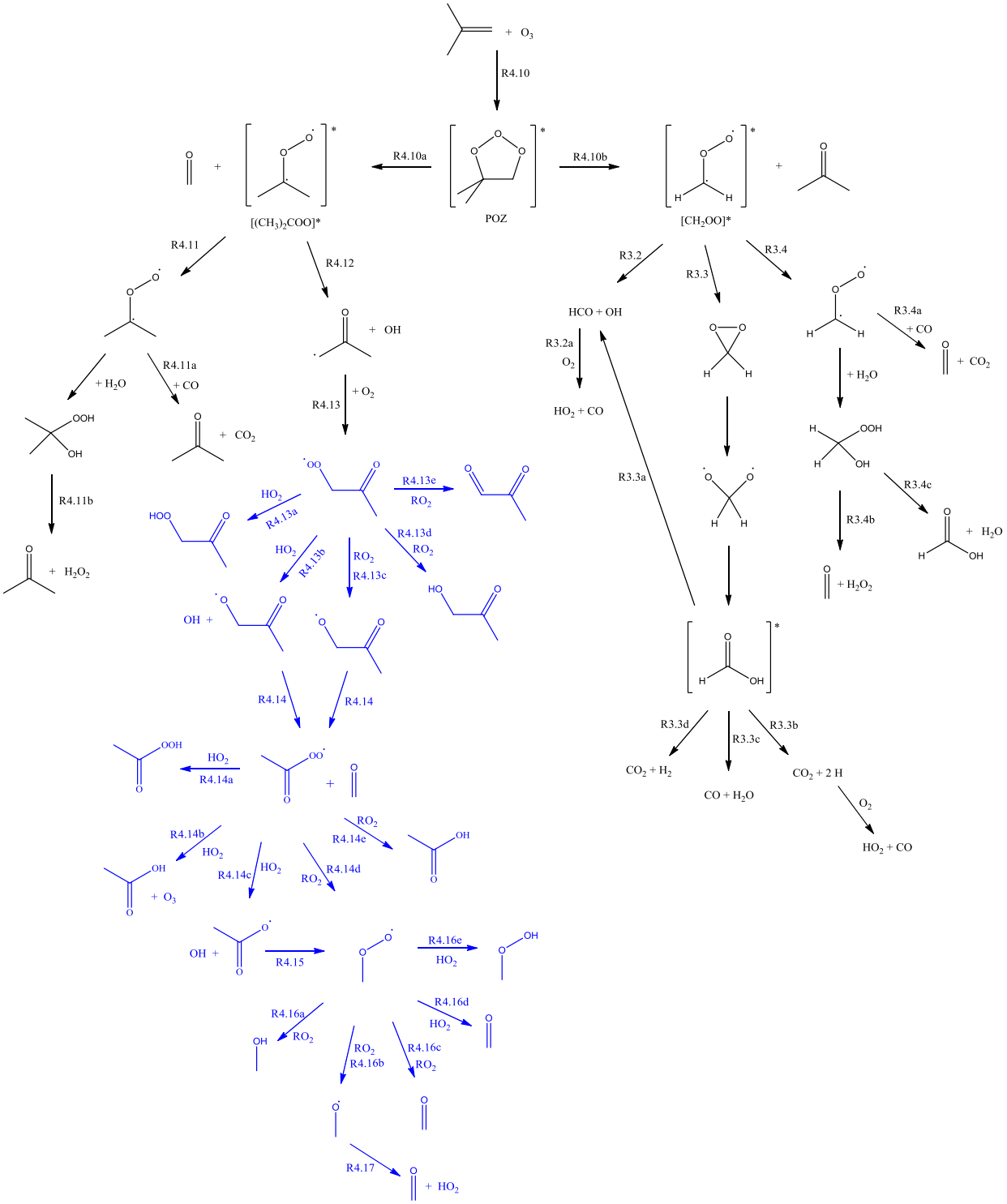


**Figure 4.6.** Schematic representation of the 2-methylpropene ozonolysis reaction system. Fast ozonolysis (black) – isomerisation / decomposition pathways adapted from IUPAC (2007), Johnson & Marston (2008) and Alam et al. (2011). Subsequent slow chemistry (blue) from standard MCM.

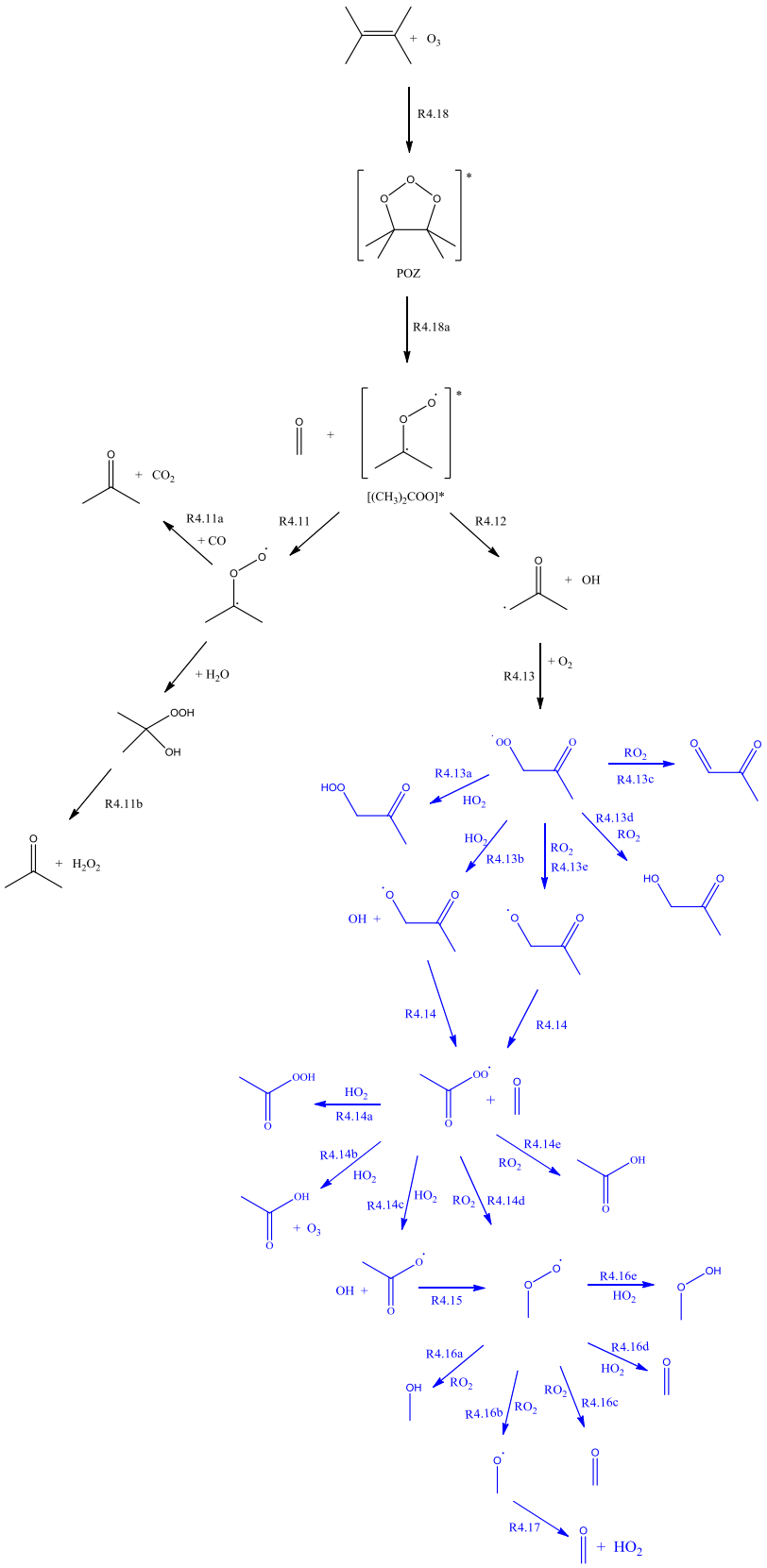


**Figure 4.7.** Schematic representation of the 2,3-dimethyl-2-butene ozonolysis reaction system. Fast ozonolysis (black) – isomerisation / decomposition pathways adapted from IUPAC (2007) and Johnson & Marston (2008). Subsequent slow chemistry (blue) from standard MCM.

### 4.2.3 Decomposition Channels $[C_2H_5CHOO]^*$

The ethyl mono-substituted Criegee intermediate $[C_2H_5CHOO]^*$ is formed from the ozonolysis of 1-butene (and other species not studied here such as *trans*-3-hexene) as illustrated in Figure 4.8. The initial POZ rapidly decomposes to two sets of species: $[C_2H_5CHOO]^*$ + HCHO (R4.19a) and $[CH_2OO]^*$ + $CH_3CH_2CHO$ (propanal) (R4.19b). In general unbranched terminal alkenes show no preference for the less substituted aldehyde. Experimental studies suggest, however, that the fragmentation of the POZ from 1-butene ozonolysis results in unequal ratios of the two sets of species. Grosjean et al. (1996) measured yields of 0.630 ± 0.031 and 0.350 ± 0.031 for HCHO and propanal respectively; whereas Paulson et al. (1999a) report a more equal branching ratio obtaining a yield of 0.45 ± 0.02 for propanal. Hasson et al. (2001a), however, reported propanal yields of 0.36 ± 0.03 and 0.52 ± 0.05 at < 0.5 % and > 50 % relative humidities.

The $[C_2H_5CHOO]^*$ can exist in a *syn*- or *anti*- configuration where it is likely that the *anti*-CI can undergo collisional stabilisation (R4.20). The SCI can then react with water forming propanal and $H_2O_2$ (R4.20b). It was suggested that it was the SCI + $H_2O$ reaction (R4.20b) that resulted in the observed increase in the propanal yield with increased humidity and a stabilised $C_2H_5CHOO$ yield of 0.10 – 0.16 was reported (Hasson et al., 2001a). The IUPAC recommendation for the SCI yield at 298 K is ~ 0.20. The *syn*-CI may undergo isomerisation / decomposition to yield OH *via* the vinyl hydroperoxide mechanism (R4.22). OH yields of 0.41 (+ 0.21 / – 0.14) (Atkinson and Aschmann, 1993) 0.29 ± 0.04 (Paulson et al., 1999a) and 0.26 (Fenske et al., 2000b) have been determined from 1-butene. (http://www.iupac-

kinetic.ch.cam.ac.uk/, 2009) Other stable products yields have been reported including $CH_3CHO$ (0.13 ± 0.01) and methylglyoxal and/or 2-hydroxypropanal ($CH_3CH(OH)CHO$, 0.03 ± 0.01) (Grosjean et al., 1996). The chemical scheme used for the modelling purposes of this study for 1-butene is shown in Figure 4.8, which illustrates the fast ozonolysis isomerisation / decomposition pathways, as well as standard (slow) chemistry from the MCM *i.e.* peroxy radical and subsequent chemistry formed, *via* the hydroperoxide mechanism, to their reaction products (R4.23 – R4.26).

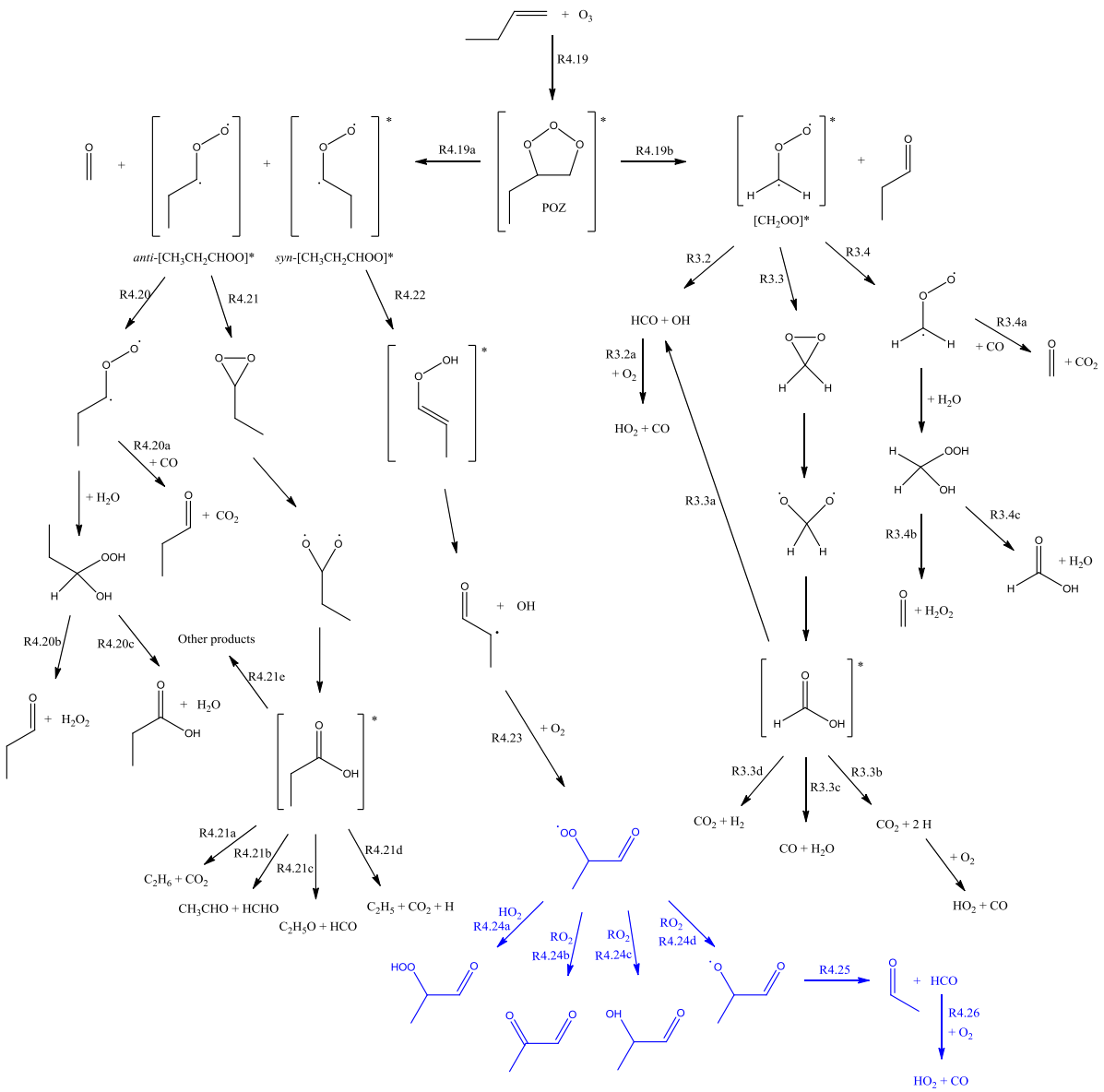


**Figure 4.8.** Schematic representation of the 1-butene ozonolysis reaction system. Fast ozonolysis (black) – isomerisation / decomposition pathways adapted from IUPAC (2007), Johnson & Marston (2008) and Alam et al. (2011). Subsequent slow chemistry (blue) from standard MCM.

## 4.3 Methodology

The experimental approach, initial concentrations, box model and analysis methodology is discussed in detail in Chapter 2. In this section, a brief methodology is presented in the form of the flow diagram below:

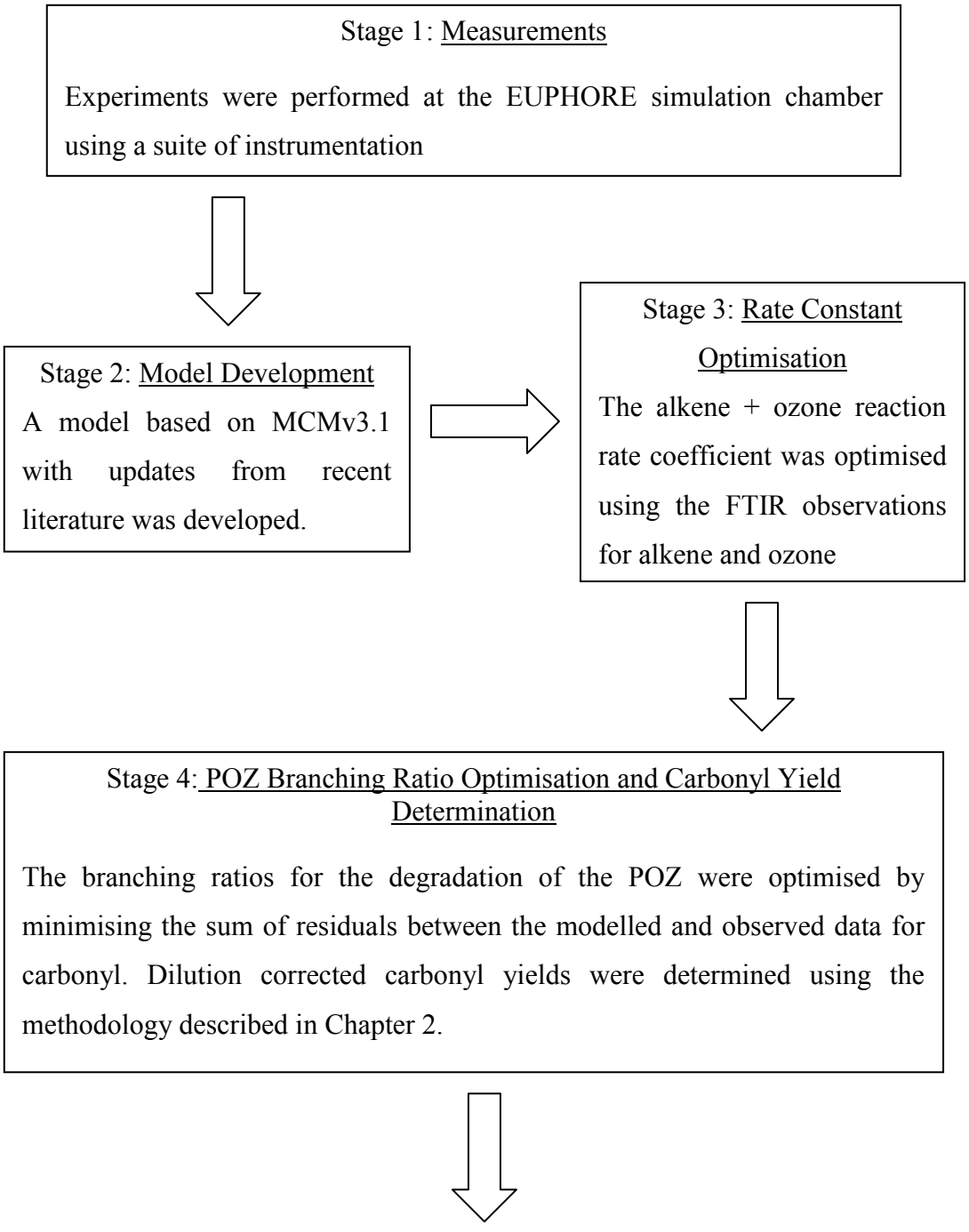

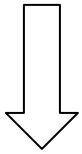

Stage 5: OH Optimisation

The yield of OH was optimised for simple alkene + ozone reactions (absence of OH scavenger), by minimising the sum of residuals between the LIF observations and modelled data. A derived branching ratio was then applied to the ozonolysis mechanism

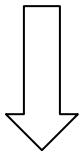

Stage 6: $HO_2$ Optimisation

The yield of $HO_2$ was optimised for all experiment types, by minimising the sum of residuals between the observations (LIF) and numerical simulations of $HO_2$.

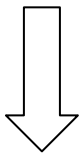

Stage 7: Branching Ratios

All experimental data were then used to derive branching ratios for various channels within the reaction mechanisms illustrated in Figures 4.4 – 4.8.

## 4.4 Results

In order to simplify the presentation of the findings of this study, the results are considered in four different sections: *(i)* Reaction rate coefficients, *(ii)* Primary carbonyl yields and POZ branching ratios, *(iii)* OH yields, and *(iv)* $HO_2$ yields.

### 4.4.1 Reaction Rate Coefficients

The alkene + ozone reaction rate coefficients, $k_{O_3+alkene}$, calculated from OH scavenger experiments are shown in Table 4.1, where the indicated uncertainty is the combined precision (1σ) and systematic uncertainty of the instrumentation. Average reaction rate coefficients at 298 K were calculated for 2-methylpropene and *trans*-2-butene (Table 4.1), by deriving the Arrhenius expression, as well as optimising the '*A*' parameter in the Arrhenius equation (EQ 4.1) within FACSIMILE.

$$k = Ae^{-\frac{Ea}{RT}} \qquad \text{(EQ 4.1)}$$

The Arrhenius expressions for 2-methylpropene and *trans*-2-butene, calculated from a limited temperature range of *ca.* 9 K, were $(2.94 \pm 0.38) \times 10^{-15}.\exp^{(-1618\ (\pm\ 114)\ /\ T)}$ and $(7.31 \pm 0.26) \times 10^{-15}.\exp^{(-1076\ (\pm\ 78)\ /\ T)}$ respectively, and were used for all subsequent simulations performed. The derived rate coefficients, $k_{O_3+alkene}$, are in good agreement with previous studies (see Table 4.1), and are all within 15 % of the IUPAC recommendations (http://www.iupac-kinetic.ch.cam.ac.uk/, 2007). Figure 4.9 shows a comparison between observed and modelled (optimised) temporal evolution of each

alkene and ozone (measured by FTIR), for experiments performed in the presence of an OH scavenger.

**Table 4.1.** Comparison of reaction rate coefficient ($k_{O_3+Alkene}$)

| Alkene | Rate constant / $cm^3$ $molecule^{-1}$ $s^{-1}$ | at T / K | Reference |
|---|---|---|---|
| Propene | $(1.15 \pm 0.11) \times 10^{-17}$ | 300 | *This study* [a] |
| | $(1.16 \pm 0.11) \times 10^{-17}$ | 300 | *This study* [b] |
| | $(1.01 \pm 0.25) \times 10^{-17}$ | 298 | IUPAC |
| | $(1.04 \pm 0.25) \times 10^{-17}$ | 300 | IUPAC |
| | $(9.6 \pm 0.4) \times 10^{-18}$ | 298 | Treacy et al. (1992) |
| 1-butene | $(1.24 \pm 0.38) \times 10^{-17}$ | 301 | *This study* [a] |
| | $(9.64 \pm 0.25) \times 10^{-18}$ | 298 | IUPAC |
| | $(1.08 \pm 0.25) \times 10^{-17}$ | 301 | IUPAC |
| | $(8.8 \pm 0.6) \times 10^{-18}$ | 298 | Treacy et al. (1992) |
| | $(1.09 \pm 0.08) \times 10^{-17}$ | 298 | Avzianova & Ariya (2002) |
| 2-Methylpropene | $1.29 \times 10^{-17}$ * | 298 | *This study (average)* |
| | $(1.27 \pm 0.15) \times 10^{-17}$ | 297 | *This study* [a] |
| | $(1.21 \pm 0.14) \times 10^{-17}$ | 295 | *This study* [a] |
| | $(1.24 \pm 0.14) \times 10^{-17}$ | 296 | *This study* [a] |
| | $(1.28 \pm 0.15) \times 10^{-17}$ | 297 | *This study* [b] |
| | $(1.13 \pm 0.30) \times 10^{-17}$ | 298 | IUPAC |
| | $(1.09 \pm 0.18) \times 10^{-17}$ | 298 | Treacy et al. (1992) |
| | $(1.08 \pm 0.10) \times 10^{-17}$ | 298 | Avzianova & Ariya (2002) |
| *cis*-2-butene | $(1.19 \pm 0.12) \times 10^{-16}$ | 299 | *This study* |
| | $(1.25 \pm 0.25) \times 10^{-16}$ | 298 | IUPAC |
| | $(1.27 \pm 0.25) \times 10^{-16}$ | 299 | IUPAC |
| | $(1.23 \pm 0.18) \times 10^{-16}$ | 298 | Treacy et al. (1992) |
| *trans*-2-butene | $1.98 \times 10^{-16}$ † | 298 | *This study (average)* |
| | $(1.80 \pm 0.25) \times 10^{-16}$ | 291 | *This study* [a] |
| | $(1.88 \pm 0.26) \times 10^{-16}$ | 294 | *This study* [c] |
| | $(1.87 \pm 0.26) \times 10^{-16}$ | 294 | *This study* [a] |
| | $(1.89 \pm 0.26) \times 10^{-16}$ | 295 | *This study* [b] |
| | $(2.08 \pm 0.28) \times 10^{-16}$ | 299 | *This study* [a] |
| | $(1.90 \pm 0.35) \times 10^{-16}$ | 298 | IUPAC |
| | $(1.81 \pm 0.06) \times 10^{-16}$ | 298 | Treacy et al. (1992) |
| | $(1.82 \pm 0.11) \times 10^{-16}$ | 298 | Avzianova & Ariya (2002) |
| 2,3-Dimethyl-2-butene | $(1.08 \pm 0.34) \times 10^{-15}$ | 292 | *This study* [a] |
| | $(1.13 \pm 0.35) \times 10^{-15}$ | 298 | IUPAC |
| | $(1.11 \pm 0.35) \times 10^{-15}$ | 292 | IUPAC |

[a] excess CO as OH scavenger
[b] excess CO as OH scavenger / relative humidity ~ 30 %
[c] excess cyclohexane as OH scavenger / relative humidity ~ 30 %
* calculated from derived Arrhenius expression $2.94 (\pm 0.38) \times 10^{-15}.\exp^{(-1618 (\pm 114) / T)}$
† calculated from derived Arrhenius expression $7.31 (\pm 0.26) \times 10^{-15}.\exp^{(-1076 (\pm 78) / T)}$
Indicated uncertainty is the combined precision (1σ) and systematic uncertainty of the instrumentation

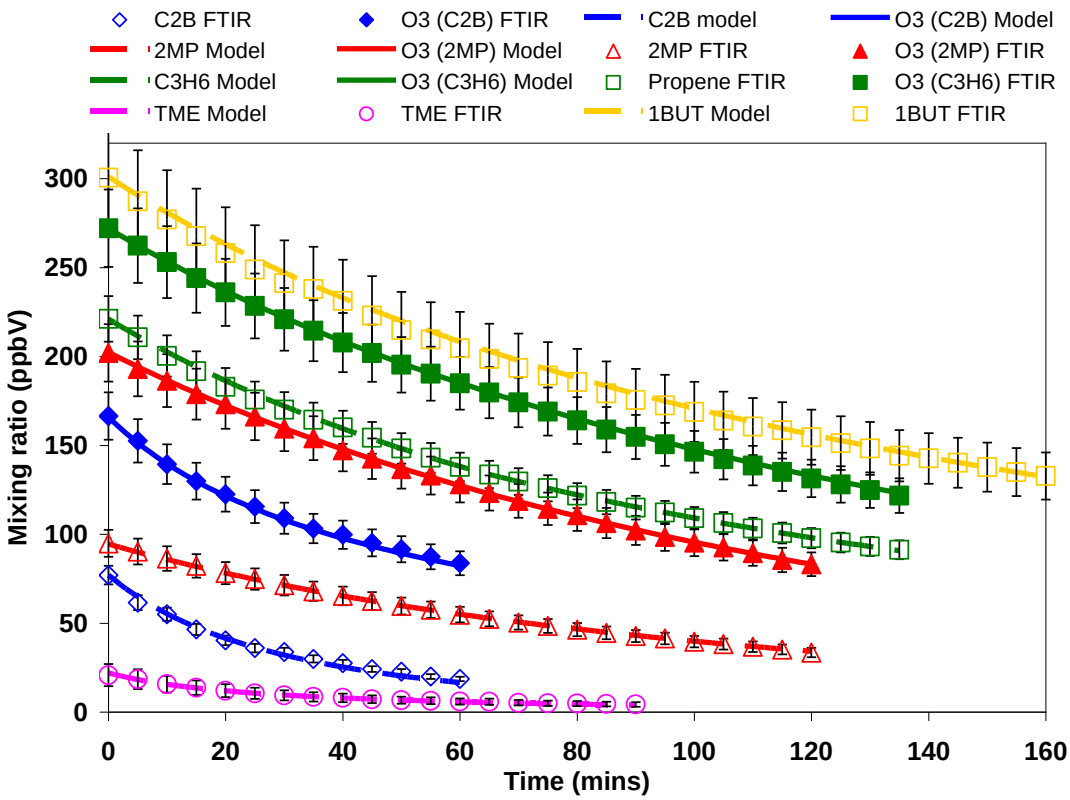


**Figure 4.9.** FTIR observed temporal profiles for alkene (open shapes) and ozone (closed shapes – same colours) for corresponding experiments, plus optimised rate *k* model profiles for alkene (dashed lines) and ozone (solid lines). Figure key abbreviations are as follows: C3H6 – propene, C2B – *cis*-2-butene, 2MP – 2-methylpropene, 1BUT – 1-butene, TME – 2,3-dimethyl-2-butene and O3 – ozone.

As mentioned in the Chapter 3, depending upon the initial concentrations of alkene and ozone, the slower the value of $k_{O_3+alkene}$, the more significant the contribution to the loss of alkene by dilution in the chamber. This is illustrated in Figure 4.10, where > 95 % of the loss of *trans*-2-butene is due to the reaction with ozone, whereas *ca.* 43 % of the loss of propene is due to dilution. Figure 4.10 also shows that OH does not react with either alkene or ozone during the experiments. This confirms that > 99 % of the OH formed from alkene ozonolysis is scavenged by CO (in experiments where excess CO was present), thus allowing us to derive a value for $k_{O_3+alkene}$ from these data.

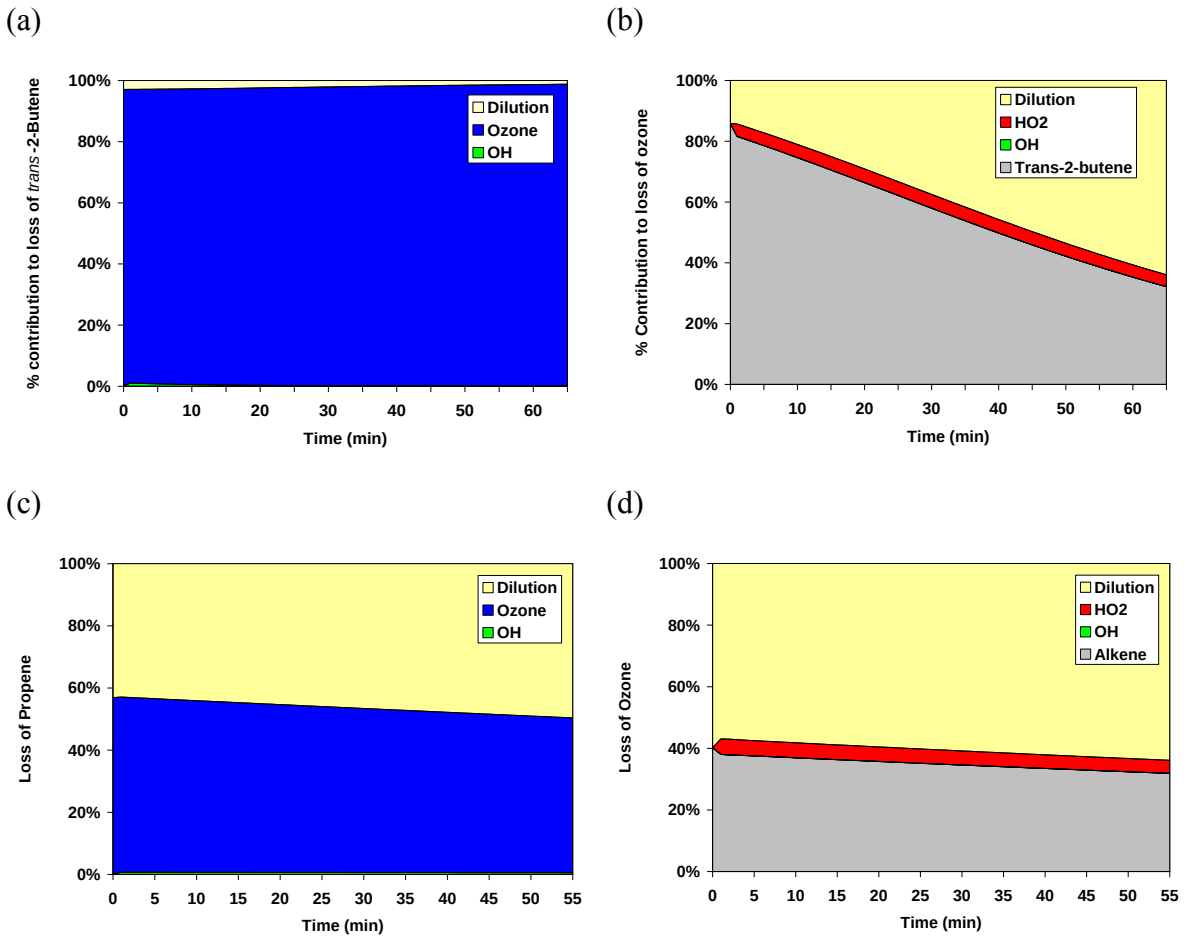


**Figure 4.10**. Percentage contribution of each process / reaction to the loss of a) *trans*-2-butene and b) ozone in an excess CO experiment and c) Propene and (d) ozone in an excess CO experiment. Blue – reaction with ozone; yellow – dilution; grey – reaction with alkene; red – reaction with $HO_2$

## 4.4.2 Primary Carbonyl Yields and POZ Decomposition Branching

### 4.4.2.1 Primary Carbonyl Yields

The yields reported in Tables 4.2 – 4.6 have been derived by calculating the dilution corrected production of carbonyl species as a function of alkene reacted, as explained in Chapter 2. The reported uncertainty (Tables 4.2 – 4.6) is the combined precision

(1σ) and systematic uncertainty of the instrumentation. It must be taken into account that dependent upon the reaction mechanism and experimental conditions, the "primary" carbonyl species formed by $O_3$ + alkene can also be (i) produced by another reaction pathway of the $O_3$ + alkene mechanism, (ii) consumed by its reaction with OH or (iii) a secondary product of the alkene + OH or other secondary organics + OH reactions. The "primary" carbonyl yields for experiments performed in the presence of an OH scavenger therefore do not directly relate to the branching ratios of the degradation of the POZ; for example the observed increase in aldehyde yields following their formation *via* the reaction of the SCI + CO. Thus, the branching ratios of the fragmentation of the POZ were optimised within the model, to reproduce the observed measurements (see Chapter 2, Section 2.5), taking into account any secondary formation (and loss) of 'primary' carbonyl species, using the postulated mechanisms discussed in Section 4.3.

In general, for the range of alkenes studied, it is found that the HCHO yield is enhanced by approximately 8 – 35 % in the presence of excess CO, with the exception of *cis*-2-butene (Table 4.5) and *trans*-2-butene (Table 4.6) which do not form HCHO as a primary carbonyl product. These two alkenes show an increase of approximately 20 – 23 % for the 'primary' carbonyl yield, acetaldehyde ($CH_3CHO$), in the presence of CO. Figure 4.11 shows the range of derived yields of acetaldehyde from *trans*-2-butene ozonolysis performed under different conditions. An average yield of acetaldehyde of 0.89 was calculated from OH scavenger experiments only and is illustrated by the solid line in Figure 4.11. In the ozonolysis of propene (Table 4.2), the yields for both primary carbonyls acetaldehyde ($CH_3CHO$) and HCHO increase in the presence of both CO and $H_2O$.

In the ozonolysis of 2-methylpropene (Table 4.4) and 2,3-dimethyl-2-butene (Table 4.7), the formation of HCHO is not exclusive to the fast ozonolysis isomerisation / decomposition pathways (see Figures 4.6 and 4.7). The HCHO yields determined from these systems appear to have a strong dependence on the reactions of the peroxy radicals formed, which is discussed in Section 4.6.2. Figure 4.12 shows the production of carbonyl species, HCHO, acetone and methyl-glyoxal as a function of 2-methylpropene consumed, for a typical ozonolysis experiment, whereas Figure 4.13 shows the range of derived HCHO yields under different conditions and different initial alkene / ozone concentrations.

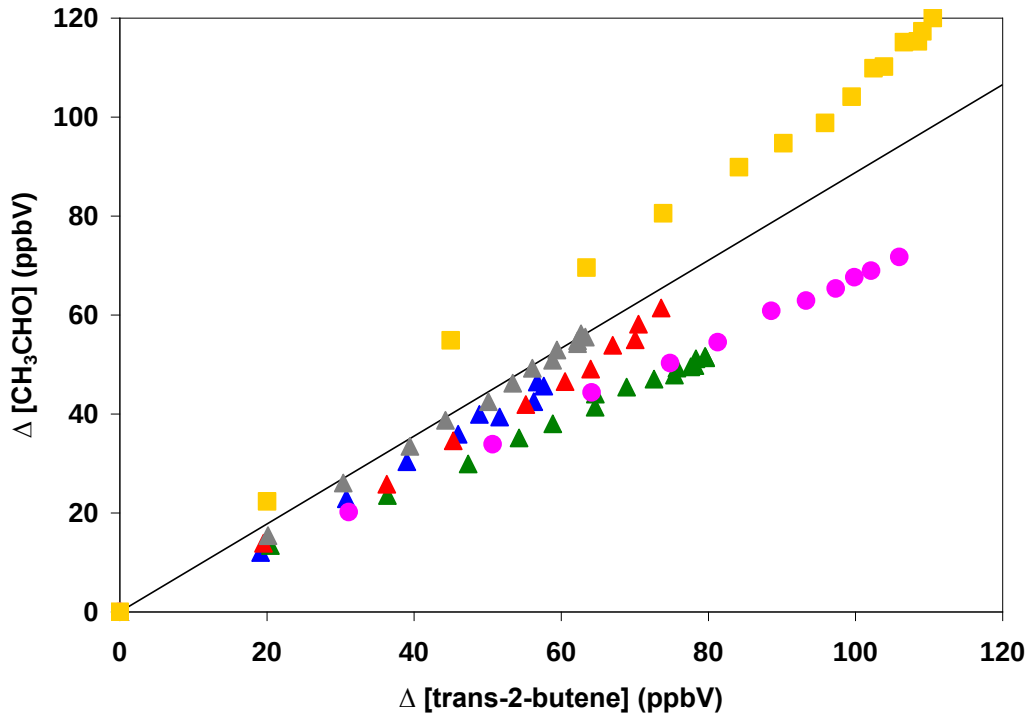


**Figure 4.11.** Acetaldehyde ($CH_3CHO$) production as a function of reacted *trans*-2-butene. Different colours illustrate the range of experiments. Triangles – excess CO experiments, circles – simple *trans*-2-butene + ozone experiment, squares – excess cyclohexane + $H_2O$ experiment. Solid line signifies the average derived yield from OH scavenger experiments – 0.84.

**Table 4.2.** Product yields from the reaction of ozone with propene

| Experiment Type | HCHO | $CH_3CHO$ | Reference |
|---|---|---|---|
| *Simple $C_3H_6 + O_3$* | 0.64 ± 0.04 | 0.44 ± 0.06 | *This study* |
| *Excess CO* | 0.81 ± 0.05 | 0.38 ± 0.06 | *This study* |
| *Excess CO + $H_2O$* | 0.97 ± 0.07 | 0.62 ± 0.08 | *This study* |
| *Simple $C_3H_6 + O_3$* | 0.490 | 0.394 | Horie and Moortgat (1991) |
| Excess cyclohexane | 0.780 ± 0.015 | 0.520 ± 0.026 | Grosjean and Grosjean (1996) |
| Excess cyclohexane | 0.645 ± 0.048 | 0.446 ± 0.092 | Tuazon *et al.* (1997) |
| Excess $C_3H_6$ | 0.62 ± 0.02 | 0.38 ± 0.02 | Schäfer *et al.* (1997) |
| Excess cyclohexane | | 0.34 ± 0.01 | Rickard *et al.* (1999) |
| Average* | | 0.52 ± 0.10 | Wegener *et al.* (2007) |

* Average of Simple $C_3H_6 + O_3$ (0.55), excess $H_2O$ (0.53), excess CO (0.47) and excess CO + $H_2O$ (0.53); authors report 20 % uncertainty

**Table 4.3.** Product yields from the reaction of ozone with 1-butene

| Experiment Type | HCHO | $CH_3CH_2CHO$ | Reference |
|---|---|---|---|
| *Simple $C_4H_8 + O_3$* | 0.41 ± 0.12 | 0.35 ± 0.14 | *This study* |
| *Excess CO* | 0.51 ± 0.15 | 0.41 ± 0.16 | *This study* |
| Excess cyclohexane | 0.630 ± 0.031 | 0.350 ± 0.031 | Grosjean and Grosjean (1996) |
| Simple $C_4H_8 + O_3$ | 0.80 ± 0.06 | - | Wegener *et al.* (2007) |
| $C_4H_8 + O_3 + H_2O$[a] | 0.86 ± 0.06 | - | Wegener *et al.* (2007) |
| Excess cyclohexane | | 0.45 ± 0.02 | Paulson *et al.* (1999) |
| Excess cyclohexane[b] | | 0.36 ± 0.03 | Hasson *et al.* (2001) |
| Excess cyclohexane + $H_2O$[c] | | 0.52 ± 0.05 | Hasson *et al.* (2001) |

[a] Relative humidity ~ 40 % ; [b] Relative humidity < 0.5 % ; [c] Relative humidity > 50 %

**Table 4.4.** Product yields from the reaction of ozone with 2-Methylpropene *

| Experiment Type | HCHO | $CH_3COCH_3$ | m-glyoxal $CH_3C(O)CHO$ | Reference |
|---|---|---|---|---|
| *Simple $C_4H_8 + O_3$* | 1.28 ± 0.11 | no data | 0.29 ± 0.05 | *This study* |
| *$C_4H_8 + O_3 + H_2O$* | 1.41 ± 0.12 | no data | no data | *This study* |
| *Excess CO* | 1.76 ± 0.16 | no data | 0.43 ± 0.08 | *This study* |
| *Excess CO* | 1.69 ± 0.15 | no data | 0.20 ± 0.03 | *This study* |
| *Excess cyclohexane* | 1.56 ± 0.14 | 0.42 ± 0.11[a] | no data | *This study* |
| *Excess cyclohexane + $H_2O$* | 1.59 ± 0.14 | 0.76 ± 0.20[a] | no data | *This study* |
| *Excess CO* | 1.39 ± 0.13[a] | 0.45 ± 0.12[a] | no data | *This study* |
| *Excess CO + $H_2O$* | 1.99 ± 0.83[a] | 0.37 ± 0.10[a] | no data | *This study* |
| *Simple $C_4H_8 + O_3$* | 0.57 ± 0.05 | 0.22 ± 0.04 | 0.10 ± 0.02 | *This study* |
| Excess cyclohexane | 0.950 ± 0.098 | 0.340 ± 0.031 | 0.190 ± 0.016[b] | Grosjean and Grosjean (1996) |
| Excess cyclohexane | 1.01 ± 0.07 | 0.294 ± 0.030[c]<br>0.323 ± 0.030[d] | - | Tuazon *et al.* (1997) |
| Excess $C_4H_8$ | 0.83 ± 0.02 | 0.40 ± 0.02 | 0.10 ± 0.02 | Schäfer *et al.* (1997) |
| Simple $C_4H_8 + O_3$ | 1.21 ± 0.13 | 0.51 ± 0.06 | 0.17 ± 0.03 | Neeb and Moortgat (1999) |
| Excess CO | 0.97 ± 0.11 | 0.30 ± 0.03 | 0.15 ± 0.03 | Neeb and Moortgat (1999) |
| Simple $C_4H_8 + O_3$ | 1.80 ± 0.14 | - | - | Wegener *et al.* (2007) |
| $C_4H_8 + O_3 + H_2O$ | 1.67 ± 0.14[f] | - | - | Wegener *et al.* (2007) |

[a] Using CIR-TOF-MS
[b] No differentiation between methyl-glyoxal and/or hydroxyacetone could be made
[c] Using FTIR
[d] Using GC-FID
[f] Relative humidity ~ 40 %
* Table is organised in chronological order, rather than experimental type.

**Table 4.5.** Product yields from the reaction of ozone with *cis*-2-Butene

| Experiment Type | HCHO | $CH_3CHO$ | Reference |
|---|---|---|---|
| *Simple $C_4H_8 + O_3$* | 0.13 ± 0.01 | 0.74 ± 0.11 | *This study* |
| *Excess CO* | 0.13 ± 0.01 | 0.92 ± 0.14 | *This study* |
| Excess cyclohexane | 0.126 ± 0.019[a] | 1.150 ± 0.104[a] | Grosjean and Grosjean (1996) |
| Excess $C_4H_8$ | 0.18[b] | 1.2[b] | Horie *et al.* (1997) |
| Excess cyclohexane | 0.161 ± 0.030 | 1.08 ± 0.08[c]<br>1.19 ± 0.14[d] | Tuazon *et al.* (1997) |
| Excess $C_4H_8$ | 0.13 ± 0.02 | 0.99 ± 0.04 | Schäfer *et al.* (1997) |
| Excess cyclohexane | | 0.83 ± 0.08 | Rickard *et al.* (1999) |
| Excess cyclohexane | | 0.86 ± 0.03 | McGill *et al.* (1999) |
| Simple $C_4H_8 + O_3$ | | 1.65 ± 0.33 | Wegener *et al.* (2007) |
| $C_4H_8 + O_3 + H_2O$ | | 1.20 ± 0.24 | Wegener *et al.* (2007) |

[a] calculated from a mixture of *cis*- & *trans*-2-butene
[b] errors not reported. Instrumental uncertainty for HCHO and $CH_3CHO$ was 10 % and 20 % respectively
[c] Using FTIR
[d] Using GC-FID

**Table 4.6.** Product yields from the reaction of ozone with *trans*-2-Butene*

| Experiment Type | HCHO | $CH_3CHO$ | Glyoxal CHOCHO | Reference |
|---|---|---|---|---|
| *Excess CO* | 0.13 ± 0.01 | 0.78 ± 0.13 | 0.03 ± 0.01 | *This study* |
| *Excess cyclohexane + $H_2O$* | no data | 1.06 ± 0.28[†] | no data | *This study* |
| *Excess CO* | 0.12 ± 0.01 | 0.65 ± 0.11 | 0.03 ± 0.01 | *This study* |
| *Excess CO + $H_2O$* | 0.14 ± 0.01 | 0.82 ± 0.14 | 0.03 ± 0.01 | *This study* |
| *Simple $C_4H_8 + O_3$* | 0.14 ± 0.01 | 0.67 ± 0.11 | 0.03 ± 0.01 | *This study* |
| *Excess CO* | 0.17 ± 0.02 | 0.87 ± 0.15 | no data | *This study* |
| Excess cyclohexane | 0.126 ± 0.019[a] | 1.150 ± 0.104[a] | 0.160 ± 0.011[d] | Grosjean and Grosjean (1996) |
| Excess cyclohexane | 0.168 ± 0.015 | 1.09 ± 0.09[b]<br>1.14 ± 0.14[c] | 0.099 ± 0.014 | Tuazon *et al.* (1997) |
| Excess $C_4H_8$ | 0.18 ± 0.02 | 1.02 ±0.05 | | Schäfer *et al.* (1997) |
| Excess cyclohexane | | 0.98 ± 0.20 | | Rickard *et al.* (1999) |
| Excess cyclohexane | | 0.85 ± 0.07 | | McGill *et al.* (1999) |
| Excess cyclohexane | | 0.97[e] | | Hasson *et al.* (2001) |
| Excess cyclohexane + $H_2O$ | | 1.17[f] | | Hasson *et al.* (2001) |
| Simple $C_4H_8 + O_3$ | | 1.50 ± 0.30[g] | | Wegener *et al.* (2007) |
| Excess CO | | 1.05 ± 0.21 | | Wegener *et al.* (2007) |
| Excess CO + $H_2O$ | | 1.00 ± 0.20 | | Wegener *et al.* (2007) |

[†] Using CIR-TOF-MS
[a] calculated from a mixture of *cis*- & *trans*-2-butene
[b] Using FTIR
[c] Using GC-FID
[d] No differentiation between glyoxal and/or hydroxyacetaldehyde could be made
[e] Relative humidity ~ 0 %
[f] Relative humidity ~ 80 %
[g] Same value for $C_4H_8 + O_3 + H_2O$
* Table is organised in chronological order, rather than experimental type.

**Table 4.7.** Product yields from the reaction of ozone with 2,3-Dimethyl-2-butene

| Experiment Type | HCHO | CH3COCH3 | m-glyoxal[a] $CH_3C(O)CHO$ | Reference |
|---|---|---|---|---|
| Simple $C_6H_9$ + O3 | 0.48 ± 0.14 | 0.95 ± 0.31 | 0.17 ± 0.06 | This study |
| Excess CO | 0.76 ± 0.23 | 1.05 ± 0.35 | 0.27 ± 0.09 | This study |
| Excess cyclohexane | 0.288 ± 0.023 | 1.006 ± 0.049 | 0.284 ± 0.010 | Grosjean and Grosjean (1996) |
| Excess cyclohexane | 0.426 ± 0.081 | 1.14 ± 0.19[a]<br>0.977 ± 0.086[b] | | Tuazon *et al.* (1997) |
| Excess $C_6H_9$ | 0.37 ± 0.02 | 1.00 ± 0.03 | 0.10 ± 0.02 | Schäfer *et al.* (1997) |
| Excess cyclohexane | | 1.04 ± 0.10 | | Rickard *et al.* (1999) |
| Excess cyclohexane | | 2.4[c] | | Hasson *et al.* (2001) |

[a] Using FTIR
[b] Using GC-FID
[c] Independent of humidity

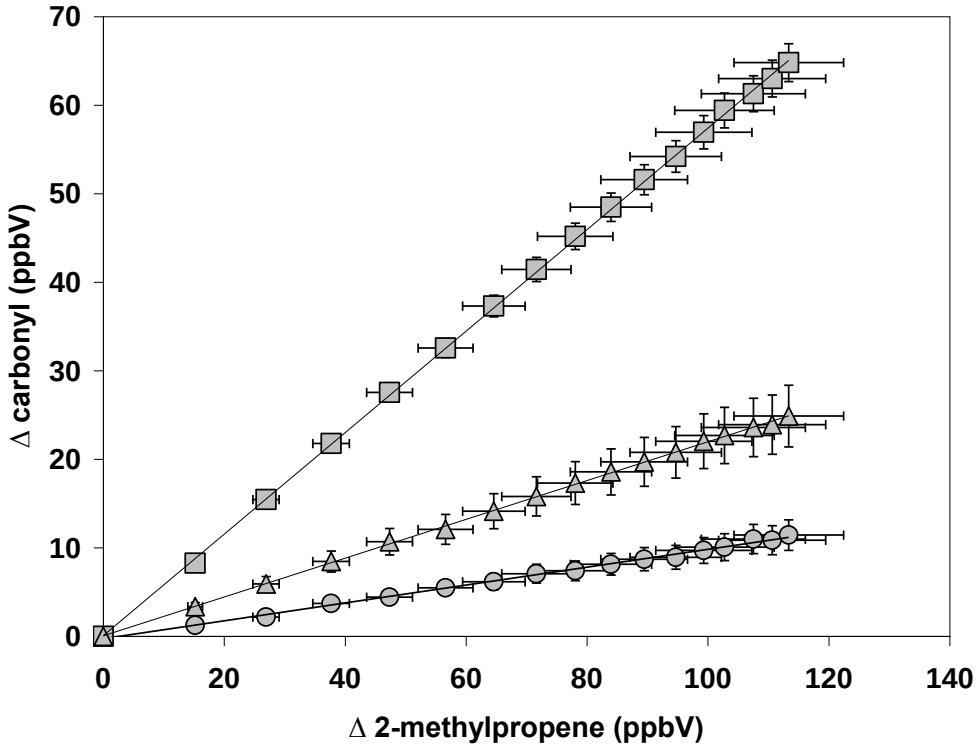


**Figure 4.12.** Derived carbonyl yields for a typical 2-methylpropene ozonolysis reaction. Product yields of 0.57 for HCHO (squares), 0.22 for acetone (triangles) and 0.10 for methyl-glyoxal (circles). See Table 4.4 for further 2-methylpropene ozonolysis experimental product yields.

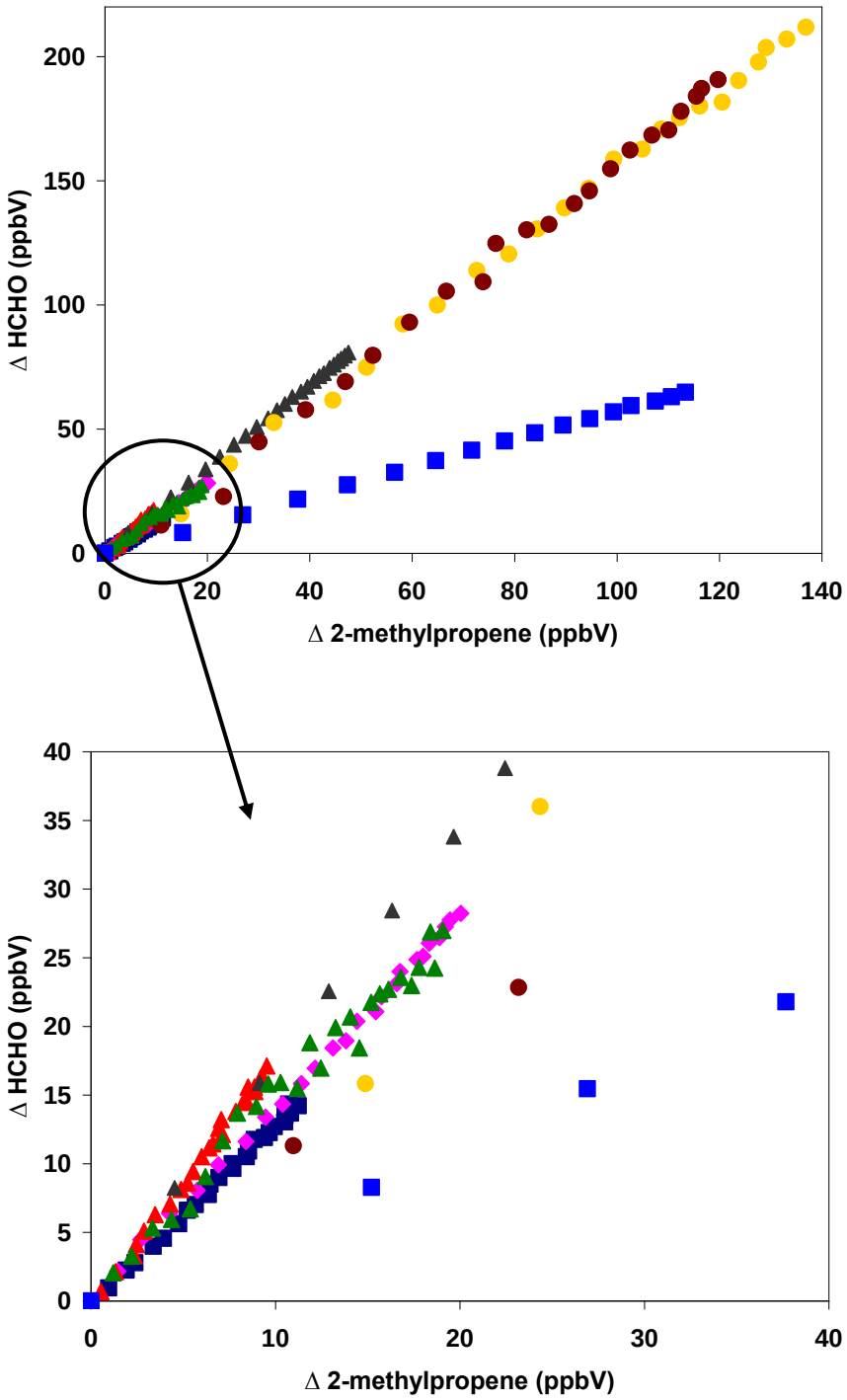


**Figure 4.13.** The dilution corrected HCHO production as a function of reacted 2-methylpropene. Derived yields range from 0.57 – 1.99 (see Table 4.4) Different colours illustrate the range of experiments performed, triangles – excess CO, circles – excess cyclohexane, squares – non scavenger.

### 4.4.2.2 Primary Ozonide Decomposition Branching Ratios

The optimised branching ratios for the decomposition of the POZ for propene, 1-butene and 2-methylpropene were 51 : 49 for $[CH_3CHOO]^*$ + HCHO (R4.1a) : $[CH_2OO]^*$ + $CH_3CHO$ (R4.1b), 59 : 41 for $[C_2H_5CHOO]^*$ + HCHO (R4.19a) : $[CH_2OO]^*$ + $CH_3CH_2CHO$ (R4.19b), and 34 : 66 for $[(CH_3)_2COO]^*$ + $CH_3COCH_3$ (R4.10a) : $[CH_2OO]^*$ + HCHO (R4.10b), respectively. Figure 4.14 shows the temporal evolution of propene ozonolysis with the optimised branching ratios for the POZ fragmentation, as a function of experimental conditions. For 2-methylpropene, the larger than unity formation yield of HCHO could not be accounted for by the simulations performed. The branching ratio for the POZ fragmentation (for 2-methylpropene) was therefore determined by simulating the average best fit for the observed acetone only, using OH scavenger (excess CO or cyclohexane) experiments.

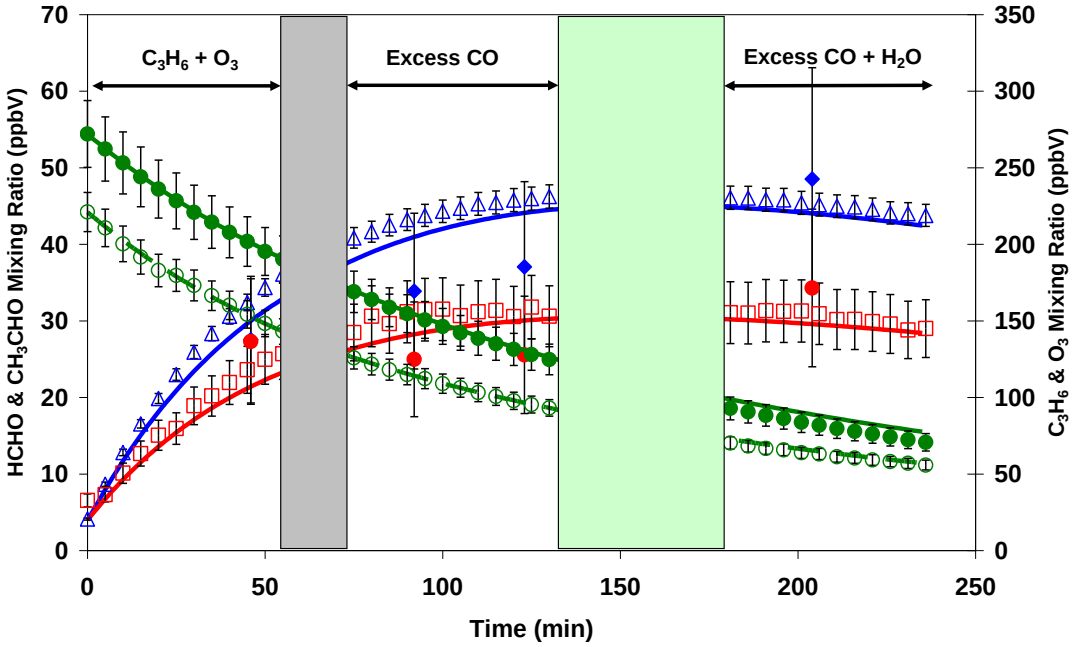


**Figure 4.14.** FTIR observed temporal profile of propene (closed green circles), ozone (open green circles), HCHO (open blue triangles) and $CH_3CHO$ (open red squares) plus optimised model simulations (solid and dashed lines). CO was added to scavenge any OH over a 15 minute period from 62 minutes (grey shaded area). $H_2O$ was introduced to increase the humidity from 1.0 to 24.0 % over a 20 minute period at 144 minutes (blue shaded area). FTIR observations were not made during addition of water due to interferences.

### 4.4.3 OH Yield

The derived OH yields ($Y_{OH}$) from ozonolysis of the alkenes studied are shown in Table 4.8. The reported uncertainty for the LIF data is 27 % which is the combined uncertainty and precision of a single calibration. The reported $Y_{OH}$ in Table 4.8 correspond to the formation of OH *via* the (fast) direct decomposition / isomerisation of the CI, after taking secondary sources into account; for example OH formation *via* $HO_2 + O_3$, the excited β-oxo peroxy radical and from the reactions of acyl peroxy

radicals + $HO_2$ (Barber and Marston, 2010, Dillon and Crowley, 2008, Hasson et al., 2004, Jenkin et al., 2007), which have been taken into account within the model. Figure 4.15 shows a typical temporal profile of OH steady state concentration measured by LIF and model simulation comparisons for *cis*-2-butene ozonolysis, and illustrates that the current MCMv3.1 overestimates (in the case of *cis*-2-butene) the OH yield (see Table 4.8).

OH yields were also determined in the presence of excess cyclohexane for *trans*-2-butene by fitting the cyclohexanone, cyclohexanol, cyclohexyl-hydroperoxide and $HO_2$ observations, (described in Chapter 2, Section 2.5), shown in Figure 14.16. The estimated error for $Y_{OH}$ derived by this scavenger technique (51 %) is the combined uncertainty of the instrumentation used in the analysis and the uncertainty associated with the branching ratio for the decomposition of the cyclohexoxy radical. It was found that the best simultaneous fit of the OH-initiated cyclohexane oxidation products (*c*-$C_6H_{10}O$, *c*-$C_6H_{11}OH$ and *c*-$C_6H_{11}OOH$) gave a $k(2(c\text{-}C_6H_{11}O_2))$ / $k(c\text{-}C_6H_{11}O_2 + HO_2)$ ($k_{2.21}$ / $k_{2.22}$) ratio of 0.45, which corresponds to a lower limit (*ca.* $5.0 \times 10^{-12}$ $cm^3$ $molecule^{-1}$ $s^{-1}$) of the previously reported $k(c\text{-}C_6H_{11}O_2 + HO_2)$ ($k_{2.22}$) determined by Boyd et al. (2003) of $1.71 \times 10^{-12}$ $cm^3$ $molecule^{-1}$ $s^{-1}$, whilst using the MCMv3.1 $RO_2$ permutation rate coefficient (for > $C_3$ alkyl) of $2.5 \times 10^{-12}$ $cm^3$ $molecule^{-1}$ $s^{-1}$ for $k(2(c\text{-}C_6H_{11}O_2))$ ($k_{2.21}$) (Jenkin et al., 1997). However the branching ratios (R2.21a) : (R2.21b) : (R2.21c) (see Chapter 2, Figure 2.6) for the *c*-$RO_2$ self reactions that gave the best simultaneous fit for the oxidation species were 0.5 : 0.2 : 0.3 respectively, in order to account for the extra cyclohexanol observed.

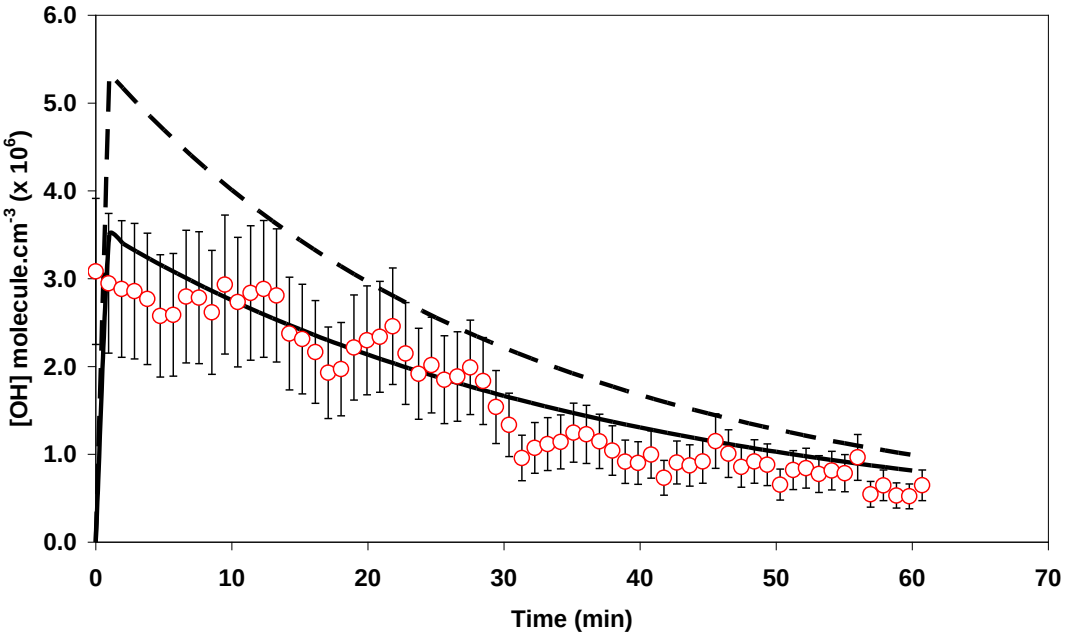


**Figure 4.15.** Temporal profile of OH (red circles) plus model simulations before (dashed line, base case MCMv3.1 chemistry) and after (solid line) optimising the OH yield to the LIF data (see Table 4.8), for *cis*-2-butene ozonolysis.

**Table 4.8.** OH formation yields from alkenes studied

| Alkene | Criegee Intermediate | OH Yield | Method | Reference |
|---|---|---|---|---|
| Propene | $CH_2OO$, $CH_3CHOO$ | 0.36 ± 0.10 | LIF | *This study* |
| | | 0.34 | - | IUPAC |
| | | 0.36 | - | MCMv3.1 |
| | | 0.33 (+ 0.17 / - 0.11) | Cyclohexane | Atkinson and Aschmann (1993) |
| | | 0.18 ± 0.01 | CO | Gutbrod *et al.*(1997) |
| | | 0.34 ± 0.06 | Cyclohexane | Neeb and Moortgat (1999) |
| | | 0.35 ± 0.07 | Tracer | Paulson *et al.* (1999) |
| | | 0.32 ± 0.08 | Tracer | Rickard *et al.* (1999) |
| | | 0.40 ± 0.06 | 2,3-butandiol | Aschmann *et al.* (2003) |
| | | 0.10 ± 0.07 (dry) | Stoichiometry | Wegener *et al.* (2007) |
| | | 0.30 ± 0.08 (wet) | | |
| | | 0.39 ± 0.08 | PERCA | Qi *et al*. (2009) |
| 1-Butene | $CH_2OO$, $C_2H_5CHOO$ | 0.56 ± 0.15 | LIF | *This study* |
| | | 0.36 | - | MCMv3.1 |
| | | 0.41 (+ 0.21 / - 0.14) | Cyclohexane | Atkinson and Aschmann (1993) |
| | | 0.29 ± 0.04 | Tracer | Paulson *et al.*(1999) |
| | | 0.26 | Tracer | Fenske *et al*. (2000) |
| | | 0.00 ± 0.08 (dry) | Stoichiometry | Wegener *et al.* (2007) |
| | | 0.30 ± 0.09 (wet) | | |

**Table 4.8.** ***continued***

| Alkene | Criegee Intermediate | OH Yield | Method | Reference |
|---|---|---|---|---|
| 2-Methylpropene | $CH_2OO$ | 0.67 ± 0.18 | LIF | *This study* |
| | $(CH_3)_2COO$ | 0.62 | - | IUPAC |
| | | 0.82 | - | MCMv3.1 |
| | | 0.84 (+ 0.42 / - 0.28) | Cyclohexane | Atkinson and Aschmann (1993) |
| | | 0.60 (+ 0.05 / - 0.07) | Cyclohexane | Neeb and Moortgat (1999) |
| | | 0.72 ± 0.12 | Tracer | Paulson *et al.*(1999) |
| | | 0.60 ± 0.15 | Tracer | Rickard *et al.* (1999) |
| | | 0.30 ± 0.14 (dry) | Stoichiometry | Wegener *et al.* (2007) |
| | | 0.80 ± 0.10 (wet) | | |
| *cis*-2-Butene | $CH_3CHOO$ | 0.26 ± 0.07 | LIF | *This study* |
| | | 0.33 | - | IUPAC |
| | | 0.57 | - | MCMv3.1 |
| | | 0.41 (+ 0.21 / - 0.14) | Cyclohexane | Atkinson and Aschmann (1993) |
| | | 0.14 ± 0.03 | Stoichiometry | Horie *et al.* (1994) |
| | | 0.17 ± 0.02 | CO | Gutbrod *et al.*(1997) |
| | | 0.33 ± 0.07 | Tracer | McGill *et al*. (1999) |
| | | 0.33 ± 0.05 | Tracer | Orzechowski and Paulson (2002) |
| | | 0.18 ± 0.09 (dry) | Stoichiometry | Wegener *et al.* (2007) |
| | | 0.40 ± 0.05 (wet) | | |
| *trans*-2-Butene | $CH_3CHOO$ | 0.63 ± 0.17 | LIF | *This study* |
| | | 0.57 (± 0.29) (wet) | Cyclohexane | *This study* |
| | | 0.64 | - | IUPAC |
| | | 0.57 | - | MCMv3.1 |
| | | 0.64 (+ 0.32 / - 0.21) | Cyclohexane | Atkinson and Aschmann (1993) |
| | | 0.24 ± 0.05 | Stoichiometry | Horie *et al.* (1994) |
| | | 0.24 ± 0.02 | CO | Gutbrod *et al.*(1997) |
| | | 0.68 ± 0.09 | LIF (5 Torr) | Donahue *et al.* (1998) |
| | | 0.54 ± 0.11 | Tracer | McGill *et al*. (1999) |
| | | (*ca.* 0.60) | LIF low pressure | Kroll *et al.* (2001) |
| | | 0.75 ± 0.19 | LIF | Siese *et al.* (2001) |
| | | 0.64 ± 0.12 | Tracer | Orzechowski and Paulson (2002) |
| | | 0.54 ± 0.05 (dry) | Tracer | Hasson *et al.* (2003) |
| | | 0.52 ± 0.04 (wet) | | |
| | | 0.70 ± 0.12 (wet) | Stoichiometry | Wegener *et al.* (2007) |
| | | 0.60 ± 0.12 (dry) | | |
| 2,3-Dimethyl-2-butene | $(CH_3)_2COO$ | 0.83 ± 0.22 | LIF | *This study* |
| | | 0.90 | - | IUPAC |
| | | 1.00 | - | MCMv3.1 |
| | | 1.00 (+ 0.5 / - 0.33) | Cyclohexane | Atkinson and Aschmann (1993) |
| | | 0.80 ± 0.12 | 2-Butanol | Chew and Atkinson (1996) |
| | | 0.36 ± 0.02 | CO | Gutbrod *et al.*(1997) |
| | | 0.70 ± 0.03 | LIF (5 Torr) | Donahue *et al.* (1998) |
| | | 0.89 ± 0.22 | Tracer | Rickard *et al.* (1999) |
| | | 0.99 ± 0.18 | Tracer | Fenske *et al*. (2000) |
| | | (*ca.* 1.00) | LIF low pressure | Kroll *et al.* (2001) |
| | | 1.00 ± 0.25 | LIF | Siese *et al.* (2001) |
| | | 0.91 ± 0.14 | Tracer | Orzechowski and Paulson (2002) |
| | | 1.07 ± 0.16 | 2,3-butandiol | Aschmann *et al.* (2003) |

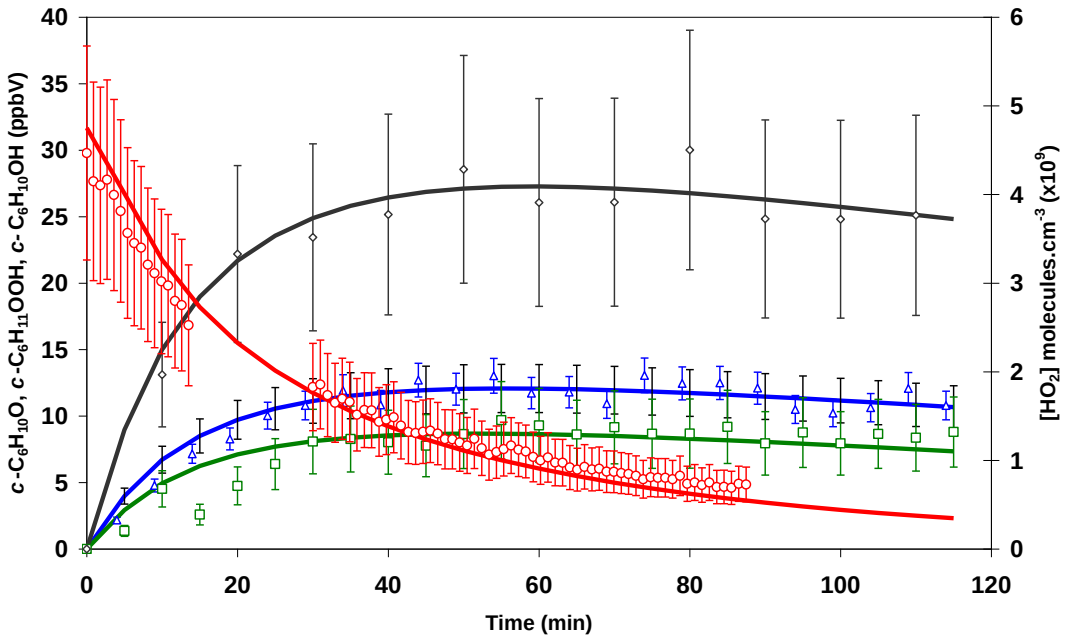


**Figure 4.16.** Observed temporal profiles of cyclohexanone (*c*-$C_6H_{10}O$ – blue triangles, from CIR-TOF-MS), cyclohexanol (*c*-$C_6H_{10}OH$ – green squares, from FTIR) cyclohexyl-hydroperoxide (*c*-$C_6H_{11}OOH$ – black diamonds, from HPLC) and steady state [$HO_2$] (red circles, from LIF) plus optimised model simulations (lines), for the ozonolysis of *trans*-2-butene in the presence of excess cyclohexane experiment.

### 4.4.4 $HO_2$ Yield

The calculated yields of $HO_2$ ($Y_{HO_2}$) for the alkenes studied are shown in Table 4.9, where the indicated uncertainty reflects the $HO_2$ observed in the LIF system. For the ozonolysis of 2-methylpropene and 2,3-dimethyl-2-butene in the absence of an OH scavenger, the $Y_{HO_2}$ are found to be greater than unity (1.51 and 1.74 respectively) which may suggest, that like HCHO yields, (Table 4.4 and 4.7) the yield of $HO_2$ may have a strong dependency on the reactions of the peroxy radicals formed from [$(CH_3)_2COO$]*. Table 4.9 shows that for all alkenes studied, a reduction in the

measured $Y_{HO_2}$ is observed in the presence of excess CO, a reduction which is further enhanced with increasing humidity. A decrease of *ca.* 81 % (average across all studied alkenes, with the exception of *trans*-2-butene (see Table 4.9)) in the calculated $Y_{HO_2}$ was seen in the presence of CO. Figure 14.17 shows the temporal profile of $HO_2$ measured by LIF in a propene ozonolysis experiment. It illustrates that the steady state $HO_2$ concentration increases when CO is introduced into the chamber (*via* the reaction of OH + CO), and decreases when the humidity is enhanced (*via* the humidity dependent $HO_2$ self reaction). Although the model takes this into account, optimised simulations suggest a change in $Y_{HO_2}$, as the simulations cannot reproduce the observed increase in $HO_2$ after increasing the CO concentration, and observed decrease in $HO_2$ after increasing the humidity (see Figure 14.17, base case MCMv3.1) with a constant $Y_{HO_2}$. The decrease in the simulated $HO_2$ observed when increasing the $H_2O$ concentration is solely due to the humidity dependence of the $HO_2$ self reaction, as there is no $H_2O$ dependence to the $HO_2$ yield in the basic mechanism within the model. The $Y_{HO_2}$ derived for *trans*-2-butene, in the simple system and in the presence of cyclohexane + $H_2O$, were over a factor of 2 different (0.89 and 0.40 respectively (see Table 4.9)). Thus, a reduction in the $Y_{HO_2}$ is observed for ethene (see Chapter 3), propene and *trans*-2-butene ozonolysis, in the presence of $H_2O$, which may indicate a humidity dependence for the $Y_{HO_2}$. Further discussion of the interpretation of these results is described in Section 4.6.6 and Chapter 5.

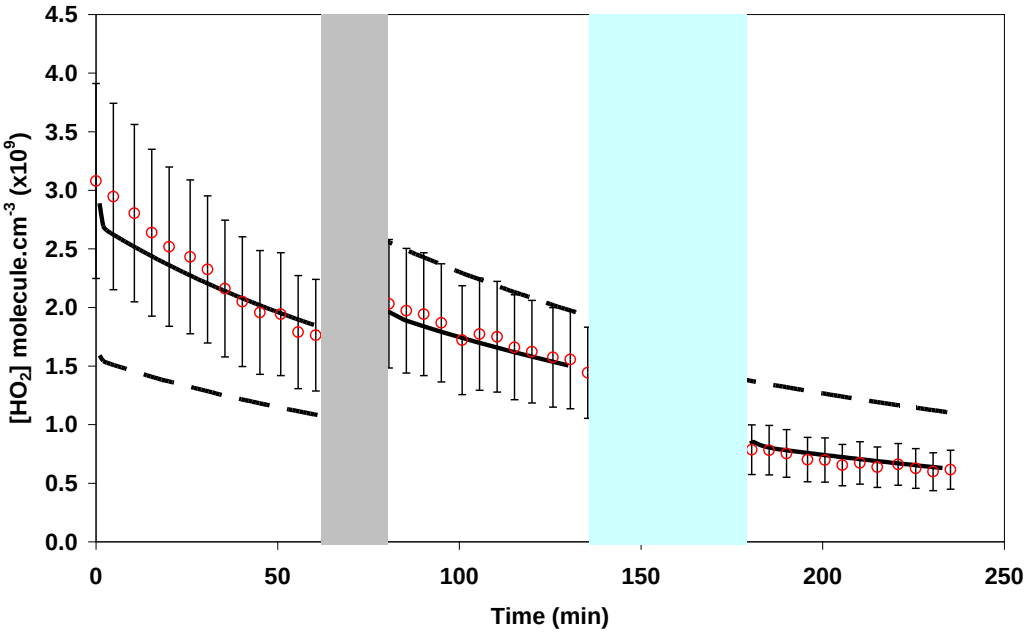


**Figure 4.17.** Observed temporal profile of $HO_2$ (red circles) plus model simulations before optimised $HO_2$ yield (base case MCMv3.1 – dashed lines) and after optimised yield (solid lines), for a propene ozonolysis experiment. Shaded areas signify introduction of CO (grey) and $H_2O$ (blue) and were not included in the optimisation of the $HO_2$ yields.

**Table 4.9.** Yield of $HO_2$ for alkenes studied under different experimental conditions

| Alkene | Experimental Type | Yield of $HO_2$ | Reference |
|---|---|---|---|
| Propene | *Simple $C_3H_6 + O_3$* | 0.61 ± 0.16 | *This study* |
| | *Excess CO* | 0.09 ± 0.02 | *This study* |
| | *Excess CO + $H_2O$* | 0.02 ± 0.00 | *This study* |
| | | 0.28 ± 0.08 | MCMv3.1 |
| | Stoichiometry | 1.50 ± 0.75 (dry) | Wegener *et al.* (2007) |
| | | 1.15 ± 0.60 (wet) | |
| | PERCA | 0.19 ± 0.04 | Qi *et al*. (2009) |
| 1-Butene | *Simple $C_4H_8 + O_3$* | 0.57 ± 0.15 | *This study* |
| | *Excess CO* | 0.18 ± 0.05 | *This study* |
| | | 0.28 | MCMv3.1 |
| | Stoichiometry | 1.60 ± 0.80 (dry) | Wegener *et al.* (2007) |
| | | 1.60 ± 0.80 (wet) | |
| 2-Methylpropene | *Simple $C_4H_8 + O_3$* | no data | *This study* |
| | *$C_4H_8 + O_3 + H_2O$* | no data | *This study* |
| | *Excess CO* | 0.36 ± 0.10 | *This study* |
| | *Excess CO* | 0.31 ± 0.08 | *This study* |
| | *Excess cyclohexane* | no data | *This study* |
| | *Excess cyclohexane + $H_2O$* | no data | *This study* |
| | *Excess CO* | 0.35 ± 0.09 | *This study* |
| | *Excess CO + $H_2O$* | 0.38 ± 0.10 | *This study* |
| | *Simple $C_4H_8 + O_3$* | 1.51 ± 0.41 | *This study* |
| | | 0.41 | MCMv3.1 |
| | Stoichiometry | 2.00 ± 1.00 (dry) | Wegener *et al.* (2007) |
| | | 1.60 ± 0.80 (wet) | |
| *cis*-2-Butene | *Simple $C_4H_8 + O_3$* | 0.58 ± 0.16 | *This study* |
| | *Excess CO* | 0.12 ± 0.03 | *This study* |
| | | 0.125 | MCMv3.1 |
| *trans*-2-Butene | *Excess CO* | 0.01 ± 0.00 | *This study* |
| | *Excess cyclohexane + $H_2O$* | 0.40 ± 0.20* | *This study* |
| | *Excess CO* | 0.03 ± 0.00 | *This study* |
| | *Excess CO + $H_2O$* | 0.00 | *This study* |
| | *Simple $C_4H_8 + O_3$* | 0.89 ± 0.24 | *This study* |
| | *Excess CO* | 0.07 ± 0.02 | *This study* |
| | | 0.125 | MCMv3.1 |
| 2,3-Dimethyl-2-butene | *Simple $C_6H_9 + O3$* | 1.74 ± 0.47 | *This study* |
| | *Excess CO* | 0.18 ± 0.05 | *This study* |
| | | 0.00 | MCMv3.1 |

* Error is the combined uncertainty of the instrumentation used in the analysis (51 %) and does not include any systematic factors inherent in the approach.

## 4.5 Discussion

Within the limited range of the next few pages, this section attempts to discuss the development and interpretation of the results obtained from the ozonolysis of alkenes studied. The scope of this section is broad and attempts to address issues involving stabilised Criegee intermediate, carbonyl and radical yields. The discussion will be considered in 6 different sections: (*i*) Reaction rate coefficient, (*ii*) Yield of stabilised Criegee intermediates ($Y_{SCI}$), (*iii*) 'Primary' carbonyl yields, (*iv*) Dependence of derived yields upon reagent concentrations, (*v*) OH yields, and (*vi*) $HO_2$ yields

### 4.5.1 Reaction Rate Coefficient

Alkene + ozone reaction rate coefficients have been subject to extensive research, utilising both absolute and relative-rate techniques (Atkinson et al., 1990, Avzianova and Ariya, 2002, Greene and Atkinson, 1992, Grosjean and Grosjean, 1995, Johnson et al., 2000, Treacy et al., 1992). It is well established that $k_{O_3+alkene}$ increases with the number of alkyl groups attached to the C=C bond (Calvert et al., 2000, Johnson and Marston, 2008), analogous to the reaction of alkenes with OH and $NO_3$ radicals. For example, the number of alkyl groups on *trans*-2-butene is twice that in propene and the $k_{O_3+T2B}$ (~ $2.0 \times 10^{-16}$ $cm^3$ $molecule^{-1}$ $s^{-1}$) is over one order of magnitude faster than the $k_{O_3+C_3H_6}$ (~ $1.0 \times 10^{-17}$ $cm^3$ $molecule^{-1}$ $s^{-1}$. Treacy et al. (1992) and Grosjean et al. (1995) demonstrated that increasing the size of the *n*-alkyl substituent, in a series of alkenes, results in a decrease in activation energy, which is consistent with the increasing substituent electron-donating ability. However, the authors also observed a

decrease in the *A* factor (EQ 4.1) consistent with the increasing substituent steric hinderance, which therefore resulted in similar rate coefficients for the 1-alkenes. Although this explains the similarities in the derived $k_{O_3+alkene}$ calculated in this study for propene ($1.15 \times 10^{-17}$ $cm^3$ $molecule^{-1}$ $s^{-1}$) and 1-butene ($1.24 \times 10^{-17}$ $cm^3$ $molecule^{-1}$ $s^{-1}$), it does not explain why 2-methylpropene also has a similar rate coefficient of $1.29 \times 10^{-17}$ $cm^3$ $molecule^{-1}$ $s^{-1}$. One would assume that 2-methylpropene, *cis*- and *trans*-2-butene, all possessing two methyl groups around the C=C bond, would have similar reaction rate coefficients, but is not the case. Treacy et al. (1992) measured near equal activation energies for *cis*- and *trans*-2-butene and attributed the difference in their rate coefficients to the differing result of the pre-exponential factor (*A* factor), which may be a consequence of steric effects.

Another way of rationalising the increasing rate constant with increasing alkyl substituents is to take into account the frontier molecular orbitals (Johnson and Marston, 2008). Increasing the substitution at the C=C bond serves to decrease the energy difference between the highest occupied molecular orbital (HOMO) and lowest unoccupied molecular orbital (LUMO), as electron donating groups (*i.e.* alkyl substitution) raise the energy of the HOMO, and subsequently lower the energy barrier to the formation of the POZ. Johnson et al. (2000) and Avzianova and Ariya (2002) report the linear relationship between the logarithm of the rate constants and the energy of the HOMO of the alkene, in particular for the simple alkenes, providing a means for the prediction of rate constants.

### 4.5.2 Yield of Stabilised Criegee Intermediates ($Y_{SCI}$)

An approximation to the yield of stabilised Criegee intermediate ($Y_{SCI}$) can be made from the observed increase in the derived 'primary' carbonyl yields in the presence of CO, using the postulated chemical mechanisms illustrated in Section 4.3. For example, the excess CO in the ozonolysis of propene scavenges > 95 % of OH radicals as well as the stabilised Criegee intermediates, *anti*-$CH_3CHOO$ (R4.1a) and $CH_2OO$ (R3.4a). An increase in the yield of $CH_3CHO$ and HCHO with CO present therefore reflects the reactions of *anti*-$CH_3CHOO$ + CO (R4.1a) and $CH_2OO$ + CO (R3.4a) respectively. HCHO is also produced by R4.5a, R4.7 and R4.3c which although included in the modelled secondary chemistry, may potentially reduce the accuracy of the calculated $Y_{SCI}$, through uncertainties in the secondary chemistry. The derived optimised branching ratios for R4.1a and R4.1b lead to a HCHO formation yield of 0.51 (R4.1a), which accounts for 63 % of the overall dilution corrected HCHO formation yield of 0.81, in the presence of excess CO (see Table 4.2). It is calculated that the OH yield from the $CH_2OO$ CI is 0.17 (see Chapter 2), which corresponds to 0.08 (0.17 × 0.49) of the overall OH yield of 0.36 calculated from propene ozonolysis (see Table 4.8). Therefore, 0.28 (0.36 - 0.08) of the overall OH yield can be attributed to the $[CH_3CHOO]^*$ CI from propene ozonolysis. Assuming that the *anti*-$[CH_3CHOO]^*$ and *syn*-$[CH_3CHOO]^*$ are formed in equal amounts indicates that the OH yield from the *syn*-$[CH_3CHOO]^*$ is 0.26. Thus, R4.5e accounts for 0.02 of the OH yield (along with 0.02 of the HCHO yield). Furthermore, as proposed by Kuwata et al. (2005) the vinoxy radical formed alongside OH (see Figure 4.2) can undergo decomposition which accounts for 0.06 (0.51 × 0.50 × 0.25) of the calculated HCHO yield (1-β pathway, Figure 4.3). The yield of HCHO *via* channel

R4.7 was calculated using the model as 0.03 (in the ozonolysis of propene), which leaves approximately 0.13 of HCHO that can be attributed to the reaction of the SCI + CO (R3.4a). This is consistent with the observed increase in the formation of HCHO for experiments conducted in the presence of excess CO with the experiments performed in the presence of excess CO and $H_2O$, for propene of 0.16 (see Table 4.2). A yield of 0.13 – 0.16 of HCHO from R3.4a corresponds to a $Y_{SCI}$ of 0.26 – 0.32 for $CH_2OO$.

The derived yield for $CH_3CHO$ of 0.44 ± 0.01 in the simple propene + ozone system is in good agreement with Horie and Moortgat (1991) and Schäfer et al. (1997) (Table 4.2). When increasing the CO concentration, a small decrease in the derived yield of $CH_3CHO$ is observed, indicating that $CH_3CHO$ may be a significant first- and multi-generation product of the propene + OH reaction, which is in qualitative agreement with Wegener et al. (2007) who see a small decrease in the yield of $CH_3CHO$ in the presence of excess CO. The calculated yield for $CH_3CHO$ of 0.38 ± 0.04 in the presence of excess CO is in good agreement with Rickard et al., (1999) who derived their yields in the presence of excess cyclohexane. The agreement with both studies suggests that the *anti*-$CH_3CHOO$ + CO reaction (R4.2a) is a minor source of $CH_3CHO$ in the ozonolysis of propene. However, when increasing the relative humidity from 0.9 to 24.0 %, the $CH_3CHO$ yield increased from 0.38 ± 0.04 to 0.62 ± 0.07, indicating that the *anti*-$CH_3CHOO$ + $H_2O$ reaction (R4.2b) may be a significant source of $CH_3CHO$, in agreement with Hasson et al. (2001b) who similarly determined a $Y_{SCI}$ by exploiting this reaction. The difference between derived $CH_3CHO$ yields under dry and humid conditions may suggest therefore that the $Y_{SCI}$ for $CH_3CHOO$ in the ozonolysis of propene is 0.24 (0.62 – 0.38). In addition a

'crude' estimation of the $Y_{SCI}$ can be made for both *cis*-2-butene (0.19) and *trans*-2-butene (0.13) by calculating the average difference between the derived yield for the primary carbonyl product, $CH_3CHO$, in the absence and presence of excess CO. The calculated $Y_{SCI}$ for 2,3-dimethyl-2-butene was 0.17 (OH yield subtracted from 1) which is discussed in Section 4.6.5. A summary of the inferred yields of stabilised Criegee intermediates are given in Table 4.10.

**Table. 4.10.** Inferred stabilised Criegee intermediate yields for alkenes studied

| **Alkene** | **Criegee Intermediate** | **SCI Yield ($Y_{SCI}$)** | **Reference** |
|---|---|---|---|
| Propene | $CH_3CHOO$ | 0.24 | *This study* |
| | | 0.16 | IUPAC |
| | | 0.24 | MCMv3.1 |
| | | 0.22 | Rickard et al. (1999) |
| | $CH_2OO + CH_3CHOO$ | 0.44 | Horie and Moortgat (1991) |
| | $CH_2OO + CH_3CHOO$ | 0.25 ± 0.02 | Hatakeyama et al. (1984) |
| 1-Butene | $C_2H_5CHOO$ | - | *This study* |
| | | 0.20 | IUPAC |
| | | 0.24 | MCMv3.1 |
| | | 0.10 – 0.16 | Hasson et al. (2001a) |
| 2-Methylpropene | $(CH_3)_2COO$ | - | *This study* |
| | | 0.18 | MCMv3.1 |
| | $(CH_3)_2COO + CH_2OO$ | 0.17 ± 0.03 | Hatakeyama et al. (1984) |
| *cis*-2-Butene | $CH_3CHOO$ | 0.19 | *This study* |
| | | 0.16 | IUPAC |
| | | 0.18 | MCMv3.1 |
| | | 0.19 | Rickard et al. (1999) |
| *trans*-2-Butene | $CH_3CHOO$ | 0.13 | *This study* |
| | | 0.16 | IUPAC |
| | | 0.18 | MCMv3.1 |
| | | 0.19 ± 0.03 | Hatakeyama et al. (1984) |
| | | 0.42 | Horie and Moortgat (1991) |
| | | 0.13 | Rickard et al. (1999) |
| 2,3-Dimethyl-2-butene | $(CH_3)_2COO$ | 0.17 | *This study* |
| | | 0.30 | Niki et al. (1987) |
| | | 0.15 | Drodz et al. (2011) |

### 4.5.3 'Primary' Carbonyl Yields

In the ozonolysis of propene, the formation yields of HCHO in the presence of CO increase from 0.81 ± 0.02 to 0.97 ± 0.05 in the presence of CO + $H_2O$ (see Table 4.2). This is in contrast to the postulated mechanism which suggests that the SCI is scavenged by CO and thus the addition of water should not increase the formation of HCHO *via* reaction R3.4a (Figure 4.4). This increase may be explained by the chemistry of the organic peroxy radical, $HCOCH_2O_2$ (see Figure 4.4). Increasing the humidity in the chamber serves to increase the reaction rate coefficient of the humidity dependent $HO_2$ self reaction, (http://www.iupac-kinetic.ch.cam.ac.uk/, 2007) and also leads to a decrease in the $Y_{HO_2}$ (see Figure 14.17). The fate of the $HCOCH_2O_2$ radical is dependent upon the concentrations of $HO_2$ and $RO_2$ present in the system, and the lower yield of $HO_2$ in the presence of water means that the competition between (R4.6a - d) is altered, forming less of the hydroperoxide *via* R4.6a. This would lead to an increase in the HCHO formation yield *via* the subsequent decomposition of the alkoxy radical (R4.7), which may account for the increase in HCHO yield with enhanced humidity. Alternatively, as the change in HCHO yield is modest, the difference may simply reflect experiment-to-experiment variability and propagated uncertainties.

The identical HCHO formation yields for *cis*-2-butene and similar HCHO & glyoxal formation yields for *trans*-2-butene under all the experimental conditions used (see Tables 4.5 and 4.6), indicate that the formation of these species is not significantly influenced by SCI and / or radical scavengers. This is consistent with the postulated mechanism, Figure 4.5, as scavenging the SCI would lead to additional $CH_3CHO$ and

not HCHO or glyoxal. However, this is inconsistent with the proposed dependence of the fate of the organic peroxy radical chemistry upon $HO_2$ and $RO_2$ concentrations, discussed for propene (above), as the difference in $Y_{HO_2}$ for the simple *trans*-2-butene + $O_3$ system of 0.86 ± 0.23 and excess CO systems of 0.03 ± 0.01, should lead to a different yield of both glyoxal and HCHO owing to the $HO_2$ / $RO_2$ competition for the organic peroxy radical, $HCOCH_2O_2$, for channels (R4.21a – d).

The variation in the derived carbonyl yields from the ozonolysis of 2-methylpropene (Table 4.4), shows that there is a strong dependency on the reactions of the peroxy radicals formed in the system. The HCHO yield for the two simple (absence of OH scavenger) 2-methylpropene + ozone experiments performed differ by a factor of 2, while the yields calculated in the presence of OH radical scavengers range from 1.39 – 1.99 (see Table 4.4). Although studies by Grosjean et al. (1996) and Tuazon et al. (1997) report yields of HCHO close to unity (Table 4.4), other studies for example, Wegener et al. (2007) report a yield of 1.80 ± 0.14. The difference between these studies, however, was that the latter was performed in the absence of a radical scavenger, which indicates that HCHO is a significant product of the OH + 2-methylpropene reaction. Neeb and Moortgat (1999) investigated the product yields from the ozonolysis of 2-methylpropene (with and without excess CO) and found that they could adequately simulate all measured product yields with the exception of methylglyoxal, which was underestimated by a factor of 3. Their results showed that the majority of the observed products from the ozonolysis of 2-methylpropene could be attributed to the secondary reactions of the acetonyl peroxy radical ($CH_3C(O)CH_2O_2$) (Neeb and Moortgat, 1999). This peroxy radical together with the chemistry of the acetyl peroxy radical may explain the variety of yields derived for

HCHO and methylglyoxal in this study for the various experiments performed under different conditions (see Appendix for experimental conditions). Figure 4.18 (below) shows the acetonyl peroxy radical chemistry (adapted from MCMv3.1) used for the modelling purposes of this study (also shown within Figure 4.6).

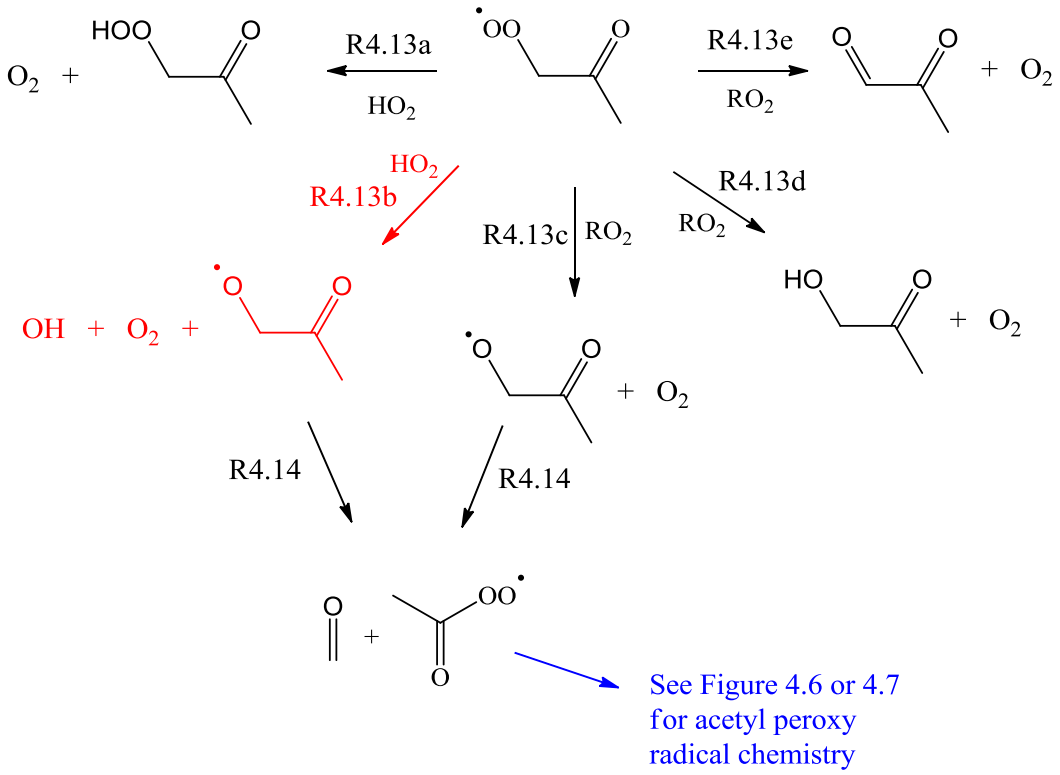


**Figure 4.18.** Acetonyl peroxy radical chemistry, adapted from MCMv3.1 (black) and Jenkin et al. (2008) (red).

The reaction rate coefficient used for R4.13c, R4.13d and R4.13e were $2.0 \times 10^{-12}$ $cm^3$ $molecule^{-1}$ $s^{-1}$, with branching ratios of 0.6, 0.2 and 0.2 respectively, adopted from the MCMv3.1. For R4.13a and R4.13b the IUPAC recommended reaction rate coefficient of $1.36 \times 10^{-13}.exp^{(1250/T)}$ $cm^3$ $molecule^{-1}$ $s^{-1}$ (http://www.iupac-kinetic.ch.cam.ac.uk/, 2007) together with branching ratios of 0.85 and 0.15 respectively (Jenkin et al., 2008) were used. It was found that in order to

best simulate the methylglyoxal observations, the reaction rate coefficient for R4.13e was increased by an order of magnitude, consistent with the results of Neeb and Moortgat (1999).

### 4.5.4 Dependence of Derived Yields Upon Reagent Concentrations

In the ozonolysis of 2-methylpropene, the formation of HCHO is not exclusive to the fast ozonolysis isomerisation / decomposition pathways R3.4a and R4.10a. The acetonyl peroxy radical (Figure 14.18) formed from R4.13 (see Figure 4.6) can react with $HO_2$ (R4.13b) and $RO_2$ (R4.13c) species to form an alkoxy radical which upon decomposition forms HCHO and an acetyl peroxy radical (R4.14). The acetyl peroxy radical (see Figure 4.6) can undergo further reactions resulting in the formation of additional HCHO *via* reactions R4.16c, R4.16d and R4.17. It is not feasible to take *all* these pathways to HCHO formation into account in a simple 'non-model' analysis approach; thus, in order to explore the variations in the differences in the derived carbonyl yields for 2-methylpropene (Table 4.4), a modelling study was conducted to indirectly simulate one of the experiments in the presence of excess CO. The model was used to account for all secondary HCHO sources and the simulated data subject to a 'simple' non-model analysis to assess the impact of these factors upon derived yields as reported in the literature. The initial concentrations (*i.e.* initial ratio of 2-methylpropene to ozone) was altered within the model (ensuring that enough CO scavenger was present in order to scavenge > 95 % of OH produced in each simulation), and the HCHO yield was calculated relative to ozone consumed and relative to alkene consumed, independently. The results showed that the simulated yield of HCHO increased when the ratio of alkene / ozone increased, when deriving

the yield relative to ozone consumed, but remain constant when deriving the yield relative to the alkene; shown in Figure 4.19. The alkene / ozone ratio is therefore important when calculating carbonyl yields relative to ozone, which was not considered by previous studies (Grosjean et al., 1996, Grosjean and Grosjean, 1996b), (Grosjean and Grosjean, 1996a) (see Figure 4.19).

An increase in the simulated HCHO yield was also observed when increasing the reaction rate coefficient of R4.13c (*i.e.* $CH_3C(O)CH_2O_2 + RO_2$, see Figure 4.19), as the fate of the peroxy radical (and formation of secondary HCHO) is dependent upon the competition between $HO_2 + RO_2$ and $RO_2 + RO_2$ chemistry (see Figure 4.18). It was found that the larger the rate constant used for R4.13c, the larger the calculated yield of HCHO (relative to alkene consumed) and the larger range of yields determined relative to ozone consumed (see Figure 4.19). When using the MCMv3.1 reaction rate coefficient of $2.0 \times 10^{-12}$ $cm^3$ $molecule^{-1}$ $s^{-1}$ and branching ratio 0.6 for R4.13c, the range of HCHO yields, calculated relative to ozone consumed, differed by a factor of 44 %, whereas increasing the rate constant by an order of magnitude lead to an increased factor of 54 %. Increasing the reaction rate coefficient of R4.13c (or increasing the branching ratio), consequently means that channels (R4.13a-b) and (R4.13d-e) become minor fates for the acetonyl peroxy radical, and thus an increase in the formation of HCHO is seen, *via* the subsequent reactions of the alkoxy radical (R4.14). The observed HCHO can be adequately simulated if the competition of $RO_2 + RO_2$ chemistry is dominant over the $HO_2 + RO_2$ chemistry, thus 'forcing' the peroxy radical chemistry to form HCHO *via* reactions R4.13c, R4.14d, R4.16b and R4.16c.

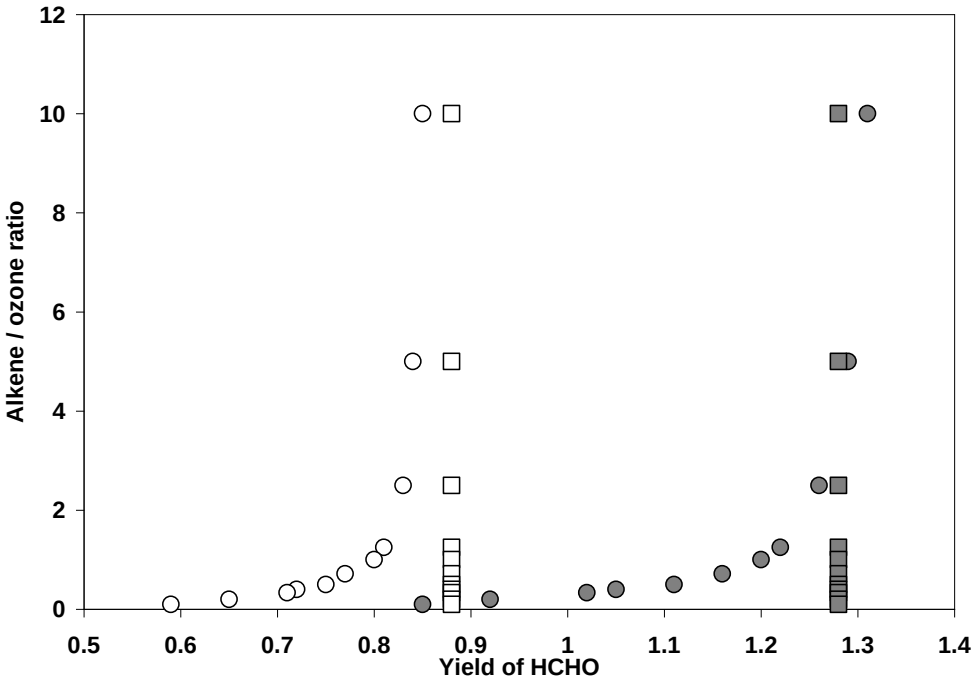


**Figure 4.19.** Derived HCHO yields from the simple non-model analysis approach for the ozonolysis of 2-methylpropene, with respect to ozone (circles) and with respect to alkene (squares) at different 2-methylpropene / ozone ratios. An increase in the simulated HCHO yield is observed on increasing the reaction rate coefficient for (R4.13c) by an order of magnitude (closed squares) (R4.13c rate coefficient for open squares is adopted from MCMv3.1 of $2.0 \times 10^{-12}$ $cm^3$ $molecule^{-1}$ $s^{-1}$)

## 4.5.5 OH Yields

The OH steady state measurements and derived yields presented in this study are the first direct observations reported for a homologous series of alkenes, under tropospherically relevant conditions; and are the first direct measurements for propene, 1-butene and 2-methylpropene. The OH yields obtained here are compared with literature values in Table 4.8 and are illustrated in Figure 14.20, where datasets from various groups (Atkinson, 1997b, McGill et al., 1999, Mihelcic et al., 1999, Qi

et al., 2006, Qi et al., 2009, Rickard et al., 1999) are correlated with the IUPAC recommended OH yield (http://www.iupac-kinetic.ch.cam.ac.uk/, 2009) for ethene, propene, 1-butene, 2-methylpropene, *cis*-2-butene, *trans*-2-butene and 2,3-dimethyl-2-butene. These literature studies, however, exploit indirect methods to detect OH, by the use of OH scavenger (Atkinson, 1997b) and tracer (Rickard et al., 1999) techniques, with the exception of Mihelcic et al. (1999) and Qi et al. (2009) who use MIESR and PERCA techniques respectively. The agreement within the different studies, particularly between this study and the IUPAC recommendations, shows that the results are consistent with the isomerisation / decomposition of a given CI to a vinyl hydroperoxide and OH; the basis of the OH yield structure activity relationship (SAR) of Rickard et al. (1999)

The first direct evidence for OH formation in the ozonolysis of alkenes was obtained by Donahue et al. (1998) from LIF observations at total pressures of 4 – 6 Torr (see Table 4.8). Short timescale (*ca.* 10 ms) measurements at various pressures between 1 Torr and several hundred Torr were made by Kroll and co workers (Kroll et al., 2001a, Kroll et al., 2001b, Kroll et al., 2001c) who found that for substituted alkenes, prompt formation is effectively quenched as pressures approach ~ 400 Torr. Longer timescale (*ca.* 1 s) measurements at atmospheric pressure, however, indicated that the OH yield increased (Kroll et al., 2001c) approaching values consistent with both prompt, low pressure measurements and other atmospheric pressure measurements from radical scavenger / tracer experiments (see Table 4.8).

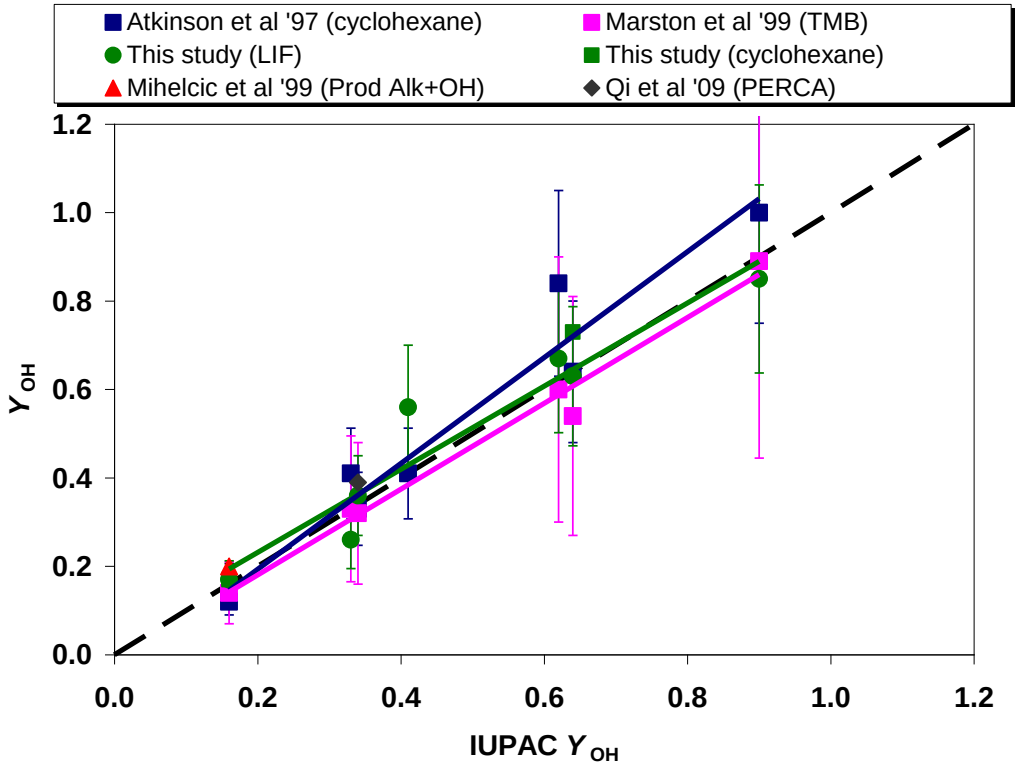


**Figure 4.20.** Comparison of IUPAC OH yield recommendations *vs.* literature OH yields. Studies conducted by Atkinson *et al.* (1997); the Marston group (*i.e.* Rickard *et al.* (1999) and McGill *et al.* (1999)); Qi *et al.* (2009); Mihelcic *et al.* (1999) and this study. The dashed line shows the 1:1 correlation. All studies regardless of the direct / indirect methods used are in good agreement.

This shows that OH formation from alkene ozonolysis can result from both prompt formation from a vibrationally excited CI and formation from the decomposition of an initially stabilised CI at longer timescales (Johnson and Marston, 2008) as discussed in Chapter 3, Section 3.4 (see Figure 3.6). Thus, there is the possibility for bimolecular reactions to occur with the partially thermalised CI interrupting the decomposition process. This could account for the sub-unity OH yield observed for the substituted alkene species 2,3-dimethyl-2-butene (http://www.iupac-kinetic.ch.cam.ac.uk/, 2007) where the hydroperoxide channel should be dominant with an expected OH yield of 1, but for which many studies measure a yield of < 1,

including the direct measurements reported in this study of 0.83 ± 0.22 (see Table 4.8). This is in contrast with the findings of Kuwata et al. (2010) who predict that the hydroperoxide mechanism proceeds 3 – 8 orders of magnitude faster than the thermalised CI reaction with water, indicating that water cannot interrupt the production of OH at least for *trans*-2-butene and isoprene. Nonetheless, this does not preclude the possibility of intercepting the hydroperoxide mechanism by reaction of the thermalised CI with other species, such as CO. On the other hand, it does indicate that a humidity dependence in the OH yield should not be observed, consistent with the findings of this study for *trans*-2-butene (see Table 4.8). More recently, the pressure dependence of the SCI yield was investigated (Drozd et al., 2011), where an increase in the yield of SCI with increasing pressure was observed. The authors report (by extrapolation) that ~ 15 % of the initially formed CI is formed below the barrier to isomerisation, which may account for the reported OH yield in this study of 0.83, considering that ~ 15 % of the CI may undergo bimolecular reaction. This suggests that the $Y_{SCI}$ from the ozonolysis of 2,3-dimethyl-2-butene calculated in this study is 0.17, consistent with Drozd et al. (2011).

The humidity dependencies to $Y_{OH}$ recently reported by Wegener et al. (2007) for propene, 1-butene, 2-methylpropene and *cis*-2-butene and by Tillmann et al. (2010) for α-pinene appear to be inconsistent with the results reported here and those of Kuwata et al. (2010). The majority of experimental studies, however, predict that the OH yield from alkene ozonolysis remain unaffected under enhanced humidity (Aschmann et al., 2002, Atkinson and Aschmann, 1993, Atkinson et al., 1992, Hasson et al., 2003). *Ab initio* calculations by Anglada et al. (2002) indicated the possibility for the formation of a hydroxy-alkyl-hydroperoxide from the reaction of the

SCI + $H_2O$, subsequently decomposing to yield OH or aldehydes. They also showed that the reaction of the *syn*-CI with $H_2O$ could form a vinyl hydroperoxide *via* the hydroperoxide mechanism, which in fact would cause the $Y_{OH}$ to be unaffected under enhanced humidity, as this would be an alternative reaction pathway forming OH *via* the same hydroperoxide channel. However, to account for the increased humidity OH yield observed by recent studies, Kuwata et al. (2010) proposed the *anti*-CI + $H_2O$ reaction analogous to that of Anglada et al. (2002) forming a vinyl hydroperoxide with an unstable peroxy bond.

Kroll et al. (2002) investigated the possibility of OH formation from the *anti*-CI by measuring yields of OD and OH radicals from deuterated (and un-deuterated) *cis*- and *trans*-3-hexene. The authors measured larger OH yields than OD yields for *trans*-3-hexene-3,4-$d_2$ respectively; and OH yields equivalent to the approximate combined total yields of OH + OD (measured for the deuterated species) for *cis*-and *trans*-3-hexene. This suggests that OH formation from *anti*-CIs may also play a significant role in the total OH yield, as approximately one third of the total OH yield comes from the *anti*-CI in the ozonolysis of *cis*-3-hexene (Kroll et al., 2002).

In this study, dependent upon the alkene, OH formation can be attributed to 4 sources, 2 primary (dominant) and 2 secondary:

*i)* Hydroperoxide mechanism – most likely dominant OH route for the *syn*-CI

*ii)* "Hot" acid – route to OH formation may play a part in the decomposition of *anti*-CIs, as demonstrated by Kroll et al. (2002).

*iii)* Excited β-oxo peroxy radical – formed from the reaction of vinoxy radical (formed alongside OH *via* the hydroperoxide mechanism) and $O_2$, which may

decompose to form OH (Figure 4.3), as proposed by Kuwata et al. (2005) with a yield of 0.25 (if an aldehydic H is present). This α-oxo peroxy radical is present in the ozonolysis of propene and 2-butenes.

*iv)* Reactions of $RO_2$ + $HO_2$ – Reaction of the acetonyl peroxy radical ($CH_3C(O)CH_2O_2$) with $HO_2$ producing OH with a 0.15 yield, as proposed by Jenkin et al. (2008), see Figure 4.19; and the reaction of the acetyl peroxy radical ($CH_3C(O)O_2$) with $HO_2$ which can also form OH, with reported yields of 0.37 – 0.50 presented by various studies (Barber and Marston, 2010, Dillon and Crowley, 2008, Hasson et al., 2004, Jenkin et al., 2007, Jenkin et al., 2008). These peroxy radicals are formed in the ozonolysis of 2-methylpropene and 2,3-dimethyl-2-butene.

For example, from the postulated mechanism for the ozonolysis of propene (Figure 4.4), the calculated branching ratio for the decomposition of the POZ to R4.1a and R4.1b is 0.51 and 0.49, respectively. As previously discussed in Chapter 3, $[CH_2OO]^*$ forms OH with a yield of 0.17, which corresponds to an OH formation yield of 0.08 (0.49 × 0.17) from this. In addition, if it is assumed that equal amounts of *anti*-$[CH_3CHOO]^*$ and *syn*-$[CH_3CHOO]^*$ are formed from R4.1a and the *syn*-CI predominantly decomposes to give OH and a vinoxy radical (R4.4), whereby the vinoxy radical reaction with $O_2$ followed by decomposition to OH (with a yield of 0.25) is taken into account within the model, then this together with the OH formation yield of 0.08 from $[CH_2OO]^*$ will account for 93 % of the overall OH yield derived in this study (0.36 ± 0.10). Thus, to account for the remaining 7 % of the total derived OH yield, a branching ratio of 0.05 of OH is required from the decomposition of the "hot" acetic acid. However, uncertainties in the commonly assumed equal branching

of the *syn* / *anti*-CI and the OH formation yield of 0.25 from the decomposition of the β-oxo peroxy radical may also account for this value.

### 4.5.6 $HO_2$ Yields

The $HO_2$ yields calculated from this study from the non-scavenger and excess CO experiments are compared with the limited literature values available in Figure 4.21. The $Y_{HO_2}$ determined for the experiments performed in the absence of radical scavenger suggests that the current yields of $HO_2$ used in the MCMv3.1 are underestimated, as shown in Figure 4.21. The $Y_{HO_2}$ in the MCMv3.1, however, are in good agreement with the $Y_{HO_2}$ determined for excess CO experiments. Literature reports of $HO_2$ formation are scarce (see Table 4.9), and $HO_2$ yields employed in the MCM are largely deduced from observations of other reaction products (*i.e.* radical yields inferred through the observation of stable products using assumed mechanisms).

The calculated $Y_{HO_2}$ of 0.61 ± 0.16 obtained in the non-scavenger propene + ozone system is intermediate to the previously reported yields of 0.19 ± 0.04 (Qi et al., 2009) and 1.50 ± 0.75 (Wegener et al., 2007). Qi et al. (2009) determined yields of OH, $HO_2$ and $RO_2$ by calculating the total radical yield of 0.97 ± 0.17 relative to consumed ozone, followed by radical partitioning derived from a box model to obtain yields of 0.39 ± 0.08, 0.19 ± 0.04 and 0.39 ± 0.08 for OH, $HO_2$ and $RO_2$, respectively. The authors comment that their derived total radical yield ranged from 0.83 to 1.18, when altering the branching ratio R4.1b from 0.5 to 0.2. Their model calculations also

demonstrated that radical yields were unchanged when the branching ratios forming HCO + $CH_3O$ and H + $CH_3$ + $CO_2$ ranged from 0 to 0.17. This appears to be contradictory when looking at the radicals produced from these reactions. HCO and $CH_3O$ radicals react near instantaneously with $O_2$ in the atmosphere forming 2 $HO_2$, CO and HCHO; whereas H and $CH_3$ radicals react near instantaneously with $O_2$ to form $HO_2$ and $CH_3O_2$. Although this would lead to the same total radical yield, it would alter the $HO_2$ and $CH_3O_2$ yields; the extent of which would be dependent on the branching ratios of R4.1a and R4.1b used (Qi et al., 2009).

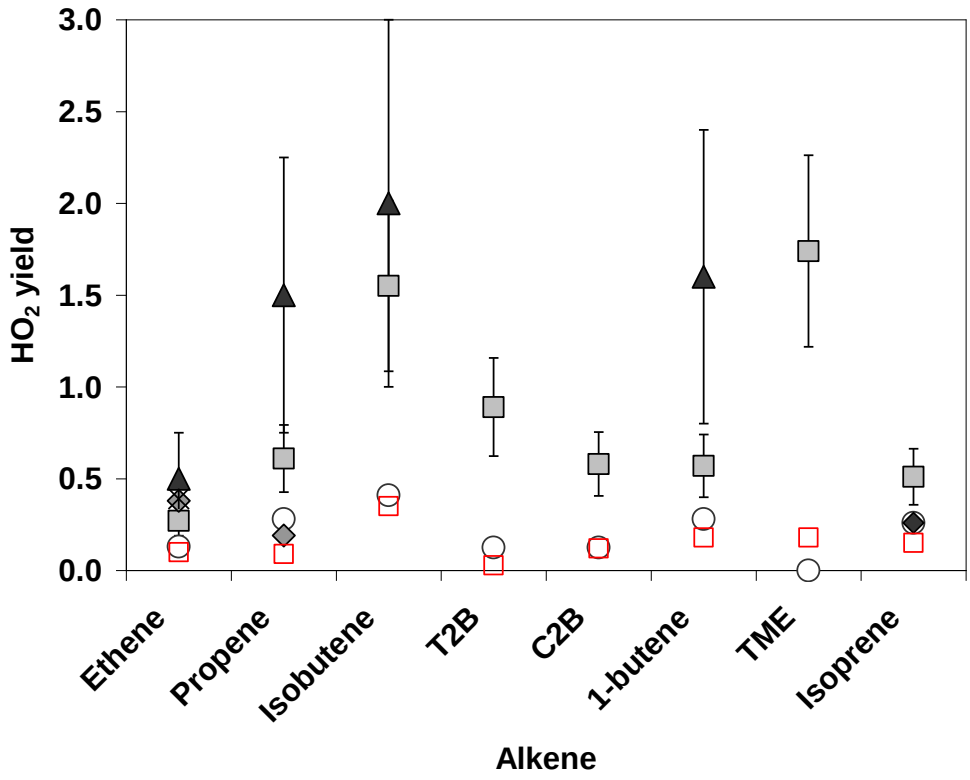


**Figure 4.21.** Comparison of $HO_2$ yields for small chain alkenes investigated during this study with literature. The abbreviations T2B, C2B and TME are *trans*-2-butene, *cis*-2-butene and 2,3-dimethyl-2-butene respectively. Grey squares and red open squares are $HO_2$ yields calculated from this study (by LIF) for non-scavenged and excess CO experiments respectively. Black triangles – Wegener et al. (2007); open circles – MCMv3.1; Grey diamonds – Qi et al. (2006) and Qi et al. (2009); black diamonds – Malkin et al. (2010); black star – Mihelcic et al. (1999)

The $HO_2$ yields reported by Wegener et al. (2007) exploited the reaction $HO_2 + O_3 \rightarrow OH + 2O_2$ to evaluate $HO_2$ formation from the additional ozone turnover in excess CO experiments. The secondary formation of OH *via* the $HO_2 + O_3$ reaction disturbs the accurate determination of $Y_{OH}$, making it difficult to optimise reaction conditions for sensitively calculating both $Y_{OH}$ and $Y_{HO_2}$ at the same time. Wegener *et al.*'s reaction conditions were chosen such that OH would preferentially be produced by ozonolysis and consumed by the reaction with ethene, while suppressing the turnover for the reaction of $HO_2 + O_3$. The contribution of ozone removal *via* reaction with $HO_2$, relative to the removal *via* reaction with ethene or dilution was therefore small, resulting in a large uncertainty in the derived $Y_{HO_2}$.

The observed decrease in the calculated $Y_{HO_2}$ for the excess CO experiments in this work is consistent with the measurements for ethene ozonolysis, and is discussed in Chapter 3. Briefly, potential explanations for the observed decrease are: (*i*) bimolecular reaction of the partially thermalised CI interrupting the decomposition through isomerisation to the vinyl hydroperoxide process; (*ii*) the reaction of CO + dioxirane, leading to the formation of an acid anhydride; (*iii*) an additional $HO_2$ production channel from the bimolecular reactions of the SCI, competing with CO and $H_2O$. This would also account for the observed decrease in $Y_{HO_2}$ seen in enhanced humidity ozonolysis reactions of propene and *trans*-2-butene. Very recently, Fuchs et al. (2011) have reported potential interferences in the $HO_2$ mode of detection by LIF. This may offer an alternative perspective for the interpretation of the observed decrease in the calculated $Y_{HO_2}$ for the excess CO experiments. This is explored in Chapter 5.

However, in the ozonolysis of 2-methylpropene, the calculated $Y_{HO_2}$ of 0.38 ± 0.10 for the excess CO with enhanced humidity system (see Table 4.9) is inconsistent with the potential explanations above, as the derived yield is in good agreement with other 'dry' excess CO experiments of 0.36 ± 0.10, 0.31 ± 0.08 and 0.35 ± 0.10. This suggests that there may be a significant source of $HO_2$ from the subsequent peroxy radical chemistry in the ozonolysis of 2-methylpropene and may also explain the greater than unity $Y_{HO_2}$ derived for the simple ozonolysis reactions of 2,3-dimethyl-2-butene (1.74 ± 0.47) and for 2-methylpropene (1.51 ± 0.41) (both alkenes possess $[(CH_3)_2COO]$* Criegee intermediates).

From the postulated mechanisms, adapted from Calvert et al. (2000), Johnson and Marston (2008) and Paulson et al. (1999a) (see Section 4.3), it can be seen that the source of $HO_2$ is mainly expected to be from the decomposition of the "hot" acid intermediate which results from isomerisation of the *anti*-CI (and / or $[CH_2OO]$*). Any secondary formation of $HO_2$ is accounted for within the model (*e.g.* subsequent $HO_2$ formation from the chemistry of peroxy and alkoxy radicals, see Figure 4.4). Again, if the postulated mechanism for the ozonolysis of propene is taken into account, it can be assumed that a yield of 0.27 for $HO_2$ comes from the subsequent chemistry of channel R4.7b, which has been discussed in Chapter 3, for the $[CH_2OO]$* intermediate. This would mean that a branching ratio of 0.94 for $HO_2$ is required from the *anti*-$[CH_3CHOO]$* intermediate (or 0.47 from both *syn*- and *anti*-$[CH_3CHOO]$*), which is clearly not feasible owing to the production of other reported stable species formed from the *anti*-CI (Calvert et al., 2000).

The source of $HO_2$ is of significant interest in the ozonolysis of alkenes, as the large yields of $HO_2$ derived cannot be attributed to the postulated mechanisms, other than for ethene. Interestingly, there is a good correlation ($R^2$ = 0.74 – 0.79) between the derived OH yields and $HO_2$ yields in this study, as shown in Figure 4.22. This may suggest that OH formation *via* the vinyl hydroperoxide mechanism may also form a route for $HO_2$ production, which is not included in the postulated mechanisms. Further discussion of the interpretation of these results is described in Chapter 5 (Interpretation and Atmospheric Implications).

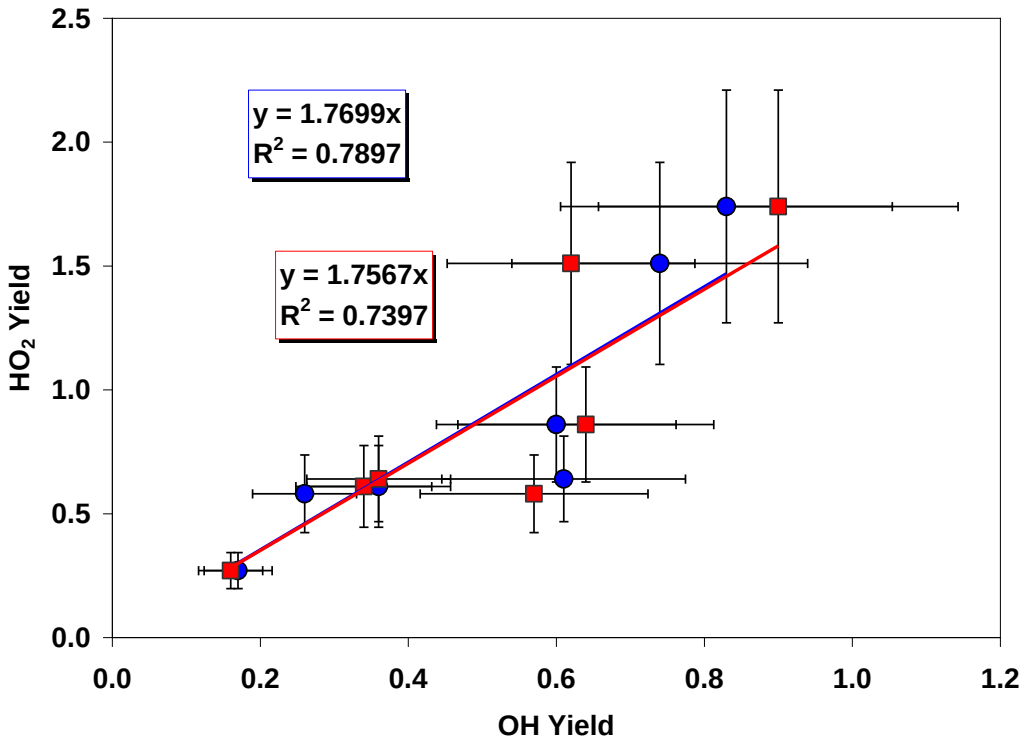


**Figure 4.22.** Correlation of OH yields derived from this study (blue circles) and IUPAC (red squares) *vs.* $HO_2$ yields determined during this study.

## 4.6 Summary of Branching Ratios for Reaction Pathways

The yields of OH, $HO_2$ and carbonyls reported in this study were used to obtain branching ratios for the reaction mechanisms illustrated in Section 4.3. The branching ratio of the initial POZ fragmentation for propene, 1-butene and 2-methylpropene, was calculated in Section 4.5.2. *syn*-CIs are expected to undergo isomerisation / decomposition to OH *via* the hydroperoxide mechanism, which in most cases accounts for 100 % of the measured $Y_{OH}$ in this study. Any additional OH that cannot be accounted for by the *syn*-CI is attributed to OH formation *via* the *anti*-CI. As mentioned previously, OH production from alkene ozonolysis can be rationalised by two dominant (fast) and two secondary sources, which could not be differentiated by these experiments. However, recent reports of OH yields from the secondary chemistry of the β-oxo peroxy radical and other peroxy radicals has enabled the deduction of the combined branching ratios for the 2 fast ozonolysis OH sources (*anti*-CI and *syn*-CI decomposition / isomerisation). The calculated $Y_{SCI}$ discussed in Section 4.6.2 (see Table 4.10), were used to assign stabilisation branching ratios for propene, *cis*- / *trans*-2-butene and 2,3-dimethyl-2-butene, for their respective postulated mechanisms (see Figures 4.4 – 4.8). It is difficult to account for the large $HO_2$ yields derived from the alkenes studied prima facie, presenting a challenge in determining branching ratios for individual reactions within each postulated mechanism (Figures 4.4 – 4.8). Thus, when determining the decomposition branching ratios for these alkenes, it was not possible to account for all the observed $HO_2$ formation. Further insight to the interpretation of $HO_2$ yields is given in Chapter 5. The decomposition branching ratios from the $[CH_2OO]^*$ CI resulting from the ozonolysis of propene, 1-butene and 2-methylpropene were adopted from Chapter 3.

Tables 4.11 – 4.13 shows the deduced branching ratios for the $[CH_3CHOO]^*$ CI for the ozonolysis of propene, *cis*-2-butene and *trans*-2-butene respectively. The calculated branching ratios for the $[(CH_3)_2COO]^*$ CI for the ozonolysis of 2-methylpropene and 2,3-dimethyl-2-butene are tabulated in Tables 4.14 – 4.15; and the branching ratios for the $[CH_3CH_2CHOO]^*$ CI for the ozonolysis of 1-butene is shown in Table 4.16.

**Table 4.11.** Summary for the branching ratios derived for reactions of the $[CH_3CHOO]^*$ CI formed in the ozonolysis of propene

| **Reaction Number (see Figure 4.4)** | **Reaction** | **Branching Ratio** |
|---|---|---|
| (R4.1a) | $POZ \rightarrow [CH_3CHOO]^* + HCHO$ | 0.51 [a] |
| (R4.1b) | $POZ \rightarrow [CH_2OO]^* + CH_3CHO$ | 0.49 [a] |
| (R4.2) | $[CH_3CHOO]^* + M \rightarrow CH_3CHOO$ | 0.24 [b] |
| (R4.3a)<br>(R4.3b) | $[CH_3CHOO]^* \rightarrow CH_4 + CO_2$<br>$[CH_3CHOO]^* \rightarrow CH_3OH + CO$ | |
| (R4.3c) | $[CH_3CHOO]^* \rightarrow CH_3O + HCO$ | $\leq 0.21$ [c] |
| (R4.3d)<br>(R4.3e) | $[CH_3CHOO]^* \rightarrow CH_2CO + H_2O$<br>$[CH_3CHOO]^* \rightarrow$ other products [d] | |
| (R4.4) | $[CH_3CHOO]^* \rightarrow OH + CH_2CHO$ | 0.55 [e] |

[a] deduced from optimised POZ branching ratio (Section 4.5.2)

[b] $Y_{SCI}$ determined in Section 4.6.2

[c] remaining ratio is attributed to this channel which results in the formation of 2 $HO_2$ molecules from subsequent reactions of $CH_3O$ and HCO with $O_2$. This ratio only accounts for 57 % of the total derived $HO_2$ yield from the non-scavenger propene + ozone experiment (see Table 4.9)

[d] other products can be *e.g.* $OH + CO + CH_3O_2$

[e] $Y_{OH}$ determined in Section 4.5.3. The $[CH_2OO]^*$ CI accounts for 23 % of the OH produced from the ozonolysis of propene. The remaining 77 % is therefore attributed to the $[CH_3CHOO]^*$ CI which results in a branching ratio of 0.55. If an equal branching of the *syn*- and *anti*-CI configuration is assumed, then a ratio of 0.05 would be attributed to R4.3e (formation of $OH + CO + CH_3O_2$ )

**Table 4.12.** Summary for the branching ratios derived for reactions of the $[CH_3CHOO]^*$ CI formed in the ozonolysis of *cis*-2-butene

| Reaction Number (see Figure 4.5) | Reaction | Branching Ratio |
|---|---|---|
| (R4.9a) | POZ → $[CH_3CHOO]^*$ + $CH_3CHO$ | 1.00 |
| (R4.2) | $[CH_3CHOO]^*$ + M → $CH_3CHOO$ | 0.19 [a] |
| (R4.3c) | $[CH_3CHOO]^*$ → $CH_3O$ + HCO | ≤ 0.29 [b] |
| (R4.3a)<br>(R4.3b)<br>(R4.3d)<br>(R4.3e) | $[CH_3CHOO]^*$ → $CH_4$ + $CO_2$<br>$[CH_3CHOO]^*$ → $CH_3OH$ + CO<br>$[CH_3CHOO]^*$ → $CH_2CO$ + $H_2O$<br>$[CH_3CHOO]^*$ → other products [d] | 0.21[c] |
| (R4.4) | $[CH_3CHOO]^*$ → OH + $CH_2CHO$ | 0.26 [e] |

[a] $Y_{SCI}$ determined by 'crude' estimation in Section 4.6.2 and is in excellent agreement to that reported by Rickard et al. (1999)
[b] This ratio is an upper limit of $HO_2$ formation and accounts for 100 % of measured $HO_2$ yield from the simple *cis*-2-butene + ozone experiment (see Table 4.9). 2 $HO_2$ molecules are formed from subsequent reactions of $CH_3O$ and HCO with $O_2$
[c] remaining ratio is attributed to the combined channels (R4.3a – b) and (R4.3d – e)
[d] examples of other products can be H + $CO_2$ + $CH_3$
[e] $Y_{OH}$ determined in Section 4.5.3

**Table 4.13.** Summary for the branching ratios derived for reactions of the $[CH_3CHOO]^*$ CI formed in the ozonolysis of *trans*-2-butene

| Reaction Number (see Figure 4.5) | Reaction | Branching Ratio |
|---|---|---|
| (R4.9a) | POZ → $[CH_3CHOO]^*$ + $CH_3CHO$ | 1.00 |
| (R4.2) | $[CH_3CHOO]^*$ + M → $CH_3CHOO$ | 0.13 [a] |
| (R4.3a)<br>(R4.3b) | $[CH_3CHOO]^*$ → $CH_4$ + $CO_2$<br>$[CH_3CHOO]^*$ → $CH_3OH$ + CO | |
| (R4.3c) | $[CH_3CHOO]^*$ → $CH_3O$ + HCO | 0.27 [b] |
| (R4.3d) | $[CH_3CHOO]^*$ → $CH_2CO$ + $H_2O$ | |
| (R4.3e) | $[CH_3CHOO]^*$ → other products [c] | |
| (R4.4) | $[CH_3CHOO]^*$ → OH + $CH_2CHO$ | 0.60 [d] |

[a] $Y_{SCI}$ determined by 'crude' estimation in Section 4.6.2 and is in excellent agreement to that reported by Rickard et al. (1999)
[b] remaining ratio is attributed to this channel which results in the formation of 2 $HO_2$ molecules from subsequent reactions of $CH_3O$ and HCO with $O_2$. This ratio only accounts for 61 % of the total derived $HO_2$ yield in this study from the simple *trans*-2-butene + ozone experiment (see Table 4.9)
[c] other products can be OH + CO + $CH_3O_2$
[d] $Y_{OH}$ determined in Section 4.5.3, using an average of 0.60 from excess cyclohexane (0.57) and non scavenger (0.63) ozonolysis experiments. If an equal branching of the *syn*- and *anti*-CI configuration is assumed, then a ratio of 0.10 would be attributed to R4.3e for the formation of OH + CO + $CH_3O_2$

**Table 4.14.** Summary for the branching ratios derived for reactions of the $[(CH_3)_2COO]^*$ CI formed in the ozonolysis of 2-methylpropene

| **Reaction Number (see Figure 4.6)** | **Reaction** | **Branching Ratio** |
|---|---|---|
| (R4.10a) | POZ → $[(CH_3)_2COO]^*$ + HCHO | 0.66 [a] |
| (R4.10b) | POZ → $[CH_2OO]^*$ + $CH_3C(O)CH_3$ | 0.34 [a] |
| (R4.11) | $[(CH_3)_2COO]^*$ + M → $(CH_3)_2COO$ | ≤ 0.07 [b] |
| (R4.12) | $[(CH_3)_2COO]^*$ → OH + $CH_3C(O)CH_2$ | 0.93 [c] |
| - | $[(CH_3)_2COO]^*$ → other products [d] | - |

[a] deduced from determined POZ branching ratio optimisation (Section 4.5.2)
[b] the remaining ratio is attributed to this channel and is therefore an upper limit, calculated from 1 – OH yield
[c] $Y_{OH}$ determined in Section 4.5.3. The $[CH_2OO]^*$ CI accounts for 9 % of the OH produced in the ozonolysis of 2-methylpropene. The remaining 91 % is therefore attributed to the $[CH_3CHOO]^*$ CI which results in a branching ratio of 0.93
[d] other products may include $HO_2$ formed *via* a dioxirane structure from the isomerisation of the initially thermalised CI. The production of $HO_2$ cannot be accounted for using the postulated mechanism

**Table 4.15.** Summary for the branching ratios derived for reactions of the $[(CH_3)_2COO]^*$ CI formed in the ozonolysis of 2,3-dimethyl-2-butene

| **Reaction Number (see Figure 4.7)** | **Reaction** | **Branching Ratio** |
|---|---|---|
| (R4.10a) | POZ → $[(CH_3)_2COO]^*$ + $CH_3COCH_3$ | 1.00 |
| (R4.11) | $[(CH_3)_2COO]^*$ + M → $(CH_3)_2COO$ | ≤ 0.17 [a] |
| (R4.12) | $[(CH_3)_2COO]^*$ → OH + $CH_3C(O)CH_2$ | 0.83 [b] |
| - | $[(CH_3)_2COO]^*$ → other products [c] | - |

[a] the remaining ratio is attributed to this channel and is therefore an upper limit, calculated from 1 – OH yield.
[b] $Y_{OH}$ determined in Section 4.5.3.
[c] other products may include $HO_2$ formed *via* a dioxirane structure from the isomerisation of the initially thermalised CI. The production of $HO_2$ can not be accounted for using the postulated mechanism

**Table 4.16.** Summary for the branching ratios derived for reactions of the $[CH_3CH_2CHOO]^*$ CI formed in the ozonolysis of 1-butene

| **Reaction Number (see Figure 4.8)** | **Reaction** | **Branching Ratio** |
|---|---|---|
| (R4.19a) | POZ → $[C_2H_5CHOO]^*$ + HCHO | 0.59 [a] |
| (R4.19b) | POZ → $[CH_2OO]^*$ + $CH_3CH_2CHO$ | 0.41 [a] |
| (R4.20) | $[C_2H_5CHOO]^*$ + M → $C_2H_5CHOO$ | |
| (R4.21a) | $[C_2H_5CHOO]^*$ → $C_2H_6$ + $CO_2$ | |
| (R4.21b) | $[C_2H_5CHOO]^*$ → $CH_3CHO$ + HCHO | |
| (R4.21c) | $[C_2H_5CHOO]^*$ → $C_2H_5O$ + HCO | 0.07 [b] |
| (R4.21d) | $[C_2H_5CHOO]^*$ → $C_2H_5$ + $CO_2$ + H | |
| (R4.21e) | $[C_2H_5CHOO]^*$ → other products | |
| (R4.22) | $[C_2H_5CHOO]^*$ → OH + $CH_3CHCHO$ | 0.83 [c] |

[a] deduced from determined POZ branching ratio optimisation (Section 4.5.2)

[b] remaining ratio is attributed to this channel which results in the formation of 2 $HO_2$ molecules from subsequent reactions of $C_2H_5O$ and HCO with $O_2$. The ratio only accounts for 33 % of the total derived $HO_2$ yield in this study from the simple 1-butene + ozone experiment (see Table 4.9)

[c] $Y_{OH}$ determined in Section 4.5.3. The $[CH_2OO]^*$ CI accounts for 12 % of the OH produced in the ozonolysis of 1-butene. The remaining 88 % is therefore attributed to the $[C_2H_5CHOO]^*$ CI which results in a branching ratio of 0.83. If an equal branching of the *syn*- and *anti*-CI configuration is assumed, then a ratio of 0.33 would be attributed to R4.21e forming OH + CO + $C_2H_5$

# Chapter 5 - Interpretation of $HO_2$ Yields & Atmospheric Implications

In this chapter, potential interferences in the $HO_2$ mode of detection by LIF are discussed, offering an alternative perspective for the interpretation of the results obtained in Chapters 3 and 4. The results are then used to predict the contribution of OH and $HO_2$ radicals from alkene ozonolysis to the total atmospheric $HO_x$ radical budget, for both a typical summer's day and night.

## 5.1 Introduction

The importance of the measurements of OH and $HO_2$ in the atmosphere has been emphasised in Chapter 1, outlining the need for accurate high sensitivity instrumentation. Over the last few years laser induced fluorescence (LIF) has been developed in order to achieve high measurement sensitivities for $HO_2$, and has been utilised in various field campaigns (Commane et al., 2010, Fuchs et al., 2010, Smith et al., 2006). This technique, is an indirect method that exploits the chemical conversion reaction between $HO_2$ and NO (see Chapter 2), and as OH is not directly detected, may be susceptible to interferences. In this study, $HO_2$ was detected indirectly by LIF of OH, in the ozonolysis of selected alkenes. Potential explanations are discussed for the observed decrease in the calculated $HO_2$ yields for experiments performed in the presence of excess CO (OH scavenger, see Chapters 3 and 4). Very

recent literature suggests that certain $RO_2$ radicals may be detected as $HO_2$ due to the chemical conversion of peroxy radicals forming OVOCs and $HO_2$, driven by reaction with NO within the LIF system (Fuchs et al., 2011). Those $RO_2$ species identified to show a substantial interference include those formed from OH + alkene reactions.

## 5.2 Interferences and Interpretation of $HO_2$ Yields

This Section is sub-divided into two parts describing the possibilities of interferences from: (*i*) alkyl peroxy radicals and (*ii*) β-hydroxyalkyl peroxy radicals; followed by a description of the potential for such interferences to contribute to the reported $HO_2$ yields in this study.

### 5.2.1 Organic Peroxy Radical ($RO_2$) Conversion

The detection of $HO_2$ by LIF has been discussed in Chapter 2; briefly $HO_2$ is detected as OH by titration with excess NO within the instrument (R5.1).

$$HO_2 + NO \rightarrow OH + NO_2 \qquad \text{(R5.1)}$$

As mentioned in Chapter 1, $RO_2$ radical species can be formed in a number of reactions including OH- and $O_3$-initiated oxidation of alkenes. The high NO mixing ratio in the LIF detection cell (*ca.* 5.3 ppmV) ensures that all $RO_2$ radicals react rapidly and exclusively with NO forming RO radicals (R5.2), with a typical rate constant of approximately $9 \times 10^{-12}$ $cm^3$ $molecule^{-1}$ $s^{-1}$ (Atkinson and Arey, 2003,

http://www.iupac-kinetic.ch.cam.ac.uk/, 2007). The alkoxy radicals (RO) formed can subsequently go on to form $HO_2$ by reaction with $O_2$ *via* R5.3, and can also undergo decomposition, isomerisation or react with NO (R5.4) (Atkinson, 1997a, Orlando et al., 2003).

$$RO_2 + NO \rightarrow RO + NO_2 \quad \text{(R5.2)}$$

$$RO + O_2 \rightarrow RCHO + HO_2 \quad \text{(R5.3)}$$

$$RO + NO \rightarrow RONO \quad \text{(R5.4)}$$

Dependent upon the reaction rate coefficient of R5.3, the $HO_2$ produced can potentially undergo further conversion to OH *via* R5.1, in the LIF system. This has previously thought to be negligible (Heard and Pilling, 2003); for example, owing to the low partial pressure of $O_2$ in the fluorescence chamber and the slow rate coefficient of R5.3, for the methoxy radical, $CH_3O$, (*ca.* $1.9 \times 10^{-15}$ $cm^3$ $molecule^{-1}$ $s^{-1}$) (http://www.iupac-kinetic.ch.cam.ac.uk/, 2007) only a small fraction (~ 1 %) of $CH_3O$ is converted to $HO_2$ (Holland et al., 2003), which subsequently reacts with NO to form OH *via* R5.1. This multistep conversion is too slow in comparison to the reaction time of a few milliseconds between the injection of NO and the fluorescence detection (Fuchs et al., 2011), where a detection sensitivity of 5 % of the $HO_2$ value has been reported (Holland et al., 2003). The sensitivity of LIF towards the peroxy radical $C_2H_5O_2$ was investigated by exploiting the ethane + OH reaction, where an increase in 5 % for the measured OH signal was observed upon addition of NO (Kanaya et al., 2001). Negligible interferences from $C_1$ - $C_4$ alkyl peroxy radicals in the LIF system have also been reported (Ren et al., 2004). Conventionally, field observations of $HO_2$ performed by LIF have largely been

interpreted as being free of $RO_2$ interferences (*e.g.* Heard & Pilling, 2003). However, potential interferences from larger alkyl peroxy radicals may be greater than that reported for $C_1 - C_4$ alkyl peroxy radicals, since the subsequent reactions of the alkoxy radicals with $O_2$ (R5.3) are expected to be faster by a factor of ~ 5 (Atkinson and Arey, 2003, Orlando et al., 2003). More complex $RO_2$ radicals may therefore lead to relatively large interferences in the measurements of $HO_2$, owing to the fast rate coefficient of R5.3, for the corresponding RO species.

Fuchs et al. (2011) have very recently reported detection sensitivities for cyclohexyl peroxy radicals under two different LIF instrumental configurations. The configurations differed in the diameter of the sampling nozzle (see Chapter 2, Figure 2.2 for schematic representation of the LIF system). This determines the sampling flows drawn into the detection cell and thus the concentration of NO needed to convert $HO_2$ into OH. The authors reported that the conversion reaction time of $HO_2$ to OH decreased from 2.7 ms to 0.18 ms for nozzles with diameters of 0.4 mm and 0.2 mm respectively. This indicates that inlet orifices with smaller diameters may be less susceptible to interferences, owing to the reduced conversion reaction time within the detection cell. Fuchs et al. (2011) reported detection sensitivities of 0.48 ± 0.14 and 0.03 ± 0.00 for cyclohexyl peroxy radicals, relative to $HO_2$, when sampling through a 0.4 mm and 0.2 mm nozzle respectively. The LIF system utilised at EUPHORE samples through a 0.38 mm nozzle indicating that there may be a potential interference in the $HO_2$ measurements for experiments performed in the presence of cyclohexane (*i.e.* ethene and *trans*-2-butene).

### 5.2.2 Interference of β-hydroxyalkyl peroxy radical

An example of a species that may undergo (fast) chemical conversion leading to the formation of $HO_2$ in the fluorescence detection cell is the β-hydroxyalkyl peroxy radical formed from the OH + alkene reaction, as illustrated in Figure 5.1 for *trans*-2-butene. These radicals react with NO (R5.5a) forming β-hydroxyalkoxy radicals (see Figure 5.1) which subsequently undergo decomposition (R5.6) at rates in the order of $10^4$ - $10^7$ $s^{-1}$ (Atkinson, 2007, Atkinson, 1997a), leading to the hydroxyalkyl radical and $CH_3CHO$ (in the case of *trans*-2-butene). The hydroxyalkyl radical reacts near-instantaneously with $O_2$ forming $CH_3CHO$ and $HO_2$ (R5.7). Thus, the decomposition reaction of the β-hydroxyalkoxy radical (R5.6 – R5.7) is fast in comparison to the slow alkoxy radical + $O_2$ reaction (R5.3) discussed in Section 5.2.1. The much shorter lifetime of the β-hydroxyalkoxy radical in comparison to the residence time of a few milliseconds between the injection of NO and the fluorescence detection, leads to substantial conversion of the peroxy radical to $HO_2$, and subsequently (through reaction with NO) to OH. Fuchs et al. (2011) demonstrated that [NO] limits the conversion efficiency of $RO_2 \rightarrow NO_2 \rightarrow OH$, where the interference in the $HO_2$ measurements decreases with decreasing [NO]. When sampling through a 0.4 mm orifice, the authors report detection sensitivities of 0.85 ± 0.05 and 0.95 ± 0.03 for the peroxy radicals formed from OH + ethene and OH + propene, respectively. These relative detection sensitivities for $RO_2$ species in the $HO_2$ detection cell decrease to 0.17 ± 0.03 and 0.15 ± 0.03 for ethene and propene respectively when sampling through a 0.2 mm nozzle.

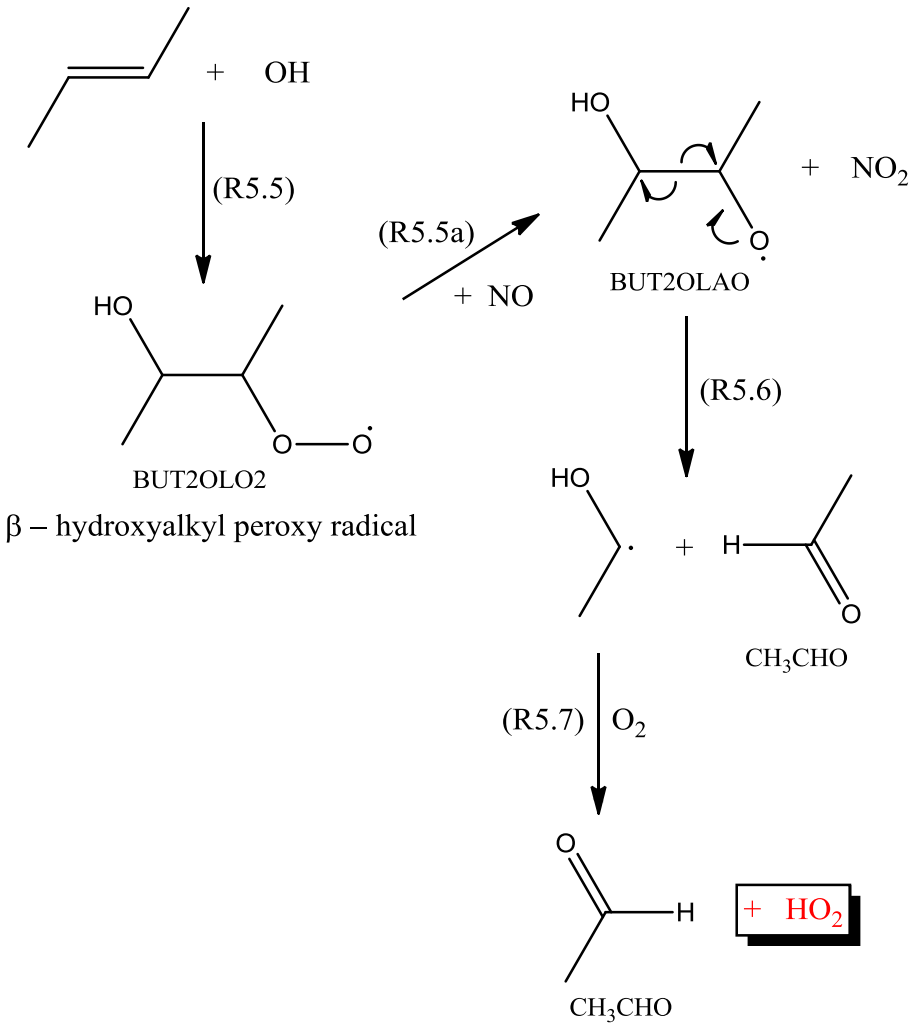


**Figure 5.1.** Proposed reactions leading to an interference of β-hydroxyalkyl peroxy radicals within the LIF system. Example shown for *trans*-2-butene + OH.

### 5.2.3 Potential Interference of Calculated $HO_2$ Yields

The potential interference from the β-hydroxyalkyl and cyclohexyl peroxy radicals, discussed in the previous Section, may affect the results of the EUPHORE experiments reported here. This is a potential issue for the experiments performed in the absence of radical scavengers and in the presence of excess cyclohexane. For

example, ozonolysis reactions performed in absence of OH radical scavenger leads to the formation of β-hydroxyalkyl peroxy radicals, through the alkene + OH reaction. The OH-initiated oxidation of cyclohexane in ozonolysis experiments performed in the presence of excess cyclohexane (where ≥ 95 % of OH produced is scavenged by cyclohexane) leads to the formation of cyclohexyl peroxy radicals (see Chapter 2, Section 2.5). These experiments may therefore be more susceptible to interferences from these $RO_2$ radicals. However, for experiments conducted in the presence of excess CO, the formation of β-hydroxyalkyl peroxy radicals is suppressed, as in the presence of CO ≥ 95 % of OH is scavenged. This indicates that $HO_2$ yields determined in the presence of excess CO may be less susceptible to the interferences mentioned above and are therefore more robust.

The potential interference from the β-hydroxyalkyl peroxy radicals, discussed in the previous Section is consistent with the large $Y_{HO_2}$ calculated for the experiments performed in the absence of OH scavenger (see Chapter 4, Table 4.9). The magnitude of the potential interference for ethene, propene and 1-butene may be smaller than that for 2-methylpropene, *trans*-2-butene and 2,3-dimethly-2-butene, owing to the latter group of alkenes having both faster OH + alkene reaction rate coefficients (http://www.iupac-kinetic.ch.cam.ac.uk/, 2007) forming the respective β-hydroxyalkyl peroxy radicals, and their faster subsequent decomposition rates ($\sim 10^7$ $s^{-1}$) (Atkinson, 1997a). This leads to shorter lifetimes of their corresponding β-hydroxyalkoxy radicals and thus greater conversion efficiencies to $HO_2$, which may be reflected in the larger than unity measured $Y_{HO_2}$ for 2-methylpropene and 2,3-dimethly-2-butene (see Table 4.9). Such an interference is also a potential explanation for the observed decrease in the $Y_{HO_2}$ in the presence of excess CO, as in

the presence of CO ≥ 95 % of OH is scavenged, suppressing the formation of β-hydroxyalkyl peroxy radicals *via* the OH + alkene reaction. The calculated $Y_{HO_2}$ in the presence of excess CO may therefore give a more realistic indication of the 'real' $HO_2$ yield, for the ozonolysis of alkenes (Table 4.9), as under these experimental conditions the measured $HO_2$ values will not be affected by interferences from either β-hydroxyalkyl peroxy radical (from OH + alkene) or cyclohexyl peroxy radical (from OH + cyclohexane) interferences.

## 5.3 Atmospheric Significance

In this Section, the derived radical yields of OH and $HO_2$ (see Chapters 3 and 4) from ozonolysis of the alkenes studied are used to predict the overall contribution of ozonolysis to the total $HO_x$ production for both day and night, compared to that calculated using the "base case" MCM (v3.1). Three sets of model simulations were performed, a base case run using the standard MCM mechanism, and two runs to explore the impact of the results obtained here, using two different approaches to determine the $HO_2$ yields to employ :

1. Upper limit – $Y_{HO_2}$ taken from experiments performed in the absence of an OH scavenger. This provided an upper limit to the predicted $HO_2$ formation from alkene ozonolysis, but may overestimate the true yield owing to $RO_2$ interference.

2. Excess CO – $Y_{HO_2}$ taken from the experiments performed in the presence of excess CO. This may provide a more realistic interpretation to the predicted $HO_2$ formation from alkene ozonolysis, as the yields of $HO_2$ are less susceptible to $RO_2$ interferences as discussed above.

As mentioned in Chapter 1, OH largely controls the oxidising capacity of the atmosphere and influences the lifetime of almost all anthropogenic and biogenic VOCs. The short lifetime of OH means that its abundance is controlled by local concentrations of $O_3$, VOCs, $NO_x$, CO, $H_2O$ and sunlight. In urban environments, OH can be rapidly cycled to $HO_2$ and $RO_2$ radical species, following their reaction with VOCs in the presence of $NO_x$ (see Chapter 1). A number of studies have demonstrated the atmospheric significance of the radical production (OH + $HO_2$) from gas-phase alkene ozonolysis, drawing attention to the overall contribution to the total $HO_x$ budget in urban environments (Emmerson et al., 2005a, Emmerson et al., 2007, Emmerson et al., 2005b, Johnson and Marston, 2008, Paulson and Orlando, 1996, Heard et al., 2004).

The next Section describes the use of a zero-dimensional photochemical box model and identifies which reactions and species are important for driving the $HO_x$ chemistry in an urban environment, by performing a rate of production analysis (ROPA).

## 5.4 Model Description

The complete gas-phase photo-oxidation mechanism for a range of parent hydrocarbons (see Table 5.1) to be included in the zero-dimensional photochemical box model was extracted (including a suitable set of inorganic reactions) directly from the MCMv3.1 website. The alkene photo-oxidation mechanisms were updated to include a more explicit representation of the ozonolysis reaction mechanisms (see Chapter 4, Section 4.3); including the calculated rate constants and radical formation yields determined in Chapters 3 and 4.

The model was constrained to average measured concentrations of 5 $C_2$ – $C_5$ alkanes, 7 $C_2$ – $C_6$ alkenes, isoprene, methanol, ethanol, formaldehyde and acetaldehyde (see Table 5.1). The observations were made during the Tropospheric ORganic CHemistry experiment (TORCH) (Lee et al., 2006, Emmerson et al., 2007). The selected species accounted for ~ 92 % of the total OH reactivity from all measured species during the TORCH campaign. The initial concentrations of $O_3$, NO, $NO_2$, CO, $CH_4$, temperature and relative humidity used in the model are shown in Table 5.2, and correspond to the average observed conditions during the day and night. Photolysis rate coefficients (*e.g.* $j(NO_2)$, $j(O^1D)$, $j$(HCHO), *etc*) were determined as a function of solar zenith angle (SZA) using a two stream scattering model (Hough, 1988).

The ROPA consisted of isolating all the reactions that involved the production of OH and $HO_2$, to identify the significance of each individual process that contributed to the overall radical budget. Parent VOC concentrations were kept constant throughout the simulations as no emissions were simulated. The models were run from 11.00 – 15.00

and 23.00 – 03.00 hours, for day and night simulations respectively. The model was allowed to stabilise for an hour, after which OH and $HO_2$ radical initiation and contribution of alkene ozonolysis to the radical budget at a specific instant was averaged over the remaining 3 hours. The results of these simulations are discussed in the next section.

**Table 5.1.** Concentration of measured hydrocarbons used in model simulations

| | **Mixing Ratio (pptV)** | |
|---|---|---|
| **Species** | **Day** | **Night** |
| Ethene | 1595 | 605 |
| Propene | 350 | 185 |
| *trans*-2-Butene | 20 | 15 |
| 1-butene | 90 | 50 |
| 2-methylpropene | 95 | 55 |
| *cis*-2-Butene | 15 | 10 |
| Isoprene | 560 | 105 |
| 2,3-dimethyl-2-butene | 10 | 9 |
| Propane | 2640 | 1720 |
| 2-methylbutane | 1740 | 1000 |
| n-Butane | 1890 | 1030 |
| n-Pentane | 815 | 490 |
| Ethanol | 5280 | 3200 |
| Methanol | 6180 | 3520 |
| Acetaldehyde | 5700 | 4100 |
| Formaldehyde | 1610 | 1390 |

**Table 5.2.** Concentrations of species and physical parameters used in model simulations

| | **Mixing Ratio (ppbV)** | |
|---|---|---|
| | **Day** | **Night** |
| Methane | 1800 | 1800 |
| Ozone | 40 | 20 |
| NO | 10 | 2 |
| $NO_2$ | 20 | 8 |
| CO | 100 | 100 |
| Temp / K | 303 | 296 |
| Relative humidity / % | 50 | 70 |

# 5.5 Results and Discussion

## 5.5.1 Daytime OH Production

As mentioned in Chapter 1, the major OH production route in the troposphere is usually assumed to be reaction of electronically excited oxygen atoms, $O^1(D)$, with water vapour (R5.8), where the source of $O^1(D)$ is the photolysis of ozone at wavelengths below 330 nm. The production rate of OH is therefore dependent upon the availability of suitable photons, and thus varies both diurnally and seasonally.

$$O^1(D) + H_2O \rightarrow OH + OH \qquad \text{(R5.8)}$$

Another OH initiation route in the troposphere is the photolysis of nitrous acid (HONO), suggested as an important source of OH in urban areas (R5.9) (Heard et al., 2004)

$$HONO + h\nu\ (\lambda \leq 400\ nm) \rightarrow OH + NO \qquad \text{(R5.9)}$$

Unfortunately measurements of HONO were not made during the TORCH campaign (Lee et al., 2006) and thus the contribution of OH production *via* R5.9 was not quantified in this study, as an initial concentration of HONO could not be accurately included in the model. Previous studies have reported that the contribution of OH from HONO photolysis may account for up to 30 % of the total OH production (Emmerson et al., 2007). However, this is uncertain as the authors parameterise an estimated production rate of HONO within their model. At night, VOC oxidation is

dominated by $NO_3$ (see Chapter 1), however, alkene-ozone reactions are believed to be the dominant source of OH radicals, owing to the absence of sunlight (*i.e.* no availability of photons for R5.8 and R5.9). In this study, the percentage contribution of OH formation from the above *primary* sources were quantified and described below.

The maximum simulated [OH] were 2.60, 2.88 and 2.56 × $10^6$ molecule $cm^{-3}$ for base case MCMv3.1, 'upper limit' and 'excess CO' simulations, respectively; indicating little difference in the overall [OH] when altering the $HO_2$ radical formation yield from alkene ozonolysis within the model. Table 5.3 illustrates that during the daytime, 71 % of primary OH formation occurred through the $O(^1D) + H_2O$ route and 29 % from alkene + $O_3$. The change in the $HO_2$ yields in the model chemistry did not significantly alter the contribution of alkene ozonolysis to the overall primary OH formation. The MCM therefore adequately predicts the OH radical contribution from alkene ozonolysis, as shown in Table 5.3. Other non-initiation fluxes leading to the formation of OH include propagation reactions $HO_2$ + NO and $HO_2$ + $O_3$ which produce ~ 85 % and ~ 3 % of the *overall* daytime OH radicals.

**Table 5.3.** Modelled percentage contribution to the overall OH initiation

| **Reaction** | **MCMv3.1** | **This study (upper limit)** [a] | **This study (excess CO)** [b] |
|---|---|---|---|
| $O(^1D) + H_2O$ | 72 | 71 | 71 |
| Alkene + $O_3$ | 28 | 29 | 29 |

[a] set 1 – $Y_{HO_2}$ used from simple alkene and ozone reactions (upper limit)

[b] set 2 – $Y_{HO_2}$ used from excess CO experiments

The percentage contribution from alkene ozonolysis to the primary OH formation routes are consistent with Emmerson et al. (2007) who performed detailed radical modelling studies for the TORCH campaign. They reported that the reaction $O(^1D) + H_2O$ dominated, while the photolysis of HONO and $O_3$ + alkene both accounted for 29 % each. The authors report that during the heatwave period 43 % of OH formation occurred through alkene + $O_3$, while only 3 % of initiation occurred through HONO photolysis (Emmerson et al., 2007). However, during the Pollution of Urban Midlands Atmosphere (PUMA) campaign (Harrison et al., 2006), it was found that in the summer $O_3$ + alkene reactions accounted for 46 % of the overall OH measurements, while the photolysis of HONO and $O(^1D) + H_2O$ accounted for 29 and 24 % respectively (Emmerson et al., 2005b, Heard et al., 2004). In the winter, OH initiation was dominated by alkene ozonolysis (62 %), HONO photolysis (36 %) and $O(^1D) + H_2O$ (< 1 %), owing to the much larger concentrations of alkenes present in the atmosphere (Emmerson et al., 2005b) and less sunlight hours. In both the above cases, MCMv3.1 chemical mechanisms / ozonolysis radical yields were employed.

### 5.5.2 Daytime $HO_2$ Production

The reactions leading to the primary formation of $HO_2$ are the photolysis of HCHO (R5.10 – R5.12), $CH_3CHO$ (R5.13) and of other carbonyl species, as well as $O_3$ + alkene reactions.

$$HCHO + h\nu\ (\lambda \leq 338\ nm) \rightarrow H + HCO \quad \text{(R5.10)}$$

$$HCO + O_2 \rightarrow HO_2 + CO \quad \text{(R5.11)}$$

$$H + O_2 + M \rightarrow HO_2 + M \quad \text{(R5.12)}$$

$$CH_3CHO + h\nu\ (\lambda \leq 330\ nm)\ (+O_2) \rightarrow HO_2 + CH_3O_2 + CO \quad (R5.13)$$

$HO_2$ production *via* HCHO (R5.10 – R5.12) and $CH_3CHO$ (R5.13) photolysis is reported to be significantly less important in the winter than in the summer (Heard et al., 2004). During the PUMA campaign, HCHO photolysis accounted for 56 and 6 % of the overall $HO_2$ initiation reactions in the summer and winter, respectively (Heard et al., 2004). In the winter the photolysis of other carbonyl (RCHO) species were more important in the formation of $HO_2$, accounting for 72 % of the primary $HO_2$ sources. $O_3$ + alkene reactions may also be the dominant source of $HO_2$ radicals during the night (Emmerson et al., 2005b), owing to the absence of photolysis driven chemistry, but has been reported as a minor source during the day (Emmerson et al., 2005b). However, in the winter alkene ozonolysis has been reported to account for 19 % of the $HO_2$ production during the day (Heard et al., 2004).

The maximum simulated [$HO_2$] were 1.44, 1.55 and 1.42 × $10^9$ molecule $cm^{-3}$ for base case MCMv3.1, 'upper limit' and 'excess CO' simulations, respectively; indicating little difference in the overall [$HO_2$] when altering the $HO_2$ radical formation yield from alkene ozonolysis within the model. Table 5.4 illustrates that during the daytime, the formation of $HO_2$ is dominated by the photolysis of HCHO.

**Table 5.4.** Modelled percentage contribution to the overall $HO_2$ initiation

| **Reaction** | **MCMv3.1** | **This study (upper limit)** [a] | **This study (excess CO)** [b] |
|---|---|---|---|
| HCHO + h$\nu$ | 84 | 78 | 84 |
| $CH_3CHO$ + h$\nu$ | 4 | 4 | 4 |
| Alkene + $O_3$ | 4 | 17 | 4 |
| Other carbonyls + h$\nu$ | 8 | 1 | 8 |

[a] set 1 – $Y_{HO_2}$ used from simple alkene and ozone reactions (upper limit)

[b] set 2 – $Y_{HO_2}$ used from excess CO experiments

The contribution of alkene ozonolysis to the primary $HO_2$ formation is small (4 %) in the 'base case MCM' and 'excess CO' simulations, due to the similarity in $HO_2$ formation yields in the alkene ozonolysis chemical schemes within the models. The contribution to the total primary $HO_2$ formation from alkene ozonolysis in the 'upper limit' simulation is calculated as 17 %, which is significantly larger than previously reported. This is, however, an upper limit as the $Y_{HO_2}$ calculated in Chapter 4 for the alkenes studied may be subject to interferences, as discussed in Section 5.2.

### 5.5.3 Night-time $HO_x$ Chemistry

The night-time (primary) radical routes of 'initiation' for both OH and $HO_2$ are dominated entirely by alkene + $O_3$ reactions, owing to the absence of photolysis reactions. Non-initiation fluxes include the reaction of $NO_3$ with organic compounds, such as alkenes, alkanes and aldehydes; discussed in Chapter 1. These reactions can form alkyl (and acyl) radicals that react near-instantaneously with $O_2$, forming peroxy radicals. $RO_2$ radicals can subsequently react with $NO_2$ (and/or $NO_3$) forming alkoxy radicals which can react with $O_2$ forming $HO_2$. Other fluxes also include OH → $HO_2$ and $HO_2$ → OH propagation routes such as R5.14 – R5.16 (see Chapter 1, Section 1.3 for more information).

$$NO_3 + OH \rightarrow NO_2 + HO_2 \quad \text{(R5.14)}$$

$$NO_3 + HO_2 \rightarrow NO_2 + OH + O_2 \quad \text{(R5.15)}$$

$$O_3 + HO_2 \rightarrow OH + 2O_2 \quad \text{(R5.16)}$$

The non-initiation and propagation routes to OH and $HO_2$ formation were not quantified in this study, as the focus was to determine the contribution of the 'primary' routes of OH and $HO_2$ formations. The concentrations for base case MCM, 'upper limit' and 'excess CO' for OH and $HO_2$ were 7.71, 7.65 and 7.15 $\times 10^4$ molecule $cm^{-3}$ and 1.38, 2.59 and 1.42 $\times 10^7$ molecule $cm^{-3}$, respectively. The observed increase (~ factor of 2) in the $HO_2$ concentration for the 'upper limit' simulation demonstrates the significance of $HO_2$ production from alkene ozonolysis at night and the overall contribution to the total primary $HO_2$ production. The percentage contributions to the primary rate of OH and $HO_2$ production are illustrated for each individual alkene + $O_3$ reaction in Figure 5.2.

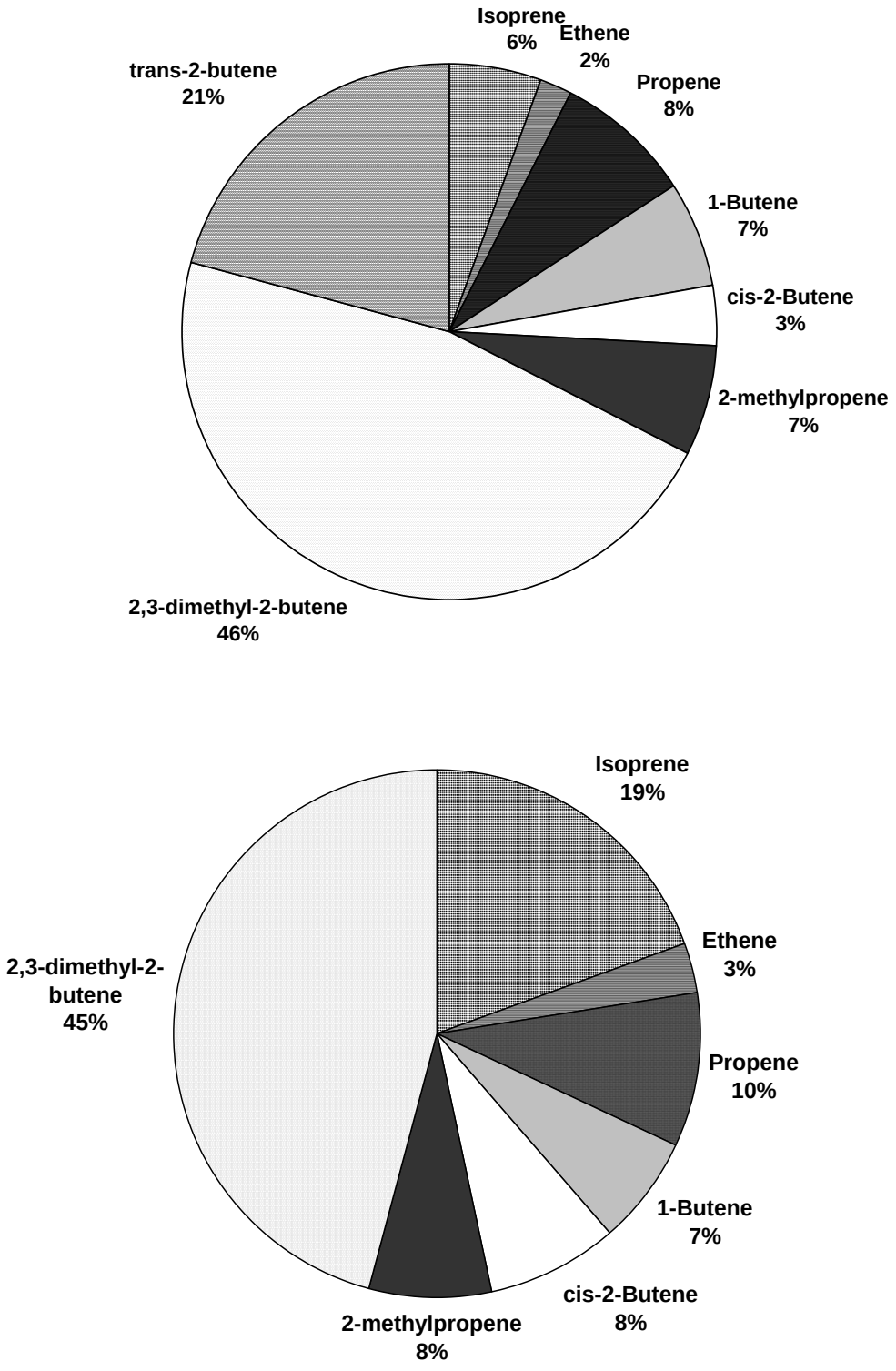


**Figure 5.2.** Percentage contribution to the primary rate of OH (top) and $HO_2$ (bottom) production from alkene ozonolysis, for 'excess CO' simulation at night (*i.e.* $Y_{HO_2}$ from excess CO experiments included in the alkene-ozone photo-oxidation chemical scheme).

## 5.6 Summary

Although alkenes are measured at relatively low concentrations in the atmosphere, their ability to form $HO_x$ radicals *via* reaction with ozone means that they significantly contribute to the total $HO_x$ budget, in urban environments. The calculated daytime contribution from alkene ozonolysis to the primary initiation routes to OH and $HO_2$ in this study was 29 and 4 – 17 % respectively. The 13 % difference in the contribution to $HO_2$ reflects the two sets of $HO_2$ yields employed in the modelled alkene-ozone chemistry (upper limit and excess CO). The contribution of alkene ozonolysis to the primary initiation route to OH production was not significantly affected when employing the two different sets of $HO_2$ yields (see Table 5.3), indicating that the MCM adequately simulates OH production from alkene ozonolysis. However, an increase of approximately 10 % was observed for the modelled levels of OH during the day, when employing 'upper limit' $HO_2$ yields. This may reflect the ~ 9 % increase in the modelled levels of $HO_2$ which subsequently undergo propagation reaction with NO to form OH; this reaction was reported as being responsible for the production of ~ 80 % of [OH] during the day (Emmerson et al., 2007).

The overall contribution of alkene ozonolysis to the primary initiation route to $HO_2$ production (using the upper limit $HO_2$ yields) was 13 % larger than that simulated using standard MCM alkene-ozone chemistry, during the day. The modelled levels of $HO_2$ at night were also a factor of ~ 2 larger, indicating that the $HO_2$ production simulated using the OH and $HO_2$ yields determined from non-scavenger experiments is considerably larger in comparison to the MCM. However, the results of the simulations performed using the $HO_2$ yields determined from excess CO experiments,

show that the contribution to $HO_2$ production (and modelled levels) is in excellent agreement with the standard MCM (see Table 5.4). This exemplifies the importance in the interpretation of the $HO_2$ yields determined in Chapters 3 and 4, where further work is needed in order to quantify any potential interferences within the LIF instrumentation.

# Chapter 6. Alkene Interferences in Chemiluminescence $NO_x$ Monitors

In this chapter the importance of accurately measuring ambient concentrations of the oxides of nitrogen ($NO_x$) is discussed, with particular emphasis on the use of chemiluminescence in NO / $NO_2$ detection monitors. During the course of alkene-ozone experiments performed at EUPHORE, an increase in the apparent NO signal was observed (by chemiluminescence $NO_x$ analyser) on addition of alkene to the chamber, illustrated in Figure 6.1.

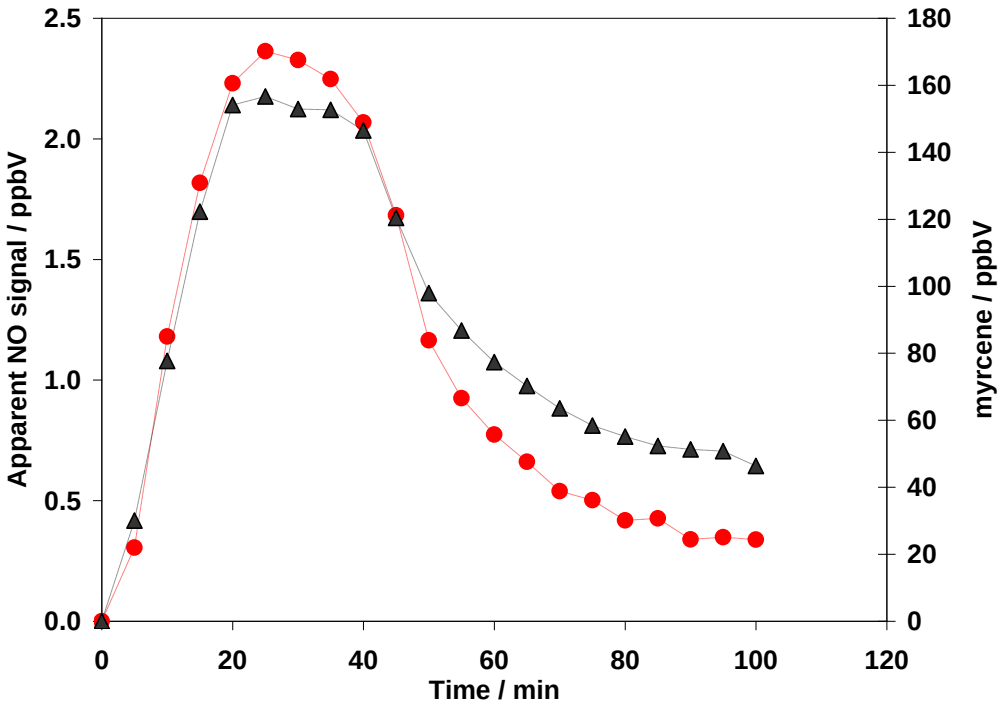


**Figure 6.1**. Temporal profile of myrcene (grey triangles) and apparent NO mixing ratio (red circles) for an ozonolysis experiment

The interference observed for a range of alkenes, during alkene-ozone chamber experiments provided the basis of the research presented in this chapter. The chapter is subdivided into two sections: (*A*) a review of the use of chemiluminescence monitors in the detection of NO (and other species) and the potential interferences associated with this technique; and (*B*) a description of experimental work carried out, identifying a series of alkenes as possible interferants. The chapter concludes with a discussion of likely reasons for the observed interferences.

# *Section A*

## 6.1 Importance of Accurate Measurements of $NO_x$

Nitrogen oxides ($NO_x$ = NO + $NO_2$) are important components in the modelling of air pollution processes, as they are central to the production and destruction of ozone in the troposphere and stratosphere (Heard, 2006). The regulation of $NO_x$ in the environment is important, as increased emissions can lead to detrimental health effects. The need for accurately measuring ambient concentrations of the oxides of nitrogen is therefore important not just for air quality modelling, but for regulatory purposes also. The necessity in accurately measuring nitrogen oxides is also emphasised by their oxidation products. For example, peroxyacetyl nitrate (PAN), a secondary pollutant present in photochemical smog, is a product of reactions involving $NO_2$ and $RO_2$ species (see Chapter 1, Figure 1.3) and is known for its mutagenic and phytotoxic (*i.e.* detrimental to plant cells, inhibiting photosynthesis) properties (Navas et al., 1997). $NO_2$ can also act as a sink for OH forming nitric acid, a key constituent of acid precipitation (Bollinger et al., 1983). Currently, there are

various techniques available for monitoring *in situ* NO and $NO_2$ concentrations, including chemiluminescence and Laser Induced Fluorescence (LIF). Techniques that can provide sensitive, real-time measurements with good time resolution, and are "free from" interferences are required to help further our understanding of tropospheric chemistry. Most commercially available $NO_x$ analysers, used for ground-based measurements, exploit the chemiluminescence technique to detect NO. Measurement of $NO_2$ is somewhat difficult to detect, as conventional techniques involve the reduction of $NO_2$ to NO followed by subsequent detection. Such methods are prone to interferences in the presence of high concentrations of other oxidised nitrogen species ($NO_y$) (Farmer and Cohen, 2008). This chapter focuses on the interferences posed by alkenes in chemiluminescence $NO_x$ analysers, where the results of both chamber and lab experiments are presented.

## 6.2 Introduction to Chemiluminescence

Chemiluminescence is the process by which a chemical reaction forms an excited-state product that can undergo one or more relaxation processes to return to its ground state. Such reactions must be sufficiently exothermic (125 – 1250 kJ $mol^{-1}$) to generate a significant proportion of products in an excited state (Fontijn, 1985). The excess energy from these reactions is divided into a combination of rotational, vibrational, translational and electronic states of the product. These excited products can undergo collisional quenching or produce chemiluminescence, by the emission of a photon in the UV/visible region. The emission of a photon in general, requires that the reaction of a product is in an excited electronic state; however vibrational overtone

emission has been reported by various authors *e.g.* for HF in the reaction of fluorine with certain sulphur containing compounds (Garcia-Campana and Baeyens, 2001, Glinski et al., 1985, Turnipseed and Birks, 1991). Few chemical reactions are known to produce intense chemiluminescence in the UV/visible region; an example of such a reaction is that of NO with $O_3$, which is described in the next section.

## 6.3 The NO + $O_3$ Chemiluminescence Reaction

The reaction of NO with $O_3$ is conceivably the best known and analytically most useful gas-phase chemiluminescence reaction (Garcia-Campana and Baeyens, 2001). The mechanism of reaction (R6.1 – R6.4) has an exothermicity of ~ 200 kJ $mol^{-1}$ and has been thoroughly investigated (Clyne et al., 1964, Michael et al., 1981, Schurath et al., 1981, Clough and Thrush, 1967, Lippmann et al., 1980, Ray and Watson, 2002).

$$NO + O_3 \rightarrow NO_2^* + O_2 \qquad \text{(R6.1)}$$

$$NO + O_3 \rightarrow NO_2 + O_2 \qquad \text{(R6.2)}$$

$$NO_2^* \rightarrow NO_2 + h\nu \qquad \text{(R6.3)}$$

$$NO_2^* + M \rightarrow NO_2 + M \qquad \text{(R6.4)}$$

The mechanism involves the formation of an electronically excited $NO_2$ molecule (R6.1) which can undergo chemiluminescence (R6.3) or quenching (R6.4). Chemiluminescence is observed in the range 600 – 3000 nm, where only a small fraction of emission occurs below 800 nm and emission peaks at 1200 nm. There have been numerous studies reporting rate constants for the formation of $NO_2$ in its ground

state (R6.2) and $NO_2$ in its electronically excited state (R6.1) (Clyne et al., 1964, Michael et al., 1981, Schurath et al., 1981). The IUPAC recommended rate constant for the overall reaction is $k_{(R6.1+R6.2)}$ = 1.8 x $10^{-14}$ $cm^3$ $molecule^{-1}$ $s^{-1}$ at 298 K (http://www.iupac-kinetic.ch.cam.ac.uk/, 2006). The estimated rate constant for the formation of electronically excited state $NO_2$ molecules is $k_{(R6.1)}$ = 1.1 x $10^{-15}$ $cm^3$ $molecule^{-1}$ $s^{-1}$ at 298 K (Clough and Thrush, 1967). Correspondingly, the fraction of the reaction that produces excited states is approximately 6 % at 298 K. However, Schurath et al. (1981) reported that the quantum yield is somewhat higher at 20%. A number of studies have found that this quantum yield increases with temperature (Clough and Thrush, 1967, Lippmann et al., 1980, Ray and Watson, 2002, Schurath et al., 1981). The NO / $O_3$ reaction system has been exploited by various methods to measure either $O_3$ or NO in polluted urban environments, which is described in the subsequent section.

## 6.4 Exploiting Chemiluminescence to Detect Species

The first *in situ* measurements of NO using the chemiluminescence NO + $O_3$ reaction was in the 1970's, reporting mixing ratios 4 – 100 ppmV (Fontijn et al., 1970). No interferences were observed from $NO_2$, $CO_2$, CO, ethene, $NH_3$, $SO_2$ and $H_2O$, but further work confirmed interferences from metal carbonyls and ethene (Stedman et al., 1972). These interferences were removed by using a filter to cut off chemiluminescence emission at $\lambda < 648$ nm. Various studies have since improved this analytical method of detecting NO, optimising temperature, pressure and flow rates within the instrument (Kley et al., 1981, Mehrabzadeh et al., 1983, Steffenson. D. M

and Stedman, 1974). Commercial nitric oxide(s) analysers are used for measuring NO and $NO_2$ in the troposphere in the low pptV range.

The chemiluminescence detection of NO was developed further by Sigsby et al. (1973), who exploited the thermal decomposition reaction of $NO_2$ to NO, by using a 6 ft long stainless steel tube heated to 750 – 900 ºC, to measure $NO_2$. The thermal decomposition reaction also converted $NH_3$ to NO, but was corrected by the use of an $NH_3$ scrubber (Sigsby et al., 1973). This analysis enabled the detection of NO *via* chemiluminescence and $NO_x$ ($NO + NO_2$) *via* thermal decomposition of $NO_2$ to NO followed by subsequent chemiluminescence of NO; the difference between the two measurements being assumed equal to $NO_2$. Numerous studies have investigated possible techniques converting $NO_2$ to NO, for example: by photolysis (Kley and McFarland, 1980), by reaction with $FeSO_4$ (Kelly et al., 1980), molybdenum metal (Joseph and Spicer, 1978) and gold surfaces (Bollinger et al., 1983). Currently, most commercial NO-$NO_2$-$NO_x$ instruments employ molybdenum converters heated to 300 – 350 ºC, to detect $NO_x$. Data obtained from such thermal decomposition techniques are difficult to interpret as they may yield measurements closer to the total oxides of nitrogen ($NO_y$) rather than $NO_x$; where $NO_y$ is the sum of $NO_x$ and all oxidised nitrogen species that represent sources of oxides of nitrogen, which can include $HNO_3$, $N_2O$, $N_2O_5$, PAN and various other organic nitrates (Farmer and Cohen, 2008). Potential interferences are discussed in detail in Section 6.5. A more specific technique to convert $NO_2$ to NO exploited the use of UV light, converting $NO_2$ to NO by photolysis (Kley and McFarland, 1980). In such instruments, sampled air is passed through a photolysis cell, illuminated by a UV lamp. The sampled air has a residence time of approximately 5 seconds in the photolysis cell, resulting in conversion

efficiencies of ~ 50% (Fehsenfeld et al., 1990). The chemiluminescence NO signal is then subtracted from the signal obtained using the illuminated photolysis cell, and divided by the measured conversion efficiency to yield $NO_2$.

A generic schematic representation of a typical chemiluminescence $NO_x$ instrument is shown in Figure 6.2. It consists of inlets for analyte and reagent gas streams, pre- and main reaction chambers, a vacuum pump to regulate the pressure, a filter and a photomultiplier tube (PMT).

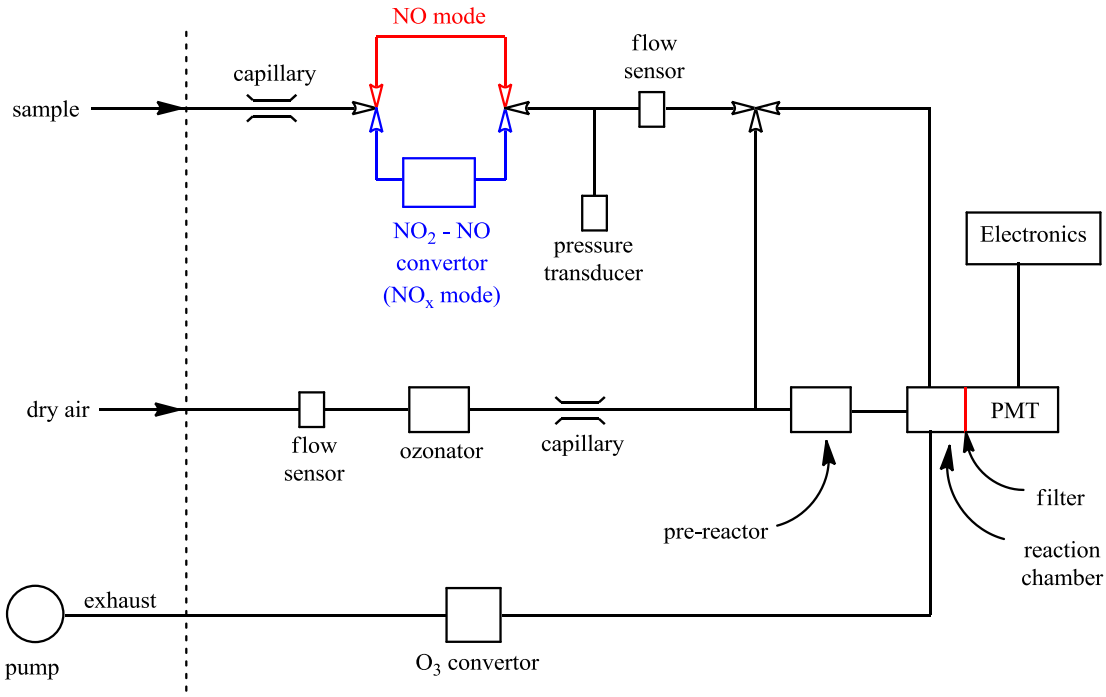


**Figure 6.2.** Schematic representation of a typical chemiluminescence $NO\text{-}NO_2\text{-}NO_x$ instrument. Adapted from Thermo Electron 42*i*-TL manual

Dry air (or $O_2$) is drawn into the instrument *via* an inlet and into the ozone generator, where ozone is produced from the oxygen in the dry air through ionisation. The

sample analyte is drawn into the instrument *via* a different inlet and passes through the capillary to a mode solenoid valve, which determines the path that the sample analyte takes. As mentioned above the instrument can run in either of two modes; NO mode or *via* the $NO_2$ converter, the $NO_x$ mode. The sample then reaches the second solenoid valve which determines whether the sample is sent to the pre- or main reaction chamber, corresponding to background or measurement modes respectively. The pre-reaction chamber is designed to allow 99% of a 200 ppb NO sample to be consumed by reaction with ozone prior to entering the main reactor, enabling a dynamic zero reading for the analyser to be taken (Thermo Electron 42*i*-TL manual). It must be noted that ozone is added to the sample analyte prior to the pre-reactor. The sample analyte can also bypass the pre-chamber and be directly transported to the main chamber, where it reacts with ozone, producing chemiluminescence which is detected by the red sensitive photomultiplier (PMT). To ensure an optimised NO selectivity a red filter is positioned between the main reaction chamber and the PMT. This removes potential interferants with chemiluminescence emission with $\lambda < 648$ nm. An external vacuum pump is used, not only to draw sample gas and dry air into the instrument, but to generate a main reaction chamber pressure of 1 – 10 Torr to minimise quenching. The exact pressure within the reaction chamber is dependent on the flow rates of the sample and ozone gas streams as well as the speed of the vacuum pump.

The generic schematic diagram shown in Figure 6.2, illustrates the incorporation of the $NO_2$-NO converter within the instrument. As mentioned previously this conversion can be through thermal decomposition or through a photolytic convertor.

In the case of a photolytic convertor, Eco Physics PLC 760 (utilised during alkene-ozone chamber experiments at EUPHORE) – the sample analyte enters the photolysis chamber with a residence time of approximately 5 seconds, where it is subjected to UV light. An optical filter is placed on the lamp window to allow only wavelengths shorter than approximately 500 nm to pass into the photolysis cell. The emission of the lamp cuts off at 320 nm, preventing any interference from the photolysis of nitrogen containing species, such as $HNO_3$, $N_2O$ and PAN (Fehsenfeld et al., 1990). Any $NO_2$ present in the sample analyte is converted into NO *via* (R6.5) and detected as previously described for NO through the chemiluminescence reaction.

$$NO_2 + h\nu \rightarrow NO + O(^3P) \qquad (R6.5)$$

## 6.5 Interferences in chemiluminescence $NO_x$ monitors

There have been numerous studies investigating interferences in chemiluminescent detectors. Gerboles et al. (2003) reported two types of interferences that could occur; the first type involves the quenching of chemiluminescence intensity and causes a bias in both NO and $NO_x$ measurements, and a second involves the conversion of other nitrogen containing species to NO, consequently affecting the $NO_x$ signal. As mentioned previously, if third body molecules with widely spaced vibrational levels are present, then these molecules are able to accept the larger quantum of electronic energy from the excited state, resulting in the quenching of chemiluminescence. Although the molybdenum converter efficiency is unaffected by humidity, a quenching affect of up to 8 % is seen in the chemiluminescent detector, when the

relative humidity is increased from dry air to 80% (Gerboles et al., 2003). Major quenching effects due to $H_2O$, $CO_2$, $H_2$ and hydrocarbons with high hydrogen/carbon ratio have also been reported (Matthews et al., 1977). However, only a small effect is observed at ambient concentrations of these species in comparison to $H_2O$. The humidity dependence of NO chemiluminescence detectors from Horiba, Monitor Labs, Thermo Environmental Instruments (TEI), and Eco Physics was investigated, and quenching effects of 2.5, 7, 8 and 7 % respectively were reported (Steinbacher et al., 2007). Horiba instruments demonstrate reduced humidity dependence due to the incorporation of an integrated heated permeation capillary drier (Gerboles et al., 2003).

To date the most significant issue with chemiluminescence $NO_x$ analysers is the inability to specifically detect $NO_2$. It is now widely recognized that the use of molybdenum catalysts in these analysers not only converts $NO_2$ to NO but also converts other gas phase nitrogen containing compounds. The response of commercial analysers to other nitrogen containing compounds was first investigated by Winer et al. (1974) where a measured response to PAN, ethyl nitrate and ethyl nitrite was recorded. The authors quantified the conversion efficiency of these compounds as 92, 103 and 92 % respectively and also reported 6 and 7 % responses to nitroethane and nitric acid respectively.

Comparisons between carbon and molybdenum convertors were also performed, where the latter converter demonstrated 10 times greater sensitivity to $NO_2$ and a 5 % more rapid converter response (Winer et al., 1974). Carbon converters were, however, later associated with chlorinated compound interferences (Joshi and Bufalini, 1978).

Measurements performed by Grosjean and Harrison (1985) revealed positive interferences for $NO_2$ with nitric acid, methyl nitrate, PAN, *n*-propyl nitrate and *n*-butyl nitrate with conversion efficiencies of > 98%. Small positive interferences with organosulphur compounds in NO measurement mode were also reported. However, the species responsible for this interference was destroyed by the catalytic molybdenum converter, as a small negative interference was observed in the $NO_2$-$NO_x$ mode (Grosjean and Harrison, 1985). Molybdenum oxide catalysts are now known to efficiently reduce compounds such as $NO_2$, $NO_3$, $HNO_3$, $N_2O_5$, $CH_3ONO_2$, $CH_3CH_2ONO_2$, *n*-$C_3H_7ONO_2$, *n*-$C_4H_9ONO_2$ and $CH_3CHONO$; as well as $HO_2NO_2$, HONO, $RO_2NO_2$, $NH_3$ and particulate phase matter, to a lesser extent (Dunlea et al., 2007). In a study evaluating $NO_2$ chemiluminescence monitors in an urban polluted environment, $HNO_3$ was identified as being responsible for a considerable portion of the total observed interference (Dunlea et al., 2007). However, as $HNO_3$ is lost on stainless steel and other surfaces, as commonly employed within these instruments, it was difficult to quantify the interference. The efficiency at which $HNO_3$ reaches the converter is different for each chemiluminescence monitor, as different monitors have different properties with varying amounts of stainless steel surface areas within the instrument.

Despite the interferences in the molybdenum catalyst conversion technique, most commercial chemiluminescent analysers still employ this technique for $NO_2$ and $NO_x$ measurements. This is due to atmospheric concentrations of interfering pollutants being generally low relative to $NO_2$; allowing legitimate measurements of $NO_2$ possible. However, in polluted regions, the concentrations of these interfering compounds may be higher relative to $NO_2$, in which case $NO_2$ measurements will be

overestimated. Steinbacher et al., (2007) reported an overestimation of $NO_2$ measured by molybdenum converter $NO_x$ chemiluminescent analysers; where they report 43 – 76 % of the apparent $NO_2$ measurements to be real. This emphasises the fact that the use of molybdenum catalysts in $NO_x$ chemiluminescence analysers is in fact a technique that better represents $NO_y$ rather than $NO_x$. It is found that the only difference between chemiluminescence $NO_x$ and $NO_y$ monitors is the position at which the catalyst is placed. In $NO_y$ monitors the catalyst is placed very close to the sampling inlet in order to convert all $NO_y$ species, whereas in $NO_x$ monitors it is placed after the capillary and before the main chamber (see Figure 6.1), therefore converting all nitrogen containing compounds that have not already been removed by the capillary filter or by passive loss on surfaces.

The drawbacks of thermal decomposition techniques highlight the increasing importance in developing inexpensive techniques that selectively measure $NO_2$ (Steinbacher et al., 2007). The use of photolytic converters to convert $NO_2$ to NO is becoming increasingly popular, due to the reduced number of interferences. Although the use of filters have ensured well defined wavelength ranges, preventing the photolysis of nitrogen containing species such as $HNO_3$, $N_2O$ and PAN, other potential interferences have been reported (*i.e.* HONO). The Eco Physics PLC 760 photolytic converter used at EUPHORE, report conversion efficiencies for PAN and HONO as 1 – 5 % and 20 % respectively. Other studies have reported conversion efficiencies for HONO as 37 % (Ryerson et al., 2000). Under polluted conditions, the $NO_x$ concentration measured by a photolytic converter was significantly lower than expected, which was attributed to unknown chemical reactions of hydrocarbons, within the converter (Kurtenbach et al., 2001).

Hitherto, interferences from the quenching of chemiluminescence intensity and the efficiency of converting $NO_2$ to NO have been discussed. A further potential interference to $NO_x$ analysers is the gas phase chemiluminescent reaction of alkenes with ozone, where the resulting chemiluminescence is recorded as NO and $NO_2$; discussed in the next section.

## 6.6 Alkenes as Potential Interferants

Alkene-ozone reactions are highly complex (as described in Chapters 3 and 4) and may have numerous chemiluminescence emitters. Pitts et al. (1972) observed chemiluminescence from 14 alkene species, which were grouped into three classes based on their emission spectra. The studies were conducted at 298 K and at total pressures of 2 – 10 Torr, similar to the conditions of the main reaction chamber within a chemiluminescence $NO_x$ monitor (Pitts et al., 1972). Chemiluminescence emission was observed from electronically excited HCHO, vibrationally excited OH and electronically excited OH in the wavelength regions 350 – 520 nm, 700 – 1100 nm and 306 nm respectively (Finlayson et al., 1974). Furthermore, phosphorescence of glyoxal and methylglyoxal was identified for *cis*- and *trans*-2-butene, peaking at 520 nm (Finlayson et al., 1974, Garcia-Campana and Baeyens, 2001, Kummer et al., 1971).

As discussed previously, chemiluminescence $NO_x$ monitors ensure sensitivity to NO by the inclusion of a red filter between the main reaction chamber and the PMT. This

ensures the filtering of chemiluminescence emission from alkene ozonolysis at wavelengths below 650 nm, and therefore does not filter the emission of the vibrationally excited OH observed in wavelength regions 700-1100 nm. In general, for the emission of a photon to occur, the product of the reaction is required to be in an excited electronic state. The reaction of alkenes and ozone may be an exception to this rule, similar to the vibrational overtone emission of HF observed in the reaction with fluorine and certain sulphur compounds (Garcia-Campana and Baeyens, 2001, Glinski et al., 1985, Turnipseed and Birks, 1991). Finlayson et al. (1974) attributed a fraction of the chemiluminescence emission observed to vibrationally excited OH *via* R6.6.

$$H + O_3 \rightarrow OH + O_2 \qquad \text{(R6.6)}$$

It was also found that $O_2$ quenched this chemiluminescence from the ethene + $O_3$ system, but not for *cis*-2-butene or isobutene systems (Calvert et al., 2000, Finlayson et al., 1974). This led to the conclusion that the cause of $O_2$ inhibition was not the scavenging of H-atoms, but that it may involve one or more reactive precursors (Calvert et al., 2000). This conclusion has initiated extensive research in attempting to explain the mechanism of the production of OH from alkene ozonolysis (Johnson and Marston, 2008), as discussed in previous chapters.

A Fast Olefin Sensor (FOS) based on the chemiluminescent alkene-ozone reaction was utilised during a field campaign in Mexico City (Velasco et al., 2007). Response characteristic for ethene, propene, isoprene, 1-butene and 1,3-butadiene were measured, with no interference from NO observed. Consequently, no relationship was observed when correlating these five observed alkene species with the apparent

measured NO interference reported by Dunlea et al. (2007). Zafiriou and True (1986) studied the interferences of ethene, acetylene, α-pinene and benzene, but found response factors to be less than 0.1 % of that for NO.

As mentioned previously, chemiluminescence $NO_x$ analysers encompass two reaction chambers, a pre chamber and a main reaction chamber. The role of the pre-chamber is to calculate a background NO reading. It is designed to allow 99 % of a 200 ppb NO sample to be consumed by reaction with ozone prior to entering the main reactor, enabling a dynamic zero reading for the analyser to be taken. Fast reacting alkenes relative to $NO + O_3$ may therefore contribute to an interfering NO signal, as a larger percentage of alkene would have been consumed with $O_3$ within the pre-chamber. The difference between the apparent background mode and measurement mode would therefore be larger. Slower reacting alkenes relative to $NO + O_3$, however, would not be consumed in the pre-chamber and may pass through to the main chamber and undergo chemiluminescence. This concept is described in detail in Section 6.9.

### *Uses of Alkene Chemiluminescence Reactions*

The chemiluminescence reaction of ethene and ozone was utilised as a means to detect ozone, exploited for atmospheric monitoring on aircrafts with a detection limit of 2 ppbV (Gregory et al., 1983). This method, however, is not the preferred choice of measuring ozone, as most commercial monitors exploit the 254 nm UV absorbance technique (see Chapter 2).

Other studies have used ozone chemiluminescence as a means to detect hydrocarbons (Bruening and Concha, 1977, Bruening and Concha, 1975, Hills and Zimmerman,

1990, Marley et al., 1998). As discussed previously, at 298 K chemiluminescence is observed for alkene + ozone reactions, but when increasing the temperature of the main reaction chamber within the instrument to 100 – 250 ºC, chemiluminescence is also observed for aromatics and alkanes. Bruening and Concha (1977) developed a gas chromatographic ozone chemiluminescence detector, which exploited the temperature dependence of hydrocarbon chemiluminescence, reporting linear responses for $C_6$-$C_9$ hydrocarbons and thiophenes. Marley et al. (1998) developed a total non-methane hydrocarbon detector using the temperature dependencies of hydrocarbon chemiluminescence. They reported little increase in chemiluminescence signal when increasing the temperature for simple alkenes (including isoprene) but an increase in signal for monoterpenes, limonene and α-pinene. The authors believed that this was an indication of a change in mechanism at higher temperatures; and reported sensitivities 50-1250 times better than flame ionization detection techniques for hydrocarbons (Marley et al., 1998).

Hills and Zimmermann (1990) developed an isoprene detector by ozone induced chemiluminescence, with a detection limit of 400 pptV. The authors used a blue sensitive PMT to maximize the sensitivity for isoprene detection and to avoid any interference from the NO + $O_3$ reaction, which as mentioned previously, occurs in the red and near-IR spectral regions. They report significant interferences with propene and to a lesser extent with ethene, 3-butene-2-one, 2-methylpropanal and dimethyl sulfide (Hills and Zimmerman, 1990). Surprisingly, no interferences were reported for α-pinene, β-pinene, limonene and a neat mixture of 33 different monoterpenes. Although chemiluminescence from these monoterpenes was observed with the PMT, it was too weak to record spectra. The authors comment that this may

be due to the monoterpenes not producing excited species upon reaction with ozone, or that other reaction products quench these species prior to fluorescence. They do however, report response factors for NO, α-pinene, β-pinene as 2.5, 3.6 and 3.9 % respectively. This method of detecting isoprene was developed and utilized in a field campaign in Mexico City, as mentioned previously (Velasco et al., 2007).

*Section B*

## 6.7 Experimental

This section describes the experiments performed to assess the extent of NO interference from alkene chemiluminescence, in conventional $NO_x$ analysers. Two sets of experiments were conducted: (*i*) EUPHORE experiments – these were performed (serendipitously) while conducting alkene ozonolysis experiments in the EUPHORE chamber; and (*ii*) Laboratory experiments – these were subsequently performed in Birmingham to expand on the results of the experiments conducted at EUPHORE.

### 6.7.1 EUPHORE Experiments

The alkene-ozone experiments were carried out in the EUPHORE atmospheric simulation chamber. Details of the experimental facility and conditions are described

in Chapter 2. Briefly, $NO_x$ measurements were performed by Eco Physics CLD 770 chemiluminescence $NO_x$ analyser, coupled to Eco Physics PLC 760 photolytic convertor. The experiments were performed with the chamber housing closed, under $NO_x$ free conditions. Ozone was added to the chamber prior to alkene addition, ensuring that any $NO_x$ present would be $NO_2$ / $NO_3$ / $N_2O_5$, rather than NO.

When injecting different alkenes into the chamber, an increase in the apparent NO signal was observed in the chemiluminescence $NO_x$ analyser, which followed the evolution of alkene concentration over the duration of the experiment, as illustrated in Figure 6.1. The 1 minute sampling times for the $NO_x$ analyser were averaged over 5 minutes and correlated to the alkene concentration (monitored by FTIR) to give an NO response factor. This provided a basis for the designation of laboratory experiments performed in Birmingham.

### 6.7.2 Laboratory Experiments

The alkene interference was also investigated in the lab in Birmingham, UK, using nitric oxide(s) analyser (Thermo Electron 42*i*-TL, chemiluminescence / thermal $NO_2$). This involved using the NO response factors calculated from the EUPHORE experiments and diluting the selected alkene to mixing ratios that would potentially show evidence of an interference. The alkenes investigated, ethene (purity ≥ 99.95 %, Fluka), *trans*-2-butene (purity ≥ 99 %, Aldrich) and 2,3-dimethyl-2-butene (purity ≥ 99 %, Aldrich), were diluted by adding pure synthetic air using a 7 L glass bulb equipped with a pressure monitor, to the required mixing ratios. The glass bulb was evacuated to ~ 1 – 3 Torr and flushed with pure air

prior to the addition of alkene, to ensure the absence of NO and impurities. After dilution, the bulb was pressurized to ~ 1000 Torr to achieve sufficient flows for the instrumental set up, shown in Figure 6.3. The alkene was further diluted by varying the flows of air / alkene, using mass flow controllers (MFCs), to the $NO_x$ analyser. The experiment was repeated several times with each individual alkene with different mixing ratios.

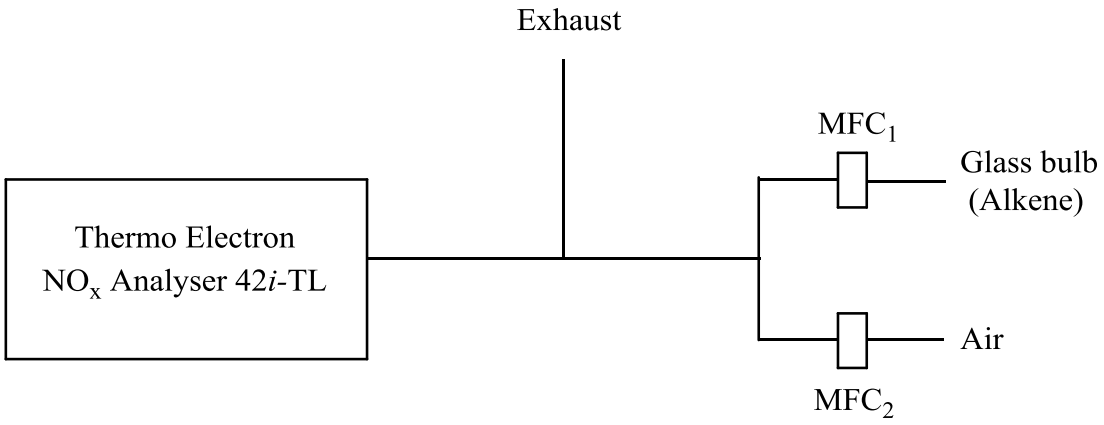


**Figure 6.3.** Schematic representation of laboratory experimental setup to assess the interference of alkenes in chemiluminescence $NO_x$ analysers

## 6.8 Results

In order to simplify the presentation of the findings of this study, the results are considered in two different sections: (*i*) EUPHORE results, and (*ii*) Laboratory results.

### 6.8.1 EUPHORE Results

The results presented in this section are for the Eco Physics CLD 770 chemiluminescence $NO_x$ analyser coupled to Eco Physics PLC 760 photolytic convertor. Although direct correlations between [alkene] and [NO] are presented within this section, the NO response factors reported are calculated by the Guggenheim approach (*i.e.* $\Delta$ [alkene] / $\Delta$ [NO]), in order to reduce noise. The two methods (direct correlation and Guggenheim approach) were calculated independently, giving quantitatively similar NO response factors (within 10 %).

Figure 6.4 illustrates that when injecting *trans*-2-butene into the chamber, an increase in the NO mixing ratio is measured by the chemiluminescence $NO_x$ analyser. The similar temporal profiles of both NO and *trans*-2-butene for the duration of the experiment demonstrates the presence of an interference. The interference cannot be attributed to NO itself, as any NO present in the chamber would react with $O_3$ two orders of magnitude faster than *trans*-2-butene + $O_3$, resulting in different temporal profiles for both species. The absence of light also ensures that no NO was formed from $NO_2$ photolysis *via* R6.5.

$$NO_2 + h\nu \rightarrow NO + O(^3P) \qquad \text{(R6.5)}$$

Correlations between alkene and NO mixing ratios were seen for *cis*- / *trans*-2-butene, 2,3-dimethyl-2-butene and myrcene, with NO response factors between 1.3 and 84.4 %. The NO response factors for limonene, α-pinene and β-pinene, however, were less than 1 %. No correlation between alkene and NO mixing ratios were observed for

ethene, propene, 1-butene, isobutene and isoprene. Terpenes, α-cedrene and methylchavicol also demonstrated interferences, but could not be quantified, probably due to the tendency for these species to stick to the inlets and the walls within the $NO_x$ instrument (and due to limited data).

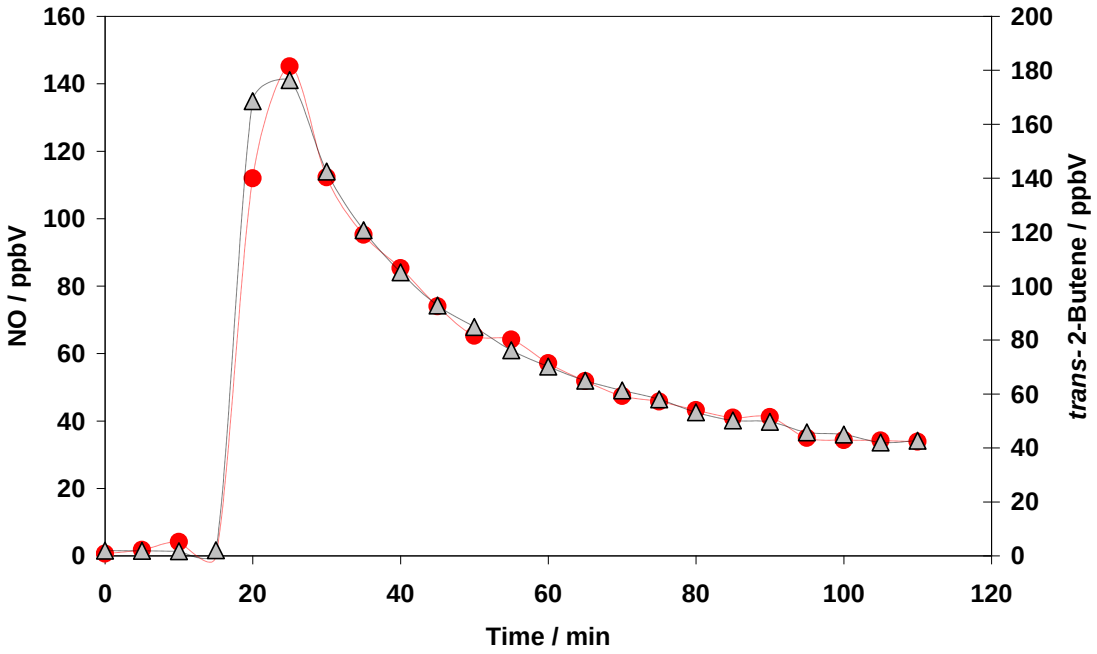


**Figure 6.4.** Temporal profile of *trans*-2-butene (grey triangles) and apparent NO mixing ratio (red circles) for an ozonolysis experiment in the absence of OH radical scavenger.

The NO response factors (calculated by the Guggenheim approach) are shown in Table 6.1. The response factors varied with both identity / structure and with different experimental conditions. The two alkenes showing the largest interferences were *trans*-2-butene and 2,3-dimethyl-2-butene, possessing NO response factors of up to 84.4 ± 2.9 % and 50.1 ± 2.0 % respectively. Figure 6.5 illustrates the correlation between the apparent NO mixing ratio and the abundance of *cis*-2-butene, *trans*-2-butene and 2,3-dimethyl-2-butene. The response factors for *cis*-2-butene and

2,3-dimethyl-2-butene are larger for experiments performed in the presence of excess CO (which is added to scavenge ≥ 95 % of OH) than experiments performed in the absence of a radical scavenger. The NO response factor for *trans*-2-butene, however, is larger for the experiment performed in the absence of radical scavenger (84.4 *vs.* 4.6 %). Figure 6.6 illustrates the correlation between Δ [2,3-dimethyl-2-butene] and Δ [NO] for 5 minute average time steps, with NO response factor 50.1 %.

**Table 6.1.** Different initial conditions of alkene ozonolysis experiments and their NO response factors. For EUPHORE experiments, using NOx analyser - Eco Physics CLD 770

| | | | Initial Conditions | | | |
|---|---|---|---|---|---|---|
| **Alkene** | **Radical Scavenger** | **NO Response Factor / %** | **Alkene / ppbV** | **$O_3$ / ppbV** | **CO / ppbV** | **$H_2O \times 10^{15}$ / molec.cm$^{-3}$** |
| *trans*-2-Butene | CO | 4.6 ± 0.3 | 90.1 | 182.9 | 720,000 | 1.82 |
| | - | 84.4 ± 2.9 | 176.4 | 87.4 | 150 * | 1.88 |
| | CO | 11.1 ± 0.3 | 76.0 | 173.1 | 700,000 | 1.98 |
| *cis*-2-Butene | - | 1.3 ± 0.1 | 49.0 | 191.0 | 150 * | 1.96 |
| | CO | 4.5 ± 1.5 | 77.0 | 166.0 | 640,000 | 2.15 |
| 2,3-Dimethyl-2-butene | - | 3.3 ± 0.3 | 35.0 | 20.2 | 700 | 1.70 |
| | CO | 50.1 ± 2.0 | 20.7 | 20.6 | 460,000 | 1.76 |
| Myrcene | - | 3.0 ± 0.2 | 121.6 | 113.2 | 340 | 1.38 |
| | $C_6H_{12}$ | 2.0 ± 0.1 | 97.9 | 105.3 | 170 | 1.57 |

* CO mixing ratio is an estimation as no data were available.
Indicated uncertainties are calculated from the scatter of the graph.

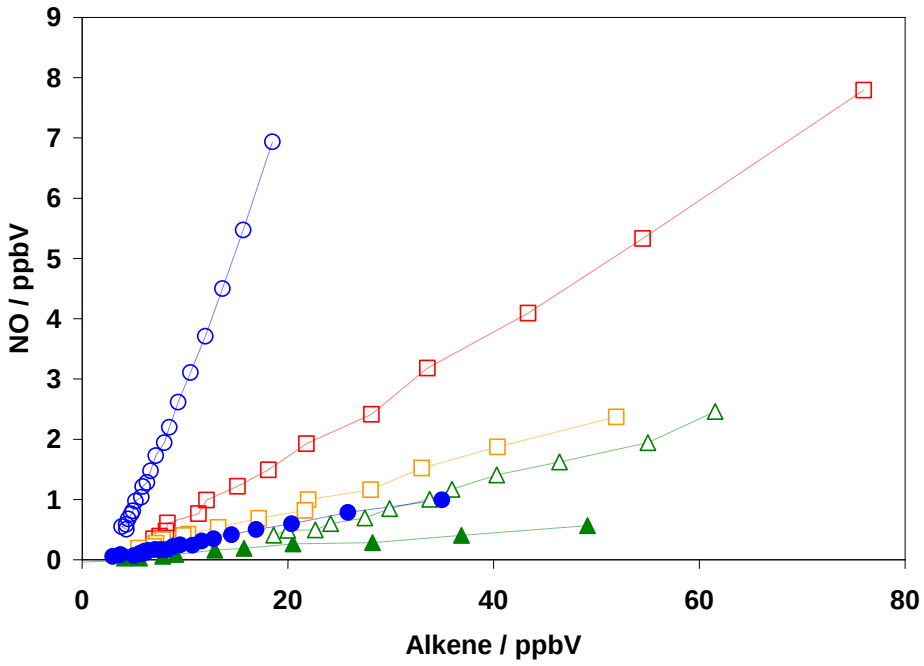


**Figure 6.5.** Correlation of alkene and NO mixing ratios for *trans*-2-butene (open red and orange squares – excess CO experiments), *cis*-2-butene (open green triangle – excess CO experiment, closed green triangle – no OH scavenger), and 2,3-dimethyl-2-butene (open blue circle – excess CO experiment, closed blue circle – no OH scavenger). Calculated NO response factors (Δ [alkene] / Δ [NO]) = 1.3 – 50.1 % (see Table 6.1).

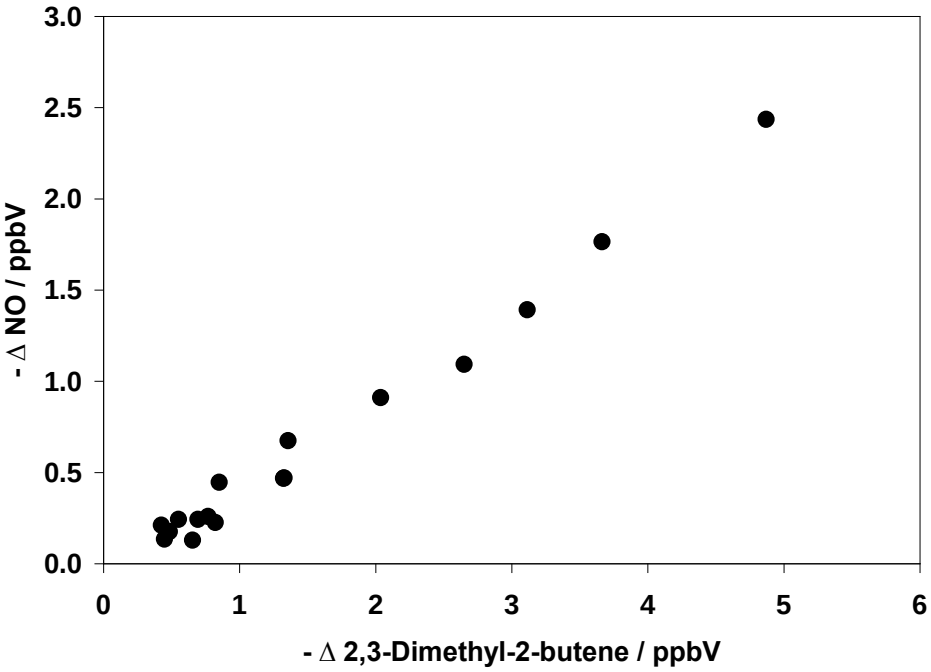


**Figure 6.6.** Δ [2,3-dimethyl-2-butene] and Δ [NO] for 5 minute average time steps, with NO response factor (50.1 ± 2.0) %.

### 6.8.2 Laboratory Results

The results presented in this section are for the Thermo Electron 42*i*-TL chemiluminescence $NO_x$ analyser, which utilises the thermal decomposition conversion of $NO_2$ to NO. The three alkenes that were investigated in the laboratory, ethene, *trans*-2-butene and 2,3-dimethyl-2-butene, show little evidence of an interference at low concentrations, in comparison to the chamber study. However, the results of the two experimental studies are in qualitative agreement (*i.e.* no interference is observed for ethene, even at high concentrations; and the largest interference observed is for *trans*-2-butene). The NO response factors calculated for trans-2-butene and 2,3-dimethyl-2-butene are shown in Table 6.2. The measured NO mixing ratio as a function of *trans*-2-butene mixing ratio is illustrated in Figure 6.7, with an overall NO response factor of 0.02 %.

**Table 6.2.** NO response factors for *trans*-2-butene and 2,3-dimethyl-2-butene for experiments performed in Birmingham, UK, investigating the potential interference from a range of different alkene mixing ratios, using NOx analyser – Thermo Electron 42*i*-TL

| **Alkene** | **Alkene / mixing ratio** | **NO Response Factor / %** |
|---|---|---|
| *trans*-2-butene | 0 – 500 ppm | 0.02 |
| | 0 – 600 ppb | 0.04 |
| | 0 – 30 ppm | 0.02 |
| 2,3-Dimethyl-2-butene | 0 – 600 ppm | $8.2 \times 10^{-4}$ |
| | 0 – 400 ppm | $6.4 \times 10^{-4}$ |

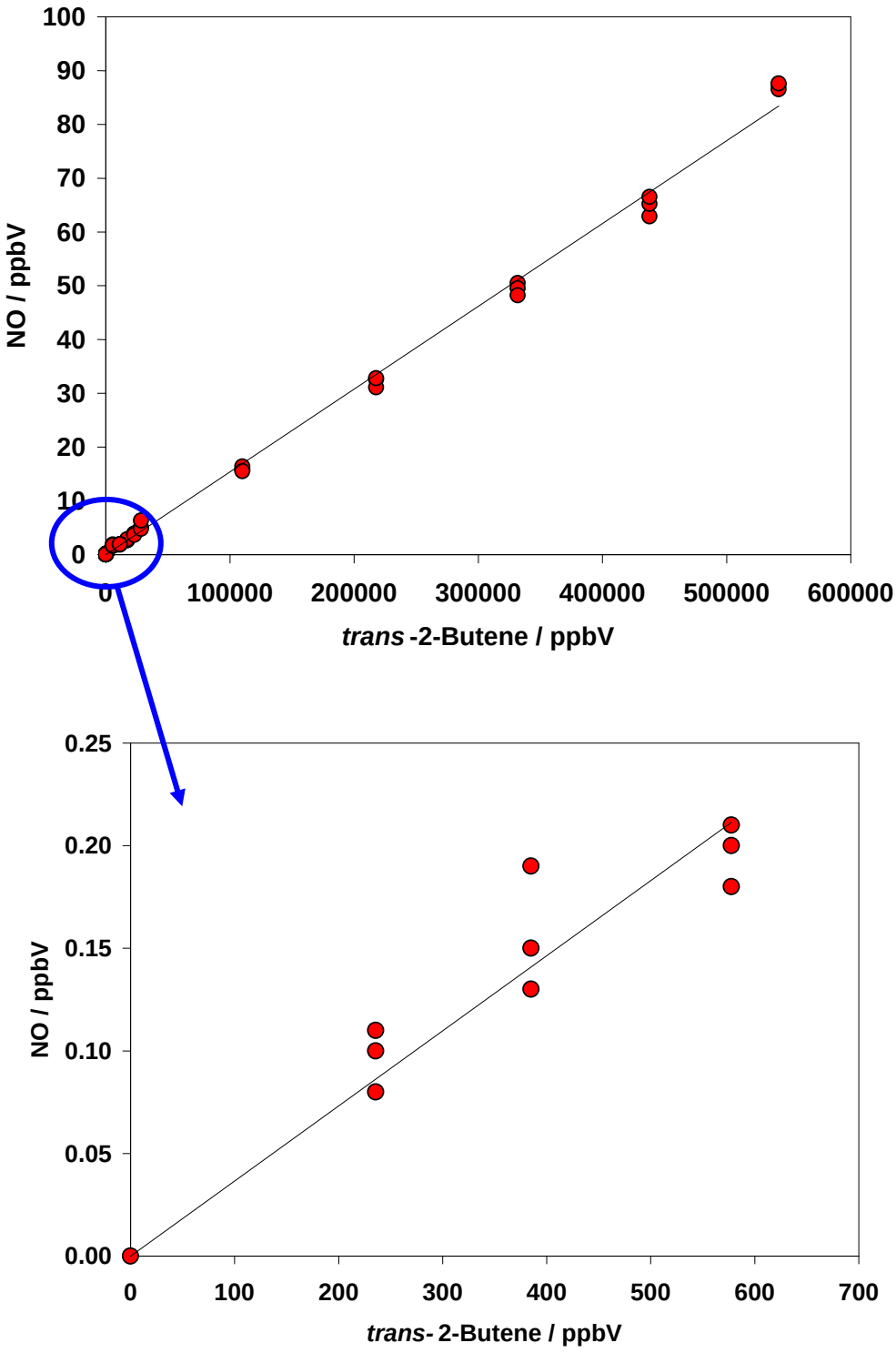


**Figure 6.7.** Correlation between *trans*-2-butene and NO mixing ratios for experiments performed in Birmingham. Overall NO response factor is 0.02 % (see Table 6.2).

## 6.9 Discussion

The results from the chamber experiments (EUPHORE results) show that *cis*-2-butene, *trans*-2-butene, 2,3-dimethyl-2-butene and myrcene all show interferences greater than 1.3 % within the Eco Physics $NO_x$ analyser. Limonene, α-pinene and β-pinene, however, show negligible interferences consistent with the 0.1 % interference reported previously (Zafiriou and True, 1986). The chamber experimental results also demonstrate no interferences for ethene, propene, 1-butene, isobutene and isoprene. This indicates that studies like that of Velasco et al. (2007) and Dunlea et al. (2007) where alkenes such as ethene, propene, isoprene, 1-butene and 1,3-butadiene were monitored and correlated with NO to measure potential interferences, may not be a good representation of alkene interference in general; as this work suggests that other alkenes behave in a different manner.

The alkenes that demonstrated interferences in the $NO_x$ analyser during the EUPHORE experiments all possessed an internal C=C bond. No NO interference was observed for ethene either during chamber or laboratory experiments. As described in Chapter 3, the Criegee intermediate (CI), $[CH_2OO]^*$, formed from the ozonolysis of ethene is also a product formed from the ozonolysis of all terminal alkenes, including isoprene, β-pinene and limonene. $[CH_2OO]^*$ is the simplest CI which cannot follow the 'hydroperoxide' mechanism to form OH (see Chapter 3, Figure 3.1). As this is the only CI formed from the ozonolysis of ethene, it may be presumed that it is a product from the hydroperoxide mechanism that may be responsible for the interference seen in the $NO_x$ analyser. This is consistent with Finlayson et al. (1974) who observed

chemiluminescence from ethene, *cis*- and *trans*-2-butene ozonolysis in the absence of $O_2$, and attributed a fraction of the emission to vibrationally excited OH *via* R6.6.

$$H + O_3 \rightarrow OH + O_2 \qquad \text{(R6.6)}$$

It was found that $O_2$ quenched this chemiluminescence from the ethene + $O_3$ system, but not in the case of *cis*- and *trans*-2-butene systems. As mentioned in Chapter 3, the H atoms formed from the ozonolysis of ethene will react near-instantaneously with $O_2$ to form $HO_2$ radicals, rather than react *via* R6.6, which would explain why no interference is observed in $NO_x$ analysers from ethene, in 1 atmosphere of air.

No interferences were observed for the ozonolysis of other terminal alkenes studied, including propene, 1-butene and 2-methylpropene. The ozonolysis of these alkenes form 2 CIs (as described in Chapter 4): $[CH_2OO]^*$ and another CI which may undergo OH formation *via* the hydroperoxide mechanism. The CIs formed in the ozonolysis of propene and 2-methylpropene are also formed from the ozonolysis of *cis*-/*trans*-2-butene and 2,3-dimethyl-2-butene respectively. Interferences were observed for *cis*-2-butene, *trans*-2-butene and 2,3-dimethyl-2-butene and not in propene and 2-methylpropene which may indicate that decomposition products formed from $[CH_2OO]^*$ may quench any potential chemiluminescence.

As mentioned earlier chemiluminescence $NO_x$ analysers ensure sensitivity to NO by the inclusion of a red filter between the main reaction chamber and the photomultiplier. This ensures the filtering of emission from alkene ozonolysis at wavelengths below 650 nm, and includes electronically excited OH at 306 nm, but

may not block emission from vibrationally excited OH observed in wavelength regions 700 - 1100 nm. It is not known whether the formation of OH *via* the hydroperoxide mechanism (or indeed formation from the excited β-oxo peroxy radical and from $HO_2$ + $RO_2$ reactions, see Chapter 4) is in an electronically or vibrationally excited state, and thus definitive conclusions cannot be drawn in regards to the source of the potential chemiluminescence.

Larger NO response factors were observed for *cis*-2-butene and 2,3-dimethyl-2-butene ozonolysis in the presence of excess CO than for ozonolysis reactions in the absence of scavenger. The calculated levels of CO in the ozonolysis experiments were designed to scavenge > 95 % of OH produced, thus, the larger NO response factor seems contradictory to the above explanation of chemiluminescence from vibrationally excited OH. The potential for the intermediate of CO + OH reaction to chemiluminesce may be a possible explanation for this observation. The OH + CO reaction takes place *via* a transitory, excited [HOCO]* intermediate, which can either revert back to its original reactants (R6.7), decompose forming H and $CO_2$ (R6.8) or be stabilised (R6.9). Stabilised HOCO can undergo reaction with $O_2$ forming $HO_2$ and $CO_2$.

| | | | | | | | | |
|---|---|---|---|---|---|---|---|---|
| OH | + | CO | ⇄ | HOCO* | | | | (R6.7) |
| HOCO* | | | → | H | + | $CO_2$ | | (R6.8) |
| HOCO* | + | M | → | HOCO | + | M | | (R6.9) |
| HOCO | + | $O_2$ | → | $HO_2$ | + | $CO_2$ | | (R6.10) |

The reversible nature of (R6.7) is only favoured at lower temperatures. The overall rate of reaction has been reported to increase with increasing pressure (Demore, 1984). There have been various studies regarding the kinetics, pressure and temperature dependencies of the OH + CO reaction (Atkinson et al., 2006), for which it is assumed that the reactions of HOCO may be similar to the reactions of H and thus, neglected in atmospheric models. The HOCO radical was first detected in the gas phase by (Miyoshi et al., 1994) by photoionisation mass spectrometry. The authors generated HOCO radicals by the reaction Cl + HCOOH and by photolysis of acrylic acid. They found that chemically produced HOCO was stable with a lifetime of > 10 ms at 298 K while photo-produced HOCO was less stable. This was attributed to the photochemically produced HOCO possessing higher internal energy, since the total excess energy of the photolysis process is larger than that of the reaction of Cl + HCOOH (Miyoshi et al., 1994). The authors also state that in the presence of $O_2$, HOCO rapidly reacts to form $HO_2$ and $CO_2$ (R12). Additional studies have also revealed structural information on the HOCO radical (Li and Francisco, 2000, Sears et al., 1992), but there are no reports in the literature regarding the detection of HOCO using UV spectroscopy or chemiluminescence (Li and Francisco, 2000). It can not therefore be ruled out that HOCO* may have the potential to emit chemiluminescence. This may account for the larger NO response factor for 2,3-dimethyl-2-butene ozonolysis in the presence of excess CO, as the reported OH yield from 2,3-dimethyl-2-butene ozonolysis in this study is large (0.83 – see Chapter 4).

In contrast to the chamber results, the experiments performed with Thermo Electron $NO_x$ analyser in the laboratory, showed little evidence of any significant interference.

No interference was observed for ethene, and small interferences (< 0.05 %) were observed for both *trans*-2-butene and 2,3-dimethyl-2-butene. The difference in the response factors for the two experimental studies may reflect the pressure differences within the main reaction chamber of the two types of $NO_x$ analysers. The external vacuum pump connected to the Eco Physics $NO_x$ analyser (used during chamber experiments) generates a main reaction chamber pressure of 1 - 10 Torr. The Thermo Electron $NO_x$ analyser (used during laboratory experiments) has a main reaction chamber pressure of 250 – 400 Torr. The higher pressure within the main chamber of the Thermo Electron $NO_x$ analyser results in an increased susceptibility of any vibrationally / electronically excited species formed from alkene + $O_3$ to undergo quenching and is reflected in the smaller NO response factors calculated. The alkene + ozone chemiluminescence study by Finlayson et al. (1974) was conducted at pressures of 2 – 10 Torr, similar to the pressure within the main reaction chamber of the Eco Physics $NO_x$ analyser used during the EUPHORE experiments.

The influence of pressure on alkene-ozone reactions has been demonstrated previously (Donahue et al., 1998, Kroll et al., 2001a, Kroll et al., 2001c). Kroll and co workers reported OH formation yields from a number of alkene ozone reactions, using LIF at pressures between 10 – 60 Torr. They showed how the OH yield for a number of substituted alkenes decreased as the pressure increased over short timescales (~ 30 ms) (Kroll et al., 2001a). They later showed that at longer timescales the OH yield increased, approaching values that were consistent with the literature (Kroll et al., 2001c). This shows that OH formation from alkene ozonolysis can result from both prompt formation from a vibrationally excited CI, and formation from the thermal decomposition of a stabilised CI at longer timescales (Johnson and Marston, 2008), as

illustrated in Figure 6.8 (and discussed in Chapter 3). The prompt formation of OH from the decomposition of the vibrationally excited CI may result in OH having considerable vibrational energy, thus emitting chemiluminescence; whereas the longer timescale OH formation from the thermal decomposition of the stabilised CI may be more stable in comparison. This may explain the larger NO response factors derived from the chamber experiments performed using chemiluminescence Eco Physics NOx analyser, which has a main reactor chamber pressure of 1 – 10 Torr.

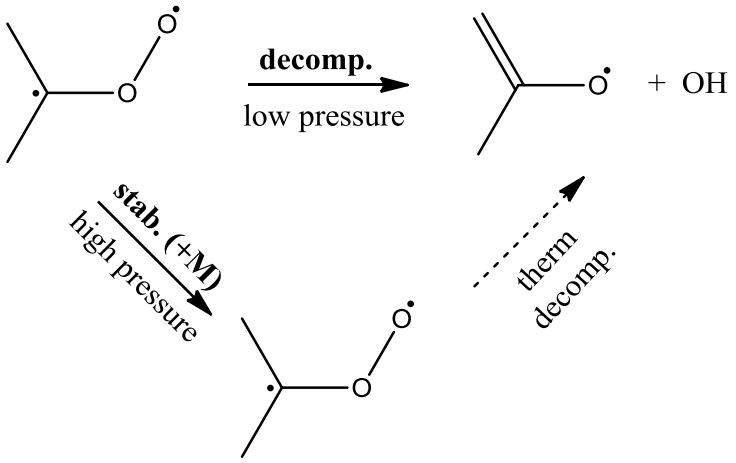


**Figure 6.8.** Possible routes to OH formation from vibrationally excited CI. Adapted from Johnson and Marston (2008).

The potential for an alkene to cause an interference in the chemiluminescence $NO_x$ analyser can also be calculated by considering the percentage of alkene reacting in the pre-reactor chamber. As mentioned previously, the pre-reactor chamber is designed to allow 99% of a 200 ppb NO sample to react with ozone prior to entering the main chamber, enabling a dynamic zero reading for the analyser (Thermo Electron 42*i*-TL manual). Using this percentage as a basis, pseudo first order rate kinetics can be exploited to calculate an approximation of the fraction of alkene reacting in the

pre-chamber. If the rate coefficient of an alkene + $O_3$ reaction is fast relative to that for the NO + $O_3$ reaction, then the contribution of alkene to an interference signal can be large, due to a larger percentage of alkene reacting in the pre-chamber. The difference between the 'background' mode (pre-chamber) and the measurement mode (main chamber) will therefore be larger, giving rise to a larger apparent overall NO signal. For example, the slow rate coefficient of ethene + $O_3$ means that ~ 99.96 % of ethene passes into the main chamber, and therefore only ~ 0.04 % of ethene has the potential to cause an interference (the percentage of reacted alkene in the pre-chamber). This percentage of alkene reacting in the pre-chamber contributes to the dynamic zero signal in the 'background' mode, and so the difference between the zero signal and the apparent NO signal is 0.04 % larger. In contrast, the fast rate coefficient of 2,3-dimethyl-2-butene + $O_3$ means that ~ 24 % of 2,3-dimethyl-2-butene reacts in the pre-reactor, which may contribute to the overall NO signal in the main chamber, as described for ethene.

## 6.10 Implications

The results of this study indicate that fast reacting alkenes (with $O_3$) may contribute considerably to NO signals within chemiluminescence $NO_x$ analysers. This is a potential problem in using such instrumentation to monitor $NO_x$ in biogenic environments, owing to the fast reaction of terpenes / sesquiterpenes including, α-terpinene / β-caryophyllene and potentially other unidentified biogenic species with $O_3$. Alkene interference may be a possible explanation to the relatively high NO and low $NO_2$ night time measurements in the tropical rainforest, which could not be

accounted for (Pugh et al., 2011). The alkene interferences reported in this study may also be a problem for chemiluminescence $NO_x$ measurements made in urban environments, owing to the presence of anthropogenic alkenes such as *trans*-2-butene, as well as high levels of CO. The results of this study, however, cannot be used to draw firm conclusions as further investigation is required.

# Chapter 7. Conclusion

The ozonolysis reactions of ethene, propene, 1-butene, 2-methylpropene, *cis*-2-butene, *trans*-2-butene and 2,3-dimethyl-2-butene have been investigated in detail under ambient boundary layer conditions using a variety of instrumentation, including FTIR, CIR-TOF-MS, HPLC, PERCA and LIF. The ozonolysis experiments were performed in the presence and absence of excess cyclohexane and/or CO in order to scavenge > 95 % of OH produced. Four analytical stages were performed, in each case to determine the *overall* yields of carbonyl and radical products from the *overall* fast ozonolysis reaction (*i.e.* the CI formation / decomposition chemistry), using detailed chemical box modelling.

Reaction rate coefficients for alkene + ozone ($k_{O_3+alkene}$) were calculated by optimising $k_{O_3+alkene}$ to best simulate the observed alkene and ozone decay traces. Carbonyl yields were determined in the absence and presence of radical scavengers and with enhanced humidity, where the derived yields for 2-methylpropene and 2,3-dimethyl-2-butene, suggest that the yields are dependent upon the initial concentration of alkene / ozone and upon $RO_2 + RO_2$ and $RO_2 + HO_2$ competition for the acetonyl and acetyl peroxy radical reactions. The increase in carbonyl yields in the presence of excess CO and/or enhanced humidity provided a means for determining the yield of stabilised Criegee intermediates (SCI). For example, the ethene-ozone postulated mechanism and previous studies indicate that the primary HCHO yield is unity; therefore, the mean measured HCHO yield of 1.54 ± 0.12 in the presence of excess CO is assumed to

reflect the reaction of $CH_2OO$ with CO (leading to $CO_2$ and HCHO), determining an SCI yield of 0.54. For the propene-ozone system, SCI yields of 0.24 were inferred by the observed additional acetaldehyde produced from the SCI + $H_2O$ reaction. Meanwhile the SCI yield for 2,3-dimethyl-2-butene (0.17) was determined by calculating the balance of the sub-unity OH yield of 0.83 ± 0.22.

The results represent the first direct OH steady state measurements and subsequent yields for a homologous series of alkenes, under tropospherically relevant conditions; and are the first direct measurements for propene, 1-butene and 2-methylpropene. OH yields were derived through numerical optimisation to observed steady state concentrations of OH by LIF. The results obtained are consistent with the so called "hydroperoxide" mechanism as previous literature suggests. The results may also indicate that the formation of an additional source of OH *via* the decomposition of the 'hot' acid is likely, though small. For ethene (where the steady-state OH concentration generated in the system were below the detection limit of the LIF) and *trans*-2-butene ozonolysis, OH yields were determined by optimisation to observed concentrations of cyclohexanol, cyclohexanone, cyclohexyl hydroperoxide, alkene, ozone and $HO_2$, from excess cyclohexane experiments. The results highlight the importance of accounting for the $HO_2$ abundance, particularly under relatively high $O_3$ / alkene conditions, and the detailed scavenger chemistry (to allow for $RO_2$ + $HO_2$ coupling and the $O_3$ + $HO_2$ contribution to the overall OH yield) when deriving radical yields in scavenger experiments.

$HO_2$ yields were determined in the presence and absence of OH scavenger, with a decrease in $HO_2$ yield observed in the presence of both CO and increased humidity (ethene and *trans*-2-butene). Potential explanations for these dependencies are: (*i*) bimolecular reaction of the partially thermalised Criegee intermediate (CI) interrupting the decomposition process, particularly for *anti*-CIs and $CH_2OO$; (*ii*) the reaction of CO + dioxirane, leading to the formation of acid anhydride; (*iii*) an additional $HO_2$ production channel from bimolecular reactions of the SCI, which competes with CO and $H_2O$; (*iv*) potential interferences of peroxy radicals in the $HO_2$ mode of detection by LIF.

The $HO_2$ yields derived for the simple alkene + ozone systems indicate that current atmospheric models (*e.g.* MCMv3.1) underestimate the formation of $HO_2$. However using the postulated mechanisms it is difficult to attribute reaction pathways for the formation of these large calculated $HO_2$ yields. The $HO_2$ yields determined for the excess CO experiments, however, indicate that $HO_2$ yields in the MCM (which are largely inferred through the observation of associated stable products using assumed mechanisms) are reasonably good estimates.

From the results presented in this study, the following rate constants / yields are suggested to be incorporated into atmospheric chemistry and air quality models where chemical detail is required:

$O_3 + C_2H_4 \rightarrow 0.17\ OH + 0.27\ (0.10)^{\dagger}\ HO_2 + 0.54\ SCI + 1.00\ HCHO$

$k_{O_3+ethene} = 1.45\ (\pm 0.25) \times 10^{-18}\ cm^3\ molecule^{-1}\ s^{-1}$ at 298 K

$O_3 + C_3H_6 \rightarrow 0.36\ OH + 0.61\ (0.09)^{\dagger}\ HO_2 + 0.24\ SCI + 0.51\ HCHO + 0.49\ CH_3CHO$

$k_{O_3+propene} = 1.15\ (\pm 0.11) \times 10^{-17}\ cm^3\ molecule^{-1}\ s^{-1}$ at 300 K

$O_3$ + 1-Butene $\rightarrow 0.56\ OH + 0.57\ (0.18)^{\dagger}\ HO_2 + 0.59\ HCHO + 0.41\ CH_3CH_2CHO$

$k_{O_3+1\text{-}butene} = 1.24\ (\pm 0.38) \times 10^{-17}\ cm^3\ molecule^{-1}\ s^{-1}$ at 301 K

$O_3$ + 2-methylpropene $\rightarrow 0.67\ OH + 1.51\ (0.35)^{\dagger}\ HO_2 + 0.66\ HCHO + 0.34\ CH_3COCH_3$

$k_{O_3+2\text{-}methylpropene} = 1.29 \times 10^{-17}\ cm^3\ molecule^{-1}\ s^{-1}$ at 298 K$^{\ddagger}$

$O_3$ + *cis*-2-butene $\rightarrow 0.26\ OH + 0.58\ (0.12)^{\dagger}\ HO_2 + 0.19\ SCI + 1.00\ CH_3CHO$

$k_{O_3+cis\text{-}2\text{-}butene} = 1.19\ (\pm 0.12) \times 10^{-16}\ cm^3\ molecule^{-1}\ s^{-1}$ at 299 K

$O_3$ + *trans*-2-butene $\rightarrow 0.60\ OH + 0.89\ (0.03)^{\dagger}\ HO_2 + 0.13\ SCI + 1.00\ CH_3CHO$

$k_{O_3+trans\text{-}2\text{-}butene} = 1.98 \times 10^{-16}\ cm^3\ molecule^{-1}\ s^{-1}$ at 298 K$^{\ddagger}$

$O_3$ + 2,3-Dimethyl-2-butene $\rightarrow 0.83\ OH + 1.74\ (0.18)^{\dagger}\ HO_2 + 0.17\ SCI + 1.00\ CH_3COCH_3$

$k_{O_3+2,3\text{-}dimethyl\text{-}2\text{-}butene} = 1.08\ (\pm 0.34) \times 10^{-18}\ cm^3\ molecule^{-1}\ s^{-1}$ at 292 K

---

$^{\dagger}$ Bracketed $HO_2$ yield values correspond to measured yields derived from experiments in the presence of excess CO

$^{\ddagger}$ Calculated from Arrhenius expression – see Chapter 4, Table 4.1

The results obtained from this study have been qualitatively considered in terms of their implications for the chemistry of the atmosphere. Of particular significance is the contribution of $HO_x$ radicals from alkene ozonolysis to the primary initiation route for OH and $HO_2$. Dependent upon the $HO_2$ yield employed in model initialisation (*i.e.* $HO_2$ yields derived from non scavenger or excess CO alkene-ozone experiments), the contribution to the primary initiation routes of $HO_2$ from alkene ozonolysis ranges from 4 – 17 %, during the daytime. This exemplifies the importance in the interpretation of the $HO_2$ yields determined, where further work is needed in order to quantify any potential interferences within the LIF instrumentation. The contribution of alkene ozonolysis to the primary initiation routes for OH was 29 %.

## *Future Work*

To date, clear isolation of the CI from gas-phase alkene ozonolysis remains a major objective, despite the direct detection of $CH_2OO$ prepared from relatively less energetic sources *e.g.* $CH_3S(O)CH_3 + O_2 \rightarrow CH_2OO + CH_3SO$ (Taatjes et al., 2008). In this study, however, SCI yields have been inferred from the observation of products from the decomposition / isomerisation of the various substituted CIs. Further mechanistic insights could therefore be attained from data from alternative experimental approaches, in which other potential product channels (for example, CO, $CO_2$) are monitored and other parameters (*e.g.* pressure) are varied.

The correlation between the derived OH and $HO_2$ non-scavenger yields in this study may suggest that OH formation *via* the vinyl hydroperoxide mechanism may also form a route for $HO_2$ production, which is not included in the postulated mechanisms.

The recent interferences reported by Fuchs et al. (2011), in the $HO_2$ mode of detection by LIF, however, may indicate that $RO_2$ radicals, from alkene + OH reactions may give rise to the apparent correlation. Quantification to the extent of various peroxy radicals and β-hydroxyalkyl peroxy radicals interfering with $HO_2$ measurements by LIF may provide insight into the missing source of $HO_x$ in environments where biogenic VOC emissions are high (Whalley et al., 2011).

The interference of alkenes in the NO signal from chemiluminescence $NO_x$ analysers observed in this study indicates that fast reacting alkenes (with $O_3$) such as α-terpinene and β-caryophyllene may contribute considerably to ambient NO signals, in regions remote from pollution sources. Quantifying such interferences may offer an alternative explanation to the relatively high NO and low $NO_2$ night time measurements observed in the tropical rainforest (Pugh et al., 2011).

## *Journal Publications Arising as a Result of this Work*

**M. S. Alam**, M. Camredon, A. R. Rickard, T. Carr, K. Hornsby, K. P. Wyche, P. S. Monks and W. J. Bloss. *Total radical yields from tropospheric ethene ozonolysis.* DOI: 10.1039/C0CP02342F. Phys. Chem. Chem. Phys., 2011

M. Camredon, J. F. Hamilton, **M. S. Alam**, K. P. Wyche, T. Carr, I. R. White, P. S. Monks, A. R. Rickard, and W. J. Bloss. *Distribution of gaseous and particulate organic composition during dark α-pinene ozonolysis.* Atmos. Chem. Phys., 10, 2893–2917, 2010

**M.S. Alam**, A. R. Rickard, M. Camredon, T. Carr, K. P. Wyche, K. Hornsby, P. S. Monks and W. J. Bloss. *Mechanistic insights into tropospheric ozonolysis of short chain alkenes (1): Radical product yields.* In preparation. J. Phys. Chem.,

**M.S. Alam**, A. R. Rickard, M. Camredon, T. Carr, K. P. Wyche, K. Hornsby, P. S. Monks and W. J. Bloss. *Mechanistic insights into tropospheric ozonolysis of short chain alkenes (2): Stable product yields.* In preparation. J. Phys. Chem.,

**M.S. Alam**, J.D. Lee, M. Martinez, A.R Rickard, M. Camredon, W.J. Bloss. *Alkene interference in chemiluminscent $NO_x$ measurements*. In preparation. Atmos. Meas. Tech. Discuss.,

# Appendix

The initial conditions for each of the alkene-ozone experiments are shown in Tables A1 – A7. The conditions were used for the initialisation of the corresponding box models. Temperature, relative humidity and dilution rates were averaged over the duration of each experiment, as the variation in these parameters was minimal (see Chapter 2, Section 2.4, Figure 2.5). The simulations were initialised at the time point at which the maximum alkene mixing ratio was observed.

**Table A1**. Initial conditions for ethene ozonolysis simulations

| Expt. Type | Ethene / ppbV | Ozone / ppbV | CO / ppmV | Cyclohexane / ppmV | Relative Humidity / % | Dilution* / $s^{-1}$ ($10^{-5}$) | Temp / k | Duration / min |
|---|---|---|---|---|---|---|---|---|
| a | 501.1 | 478.3 | 0.753 | 0 | 0.3 | 6.75 | 293 | 130 |
| b | 522.8 | 486.7 | 570 | 0 | 0.3 | 7.21 | 295 | 80 |
| c | 490.5 | 469.0 | 0.281 | 18.5 | 0.3 | 4.64 | 296 | 200 |
| b | 433.1 | 455.6 | 633 | 0 | 0.2 | 5.04 | 300 | 100 |
| b+d | 264.8 | 242.3 | 504 | 0 | 29.0 | 4.88 | 302 | 90 |

a, simple ethene and ozone; b, with added CO; c, with added cyclohexane; d, with added water
* derived from decay of $SF_6$, monitored by FT-IR

**Table A2**. Initial conditions for propene ozonolysis simulations

| Expt. Type | Propene / ppbV | Ozone / ppbV | CO / ppmV | Cyclohexane / ppmV | Relative Humidity / % | Dilution* / $s^{-1}$ ($10^{-5}$) | Temp / k | Duration / min |
|---|---|---|---|---|---|---|---|---|
| a | 221.0 | 272.0 | 0.150 | 0 | 1.3 | 4.78 | 302.0 | 60 |
| b | 117.0 | 164.0 | 538,000 | 0 | 1.3 | 4.92 | 300.8 | 55 |
| b+d | 65.0 | 93.0 | 458,000 | 0 | 20.4 | 4.99 | 300.2 | 55 |

a, simple ethene and ozone; b, with added CO; d, with added water
* derived from decay of $SF_6$, monitored by FT-IR

**Table A3**. Initial conditions for 1-butene (1-BUT) ozonolysis simulations

| Expt. Type | 1-BUT /ppbV | Ozone / ppbV | CO / ppmV | Cyclohexane / ppmV | Relative Humidity / % | Dilution* / $s^{-1}$ ($10^{-5}$) | Temp / k | Duration / min |
|---|---|---|---|---|---|---|---|---|
| a | 301.0 | 274.0 | 0.150 | 0 | 0.2 | 2.41 | 297.5 | 55 |
| b | 170.0 | 165.0 | 766,000 | 0 | 0.2 | 2.42 | 301.4 | 70 |

a, simple ethene and ozone; b, with added CO
* derived from decay of $SF_6$, monitored by FT-IR

**Table A4**. Initial conditions for 2-methylpropene (2-MP) ozonolysis simulations

| Expt. Type | 2-MP /ppbV | Ozone / ppbV | CO / ppmV | Cyclohexane / ppmV | Relative Humidity / % | Dilution* / $s^{-1}$ ($10^{-5}$) | Temp / k | Duration / min |
|---|---|---|---|---|---|---|---|---|
| a | 32.7 | 200.6 | 0.100 | 0 | 0.2 | 6.31 | 292.9 | 120 |
| a+d | 92.6 | 118.2 | 0.177 | 0 | 18.0 | 7.55 | 295.3 | 120 |
| b | 37.7 | 198.7 | 541,000 | 0 | 0.6 | 7.01 | 297.0 | 120 |
| b | 112.6 | 466.8 | 804,000 | 0 | 0.8 | 7.30 | 294.7 | 120 |
| c | 306.5 | 470.6 | 0.406 | 142,000 | 0.2 | 2.30 | 291.3 | 115 |
| c+d | 280.7 | 450.7 | 0.400 | 149,000 | 21.0 | 2.84 | 294.3 | 110 |
| b | 60.2 | 216.8 | 625,000 | 0 | 0.2 | 3.21 | 295.8 | 135 |
| b+d | 57.4 | 145.9 | 629,000 | 0 | 18.0 | 5.21 | 296.9 | 105 |
| a | 239.0 | 463.5 | 0.150 | 0 | 0.4 | 7.16 | 292.3 | 80 |

a, simple ethene and ozone; b, with added CO; c, with added cyclohexane; d, with added water
* derived from decay of $SF_6$, monitored by FT-IR

**Table A5**. Initial conditions for *cis*-2-butene (C2B) ozonolysis simulations

| Expt. Type | C2B /ppbV | Ozone / ppbV | CO / ppmV | Cyclohexane / ppmV | Relative Humidity / % | Dilution* / $s^{-1}$ ($10^{-5}$) | Temp / k | Duration / min |
|---|---|---|---|---|---|---|---|---|
| a | 49.0 | 191.0 | 0.200 | 0 | 0.2 | 6.93 | 296.7 | 60 |
| b | 77.0 | 166.0 | 637,000 | 0 | 0.2 | 7.21 | 299.3 | 60 |

a, simple ethene and ozone; b, with added CO
* derived from decay of $SF_6$, monitored by FT-IR

**Table A6**. Initial conditions for *trans*-2-butene (T2B) ozonolysis simulations

| Expt. Type | T2B /ppbV | Ozone / ppbV | CO / ppmV | Cyclohexane / ppmV | Relative Humidity / % | Dilution* / $s^{-1}$ ($10^{-5}$) | Temp / k | Duration / min |
|---|---|---|---|---|---|---|---|---|
| b | 66.8 | 199.7 | 749,000 | 0 | 0.5 | 5.11 | 290.6 | 45 |
| c+d | 245.8 | 110.1 | 0.228 | 57,400 | 21.7 | 3.80 | 293.7 | 115 |
| b | 90.1 | 182.9 | 715,000 | 0 | 0.3 | 4.22 | 293.5 | 80 |
| b+d | 85.9 | 178.1 | 748,000 | 0 | 20.4 | 3.78 | 294.6 | 70 |
| a | 176.4 | 87.4 | 0.150 | 0 | 0.3 | 5.92 | 293.5 | 80 |
| b | 76.0 | 178.1 | 704,000 | 0 | 0.2 | 6.44 | 299.4 | 65 |

a, simple ethene and ozone; b, with added CO; c, with added cyclohexane; d, with added water
* derived from decay of $SF_6$, monitored by FT-IR

**Table A7**. Initial conditions for 2,3-dimethyl-2-butene (TME) ozonolysis simulations

| Expt. Type | TME /ppbV | Ozone / ppbV | CO / ppmV | Cyclohexane / ppmV | Relative Humidity / % | Dilution* / $s^{-1}$ ($10^{-4}$) | Temp / k | Duration / min |
|---|---|---|---|---|---|---|---|---|
| a | 35.0 | 20.2 | 0.703 | 0 | 0.3 | 1.18 | 291.9 | 90 |
| b | 20.8 | 20.6 | 464,000 | 0 | 0.3 | 1.24 | 291.6 | 90 |

a, simple ethene and ozone; b, with added CO
* derived from decay of $SF_6$, monitored by FT-IR

# References

ALAM, M. S., CAMREDON, M., RICKARD, A. R., CARR, T., WYCHE, K. P., HORNSBY, K., MONKS, P. S. & BLOSS, W. J. (2011) Total Radical Yields from Tropospheric Ethene Ozonolysis. *Physical Chemistry Chemical Physics***,** DOI: 10.1039/C0CP02342F.

ALTUZAR, V., TOMAS, S. A., ZELAYA-ANGEL, O., SANCHEZ-SINENCIO, F. & ARRIAGA, J. L. (2005) Atmospheric ethene concentrations in Mexico City: Indications of strong diurnal and seasonal dependences. *Atmospheric Environment,* 39**,** 5219-5225.

ANGLADA, J. M., APLINCOURT, P., BOFILL, J. M. & CREMER, D. (2002) Atmospheric formation of OH radicals and H2O2 from alkene ozonolysis under humid conditions. *Chemphyschem,* 3**,** 215-+.

ASCHMANN, S. M., AREY, J. & ATKINSON, R. (2002) OH radical formation from the gas-phase reactions of O-3 with a series of terpenes. *Atmospheric Environment,* 36**,** PII S1352-2310(02)00355-2.

ASCHMANN, S. M., TUAZON, E. C., AREY, J. & ATKINSON, R. (2003) Products of the gas-phase reaction of O-3 with cyclohexene. *Journal of Physical Chemistry A,* 107**,** 2247-2255.

ASCHMUTAT, U., HESSLING, M., HOLLAND, F. & HOFZUMAHAUS, A. (1994) IN ANGELETTI, G. & RESELLI, G. (Eds.) *Physico-Chemical Behaviour of Atmospheric Pollutants.* (European Commision, Brussels).

ATKINSON, R. (1997a) Atmospheric reactions of alkoxy and beta-hydroxyalkoxy radicals. *International Journal of Chemical Kinetics,* 29**,** 99-111.

ATKINSON, R. (1997b) Gas-Phase Tropospheric Chemistry of Volatile Organic Compounds: 1. Alkanes and Alkenes. *Journal of Physical and Chemical Reference Data,* 26**,** 215-290.

ATKINSON, R. (2007) Rate constants for the atmospheric reactions of alkoxy radicals: An updated estimation method. *Atmospheric Environment,* 41**,** 8468-8485.

ATKINSON, R. & AREY, J. (2003) Gas-phase tropospheric chemistry of biogenic volatile organic compounds: a review. *Atmospheric Environment,* 37**,** S197-S219.

ATKINSON, R. & ASCHMANN, S. M. (1993) OH RADICAL PRODUCTION FROM THE GAS-PHASE REACTIONS OF O-3 WITH A SERIES OF ALKENES UNDER ATMOSPHERIC CONDITIONS. *Environmental Science & Technology,* 27**,** 1357-1363.

ATKINSON, R., ASCHMANN, S. M., AREY, J. & SHOREES, B. (1992) FORMATION OF OH RADICALS IN THE GAS-PHASE REACTIONS OF O3 WITH A SERIES OF TERPENES. *Journal of Geophysical Research-Atmospheres,* 97**,** 6065-6073.

ATKINSON, R., BAULCH, D. L., COX, R. A., CROWLEY, J. N., HAMPSON, R. F., HYNES, R. G., JENKIN, M. E., ROSSI, M. J. & TROE, J. (2006) Evaluated kinetic and photochemical data for atmospheric chemistry: Volume II - gas phase reactions of organic species. *Atmospheric Chemistry and Physics,* 6**,** 3625-4055 & http://www.iupac-kinetic.ch.cam.ac.uk/, IUPAC Subcommittee on Gas Kinetic Data Evaluation, 2006.

ATKINSON, R., HASEGAWA, D. & ASCHMANN, S. M. (1990) RATE CONSTANTS FOR THE GAS-PHASE REACTIONS OF O-3 WITH A

SERIES OF MONOTERPENES AND RELATED-COMPOUNDS AT 296-K +/-2-K. *International Journal of Chemical Kinetics,* 22**,** 871-887.

ATKINSON, R. & LLOYD, A. C. (1984) EVALUATION OF KINETIC AND MECHANISTIC DATA FOR MODELING OF PHOTOCHEMICAL SMOG. *Journal of Physical and Chemical Reference Data,* 13**,** 315-444.

AVZIANOVA, E. V. & ARIYA, P. A. (2002) Temperature-dependent kinetic study for ozonolysis of selected tropospheric alkenes. *International Journal of Chemical Kinetics,* 34**,** 678-684.

BAHTA, A., SIMONAITIS, R. & HEICKLEN, J. (1984) Reactions of Ozone with Olefins: Ethylene, Allene, 1,3-Butadiene, and trans-1,3-Pentadiene. *International Journal of Chemical Kinetics,* 16**,** 1227-1246.

BARBER, C. & MARSTON, G. (2010) FTIR Product Studies of RO2 + HO2 Reactions of Atmospheric Importance. *21st International Symposium on Gas Kinetics.* Leuven, Belgium.

BECKER, K. H. (1996) EUPHORE: Final Report to the European Commission, Contract EV5V-CT92-0059. *Final Report of the EC-Project.* Bergische Universität Wuppertal, Germany.

BECKER, K. H. (1999) In Situ Euphore Radical Measurement (EUROPHAM): Final Report to the European Commission, Contract ENV4-CT95-0011. *Final Report.* Bergische Universität Wuppertal, Germany.

BERNDT, T., BOGE, O. & STRATMANN, F. (2003) Gas-phase ozonolysis of alpha-pinene: gaseous products and particle formation. *Atmospheric Environment,* 37**,** 3933-3945.

BLAKE, R. S., WHYTE, C., HUGHES, C. O., ELLIS, A. M. & MONKS, P. S. (2004) Demonstration of proton-transfer reaction time-of-flight mass

spectrometry for real-time analysis of trace volatile organic compounds. *Analytical Chemistry,* 76**,** 3841-3845.

BLOSS, C., WAGNER, V., BONZANINI, A., JENKIN, M. E., WIRTZ, K., MARTIN-REVIEJO, M. & PILLING, M. J. (2005) Evaluation of detailed aromatic mechanisms (MCMv3 and MCMv3.1) against environmental chamber data. *Atmospheric Chemistry and Physics,* 5**,** 623-639.

BLOSS, W. J., GRAVESTOCK, T. J., HEARD, D. E., INGHAM, T., JOHNSON, G. P. & LEE, J. D. (2003) Application of a compact all solid-state laser system to the in situ detection of atmospheric OH, HO2, NO and IO by laser-induced fluorescence. *Journal of Environmental Monitoring,* 5**,** 21-28.

BLOSS, W. J., LEE, J. D., BLOSS, C., HEARD, D. E., PILLING, M. J., WIRTZ, K., MARTIN-REVIEJO, M. & SIESE, M. (2004) Validation of the calibration of a laser-induced fluorescence instrument for the measurement of OH radicals in the atmosphere. *Atmospheric Chemistry and Physics,* 4**,** 571-583.

BOLLINGER, M. J., SIEVERS, R. E., FAHEY, D. W. & FEHSENFELD, F. C. (1983) CONVERSION OF NITROGEN-DIOXIDE, NITRIC-ACID, AND NORMAL-PROPYL NITRATE TO NITRIC-OXIDE BY GOLD-CATALYZED REDUCTION WITH CARBON-MONOXIDE. *Analytical Chemistry,* 55**,** 1980-1986.

BOYD, A. A., FLAUD, P. M., DAUGEY, N. & LESCLAUX, R. (2003) Rate constants for RO2 + HO2 reactions measured under a large excess of HO2. *Journal of Physical Chemistry A,* 107**,** 818-821.

BRAUERS, T., BOSSMEYER, J., DORN, H. P., SCHLOSSER, E., TILLMANN, R., WEGENER, R. & WAHNER, A. (2007) Investigation of the formaldehyde differential absorption cross section at high and low spectral resolution in the

simulation chamber SAPHIR. *Atmospheric Chemistry and Physics,* 7**,** 3579-3586.

BROOKES, D. M. (2009) Characterisation of a PERCA instrument and measurements of peroxy radicals during the West African Monsoon 2006, Thesis. University of Leicester.

BRUENING, W. & CONCHA, F. J. M. (1975) SELECTIVE DETECTOR FOR GAS-CHROMATOGRAPHY BASED ON CHEMILUMINESCENCE OF OZONE REACTIONS. *Journal of Chromatography,* 112**,** 253-265.

BRUENING, W. & CONCHA, F. J. M. (1977) IMPROVED GAS-CHROMATOGRAPHIC OZONE CHEMILUMINESCENCE DETECTOR. *Journal of Chromatography,* 142**,** 191-201.

CALVERT, J. G., ATKINSON, R., KERR, J. A., MADRONICH, S., MOORTGAT, G. K., WALLINGTON, T. J. & YARWOOD, G. (2000) *The Mechanism of Atmospheric Oxidation of the Alkenes,* New York, Oxford University Press.

CAMREDON, M., HAMILTON, J. F., ALAM, M. S., WYCHE, K. P., CARR, T., WHITE, I. R., MONKS, P. S., RICKARD, A. R. & BLOSS, W. J. (2010) Distribution of gaseous and particulate organic composition during dark alpha-pinene ozonolysis. *Atmos. Chem. Phys.,* 10**,** 2893-2917.

CANTRELL, C. A., STEDMAN, D. H. & WENDEL, G. J. (1984) MEASUREMENT OF ATMOSPHERIC PEROXY-RADICALS BY CHEMICAL AMPLIFICATION. *Analytical Chemistry,* 56**,** 1496-1502.

CARPENTER, L. J., MONKS, P. S., BANDY, B. J., PENKETT, S. A., GALBALLY, I. E. & MEYER, C. P. (1997) A study of peroxy radicals and ozone photochemistry at coastal sites in the northern and southern hemispheres. *J. Geophys. Res.,* 102**,** 25417-25427.

CHEW, A. A. & ATKINSON, R. (1996) OH radical formation yields from the gas-phase reactions of O3 with alkenes and monoterpenes. *J. Geophys. Res.,* 101**,** 28649-28653.

CLEMITSHAW, K. C., CARPENTER, L. J., PENKETT, S. A. & JENKIN, M. E. (1997) A calibrated peroxy radical chemical amplifier for ground-based tropospheric measurements. *Journal of Geophysical Research-Atmospheres,* 102**,** 25405-25416.

CLOUGH, P. N. & THRUSH, B. A. (1967) MECHANISM OF CHEMILUMINESCENT REACTION BETWEEN NITRIC OXIDE AND OZONE. *Transactions of the Faraday Society,* 63**,** 915.

CLYNE, M. A. A., WAYNE, R. P. & THRUSH, B. A. (1964) KINETICS OF CHEMILUMINESCENT REACTION BETWEEN NITRIC OXIDE + OZONE. *Transactions of the Faraday Society,* 60**,** 359.

COMMANE, R., FLOQUET, C. F. A., INGHAM, T., STONE, D., EVANS, M. J. & HEARD, D. E. (2010) Observations of OH and HO2 radicals over West Africa. *Atmospheric Chemistry and Physics,* 10**,** 8783-8801.

CREHUET, R., ANGLADA, J. M. & BOFILL, J. M. (2001) Tropospheric formation of hydroxymethyl hydroperoxide, formic acid, H2O2, and OH from carbonyl oxide in the presence of water vapor: A theoretical study of the reaction mechanism. *Chemistry-a European Journal,* 7**,** 2227-2235.

CREMER, D., KRAKA, E., MCKEE, M. L. & RADHAKRISHNAN, T. P. (1991) THE CARBONYL OXIDE-ALDEHYDE COMPLEX - A NEW INTERMEDIATE OF THE OZONOLYSIS REACTION. *Chemical Physics Letters,* 187**,** 491-493.

CRIEGEE, R. (1975) MECHANISM OF OZONOLYSIS. *Angewandte Chemie-International Edition in English,* 14**,** 745-752.

CURTIS, A. R. & SWEETENHAM, W. P. (1987) *Facsimile/Checkmat User's Manual,* Harwell Laboratory, Oxfordshire.

DEMORE, W. B. (1984) RATE-CONSTANT FOR THE OH + CO REACTION - PRESSURE-DEPENDENCE AND THE EFFECT OF OXYGEN. *International Journal of Chemical Kinetics,* 16**,** 1187-1200.

DERWENT, R. G., JENKIN, M. E., MURRELLS, T. P., PILLING, M. J. & RICKARD, A. R. (2007) A Review of the Master Chemical Mechanism. Modelling of Tropospheric Ozone AQ03508.

DERWENT, R. G., JENKIN, M. E. & SAUNDERS, S. M. (1996) Photochemical ozone creation potentials for a large number of reactive hydrocarbons under European conditions. *Atmospheric Environment,* 30**,** 181-199.

DERWENT, R. G., JENKIN, M. E., SAUNDERS, S. M. & PILLING, M. J. (1998) Photochemical ozone creation potentials for organic compounds in northwest Europe calculated with a master chemical mechanism. *Atmospheric Environment,* 32**,** 2429-2441.

DILLON, T. J. & CROWLEY, J. N. (2008) Direct detection of OH formation in the reactions of HO2 with CH3C(O)O-2 and other substituted peroxy radicals. *Atmospheric Chemistry and Physics,* 8**,** 4877-4889.

DONAHUE, N. M., DRODZ, G. T., EPSTEIN, S. A., PRESTO, A. A. & KROLL, J. H. (2011) Adventures in ozoneland: donw the rabbit-hole. *Physical Chemistry Chemical Physics,* 13**,** 10848-10857.

DONAHUE, N. M., KROLL, J. H., ANDERSON, J. G. & DEMERJIAN, K. L. (1998) Direct observation of OH production from the ozonolysis of olefins. *Geophysical Research Letters,* 25**,** 59-62.

DOUSSIN, J. F., DOMINIQUE, R. & PATRICK, C. (1999) Multiple-pass cell for very-long-path infrared spectrometry. *Applied Optics,* 38**,** 4145-4150.

DROZD, G. T., KROLL, J. H. & DONAHUE, N. M. (2011) 2-3,Dimethyl-2-butene (TME) Ozonolysis: Pressure Dependence of Stabilized Criegee Intermediates and Evidence of Stabilized Vinyl Hydroperoxides. *Journal of Physical Chemistry A***,** in press.

DUNLEA, E. J., HERNDON, S. C., NELSON, D. D., VOLKAMER, R. M., SAN MARTINI, F., SHEEHY, P. M., ZAHNISER, M. S., SHORTER, J. H., WORMHOUDT, J. C., LAMB, B. K., ALLWINE, E. J., GAFFNEY, J. S., MARLEY, N. A., GRUTTER, M., MARQUEZ, C., BLANCO, S., CARDENAS, B., RETAMA, A., VILLEGAS, C. R. R., KOLB, C. E., MOLINA, L. T. & MOLINA, M. J. (2007) Evaluation of nitrogen dioxide chemiluminescence monitors in a polluted urban environment. *Atmospheric Chemistry and Physics,* 7**,** 2691-2704.

EHHALT, D. H. (1999) Photooxidation of trace gases in the troposphere. *Physical Chemistry Chemical Physics,* 1**,** 5401-5408.

ELSHORBANY, Y. F., KURTENBACH, R., WIESEN, P., LISSI, E., RUBIO, M., VILLENA, G., GRAMSCH, E., RICKARD, A. R., PILLING, M. J. & KLEFFMANN, J. (2009) Oxidation capacity of the city air of Santiago, Chile. *Atmos. Chem. Phys.,* 9**,** 2257-2273.

EMMERSON, K. M., CARSLAW, N., CARPENTER, L. J., HEARD, D. E., LEE, J. D. & PILLING, M. J. (2005a) Urban atmospheric chemistry during the PUMA

campaign 1: Comparison of modelled OH and HO2 concentrations with measurements. *Journal of Atmospheric Chemistry,* 52**,** 143-164.

EMMERSON, K. M., CARSLAW, N., CARSLAW, D. C., LEE, J. D., MCFIGGANS, G., BLOSS, W. J., GRAVESTOCK, T., HEARD, D. E., HOPKINS, J., INGHAM, T., PILLING, M. J., SMITH, S. C., JACOB, M. & MONKS, P. S. (2007) Free radical modelling studies during the UK TORCH Campaign in Summer 2003. *Atmospheric Chemistry and Physics,* 7**,** 167-181.

EMMERSON, K. M., CARSLAW, N. & PILLING, M. J. (2005b) Urban atmospheric chemistry during the PUMA campaign 2: Radical budgets for OH, HO2 and RO2. *Journal of Atmospheric Chemistry,* 52**,** 165-183.

FARMER, D. K. & COHEN, R. C. (2008) Observations of HNO3, Sigma AN, Sigma PN and NO2 fluxes: evidence for rapid HOx chemistry within a pine forest canopy. *Atmospheric Chemistry and Physics,* 8**,** 3899-3917.

FEHSENFELD, F. C., DRUMMOND, J. W., ROYCHOWDHURY, U. K., GALVIN, P. J., WILLIAMS, E. J., BUHR, M. P., PARRISH, D. D., HUBLER, G., LANGFORD, A. O., CALVERT, J. G., RIDLEY, B. A., GRAHEK, F., HEIKES, B. G., KOK, G. L., SHETTER, J. D., WALEGA, J. G., ELSWORTH, C. M., NORTON, R. B., FAHEY, D. W., MURPHY, P. C., HOVERMALE, C., MOHNEN, V. A., DEMERJIAN, K. L., MACKAY, G. I. & SCHIFF, H. I. (1990) INTERCOMPARISON OF NO2 MEASUREMENT TECHNIQUES. *Journal of Geophysical Research-Atmospheres,* 95**,** 3579-3597.

FENSKE, J. D., HASSON, A. S., HO, A. W. & PAULSON, S. E. (2000a) Measurement of absolute unimolecular and bimolecular rate constants for

CH3CHOO generated by the trans-2-butene reaction with ozone in the gas phase. *Journal of Physical Chemistry A,* 104**,** 9921-9932.

FENSKE, J. D., HASSON, A. S., PAULSON, S. E., KUWATA, K. T., HO, A. & HOUK, K. N. (2000b) The pressure dependence of the OH radical yield from ozone-alkene reactions. *Journal of Physical Chemistry A,* 104**,** 7821-7833.

FINLAYSON, B. J., PITTS, J. N. & ATKINSON, R. (1974) LOW-PRESSURE GAS-PHASE OZONE-OLEFIN REACTIONS - CHEMILUMINESCENCE, KINETICS, AND MECHANISMS. *Journal of the American Chemical Society,* 96**,** 5356-5367.

FLEMING, Z. L., MONKS, P. S., RICKARD, A. R., HEARD, D. E., BLOSS, W. J., SEAKINS, P. W., STILL, T. J., SOMMARIVA, R., PILLING, M. J., MORGAN, R., GREEN, T. J., BROUGH, N., MILLS, G. P., PENKETT, S. A., LEWIS, A. C., LEE, J. D., SAIZ-LOPEZ, A. & PLANE, J. M. C. (2006) Peroxy radical chemistry and the control of ozone photochemistry at Mace Head, Ireland during the summer of 2002. *Atmospheric Chemistry and Physics,* 6**,** 2193-2214.

FONTIJN, A. (1985) *Gas-Phase Chemiluminescence and Chemi-Ionization*, Elsevier Science

FONTIJN, A., SABADELL, A. J. & RONCO, R. J. (1970) HOMOGENEOUS CHEMILUMINESCENT MEASUREMENT OF NITRIC OXIDE WITH OZONE - IMPLICATIONS FOR CONTINUOUS SELECTIVE MONITORING OF GASEOUS AIR POLLUTANTS. *Analytical Chemistry,* 42**,** 575.

FUCHS, H., BOHN, B., HOFZUMAHAUS, A., HOLLAND, F., LU, K. D., NEHR, S., ROHRER, F. & WAHNER, A. (2011) Detection of HO2 by laser-induced

fluorescence: calibration and interferences from RO2 radicals. *Atmos. Meas. Tech. Discuss.,* 4**,** 1255-1302.

FUCHS, H., BRAUERS, T., DORN, H. P., HARDER, H., HASELER, R., HOFZUMAHAUS, A., HOLLAND, F., KANAYA, Y., KAJII, Y., KUBISTIN, D., LOU, S., MARTINEZ, M., MIYAMOTO, K., NISHIDA, S., RUDOLF, M., SCHLOSSER, E., WAHNER, A., YOSHINO, A. & SCHURATH, U. (2010) Technical Note: Formal blind intercomparison of HO2 measurements in the atmosphere simulation chamber SAPHIR during the HOxComp campaign. *Atmos. Chem. Phys. Discuss.,* 10**,** 21189-21235.

GARCIA-CAMPANA, A. M. & BAEYENS, W. R. G. (2001) *Chemiluminescence in Analytical Chemistry*, Taylor & Francis Inc.

GERBOLES, M., LAGLER, F., REMBGES, D. & BRUN, C. (2003) Assessment of uncertainty of NO2 measurements by the chemiluminescence method and discussion of the quality objective of the NO2 European Directive. *Journal of Environmental Monitoring,* 5**,** 529-540.

GLINSKI, R. J., GETTY, J. N. & BIRKS, J. W. (1985) PHOSPHORESCENCE SPECTRA OF THIOFORMALDEHYDE AND THIOFORMALDEHYDE-D2 BY CHEMI-LUMINESCENCE - IDENTIFICATION OF THE 4(1)1 BAND. *Chemical Physics Letters,* 117**,** 359-364.

GOLDSTEIN, A. H., MCKAY, M., KURPIUS, M. R., SCHADE, G. W., LEE, A., HOLZINGER, R. & RASMUSSEN, R. A. (2004) Forest thinning experiment confirms ozone deposition to forest canopy is dominated by reaction with biogenic VOCs. *Geophysical Research Letters,* 31.

GREEN, T. J., REEVES, C. E., FLEMING, Z. L., BROUGH, N., RICKARD, A. R., BANDY, B. J., MONKS, P. S. & PENKETT, S. A. (2006) An improved dual

channel PERCA instrument for atmospheric measurements of peroxy radicals. *Journal of Environmental Monitoring,* 8**,** 530-536.

GREENE, C. R. & ATKINSON, R. (1992) RATE CONSTANTS FOR THE GAS-PHASE REACTIONS OF O3 WITH A SERIES OF ALKENES AT 296-K+/-2-K. *International Journal of Chemical Kinetics,* 24**,** 803-811.

GREGORY, G. L., HUDGINS, C. H. & EDAHL, R. A. (1983) LABORATORY EVALUATION OF AN AIRBORNE OZONE INSTRUMENT THAT COMPENSATES FOR ALTITUDE SENSITIVITY EFFECTS - REPLY. *Environmental Science & Technology,* 17**,** 562-564.

GROSJEAN, D. & HARRISON, J. (1985) RESPONSE OF CHEMI-LUMINESCENCE NOX ANALYZERS AND ULTRAVIOLET OZONE ANALYZERS TO ORGANIC AIR-POLLUTANTS. *Environmental Science & Technology,* 19**,** 862-865.

GROSJEAN, E., DEANDRADE, J. B. & GROSJEAN, D. (1996) Carbonyl products of the gas-phase reaction of ozone with simple alkenes. *Environmental Science & Technology,* 30**,** 975-983.

GROSJEAN, E. & GROSJEAN, D. (1995) RATE CONSTANTS FOR THE GAS-PHASE REACTION OF C-5-C-10 ALKENES WITH OZONE. *International Journal of Chemical Kinetics,* 27**,** 1045-1054.

GROSJEAN, E. & GROSJEAN, D. (1996a) Carbonyl products of the gas-phase reaction of ozone with 1-alkenes. *Atmospheric Environment,* 30**,** 4107-4113.

GROSJEAN, E. & GROSJEAN, D. (1996b) Carbonyl products of the gas phase reaction of ozone with symmetrical alkenes. *Environmental Science & Technology,* 30**,** 2036-2044.

GUTBROD, R., KRAKA, E., SCHINDLER, R. N. & CREMER, D. (1997a) Kinetic and theoretical investigation of the gas-phase ozonolysis of isoprene: Carbonyl oxides as an important source for OH radicals in the atmosphere. *Journal of the American Chemical Society,* 119**,** 7330-7342.

GUTBROD, R., MEYER, S., RAHMAN, M. M. & SCHINDLER, R. N. (1997b) On the use of CO as scavenger for OH radicals in the ozonolysis of simple alkenes and isoprene. *International Journal of Chemical Kinetics,* 29**,** 717-723.

GUTBROD, R., SCHINDLER, R. N., KRAKA, E. & CREMER, D. (1996) Formation of OH radicals in the gas phase ozonolysis of alkenes, the unexpected role of carbonyl oxides. *Chemical Physics Letters,* 252**,** 221-229.

HARD, T. M., O'BRIEN, R. J., CHAN, C. Y. & MEHRABZADEH, A. A. (1984) Tropospheric free radical determination by fluorescence assay with gas expansion. *Environmental Science & Technology,* 18**,** 768-777.

HARRISON, R. M., YIN, J., TILLING, R. M., CAI, X., SEAKINS, P. W., HOPKINS, J. R., LANSLEY, D. L., LEWIS, A. C., HUNTER, M. C., HEARD, D. E., CARPENTER, L. J., CREASY, D. J., LEE, J. D., PILLING, M. J., CARSLAW, N., EMMERSON, K. M., REDINGTON, A., DERWENT, R. G., RYALL, D., MILLS, G. & PENKETT, S. A. (2006) Measurement and modelling of air pollution and atmospheric chemistry in the UK West Midlands conurbation: Overview of the PUMA Consortium project. *Science of the Total Environment,* 360**,** 5-25.

HASSON, A. S., CHUNG, M. Y., KUWATA, K. T., CONVERSE, A. D., KROHN, D. & PAULSON, S. E. (2003) Reaction of Criegee intermediates with water vapor - An additional source of OH radicals in alkene ozonolysis? *Journal of Physical Chemistry A,* 107**,** 6176-6182.

HASSON, A. S., HO, A. W., KUWATA, K. T. & PAULSON, S. E. (2001a) Production of stabilized Criegee intermediates and peroxides in the gas phase ozonolysis of alkenes 2. Asymmetric and biogenic alkenes. *Journal of Geophysical Research-Atmospheres,* 106**,** 34143-34153.

HASSON, A. S., ORZECHOWSKA, G. & PAULSON, S. E. (2001b) Production of stabilized Criegee intermediates and peroxides in the gas phase ozonolysis of alkenes 1. Ethene, trans-2-butene, and 2,3-dimethyl-2-butene. *Journal of Geophysical Research-Atmospheres,* 106**,** 34131-34142.

HASSON, A. S., TYNDALL, G. S. & ORLANDO, J. J. (2004) A product yield study of the reaction of HO2 radicals with ethyl peroxy (C2H5O2), acetyl peroxy (CH3C(O)O-2), and acetonyl peroxy (CH3C(O)CH2O2) radicals. *Journal of Physical Chemistry A,* 108**,** 5979-5989.

HATAKEYAMA, S. & AKIMOTO, H. (1994) REACTIONS OF CRIEGEE INTERMEDIATES IN THE GAS-PHASE. *Research on Chemical Intermediates,* 20**,** 503-524.

HATAKEYAMA, S., KOBAYASHI, H. & AKIMOTO, H. (1984) Gas-Phase Oxidation of $SO_2$ in the Ozone-Olefin Reactions. *The Journal of Physical Chemistry,* 88**,** 4736.

HATAKEYAMA, S., KOBAYASHI, H., LIN, Z. Y., TAKAGI, H. & AKIMOTO, H. (1986) Mechanism for the Reaction of $CH_2OO$ with $SO_2$. *The Journal of Physical Chemistry,* 90**,** 4131.

HEARD, D. E. (2006) *Analytical Techniques for Atmospheric Measurement*, Blackwell Publishing Ltd.

HEARD, D. E., CARPENTER, L. J., CREASEY, D. J., HOPKINS, J. R., LEE, J. D., LEWIS, A. C., PILLING, M. J., SEAKINS, P. W., CARSLAW, N. &

EMMERSON, K. M. (2004) High levels of the hydroxyl radical in the winter urban troposphere. *Geophysical Research Letters,* 31.

HEARD, D. E. & PILLING, M. J. (2003) Measurement of OH and HO2 in the troposphere. *Chemical Reviews,* 103**,** 5163-5198.

HELLPOINTNER, E. & GAB, S. (1989) DETECTION OF METHYL, HYDROXYMETHYL AND HYDROXYETHYL HYDROPEROXIDES IN AIR AND PRECIPITATION. *Nature,* 337**,** 631-634.

HERRON, J. T. & HUIE, R. E. (1977) STOPPED-FLOW STUDIES OF MECHANISMS OF OZONE-ALKENE REACTIONS IN GAS-PHASE - ETHYLENE. *Journal of the American Chemical Society,* 99**,** 5430-5435.

HILLS, A. J. & ZIMMERMAN, P. R. (1990) ISOPRENE MEASUREMENT BY OZONE-INDUCED CHEMILUMINESCENCE. *Analytical Chemistry,* 62**,** 1055-1060.

HOLLAND, F., HOFZUMAHAUS, A., SCHAFER, R., KRAUS, A. & PATZ, H. W. (2003) Measurements of OH and HO2 radical concentrations and photolysis frequencies during BERLIOZ. *Journal of Geophysical Research-Atmospheres,* 108.

HORIE, O. & MOORTGAT, G. K. (1991) DECOMPOSITION PATHWAYS OF THE EXCITED CRIEGEE INTERMEDIATES IN THE OZONOLYSIS OF SIMPLE ALKENES. *Atmospheric Environment Part a-General Topics,* 25**,** 1881-1896.

HORIE, O., NEEB, P. & MOORTGAT, G. K. (1994) OZONOLYSIS OF TRANS-2-BUTENES AND CIS-2-BUTENES IN LOW PARTS-PER-MILLION CONCENTRATION RANGES. *International Journal of Chemical Kinetics,* 26**,** 1075-1094.

HORIE, O., NEEB, P. & MOORTGAT, G. K. (1997) The reactions of the Criegee intermediate CH3CHOO in the gas-phase ozonolysis of 2-butene isomers. *International Journal of Chemical Kinetics,* 29**,** 461-468.

HORIE, O., SCHAFER, C. & MOORTGAT, G. K. (1999) High reactivity of hexafluoro acetone toward Criegee intermediates in the gas-phase ozonolysis of simple alkenes. *International Journal of Chemical Kinetics,* 31**,** 261-269.

HOUGH, A. M. (1988) The calculation of photolysis rates for use in global tropospheric modelling studies. AERE Rep. R-13259.

HTTP://WWW.IUPAC-KINETIC.CH.CAM.AC.UK/ (2006) IUPAC Subcommittee on Gas Kinetic Data Evaluation.

HTTP://WWW.IUPAC-KINETIC.CH.CAM.AC.UK/ (2007) IUPAC Subcommittee on Gas Kinetic Data Evaluation.

HTTP://WWW.IUPAC-KINETIC.CH.CAM.AC.UK/ (2009) IUPAC Subcommittee on Gas Kinetic Data Evaluation.

JACOB, D. J. (1999) *Introduction to Atmospheric Chemistry*, Princeton University Press.

JENKIN, M. E., HAYMAN, G. D., WALLINGTON, T. J., HURLEY, M. D., BALL, J. C., NIELSEN, O. J. & ELLERMANN, T. (1993) KINETIC AND MECHANISTIC STUDY OF THE SELF-REACTION OF CH3OCH2O2 RADICALS AT ROOM-TEMPERATURE. *Journal of Physical Chemistry,* 97**,** 11712-11723.

JENKIN, M. E., HURLEY, M. D. & WALLINGTON, T. J. (2007) Investigation of the radical product channel of the CH3C(O)O-2+HO2 reaction in the gas phase. *Physical Chemistry Chemical Physics,* 9**,** 3149-3162.

JENKIN, M. E., HURLEY, M. D. & WALLINGTON, T. J. (2008) Investigation of the radical product channel of the CH3C(O) CH2O2+HO2 reaction in the gas phase. *Physical Chemistry Chemical Physics,* 10**,** 4274-4280.

JENKIN, M. E., SAUNDERS, S. M. & PILLING, M. J. (1997) The tropospheric degradation of volatile organic compounds: A protocol for mechanism development. *Atmospheric Environment,* 31**,** 81-104.

JOHNSON, D., LEWIN, A. G. & MARSTON, G. (2001) The effect of Criegee-intermediate scavengers on the OH yield from the reaction of ozone with 2-methylbut-2-ene. *Journal of Physical Chemistry A,* 105**,** 2933-2935.

JOHNSON, D. & MARSTON, G. (2008) The gas-phase ozonolysis of unsaturated volatile organic compounds in the troposphere. *Chemical Society Reviews,* 37**,** 699-716.

JOHNSON, D., RICKARD, A. R., MCGILL, C. D. & MARSTON, G. (2000) The influence of orbital asymmetry on the kinetics of the gas-phase reactions of ozone with unsaturated compounds. *Physical Chemistry Chemical Physics,* 2**,** 323-328.

JOSEPH, D. W. & SPICER, C. W. (1978) CHEMILUMINESCENCE METHOD FOR ATMOSPHERIC MONITORING OF NITRIC-ACID AND NITROGEN-OXIDES. *Analytical Chemistry,* 50**,** 1400-1403.

JOSHI, S. B. & BUFALINI, J. J. (1978) HALOCARBON INTERFERENCES IN CHEMILUMINESCENT MEASUREMENTS OF NOX. *Environmental Science & Technology,* 12**,** 597-599.

KAN, C. S., SU, F., CALVERT, J. G. & SHAW, J. H. (1981) Mechanism of the Ozone-Ethene Reaction in Dilute $N_2/O_2$ Mixtures Near 1-atm Pressure. *The Journal of Physical Chemistry,* 85**,** 2359.

KANAYA, Y., SADANAGA, Y., HIROKAWA, J., KAJII, Y. & AKIMOTO, H. (2001) Development of a ground-based LIF instrument for measuring HOx radicals: Instrumentation and calibrations. *Journal of Atmospheric Chemistry,* 38**,** 73-110.

KELLY, T. J., STEDMAN, D. H., RITTER, J. A. & HARVEY, R. B. (1980) Measurements of Oxides of Nitrogen and Nitric Acid in Clean Air. *J. Geophys. Res.,* 85.

KLEINDIENST, T. E., HUDGENS, E. E., SMITH, D. F., MCELROY, F. F. & BUFALINI, J. J. (1993) Comparison of chemiluminescence and ultraviolet ozone monitor responses in the presence of humidity and photochemical pollutants. *Air and Waste,* 43**,** 213-222.

KLEY, D., DRUMMOND, J. W., MCFARLAND, M. & LIU, S. C. (1981) Tropospheric Profiles of NOx. *J. Geophys. Res.,* 86.

KLEY, D. & MCFARLAND, M. (1980) Chemiluminescence Detector for NO and $NO_2$. *Atmospheric Technology,* 12**,** 63-69.

KROLL, J. H., CLARKE, J. S., DONAHUE, N. M., ANDERSON, J. G. & DEMERJIAN, K. L. (2001a) Mechanism of HOx formation in the gas-phase ozone-alkene reaction. 1. Direct, pressure-dependent measurements of prompt OH yields. *Journal of Physical Chemistry A,* 105**,** 1554-1560.

KROLL, J. H., DONAHUE, N. M., CEE, V. J., DEMERJIAN, K. L. & ANDERSON, J. G. (2002) Gas-phase ozonolysis of alkenes: Formation of OH from anti carbonyl oxides. *Journal of the American Chemical Society,* 124**,** 8518-8519.

KROLL, J. H., HANISCO, T. F., DONAHUE, N. M., DEMERJIAN, K. L. & ANDERSON, J. G. (2001b) Accurate, direct measurements of OH yields from

gas-phase ozone-alkene reactions using an in situ LIF instrument. *Geophysical Research Letters,* 28**,** 3863-3866.

KROLL, J. H., SAHAY, S. R., ANDERSON, J. G., DEMERJIAN, K. L. & DONAHUE, N. M. (2001c) Mechanism of HOx formation in the gas-phase ozone-alkene reaction. 2. Prompt versus thermal dissociation of carbonyl oxides to form OH. *Journal of Physical Chemistry A,* 105**,** 4446-4457.

KROLL, J. H. & SEINFELD, J. H. (2008) Chemistry of secondary organic aerosol: Formation and evolution of low-volatility organics in the atmosphere. *Atmospheric Environment,* 42**,** 3593-3624.

KUHNE, H., VACCANI, S., HA, T. K., BAUDER, A. & GUNTHARD, H. H. (1976) INFRARED-MATRIX AND MICROWAVE SPECTROSCOPY OF ETHYLENE-OZONE GAS-PHASE REACTION. *Chemical Physics Letters,* 38**,** 449-455.

KUMMER, W. A., PITTS, J. N. & STEER, R. P. (1971) CHEMILUMINESCENT REACTIONS OF OZONE WITH OLEFINS AND SULFIDES. *Environmental Science & Technology,* 5**,** 1045-&.

KURTENBACH, R., BECKER, K. H., GOMES, J. A. G., KLEFFMANN, J., LORZER, J. C., SPITTLER, M., WIESEN, P., ACKERMANN, R., GEYER, A. & PLATT, U. (2001) Investigations of emissions and heterogeneous formation of HONO in a road traffic tunnel. *Atmospheric Environment,* 35**,** 3385-3394.

KUWATA, K. T., HASSON, A. S., DICKINSON, R. V., PETERSEN, E. B. & VALIN, L. C. (2005) Quantum chemical and master equation simulations of the oxidation and isomerization of vinoxy radicals. *Journal of Physical Chemistry A,* 109**,** 2514-2524.

KUWATA, K. T., HERMES, M. R., CARLSON, M. J. & ZOGG, C. K. (2010) Computational Studies of the Isomerization and Hydration Reactions of Acetaldehyde Oxide and Methyl Vinyl Carbonyl Oxide. *Journal of Physical Chemistry A,* 114**,** 9192-9204.

LEE, J. D., LEWIS, A. C., MONKS, P. S., JACOB, M., HAMILTON, J. F., HOPKINS, J. R., WATSON, N. M., SAXTON, J. E., ENNIS, C., CARPENTER, L. J., CARSLAW, N., FLEMING, Z., BANDY, B. J., ORAM, D. E., PENKETT, S. A., SLEMR, J., NORTON, E., RICKARD, A. R., WHALLEY, L. K., HEARD, D. E., BLOSS, W. J., GRAVESTOCK, T., SMITH, S. C., STANTON, J., PILLING, M. J. & JENKIN, M. E. (2006) Ozone photochemistry and elevated isoprene during the UK heatwave of August 2003. *Atmospheric Environment,* 40**,** 7598-7613.

LI, Y. M. & FRANCISCO, J. S. (2000) High level ab initio studies on the excited states of HOCO radical. *Journal of Chemical Physics,* 113**,** 7963-7970.

LIPPMANN, H. H., JESSER, B. & SCHURATH, U. (1980) THE RATE-CONSTANT OF NO+O3-]NO2+O2 IN THE TEMPERATURE-RANGE OF 283-443 K. *International Journal of Chemical Kinetics,* 12**,** 547-554.

MA, Y. & MARSTON, G. (2009) Formation of organic acids from the gas-phase ozonolysis of terpinolene. *Physical Chemistry Chemical Physics,* 11**,** 4198-4209.

MALKIN, T. L., GODDARD, A., HEARD, D. E. & SEAKINS, P. W. (2010) Measurements of OH and HO2 yields from the gas phase ozonolysis of isoprene. *Atmospheric Chemistry and Physics,* 10**,** 1441-1459.

MARLEY, N. A., GAFFNEY, J. S. & CUNNINGHAM, M. M. (1998) Ozone chemiluminescent detection of olefins: Potential applications for real-time

measurements of natural hydrocarbon emissions. *10th Joint Conference on the Applications of Air Pollution Meteorology with the a&Wma*, J42-J44.

MARTINEZ-AVILA, M., PEIRO-GARCIA, J., RAMIREZ-RAMIREZ, V. M. & NEBOT-GIL, I. (2003) Ab initio study on the mechanism of the HCO+O-2 -> HO2+CO reaction. *Chemical Physics Letters,* 370**,** 313-318.

MATTHEWS, R. D., SAWYER, R. F. & SCHEFER, R. W. (1977) INTERFERENCES IN CHEMILUMINESCENT MEASUREMENT OF NO AND NO2 EMISSIONS FROM COMBUSTION SYSTEMS. *Environmental Science & Technology,* 11**,** 1092-1096.

MCGILL, C. D., RICKARD, A. R., JOHNSON, D. & MARSTON, G. (1999) Product yields in the reactions of ozone with Z-but-2-ene, E-but-2-ene and 2-methylbut-2-ene. *Chemosphere,* 38**,** 1205-1212.

MEHRABZADEH, A. A., OBRIEN, R. J. & HARD, T. M. (1983) OPTIMIZATION OF RESPONSE OF CHEMI-LUMINESCENCE ANALYZERS. *Analytical Chemistry,* 55**,** 1660-1665.

MEYER, C. P., ELSWORTH, C. M. & GALBALLY, I. E. (1991) WATER-VAPOR INTERFERENCE IN THE MEASUREMENT OF OZONE IN AMBIENT AIR BY ULTRAVIOLET-ABSORPTION. *Review of Scientific Instruments,* 62**,** 223-228.

MICHAEL, J. V., ALLEN, J. E. & BROBST, W. D. (1981) TEMPERATURE-DEPENDENCE OF THE NO+O3 REACTION-RATE FROM 195-DEGREES-K TO 369-DEGREES-K. *Journal of Physical Chemistry,* 85**,** 4109-4117.

MIHELCIC, D., HEITLINGER, M., KLEY, D., MUSGEN, P. & VOLZ-THOMAS, A. (1999) Formation of hydroxyl and hydroperoxy radicals in the gas-phase ozonolysis of ethene. *Chemical Physics Letters,* 301**,** 559-564.

MIYOSHI, A., MATSUI, H. & WASHIDA, N. (1994) DETECTION AND REACTIONS OF THE HOCO RADICAL IN GAS-PHASE. *Journal of Chemical Physics,* 100**,** 3532-3539.

NASA-JPL (2006) Chemical Kinetics and Photochemical Data for use in Atmospheric Studies. *National Aeronautics & Space Administration and Jet Propulsion Laboratory, 15th Data Evaluation*.

NAVAS, M. J., JIMENEZ, A. M. & GALAN, G. (1997) Air analysis: Determination of nitrogen compounds by chemiluminescence. *Atmospheric Environment,* 31**,** 3603-3608.

NEEB, P., HORIE, O. & MOORTGAT, G. K. (1995) THE NATURE OF THE TRANSITORY PRODUCT IN THE GAS-PHASE OZONOLYSIS OF ETHENE. *Chemical Physics Letters,* 246**,** 150-156.

NEEB, P., HORIE, O. & MOORTGAT, G. K. (1996) Gas-phase ozonolysis of ethene in the presence of hydroxylic compounds. *International Journal of Chemical Kinetics,* 28**,** 721-730.

NEEB, P., HORIE, O. & MOORTGAT, G. K. (1998) The ethene-ozone reaction in the gas phase. *Journal of Physical Chemistry A,* 102**,** 6778-6785.

NEEB, P. & MOORTGAT, G. K. (1999) Formation of OH radicals in the gas-phase reaction of propene, isobutene, and isoprene with O-3: Yields and mechanistic implications. *Journal of Physical Chemistry A,* 103**,** 9003-9012.

NGUYEN, T. L., PEETERS, J. & VEREECKEN, L. (2009a) Theoretical study of the gas-phase ozonolysis of beta-pinene (C10H16). *Physical Chemistry Chemical Physics,* 11**,** 5643-5656.

NGUYEN, T. L., WINTERHALTER, R., MOORTGAT, G., KANAWATI, B., PEETERS, J. & VEREECKEN, L. (2009b) The gas-phase ozonolysis of beta-caryophyllene (C(15)H(24)). Part II: A theoretical study. *Phys Chem Chem Phys,* 11**,** 4173-83.

NIKI, H., MAKER, P. D., SAVAGE, C. M. & BREITENBACH, L. P. (1981) A FTIR Study of a Transitory Product in the Gas-Phase Ozone-Ethylene Reaction. *The Journal of Physical Chemistry,* 85**,** 1024.

NIKI, H., MAKER, P. D., SAVAGE, C. M., BREITENBACH, L. P. & HURLEY, M. D. (1987) FTIR SPECTROSCOPIC STUDY OF THE MECHANISM FOR THE GAS-PHASE REACTION BETWEEN OZONE AND TETRAMETHYLETHYLENE. *Journal of Physical Chemistry,* 91**,** 941-946.

OLZMANN, M., KRAKA, E., CREMER, D., GUTBROD, R. & ANDERSSON, S. (1997) Energetics, kinetics, and product distributions of the reactions of ozone with ethene and 2,3-dimethyl-2-butene. *Journal of Physical Chemistry A,* 101**,** 9421-9429.

ORLANDO, J. J., IRACI, L. T. & TYNDALL, G. S. (2000) Chemistry of the cyclopentoxy and cyclohexoxy radicals at subambient temperatures. *Journal of Physical Chemistry A,* 104**,** 5072-5079.

ORLANDO, J. J., TYNDALL, G. S. & WALLINGTON, T. J. (2003) The atmospheric chemistry of alkoxy radicals. *Chemical Reviews,* 103**,** 4657-4689.

ORZECHOWSKA, G. E. & PAULSON, S. E. (2002) Production of OH radicals from the reactions of C-4-C-6 internal alkenes and styrenes with ozone in the gas phase. *Atmospheric Environment,* 36**,** 571-581.

PAULSON, S. E., CHUNG, M. Y. & HASSON, A. S. (1999a) OH radical formation from the gas-phase reaction of ozone with terminal alkenes and the relationship between structure and mechanism. *Journal of Physical Chemistry A,* 103**,** 8125-8138.

PAULSON, S. E., FENSKE, J. D., SEN, A. D. & CALLAHAN, T. W. (1999b) A novel small-ratio relative-rate technique for measuring OH formation yields from the reactions of O-3 with alkenes in the gas phase, and its application to the reactions of ethene and propene. *Journal of Physical Chemistry A,* 103**,** 2050-2059.

PAULSON, S. E. & ORLANDO, J. J. (1996) The reactions of ozone with alkenes: An important source of HOx in the boundary layer. *Geophysical Research Letters,* 23**,** 3727-3730.

PITTS, J. N., KUMMER, W. A., STEER, R. P. & FINLAYSO.BJ (1972) CHEMILUMINESCENT REACTIONS OF OZONE WITH OLEFINS AND ORGANIC SULFIDES. *Advances in Chemistry Series***,** 246-254.

PLATZ, J., SEHESTED, J., NIELSEN, O. J. & WALLINGTON, T. J. (1999) Atmospheric chemistry of cyclohexane: UV spectra of c-C6H11 center dot and (c-C6H11)O-2(center dot) radicals, kinetics of the reactions of (c-C6H11)O-2(center dot) radicals with NO and NO2, and the fate of the alkoxy radical (c-C6H11)O-center dot. *Journal of Physical Chemistry A,* 103**,** 2688-2695.

PUGH, T., RYDER, J., MACKENZIE, A., MOLLER, S., LEE, J., HELFTER, C., NEMITZ, E., LOWE, D. & HEWITT, C. (2011) Modelling chemistry in the nocturnal boundary layer above tropical rainforest and a generalised effective nocturnal ozone deposition velocity for sub-ppbv NOx conditions. *Journal of Atmospheric Chemistry*, 1-22.

QI, B., SATO, K., IMARNURA, T., TAKAMI, A., HATAKEYAMA, S. & MA, Y. (2006) Production of the radicals in the ozonolysis of ethene: A chamber study by FT-IR and PERCA. *Chemical Physics Letters,* 427**,** 461-465.

QI, B., YANG, B., WANG, Z. Q., YANG, H. Y. & LIU, L. (2009) Production of radicals in the ozonolysis of propene in air. *Science in China Series B-Chemistry,* 52**,** 356-361.

RATHMAN, W. C. D., CLAXTON, T. A., RICKARD, A. R. & MARSTON, G. (1999) A theoretical investigation of OH formation in the gas-phase ozonolysis of E-but-2-ene and Z-but-2-ene. *Physical Chemistry Chemical Physics,* 1**,** 3981-3985.

RAVISHANKARA, A. R., HANCOCK, G., KAWASAKI, M. & MATSUMI, Y. (1998) Photochemistry of Ozone: Surprises and Recent Lessons. *Science,* 280**,** 60-61.

RAY, G. W. & WATSON, R. T. (2002) Kinetics of the reaction nitric oxide + ozone .fwdarw. nitrogen dioxide + oxygen from 212 to 422 K. *The Journal of Physical Chemistry,* 85**,** 1673-1676.

REN, X. R., HARDER, H., MARTINEZ, M., FALOONA, I. C., TAN, D., LESHER, R. L., DI CARLO, P., SIMPAS, J. B. & BRUNE, W. H. (2004) Interference testing for atmospheric HOx measurements by laser-induced fluorescence. *Journal of Atmospheric Chemistry,* 47**,** 169-190.

RICKARD, A. R., JOHNSON, D., MCGILL, C. D. & MARSTON, G. (1999) OH yields in the gas-phase reactions of ozone with alkenes. *Journal of Physical Chemistry A,* 103**,** 7656-7664.

ROWLEY, D. M., LESCLAUX, R., LIGHTFOOT, P. D., NOZIERE, B., WALLINGTON, T. J. & HURLEY, M. D. (1992) KINETIC AND MECHANISTIC STUDIES OF THE REACTIONS OF CYCLOPENTYLPEROXY AND CYCLOHEXYLPEROXY RADICALS WITH HO2. *Journal of Physical Chemistry,* 96**,** 4889-4894.

ROWLEY, D. M., LIGHTFOOT, P. D., LESCLAUX, R. & WALLINGTON, T. J. (1991) UV ABSORPTION-SPECTRUM AND SELF-REACTION OF CYCLOHEXYLPEROXY RADICALS. *Journal of the Chemical Society-Faraday Transactions,* 87**,** 3221-3226.

RYERSON, T. B., TRAINER, M., ANGEVINE, W. M., BROCK, C. A., DISSLY, R. W., FEHSENFELD, F. C., FROST, G. J., GOLDAN, P. D., HOLLOWAY, J. S., HUBLER, G., JAKOUBEK, R. O., KUSTER, W. C., NEUMAN, J. A., NICKS, D. K., PARRISH, D. D., ROBERTS, J. M. & SUEPER, D. T. (2003) Effect of petrochemical industrial emissions of reactive alkenes and NOx on tropospheric ozone formation in Houston, Texas. *Journal of Geophysical Research-Atmospheres,* 108.

RYERSON, T. B., WILLIAMS, E. J. & FEHSENFELD, F. C. (2000) An efficient photolysis system for fast-response NO2 measurements. *J. Geophys. Res.,* 105.

SALISBURY, G., MONKS, P. S., BAUGUITTE, S., BANDY, B. J. & PENKETT, S. A. (2002) A seasonal comparison of the ozone photochemistry in clean and

polluted air masses at Mace Head, Ireland. *Journal of Atmospheric Chemistry,* 41**,** 163-187.

SAUER, F., SCHAFER, C., NEEB, P., HORIE, O. & MOORTGAT, G. K. (1999) Formation of hydrogen peroxide in the ozonolysis of isoprene and simple alkenes under humid conditions. *Atmospheric Environment,* 33**,** 229-241.

SAUNDERS, S. M., JENKIN, M. E., DERWENT, R. G. & PILLING, M. J. (1997) World Wide Web site of a Master Chemical Mechanism (MCM) for use in tropospheric chemistry models. *Atmospheric Environment,* 31**,** 1249-1249.

SAUNDERS, S. M., JENKIN, M. E., DERWENT, R. G. & PILLING, M. J. (2003) Protocol for the development of the Master Chemical Mechanism, MCM v3 (Part A): tropospheric degradation of non-aromatic volatile organic compounds. *Atmospheric Chemistry and Physics,* 3**,** 161-180.

SCHAFER, C., HORIE, O., CROWLEY, J. N. & MOORTGAT, G. K. (1997) Is the hydroxyl radical formed in the gas-phase ozonolysis of alkenes? *Geophysical Research Letters,* 24**,** 1611-1614.

SCHURATH, U., LIPPMANN, H. H. & JESSER, B. (1981) TEMPERATURE-DEPENDENCE OF THE CHEMI-LUMINESCENT REACTION (1), NO+O3-]NO2(2A1-2B1,2)+O2, AND QUENCHING OF THE EXCITED PRODUCT. *Berichte Der Bunsen-Gesellschaft-Physical Chemistry Chemical Physics,* 85**,** 807-813.

SEARS, T. J., FAWZY, W. M. & JOHNSON, P. M. (1992) TRANSIENT DIODE-LASER ABSORPTION-SPECTROSCOPY OF THE NU-2 FUNDAMENTAL OF TRANS-HOCO AND DOCO. *Journal of Chemical Physics,* 97**,** 3996-4007.

SIESE, M., BECKER, K. H., BROCKMANN, K. J., GEIGER, H., HOFZUMAHAUS, A., HOLLAND, F., MIHELCIC, D. & WIRTZ, K. (2001) Direct measurement of OH radicals from ozonolysis of selected alkenes: A EUPHORE simulation chamber study. *Environmental Science & Technology,* 35**,** 4660-4667.

SIGSBY, J. E., BLACK, F. M., BELLAR, T. A. & KLOSTERM.DL (1973) CHEMILUMINESCENT METHOD FOR ANALYSIS OF NITROGEN-COMPOUNDS IN MOBILE SOURCE EMISSIONS (NO, NO2, AND NH3). *Environmental Science & Technology,* 7**,** 51-54.

SMITH, S. C., LEE, J. D., BLOSS, W. J., JOHNSON, G. P., INGHAM, T. & HEARD, D. E. (2006) Concentrations of OH and HO2 radicals during NAMBLEX: measurements and steady state analysis. *Atmospheric Chemistry and Physics,* 6**,** 1435-1453.

STEDMAN, D. H., DABY, E. E., STUHL, F. & NIKI, H. (1972) Analysis of ozone and nitric oxide by a chemiluminescent method in laboratory and atmospheric studies of photochemical smog. *Journal of Air Pollution Control Association,* 22**,** 260-263.

STEFFENSON. D. M & STEDMAN, D. H. (1974) OPTIMIZATION OF OPERATING PARAMETERS OF CHEMILUMINESCENT NITRIC-OXIDE DETECTORS. *Analytical Chemistry,* 46**,** 1704-1709.

STEINBACHER, M., ZELLWEGER, C., SCHWARZENBACH, B., BUGMANN, S., BUCHMANN, B., ORDONEZ, C., PREVOT, A. S. H. & HUEGLIN, C. (2007) Nitrogen oxide measurements at rural sites in Switzerland: Bias of conventional measurement techniques. *Journal of Geophysical Research-Atmospheres,* 112.

SU, F., CALVERT, J. G. & SHAW, J. H. (1980) FT IR SPECTROSCOPIC STUDY OF THE OZONE ETHENE REACTION-MECHANISM IN O2-RICH MIXTURES. *Journal of Physical Chemistry,* 84**,** 239-246.

TAATJES, C. A., MELONI, G., SELBY, T. M., TREVITT, A. J., OSBORN, D. L., PERCIVAL, C. J. & SHALLCROSS, D. E. (2008) Direct observation of the gas-phase Criegee intermediate (CH2OO). *Journal of the American Chemical Society,* 130**,** 11883-11885.

THOMAS, W., ZABEL, F., BECKER, K. H. & FINK, E. H. (1993) A mechanistic study on the ozonolysis of ethene. *Proceedings of the 1st European Symposium on Physico-Chemical Behaviour of Atmospheric Pollutants***,** 207-212, Varese, Italy.

TILLMANN, R., HALLQUIST, M., JONSSON, A. M., KIENDLER-SCHARR, A., SAATHOFF, H., IINUMA, Y. & MENTEL, T. F. (2010) Influence of relative humidity and temperature on the production of pinonaldehyde and OH radicals from the ozonolysis of alpha-pinene. *Atmospheric Chemistry and Physics,* 10**,** 7057-7072.

TORNQVIST, M. (1994) IS AMBIENT ETHENE A CANCER RISK FACTOR. *Environmental Health Perspectives,* 102**,** 157-160.

TREACY, J., ELHAG, M., OFARRELL, D. & SIDEBOTTOM, H. (1992) REACTIONS OF OZONE WITH UNSATURATED ORGANIC-COMPOUNDS. *Berichte Der Bunsen-Gesellschaft-Physical Chemistry Chemical Physics,* 96**,** 422-427.

TUAZON, E. C., ASCHMANN, S. M., AREY, J. & ATKINSON, R. (1997) Products of the gas-phase reactions of O-3 with a series of methyl-substituted ethenes. *Environmental Science & Technology,* 31**,** 3004-3009.

TURNIPSEED, A. A. & BIRKS, J. W. (1991) KINETICS OF THE REACTION OF MOLECULAR FLUORINE WITH DIMETHYL SULFIDE. *Journal of Physical Chemistry,* 95**,** 6569-6574.

VELASCO, E., LAMB, B., WESTBERG, H., ALLWINE, E., SOSA, G., ARRIAGA-COLINA, J. L., JOBSON, B. T., ALEXANDER, M. L., PRAZELLER, P., KNIGHTON, W. B., ROGERS, T. M., GRUTTER, M., HERNDON, S. C., KOLB, C. E., ZAVALA, M., DE FOY, B., VOLKAMER, R., MOLINA, L. T. & MOLINA, M. J. (2007) Distribution, magnitudes, reactivities, ratios and diurnal patterns of volatile organic compounds in the Valley of Mexico during the MCMA 2002 & 2003 field campaigns. *Atmospheric Chemistry and Physics,* 7**,** 329-353.

VOLKAMER, R., SHEEHY, P., MOLINA, L. T. & MOLINA, M. J. (2010) Oxidative capacity of the Mexico City atmosphere - Part 1: A radical source perspective. *Atmospheric Chemistry and Physics,* 10**,** 6969-6991.

WAYNE, R. P. (2000) *Chemistry of Atmospheres*, Oxford University Press.

WEGENER, R., BRAUERS, T., KOPPMANN, R., BARES, S. R., ROHRER, F., TILLMANN, R., WAHNER, A., HANSEL, A. & WISTHALER, A. (2007) Simulation chamber investigation of the reactions of ozone with short-chained alkenes. *Journal of Geophysical Research-Atmospheres,* 112.

WELZ, O., STRIEBEL, F. & OLZMANN, M. (2008) On the thermal unimolecular decomposition of the cyclohexoxy radical - an experimental and theoretical study. *Physical Chemistry Chemical Physics,* 10**,** 320-329.

WHALLEY, L. K., EDWARDS, P. M., FURNEAUX, K. L., GODDARD, A., INGHAM, T., EVANS, M. J., STONE, D., HOPKINS, J. R., JONES, C. E., KARUNAHARAN, A., LEE, J. D., LEWIS, A. C., MONKS, P. S., MOLLER,

S. J. & HEARD, D. E. (2011) Quantifying the magnitude of a missing hydroxyl radical source in a tropical rainforest. *Atmos. Chem. Phys. Discuss.,* 11**,** 5785-5809.

WHITE, J. U. (1942) Long optical paths of large aperture. *Journal of the Optical Society of America,* 32**,** 285-288.

WINER, A. M., PETERS, J. W., SMITH, J. P. & PITTS, J. N. (1974) RESPONSE OF COMMERCIAL CHEMILUMINESCENT NO-NO2 ANALYZERS TO OTHER NITROGEN-CONTAINING COMPOUNDS. *Environmental Science & Technology,* 8**,** 1118-1121.

WINTERHALTER, R., HERRMANN, F., KANAWATI, B., NGUYEN, T. L., PEETERS, J., VEREECKEN, L. & MOORTGAT, G. K. (2009) The gas-phase ozonolysis of beta-caryophyllene (C15H24). Part I: an experimental study. *Physical Chemistry Chemical Physics,* 11**,** 4152-4172.

WOLFF, S., BODDENBERG, A., THAMM, J., TURNER, W. V. & GAB, S. (1997) Gas-phase ozonolysis of ethene in the presence of carbonyl-oxide scavengers. *Atmospheric Environment,* 31**,** 2965-2969.

WYCHE, K. P., BLAKE, R. S., ELLIS, A. M., MONKS, P. S., BRAUERS, T., KOPPMANN, R. & APEL, E. C. (2007) Technical note: Performance of Chemical Ionization Reaction Time-of-Flight Mass Spectrometry (CIR-TOF-MS) for the measurement of atmospherically significant oxygenated volatile organic compounds. *Atmospheric Chemistry and Physics,* 7**,** 609-620.

ZADOR, J., TURANYI, T., WIRTZ, K. & PILLING, M. J. (2006) Measurement and investigation of chamber radical sources in the European Photoreactor (EUPHORE). *Journal of Atmospheric Chemistry,* 55**,** 147-166.

ZAFIRIOU, O. C. & TRUE, M. B. (1986) INTERFERENCES IN ENVIRONMENTAL-ANALYSIS OF NO BY NO PLUS O-3 DETECTORS - A RAPID SCREENING TECHNIQUE. *Environmental Science & Technology,* 20**,** 594-596.

ZHANG, L., KITNEY, K. A., FERENAC, M. A., DENG, W. & DIBBLE, T. S. (2004) LIF spectra of cyclohexoxy radical and direct kinetic studies of its reaction with O-2. *Journal of Physical Chemistry A,* 108**,** 447-454.